Investigating the role of RNA 5-methylcytosine on ribosomal and transfer RNAs in *Arabidopsis thaliana*

This dissertation is submitted for the degree of

Doctor of Philosophy (Bioscience)

Jing ZHAO

Supervisor: A/Prof Iain Searle

The University of Adelaide

Faculty of Sciences, Engineering and Technology

School of Biological Sciences

September 2022

Table of contents

List of Figures

Abstract

RNA 5-methylcytosine (m^5C) is implicated to have multiple biological and molecular roles in single cell and multicellular organisms, including regulation of mRNA translation and plant growth. However, there are still many questions waiting to be answered. In my research, I addressed the roles of m^5C on rRNAs and tRNAs in *Arabidopsis thaliana*. In Chapter 2, NOP2, a putative rRNA m^5C methyltransferase was shown to be genetically redundant and essential for ovule development. Three NOP2 orthologues, *NOP2A, NOP2B* and *NOP2C* were identified in the *A. thaliana* genome and are genetically redundant. I found *nop2a nop2b* mutants were lethal due to female gametophyte abortion at the two to eight-nucleate stages. Reduction of *NOP2A* in *nop2b nop2c* mutants using an artificial miRNA led to a range of post-embryo phenotypes, impaired ribosome activity and reduced m^5C methylation of C2268 on the 25S rRNA. In Chapter 3, I tested tRNA cleavage in T2 RNase mutants, *rns1*, *rns2, rns4* and wild type under oxidative stress by northern blotting. Small RNA sequencing suggested that loss of RNS2 results in changes of both pre-tRNA and mature tRNA profiles under oxidative stress. I also tested tRNA cleavage without m^5C methyltransferase TRM4B, and without ribonuclease RNS2, and found m^5C appears to protect $tRNA^{Asp(GTC)}$ from RNS2 cleavage. In Chapter 4, I explored the processing and molecular targets of tRNA halves originating from cleaved $tRNA^{Asp(GTC)}$. When a 35 nt 5'-half $tRNA^{Asp}$ fragment was expressed from a strong polymerase III promoter and the transgene was transformed into plants, no transgenic plants were recovered. Hence, we named this transgene, *Killer*. Subsequent transient expression of *Killer* in *Nicotiana benthamiana* leaves followed by small RNA sequencing and a targeted genetic suppressor screen in *Arabidopsis* indicated that the 35 nt 5'-half $tRNA^{Asp}$ in *Killer* was processed into several sRNAs, and involved RNA silencing proteins RDR6, DCL2, DCL3, DCL4, AGO1, AGO3, AGO4, AGO5, AGO7, AGO9 and AGO10. Two sRNAs from 5'-half $tRNA^{Asp}$ appear to silence embryo-defective genes, At1g67490 and At1g32490, thereby leading to embryo lethality. Taken together, my research addressed functions of m^5C methyltransferases NOP2 and TRM4B, and revealed a role in the processing of $tRNA^{Asp5'}$ in *A. thaliana*.

Declaration

I certify that this work contains no material which has been accepted for the award of any other degree or diploma in my name, in any university or other tertiary institution and, to the best of my knowledge and belief, contains no material previously published or written by another person, except where due reference has been made in the text. In addition, I certify that no part of this work will, in the future, be used in a submission in my name, for any other degree or diploma in any university or other tertiary institution without the prior approval of the University of Adelaide and where applicable, any partner institution responsible for the joint-award of this degree.

I acknowledge that the copyright of published works contained within this thesis resides with the copyright holder(s) of those works.

I also give permission for the digital version of my thesis to be made available on the web, via the University's digital research repository, the Library Search and also through web search engines, unless permission has been granted by the University to restrict access for a period of time.

Signature of student

23/09/2022

Acknowledgements

This extended PhD journey would not have been possible without the strong support of the following people.

First, I would like to express my deepest appreciation to my principal supervisor A/Prof Iain Searle for his dedicated support, encouragement, and guidance over the years. Your valuable suggestions, feedback and professional attitude are precious treasures that were deeply valued throughout my research training. He continuously provided encouragement and was always willing to assist me, especially, when I was grieving the unexpected loss of my brother, and during the two years I was isolated in China due to the COVID-19 pandemic. I would like to also extend my sincere thanks to my co-supervisor Prof. Frank Grutzner for his supervision. His advice and support helped me to finish my project. Thank you, Iain and Frank.

I would like to thank members of the Searle laboratory, past and present. A special thanks to Pei Qin Ng for her bioinformatics analysis undertaken in Chapters 3 and 4. I am grateful for the technical support provided by Dr. Vy Hoang Thao Nguyen, Dr. Rakesh David, Dr. Gang Li and Dr. Trung Do. In addition, many thanks to Xingyu Wu and Dr. Jun Li for their kind help when I came to the laboratory in Adelaide.

I am deeply grateful to my loving family for their endless support and love. Mom and Dad, thanks for listening to my whining and giving me advice when I have problems in life. To my younger brother, Pengfei ZHAO, I cherish the time we spent together over the 26 years. Even though you died in 2018, you are always in my heart. My appreciation also goes to my boyfriend, Yuanqiao Li, for your support throughout my PhD. Your encouragement and appreciation of me helped me to overcome the difficulties in my research. I would like to express my gratitude to my landlady Wang Wei. Thank you for never increasing my house bills. You and your family are *my family in Adelaide*.

I must thank my friends, Feng Tang, Qianhui Wan, Ying Meng, Xiaolong You, Xin Liu, Tong He and Eunice Hsiu Yee Lee for encouraging me. The time spent with you in Adelaide is an unforgettable memory in my life.

Lastly, I thankfully acknowledge the generous financial support from the University of Adelaide and the China Scholarship Council (CSC) during my PhD.

Publications

Li J, Wu X, Do T, Nguyen V, **Zhao J**, Ng PQ, *et al.* Quantitative and Single-Nucleotide Resolution Profiling of RNA 5-Methylcytosine. Methods Mol Biol. 2021; 2298:135–51.

Guo Q, Ng PQ, Shi S, Fan D, Li J, **Zhao J**, *et al. Arabidopsis* TRM5 encodes a nuclear localised bifunctional tRNA guanine and inosine-N1-methyltransferase that is important for growth. PLoS ONE. 2019;14: e0225064.

Posters

Zhao, J., Ng, P., Searle, I. R. (2019) The insights of tRNA-halves in *Arabidopsis thaliana*. Poster presented at the meeting of the Annual Genetics Society of Australia conference.

Zhao, J., Burgess, A., David, R., Searle, I. R. (2017) The effects of 5-methylcytosine on the stability of tRNAs in *Arabidopsis thaliana*. Poster presented at the meeting of Annual Combio of Australia conference.

Glossary

A-to-I (I)	Adenosine-to-inosine
A. thaliana	*Arabidopsis thaliana*
AGO	Argonaute protein
ALKBH	ALKB dioxygenase homolog
ALKBH5	Alkylation repair homologue protein 5
amiR	Artificial microRNA
Aza-IP-seq	5-Azacytidine Immunoprecipitation sequencing
bp	base pair
bsRNA-seq	RNA bisulfite sequencing
C	Cytosine
C-to-U (U)	Cytidine-to-uridine
cDNA	Complementary DNA
CDS	Coding sequence
CLIP	Crosslinking and Immunoprecipitation Sequencing
DNA	Deoxyribonucleic acid
DNMT2	DNA methyltransferase 2
eIF3	Eukaryotic initiation factor 3

eRNA	Enhancer associated RNA
FG	Female gametophyte
FIB	Fibrillarin
FIP37	FKBP12 interacting protein 37
FTO	Fat mass and obesity associated
g	Gram
GFP	Green fluorescent protein
GUS	β-glucuronidase
H_2O_2	Hydrogen peroxide
hm^5C	5-hydroxymethylcytosine
HNRNP	Heterogeneous nuclear ribonucleoprotein
hrs	Hours
Kan	Kanamycin
LB	Luria-Betrani media
lncRNA	Long non-coding RNA
LSU	Large ribosomal subunit
M	Mole
m^1A	N1-methyladenosine

m^3T	N^3-methylthymidine
m^3U	N3-methyluridine
m^5C	5-Methylcytosine
m^6A	N^6-methyladenosine
meRIP-seq	Methylated-RNA-immunoprecipitation sequencing
METTL	Methyltransferase-like
Mg	Microgam
miCLIP	Methylation Individual-Nucleotide-Resolution
min	Miniute
miRNA	microRNA
mL	Millilitre
mm	Millimetre
mM	MilliMole
mRNA	Messenger RNA
MS Media	Murashige and Skoog Media
MTA	Adenosine methyltransferase A
ncRNAs	Non-coding RNA
ng	Nanogram

NOP2	Nuclear protein 2
NOP2	Nucleolar protein 2
NOP2A	Nuclear protein 2A
NOP2B	Nuclear protein 2B
NOP2C	Nuclear protein 2C
NSUN2	NOP2/Sun domain protein 2
NSUN5	NOP2/Sun domain protein 5
nt	Nucleotide
OLI2	Oligocellula 2
ORF	Open reading frame
PCR	Polymerase chain reaction
PRC2	Polycomb repressive complex 2
PTC	peptidyl transferase center
PUS	Ψ synthases
RBS-seq	RNA-bisulfite-sequencing
RCM1	rRNA cytosine methyltransferase 1
RCMT	RNA cytosine methyltransferase
RFM	Rossmann-fold motif

rRNA	Ribosomal RNA
RT-qPCR	Real-time quantitative PCR
snoRNAs	Small nucleolar RNAs
snRNAs	Small nuclear RNAs
ssDNA	Single strand DNA
ssRNA	Single strand RNA
SSU	Small ribosomal subunit
STM	Shootmeristemless
T	Thymine
T-DNA	Transfer-DNA
TAD	tRNA-specific Adenosine Deamiase 1
TAIR	THE Arabidopsis Information Resource
TET	Ten-eleven Translocation
TRDMT1	Transfer RNA Aspartic acid Methyltransferase1
TRM4	Transfer RNA methyltransferase 4
tRNA	Transfer RNA
U	Uracil
UTR	Untranslated region

vtRNA	Vault RNA
WT	Wild type
WTAP	Wilms' tumor 1-associating protein
WUS	WUSCHEL
XIST	X-inactive specific transcript
YTHDC	YTH domain containing
µg	Microgram
µL	Microlitre
µmol	Micromole
Ψ	Pseudouridine

Chapter 1. Epitranscriptome introduction

1.1. Overview

The history and use of the term epigenetics are somewhat pliable. The hypothesis of epigenetic changes affecting the expression of genes on chromosomes was thought to be first defined by Nikolai Koltsov early last century. Soon after in 1942, Conrad Waddington coined the term epigenetics as pertaining to epigenesis, referring to the differentiation of cells from their initial totipotent state during embryonic development. He used the phrase epigenetic landscape as a metaphor for biological development in terms of how genetic components may interact with the environment to produce a phenotype. More recently Rob Holliday, in about 1990, defined epigenetics as, the study of the mechanisms of temporal and spatial control of gene activity during the development of complex organisms [1]. More recently, Arthur Riggs, Adrian Bird and others have used much stricter definitions around the inheritance of a phenotype through mitosis that is not explained by the DNA sequence [2], [3]. Analogous to epigenetics, epitranscriptomics involves understanding all functionally relevant changes to the transcriptome that do not involve a change in the ribonucleotide sequence.

The term epitranscriptome is used to describe all the biochemical modifications of the transcriptome within the cell. Now, more than 150 types of RNA modifications were identified using a suite of advanced technologies [4], [5]. Initially, most RNA modifications were found in transfer RNAs (tRNAs) and ribosomal RNAs (rRNAs). However, using high-throughput sequencing methods, RNA modifications were also discovered on less abundant messenger RNAs (mRNAs) and non-coding RNA (ncRNAs), including long non-coding RNAs (lncRNAs), microRNAs (miRNAs) and siRNAs [6]. The abundance of modifications differs amongst RNA species. For example, N1-methyladenosine (m^1A), pseudouridine (Ψ), and 2'-O-methylation (2'OMe) are much more abundant on tRNAs and rRNAs, while N6-methyladenosine (m^6A), 5-methylcytidine (m^5C), and 2'OMe are extensively enriched in mRNAs and viral RNAs [7], [8]. Among the identified RNA modifications, methylation is the most well-studied in plants and animals.

In the next section, I introduce prevalent cellular RNA modifications including m^5C, m^6A, and Ψ, and describe the so-called writer, eraser and reader proteins, the distribution and functions of these modifications on mRNAs, rRNAs and tRNAs. I then outline the production, and function of small RNAs derived from cleaved tRNAs.

1.1.1. m^5C

Among the identified RNA modifications, m^5C is formed by adding a methyl group to the fifth carbon of the cytosine base (Fig 1.1). First identified on DNA [9] and later found on RNA [10], m^5C was identified in all cellular RNAs, including mRNAs, rRNAs, tRNAs, lncRNAs, and small nuclear RNAs (snRNAs) [11].

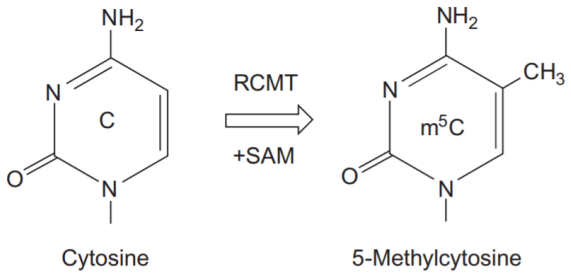

Figure 1.1: Cytosine is methylated to 5-methylcytosine by RNA cytosine methyltransferases (RCMTs).

RCMT catalyses the transfer of a methyl group, CH_3, from the donor substrate S-adenosylmethionine (SAM) to the 5-carbon position of cytosine. Figure from [12].

1.1.1.1. m^5C detection

The distribution and functional studies of m^5C are underpinned by advances in m^5C detection. Transcriptome-wide m^5C detection methods include RNA-bisulfite-sequencing (bsRNA-seq), methylated-RNA-immunoprecipitation (meRIP-seq), Aza-IP-seq and miCLIP-seq. Each method has its advantages and disadvantages. Bisulfite-sequencing was first utilised for detecting DNA m^5C in 1992 [13]. In the presence of sodium bisulfite, unmethylated cytosines are converted to uracils and sequenced as thymines, while the methylated

cytosines remained unchanged during conversion and sequencing [14]. RNA bisulphite-sequencing utilises the same principles as previously outlined for DNA and has the advantage over other techniques of providing single-nucleotide resolution and high specificity. However, this approach is unable to reliability detect low abundance m^5C in RNAs and fails to distinguish m^5C from other types of cytosine modifications, like m^3C [15].

A second detection method is meRIP-seq which was first adopted to detect m^6A in RNA transcripts [16], [17]. meRIP-seq using a m^5C antibody combined with deep-sequencing was applied to map m^5C sites in animals and plants [18], [19]. A limitation of meRIP-seq is the inability to detect modifications at single-nucleotide resolution due to the effective shearing length of IP input RNA is about 100-150 nt [15]. A disadvantage of meRIP-seq is RNA second structure that may inhibit the antibody binding and detection of potential m^5C sites [20]. A potential second disadvantage is the specificity of the antibody, as an antibody cross may react with another modification and therefore lead to erroneous datasets [21].

The last methods to detect RNA m^5C are Aza-IP-seq and miCLIP-seq that were designed to identify the target sites of RNA cytosine methyltransferases (RCMTs) by trapping and immunoprecipitation [22], [23]. RCMTs form a reversible covalent intermediate with their target cytosine substrate however both Aza-IP-seq and miCLIP-seq trap the RCMT bound to the target RNA. With Aza-IP, RNA is mixed with 5-azacytidine (5-azaC) and RNA transcripts containing m^5C are trapped the RCMT by forming a covalent enzyme-RNA adduct. Then, the protein and covalently bound RNA are immunoprecipitated and sequenced. Even though Aza-IP can identify m^5C sites at single-nucleotide resolution, it also has limitations. Examples include 5-azaC is toxic to cells at high concentrations and not all cytosines will be replaced by 5-azaC [24], [25]]. Compared to Aza-IP, the method, methylation-individual nucleotide resolution cross-linking and immunoprecipitation (miCLIP) introduces a mutation of the conserved cysteine in the catalytic domain (C271A) of the RCMT and subsequently forms a covalently linked RNA-protein complex [26]. Immunoprecipitation and deep-sequencing identify the m^5C site at the +1 site

of the sequencing read [27]. Even though it has high specificity, the method is time consuming.

Except for the above detection methods for RNA modifications, the latest nanopore sequencing technologies developed by Oxford Nanopore Technologies allows to detect endogenous and exogenous RNA modifications at the single-nucleotide and single-molecule resolution, as well as to predict RNA modifications in individual reads based on nanopore data [28]–[30]. However, the application of nanopore was limited by the lack of available data by which to recognize the location and abundance of known RNA modifications and the inevitable error rate [28], [31].

In summary, all m^5C detection methods have limitations. Therefore, to obtain reliable, nucleotide resolution m^5C data, a combination of approaches is required.

1.1.1.2. m^5C methyltransferases

Currently, two classes of RCMTs have been identified in eukaryotes. The first is the Rossmann-fold superfamily of RNA methyltransferases (MTases) due to the family sharing a Rossmann-fold motif (RFM) within the catalytic domain [32]. Among this class, five subfamilies, RCMT1, 2, 7, 8 and 9, are present in eukaryotes, and each subfamily shares conserved amino acid sequences across different species. The remaining RCMT subfamilies 3, 4, 5 and 6 are distinctly prokaryotic [33]. RCMT7 family proteins are involved in the methylation of tRNAs and mRNAs [34], [35] and NSUN2 methylates the tRNAs structural position C34 of $tRNA^{Lec(CAA)}$, C40 of $tRNA^{Gly(GCC)}$, C48 and C49 of $tRNA^{Asp(GTC)}$ in humans [35]. The NSUN2 ortholog, TRM4B, has m^5C methylation activity on tRNAs at positions C48, C49 and C50, as well in non-coding RNAs and mRNAs in *A. thaliana* [11], [36]. Members of the RCMT2 protein family mainly methylate rRNAs. For example, the Nucleolar protein 2 (NOP2)/NSUN1 catalyses methylation of C2870 in 25S rRNA in yeast [37]. Genome sequencing and characterization identified three paralogs of *NOP2* in *A. thaliana*, *NOP2A/At5g55920* as known as *OLI2*), *NOP2B/At4g26600* and

NOP2C/At1g06560. Recently published data shows that C2860 in 25S rRNA was reduced in *NOP2* RNAi *Arabidopsis* plants [38]. Besides RCMT2, the RCMT8 subfamily referred to as NSUN5 in *A. thaliana* and RCM1 (rRNA cytosine methyltransferase 1) in yeast also target rRNA methylation. The loss of RCM1 specifically abolishes m^5C at C2278 in 25S rRNA. Similarly, reduced m^5C methylation at C2268 in 25S rRNA was observed in nsun5 *A. thaliana* mutants [36], [39].

Another class of eukaryotic RCMTs is Transfer RNA Aspartic acid Methyltransferase (TRDMT1), also known as DNA methyltransferase (DNMT2) due to its shared sequence methyltransferase motifs with DNA methyltransferases [40]. TRDMT1 methylates tRNAs in various organisms including Drosophila, *A. thaliana* and Homo sapiens [41]. Initially, TRDMT1 was demonstrated to methylate $tRNA^{Asp(GTC)}$, $tRNA^{Gly(GCC)}$ and $tRNA^{Val(AAC)}$ at structural position C38 in animals [42]–[44], and only $tRNA^{Asp(GTC)}$ in *A. thaliana*. Subsequently, TRDMT1 has been demonstrated to also methylate C38 on $tRNA^{Gly(CCC)}$ and $tRNA^{Gly(GCC)}$ in *A. thaliana* [45]. Although significant progress has been made in identifying the writers of m^5C, the targeting mechanism is largely still a mystery.

1.1.1.3. m^5C distribution

Mapping of m^5C sites from various studies demonstrated that the distribution of m^5C on mRNA is not random. In *A. thaliana*, the majority of identified sites identified by bs-RNA seq are in the coding sequence (CDS), and a slight enrichment for sites in the 3' UTR and 5'UTR [11]. While a divergent result in m^5C-RIP seq showed no m^5C enrichment in the 3'UTR and 5'UTR in *A. thaliana* [46]. In Hela and mouse cells, the data from bs-RNA seq have shown that the m^5C sites are enriched in 3'UTR and 5'UTR and were not enriched in the CDS [47], [48]. The contradictory m^5C distribution could be explained by the different tissues the RNA was derived from, depth of sequencing, detection sensitivity and specificity or sensitivity to RNA secondary structure of the different methods. Exploring m^5C distribution in more species combined with genetics tools is necessary to further clarify the distribution.

1.1.1.4. m^5C Function

Although progress has been made in the detection, identification of methyltransferases and transcriptome-wide distribution of m^5C, we are only beginning to reveal the cellular and molecular roles of m^5C on RNAs. On tRNAs, m^5C methylation can stabilize tRNA secondary structure, promote translation efficiency and regulate stress responses [37], [49]. In terms of mRNAs, the functional role of 3'UTRs m^5C is unclear. It has been proposed that m^5C in 3'UTRs may be related to the binding of Argonaute I-IV proteins in humans that function in the miRNA-guided decay of mRNA and translational inhibition [50]. More recently, 5-methylation on mRNAs was shown to exert influence on RNA metabolism through, mRNA stability, splicing, nucleus-to-cytoplasm export, and alternative polyadenylation [48], [51], [52]. In humans, mutations in m^5C methyltransferases are associated with various diseases and altered expression is observed in numerous cancers [53]–[55]. Like tRNA and mRNA stability, RCMTs are linked to maintaining rRNA stability and translational efficiency [27], [56]. In other RNA types, including long non-coding RNAs (lncRNAs) and smaller non-coding RNAs, such as enhancer associated RNAs (eRNAs) or vault RNAs (vtRNAs) m^5C was also shown to play a role. Specifically, m^5C in the vital A-region of the lncRNA X-inactive specific transcript (XIST) prevents binding of the chromatin regulatory PRC2 (polycomb repressive complex 2) complex to XIST *in vitro* [57]. In *nusn7* mutants, decreased m^5C levels on eRNAs correlated with decreased eRNA abundance, demonstrating that m^5C plays a role in eRNAs stabling and therefore fine-tuning gene expression [58] Furthermore, methylation of the small non-coding RNA vtRNA1.1 effects processing into smaller RNA fragments that have a miRNA-like function [59]. Overall, these findings highlight the significance of RNA m^5C in molecular and cellular functions.

1.1.2. m^6A

RNA N-m^6A is another well-studied RNA modification in yeast [60], plants [61] and humans [62]. After being discovered on mRNAs, m^6A was later found on rRNAs and lncRNAs [63]. Compared to m^5C, a better understanding of the m^6A

writer, reader and eraser proteins has occurred in plants and mammals, which is shown in Table 1.

Table 1.1: List of writers, readers, and erasers involved in RNA methylation in *A. thaliana* and rice (Oryza sativa). Table from [64].

Type	Gene name	Arabidopsis gene ID	Target RNA	Function	Rice ortholog	Animal counterpart
Writers	MTA	At4g10760	m^6A	Embryo development	LOC_Os02g45110	METTL3
	MTB	At4g09980	m^6A	Embryo development	LOC_Os01g16180	METTL14
					LOC_Os03g05420	
					LOC_Os10g31030	
	FIP37	At3g54170	m^6A	Development	LOC_Os06g27970	WTAP
	VIRILIZER	At3g05680	m^6A	Development	LOC_Os03g35340	VIRMA
	HAKAI	At5g01160	m^6A	Development	LOC_Os10g35190	
	TRM4A	At4g40000	m^5C		LOC_Os08g37780	
	TRM4B	At2g22400	m^5C	Root development	LOC_Os09g29630	
Readers	YTH01 (ECT11)	At1g09810	m^6A m^1A		LOC_Os01g22630	YTHDF1
	YTH02 (ECT9)	At1g27960			LOC_Os08g12760	YTHDF2
	YTH03(CPSF30)	At1g30460			LOC_Os06g46400	YTHDF3
	YTH04 (ECT7)	At1g48110			LOC_Os03g20180	YTHDC1
	YTH05 (ECT4)	At1g55500		Development	LOC_Os03g53670	YTHDC2
	YTH06 (ECT8)	At1g79270			LOC_Os01g48790	
	YTH07 (ECT1)	At3g03950			LOC_Os04g51940	
	YTH08 (ECT5)	At3g13060			LOC_Os08g44200	
	YTH09 (ECT2)	At3g13460		Trichome branching	LOC_Os07g07490	
	YTH10 (ECT6)	At3g17330			LOC_Os04g51950	
	YTH11	At4g11970				
	YTH12 (ECT10)	At5g58190			LOC_Os05g04000	
	YTH13 (ECT3)	At5g61020		Trichome branching	LOC_Os05g01520	
Erasers	ALKBH1A	At1g11780			LOC_Os03g60190	ALKBH1
	ALKBH1B	At3g14140			LOC_Os11g29690	
	ALKBH1C	At3g14160				
	ALKBH1D	At5g01780				
	ALKBH2	At2g22260			LOC_Os06g17830	ALKBH2
	ALKBH6	At4g20350			LOC_Os10g28410	ALKBH6
	ALKBH8	At1g36310	tRNA mcm^5U		LOC_Os04g51360	ALKBH8
					LOC_Os11g43610	
	ALKBH8A	At1g31600	tRNA mcm^5U			
	ALKBH8B	At4g02485				
	ALKBH9A	At1g48980			LOC_Os06g04660	ALKBH5
	ALKBH9B	At2g17970	m^6A	Viral infection		
	ALKBH9C	At4g36090				
	ALKBH10A	At2g48080			LOC_Os05g33310	
	ALKBH10B	At4g02940	m^6A	Flowering	LOC_Os10g02760	

In the m^6A writer complex, methyltransferase-like 3 (METTL3), METTL14, METTL16, Wilms' tumor 1-associating protein (WTAP), and Vir-like m^6A methyltransferase-associated (VIRMA; KIAA1429) were demonstrated as essential components in animals [65]–[68]. It is noteworthy that these components are dependent on each other to regulate the m^6A methylation. For example, although METTL3 predominantly exerts a methyltransferase activity, the catalytic activity of the METTL3–METTL14 complex is much higher than METTL3 or METTL14 alone, which indicates METTL14 enhances the MTase activity of METTL3 [66], [69]. WTAP interacts with METTL3 and METTL14 and

is necessary for their localisation into nuclear speckles enriched with pre-mRNA processing factors [65]. VIRMA guides specific target methylation by recruiting the catalytic core components METTL3/METTL14/WTAP [70]. METTL16, a newly discovered independent RNA methyltransferase, is responsible for 3′ UTR m^6A in mRNAs and on A43 of U6 small nuclear RNA [71]. Additionally, bioinformatics indicated that the CCHC zinc-finger-containing protein ZCCHC4 is an RNA m^6A methyltransferase and was confirmed to be required for m^6A on human 28S rRNA [72]. Also, the CCCH zinc-finger-containing protein ZC3H13 was found to be essential for the Zc3h13-WTAP-Virilizer-Hakai complex, which is vital for RNA m^6A in mammals [73]. Based on orthology of the animal m^6A writers, the plant's methyltransferase complexes MTA (ortholog of METTL3), MTB (ortholog of METTL14), FIP37 (ortholog of WTAP) and VIRILIZER (ortholog of VIRMA) were identified. In *A. thaliana*, E3 ubiquitin ligase HAKAI was found to be an important m^6A writer component as knockdown of this protein resulted in decreased m^6A levels and pleiotropic phenotypes [74].

Eraser proteins, also known as demethylases, of m^6A are members of the alpha-ketoglutarate-dependent dioxygenase homologs (ALKBH) family and are Fe (II) and α-ketoglutaric acid-dependent. In mammals, the Fat mass and obesity-associated protein (FTO) and Alkylation repair homologue protein 5 (ALKBH5) are responsible for the removal of m^6A in RNA [75], [76]. FTO could demethylate not only m^6A but also N3-methylthymidine (m^3T) and N3-methyluridine (m^3U) from single-strand DNA (ssDNA) in mice and single-strand RNA (ssRNA) [77].. ALKBH5 and FTO were demonstrated to participate in multiple processes including splicing and production of longer 3′-UTRs of mRNAs, maintaining mRNA translation stability and several other cellular processes [78]–[81]. Another demethylase, ALKBH3, was identified for tRNA m^6A demethylation in human [82]. Sequence homology searches identified 14 ALKBH-like members in *A. thaliana* (Table 1) [83], of which only ALKBH9B (At2g17970) and ALKBH10B (At4g02940) are related to m^6A demethylation during viral infection and floral transition [84], [85]. In summary, growing numbers of m^6A eraser proteins have been identified, but the activity and substrate RNAs of most ALKBH family members in plants and animals are unclear.

Members of the YT521-B homology (YTH) domain family (YTHDF1, YTHDF2, YTHDF3, YTHDC1, and YTHDC2) have a conserved m^6A-binding domain that has high affinity to m^6A and are important m^6A readers [86], [87]. Interestingly, the different reader proteins recognize and bind different m^6A RNAs and have functional outcomes. For example, the first identified m^6A reader, YTHDF2, binds to m^6A-modified RNAs and then accelerates their degradation by recruiting the CCR4-NOT deadenylase complex [88]. Reader YTHDF1 recognises m^6A sites around mRNA stop codons and enhances mRNA translation and protein synthesis by interacting with translation initiation factors and the 40S ribosomal subunit [89]. YTHDF3 cooperates with YTHDF1 to promote the translation of methylated mRNAs and increase target RNA degradation by interacting with YTHDF2 [90]. YTHDC1 has a role in exporting m^6A-methylated mRNAs from the nucleus [91]. YTHDC2 can also promote the translation of m^6A-methylated mRNAs [92].

Besides the YTH proteins, other protein can act as m^6A readers in animal cells. One such family is the nuclear ribonucleoprotein (HNRNP). HNRNPC and HNRNPG bind to m^6A-methylated mRNAs and regulate mRNA abundance and splicing, similar to YTHDC2 [93]. Another m^6A binding protein is the insulin-like growth factor 2- IGF2BPs, including IGF2BP1, 2 and 3. IGF2BPs recognise m^6A sites and enhance mRNA stability and translation in an m^6A-dependent manner [94]. Eukaryotic initiation factor 3 (eIF3) could also bind m^6A in the 5′ UTR region of transcripts and enhance cap-independent translation [95]. In the *A. thaliana* genome, a total of 13 YTH domain proteins were predicted (Table 1), eleven of the 13 members have a highly conserved C terminus and are named ECT1 to ECT11 for Evolutionarily Conserved C Terminus. YTHD09 (ECT2), YTHD13 (ECT3), and YTH05 (ECT4) were functionally recently functional characterized [96], [97]. It was reported that ECT2 can bind m^6A RNA *in vivo*, and plants depleted of ECT2 show a trichome-branching defect. Additionally, ECT2 is cytoplasmic located protein and can regulate mRNA fate by relocating bound RNA to stress granules upon heat exposure [97]. When ECT4 was mutated, the *ect2/ect3* mutants exhibited delayed leaf emergence and leaf morphology defects [98], [99].

RNA m^{6}A in mammals was linked to various processes including RNA splicing, RNA stability, RNA export, 3'UTR processing, and translation by genetic analysis of the writer, eraser and readers (Fig 1.2). For example, in VIRMA and METTL3-depleted cell lines, the 3′UTR length of mRNA transcripts was extended by over 50% [100]. FTO was demonstrated to regulate alternative splicing via moderating m^{6}A levels and hence SRSF2 binding at splice sites [101]. YTHDF2 is mainly bound to m^{6}A near the stop codon, 3'UTR and CDS, indicating a role in mRNA stability and translation [102]. FMRP binds to m^{6}A-modified mRNAs and enhances their nuclear export to regulate neural differentiation [103]. Functional analysis of m^{6}A was also linked to cell development, proliferation, differentiation, and cell motility. For example, up-regulated ALKBH5 reduces autophagy and promotes cell proliferation [104]. On the contrary, depletion of FTO in mice can hamper the differentiation of primary myoblasts into skeletal muscle cells [105]. Perhaps unexpectedly, METTL3 was identified as an oncogene in cancer cells as METTL3 facilitated cancer-induced gene expression associated with translation initiation factors [106].

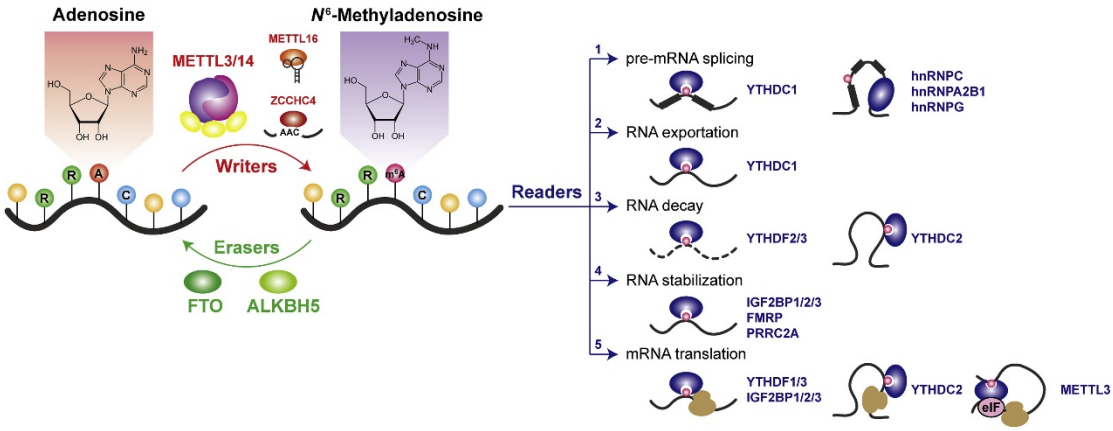

Figure 1.2: The m^{6}A Methylation Machinery and the Biological Functions of m^{6}A.

The N-m^{6}A modification is installed onto cellular RNAs by the methyltransferase complex comprising the methyltransferase-like 3 (METTL3)/METTL14 (methyltransferase-like 14) heterodimer core subunit and other cofactors including WTAP, KIAA1429, ZC3H13, and RBM15/RBM15b. Methyltransferase-like 16 (METTL16) alone can catalyse m^{6}A formation on U6 small nuclear (sn)RNA and some structural RNAs, whereas ZCCHC4 is responsible for the deposition of m^{6}A on rRNA. The RNA m^{6}A modification can be reversibly removed by RNA demethylases (erasers) fat mass and obesity-associated protein (FTO) and AlkB family member 5 (ALKBH5). The biological functions of m^{6}A modification are affected by specific recognition by RNA binding proteins (readers), which regulates RNA fate by regulating RNA splicing, export, decay, stabilisation, and translation. Figure from [107].

Functional studies of RNA m^{6}A was also linked to plant development and abiotic stress responses through genetic analysis of the writers, erasers and readers. In *A. thaliana*, lack of m^{6}A writer MTA leads to early embryonic lethality, as it is essential for formation of shoot meristems and reduced MTA abundance was linked to post-embryonic processes of lateral root growth, leaf and floral tissue development [108]. Embryonic lethality was also observed in complete depletion of FIP37, while partial loss results in the massive proliferation of shoot meristems through increasing WUSCHEL (WUS) [109]. Other m^{6}A writers in *A. thaliana*, like VIRILIZER and HAKAI, also influence root and shoot growth and cotyledon development [74]. Unlike m^{6}A writers, functional knowledge about m^{6}A erasers and readers is more limited. In *A. thaliana*, *alkbh10b* mutants displayed delayed juvenile to adult leaf transition, delayed flowering and reduced ALKBH9B results in a high abundance of m^{6}A in the alfalfa mosaic virus genome of infected plants [110], [111]. m^{6}A ECT family members were illustrated to have a role in *A. thaliana* leaf and epidermal hair development [98]. Interestingly, in rice, the analysis of microarray data showed the expression pattern of m^{6}A writers MTA and FIP37 were enhanced by cold and heat stress, and increased activity of eraser ALKBH1 was found after drought and cold treatments. In contrast, the expression of reader YTHD4 does not respond to cold stress [64]. The abiotic stress condition complicated the understanding of the status of m^{6}A, therefore disclosing the co-regulation mechanisms of writer, eraser and reader of m^{6}A under abiotic stress on other species is beneficial to

unveiling the mystery of m^6A.

1.1.3. Other RNA modifications

1.1.3.1. Pseudouridine (Ψ)

Ψ is generated from uridine through a post-transcriptional isomerisation and was identified more than sixty years ago. By now, the Ψ is the first modification to be discovered and the most abundant one in the RNA species [112]. More recently, a transcriptome-wide profiling study revealed that the Ψ sites were not only found in rRNA, tRNA, and small nuclear RNAs but also mRNAs [113]. Notably, the catalytic reaction between uridine and Ψ was achieved by two mechanisms, namely, an RNA-independent mechanism and an RNA-dependent mechanism [114]. RNA-independent pseudouridylation involves various Ψ synthases (PUSs) with specific substrates and sub-cellular domains to convert uridine into Ψ. However, the RNA-dependent mechanism is accomplished by a box H/ACA small nucleolar RNAs (snoRNAs).

The advancement of high throughput pseudouridine-seq technologies accelerates the identification of Ψ sites. Four different high throughput pseudouridine-seq methods (Pseudo-seq, Ψ-seq, PSI-seq and CeU-seq) have identified 1496 Ψ sites in 867 yeast mRNAs under normal and stress stimulus conditions. Also, there are 3083 Ψ sites in 2174 human mRNAs, which mainly accumulate in 5' and 3'UTR and CDS [114]. However, the biological role of Ψ in mRNAs is only beginning to be uncovered. Despite less evidence from the experiment, the Ψ was speculated to have the ability to modulate mRNA structure, influence pre-mRNA splicing and 5' capping and regulate RNA sub-cellular localisation [115], [116]. Furthermore, the Ψ was demonstrated to influence the mRNA stability. Such as the absence of PUS7, Pus family enzymes regulating Ψ sites, in yeast leads to the decreasing level of pseudouridylated mRNA, showing a role in stabilising mRNA stability [117]. In contrast, another study in wild-type and TgPUS1-mutant parasites indicated that genes containing a TgPUS1-dependent Ψ are relatively more abundant in mutant parasites than wide type, suggesting that pseudouridylation is able to

destabilise mRNA [118]. Therefore, studies referring to clarifying molecular mechanisms underlying Ψ-mediated regulation of mRNA stability should gain substantial attention. Investigation of Ψ on other RNAs was also carried out. Such as, it was demonstrated that Ψ sites are functionally enriched in principle rRNA regions, including the peptidyl transferase centre (PTC), the decoding centre, the A-site finger (ASF) region and sites where ribosomal subunits interact [119]. It was reported that the Ψ in rRNAs is vital for the ribosome biogenesis and protein translation in S. cerevisiae [120], [121]. Additionally, a Functional study of Ψ in tRNAs exhibited that Ψ is able to maintain the tRNA stability and decoding fidelity during translation [122].

1.1.3.2. 5-hydroxymethylcytosine (hm^5C)

In RNA and DNA, TET- enzymes catalyse the oxidisation of m^5C to hm^5C (Fig 1.3) [123]. In Drosophila melanogaster decreased hm^5C in dTet-deficient mutants had impaired brain development. Moreover, transcriptome-wide mapping revealed that hm^5C is located in exonic and intronic regions of protein-coding transcripts [124]. Further analyses identified a consensus sequence of UCCUC repeats. In contrast to m^5C, mRNAs with high hm^5C content were associated with active translation [125]. The distribution and biological functions of hm^5C in mammals and plants is actively being pursued.

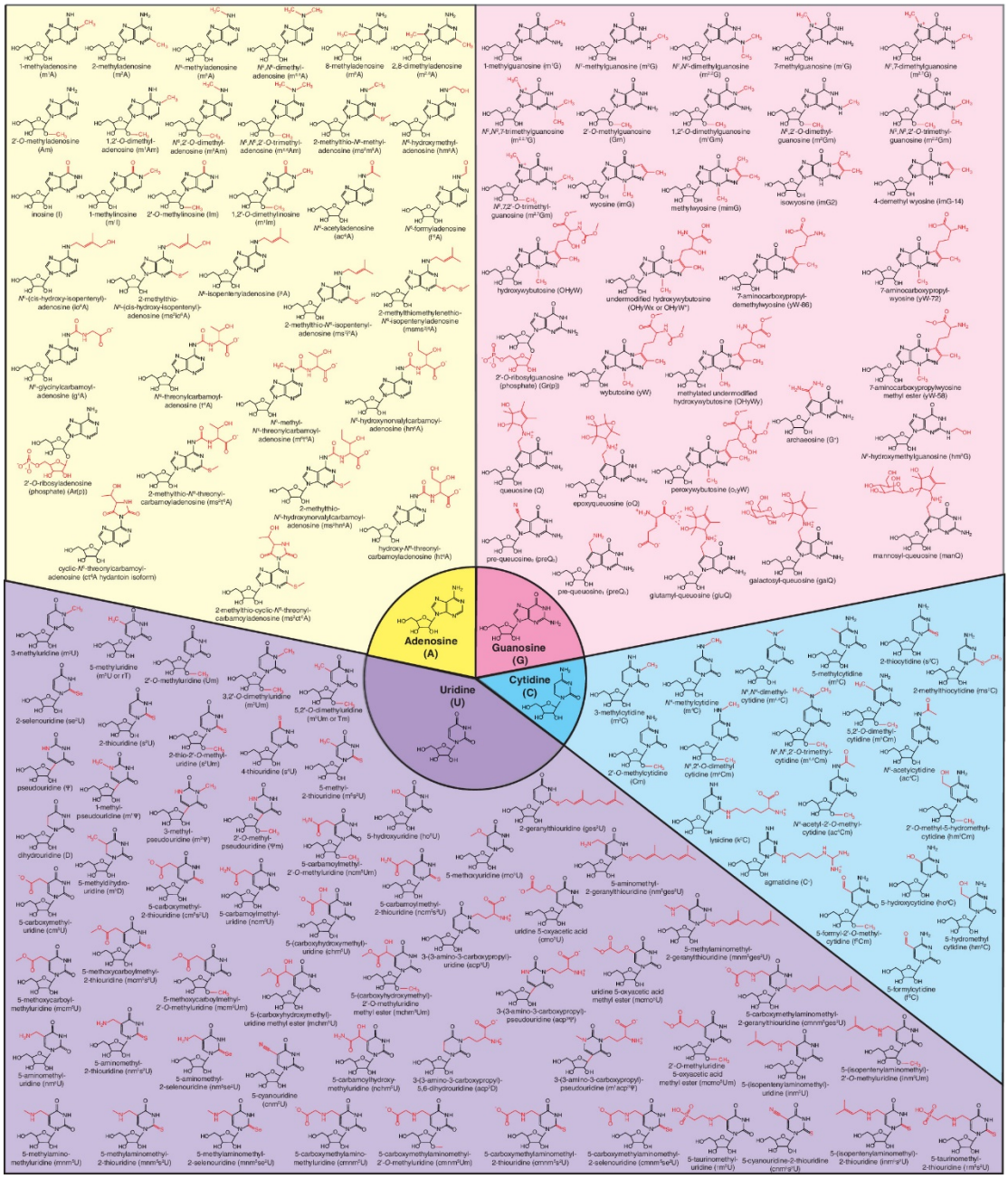

Figure 1.3: Chemical structures of all currently known RNA modifications.

Adenosine-derived (yellow), guanosine-derived (pink), uridine-derived (purple), and cytidine-derived (cyan) modifications are classified based on the parent ribonucleoside. The red moieties indicate which portion of the modified ribonucleoside is different from the parent ribonucleoside, whose structures are shown in the central circle. Figure from [126].

1.1.3.3. I and U

Adenosine-to-inosine RNA editing (A-to-I editing), termed I, is also a

transcriptional modification (Fig 1.3). It is formed by the adenosine deaminase acting on RNA (ADAR) family of enzymes [127]. And there are three members in humans, ADAR1 and ADAR2, which mainly catalyse dsRNA-binding proteins, while ADAR3 is thought to be a dominant negative regulator of the I editting [128], [129]. Roughly 50 000-150 000 I editing sites were mapped in mice and about millions in humans. Specifically, it is reported that 1741 I sites are located in CD regions of transcripts from different human tissues [130], [131]. In recent years, this modification has been discovered to influence the native secondary structure of the mRNA [132].

Cytidine-to-uridine RNA editing (C-to-U editing), also named U (Fig 1.3), is a critical post-transcriptional modification in mitochondria and chloroplasts specific to flowering plants. In rice, a total of 491 U editing sites have been identified in the mitochondria genome [133]. This editing could be found in 5′ or 3′ UTR, introns, rRNA and tRNA, regulating splicing, stabilising transcript and maintaining translation efficiency [134].

1.2. Messenger RNA modifications and functions

Among the already identified RNA modifications, the m^6A and m^5C are the best understood covalent nucleotide modifications in mRNAs. Mass spectrometric (MS) quantification also identified other modifications in mRNA, including N 1-methyladenosine (m^1A), N 4-acetylcytidine (ac4C), hydroxymethylcytosine (hm^5C), 3-methylcytidine (m^3C), cytosine to uridine (C to U) editing, m^7G, Nm, and 7,8-dihydro-8-oxoguanosine (8-oxoG) [135]. These modifications are less well understood due to their lower abundance compared to m^6A and m^5C.

In plants, the abundance of mRNA modifications m^6A and m^5C is dynamic during growth and development. In *A. thaliana*, a total of 4,881 different m^6A peaks were identified between 5-day-old seedlings and 4-week-old leaves [136]. In rice, m^6A modification profiling identified 1,792 and 6,508 m^6A-modified genes in callus and leaves, respectively [137]. In the fruit of the ripening-

deficient tomato *sidml2* mutants, more than 1,100 mRNAs showed an increase of m^6A compared to wild type [138]. In *A. thaliana*, 128, 201, and 859 m^5C sites were identified in siliques, seedling shoots, and root tissues, respectively, and only 15 sites showed varying m^5C levels amongst all three tissues [11]. In another study, m^5C sites were investigated in siliques and rosette leaves, displaying the highest (0.036%) and lowest abundance (0.010%), respectively. Of note, a slightly increasing trend of m^5C level was observed from 3-day-old to 15-day-old whole seedlings [139]. The above finding of m^6A and m^5C in different tissues and development stages indicates the dynamic regulation pattern of mRNA modifications in plants.

The molecular and biological importance roles of mRNA modifications have been elucidated in multiple species. Being the most abundant mRNA modification, m^6A is mainly near the translation start codon and translation stop codon, which confers its main roles in the translation process. To be more specific, the dynamic m^6A could be bound by some special protein and influence the lifetime of mRNA [79], [101], [103], [140]. Furthermore, the biological role of m^6A was reported to be associated with the embryo development, stem cell fate determination [109], floral transition [141], trichome and leaf morphology [98] in *A. thaliana*, fruit ripening in tomatoes [138], and sporogenesis in rice [142] (Fig 1.4). The functional versatility of m^5C on mRNA has also been gradually disclosed in plants and animals. For example, as the candidate sites were found in cis-acting regulatory motifs and miRNA/RISC binding sites, the m^5C were predicted to be involved in post-transcriptional regulation of the mRNA metabolism [50]. Also, the m^5C is related to mRNAs in low translation activity in *A. thaliana* [15]. Notably, the recent finding indicates that m^5C has a role in guiding mRNA over graft junctions to distinct parts in *A. thaliana* [19], while the mechanism behind this function is unclear and the mobility of mRNA conferred by m^5C is still waiting to be mirrored in other species. In addition, m^5C in human could be recognised by mRNA export adaptor ALYREF via a methyl-specific RNA-binding motif and modulate the export of bound mRNAs in an NSUN2-dependent way [143]. The investigation of mRNA m^5C on the growth of plants is sparse. It was only reported that the decreased m^5C levels caused by the absence of TRM4B in mRNA resulted in

the short primary roots and a reduced number of lateral roots in *A. thaliana* [11] , [15]. In summary, the mRNA modifications m^6A and m^5C are vital for the mRNA processing and the development of plants.

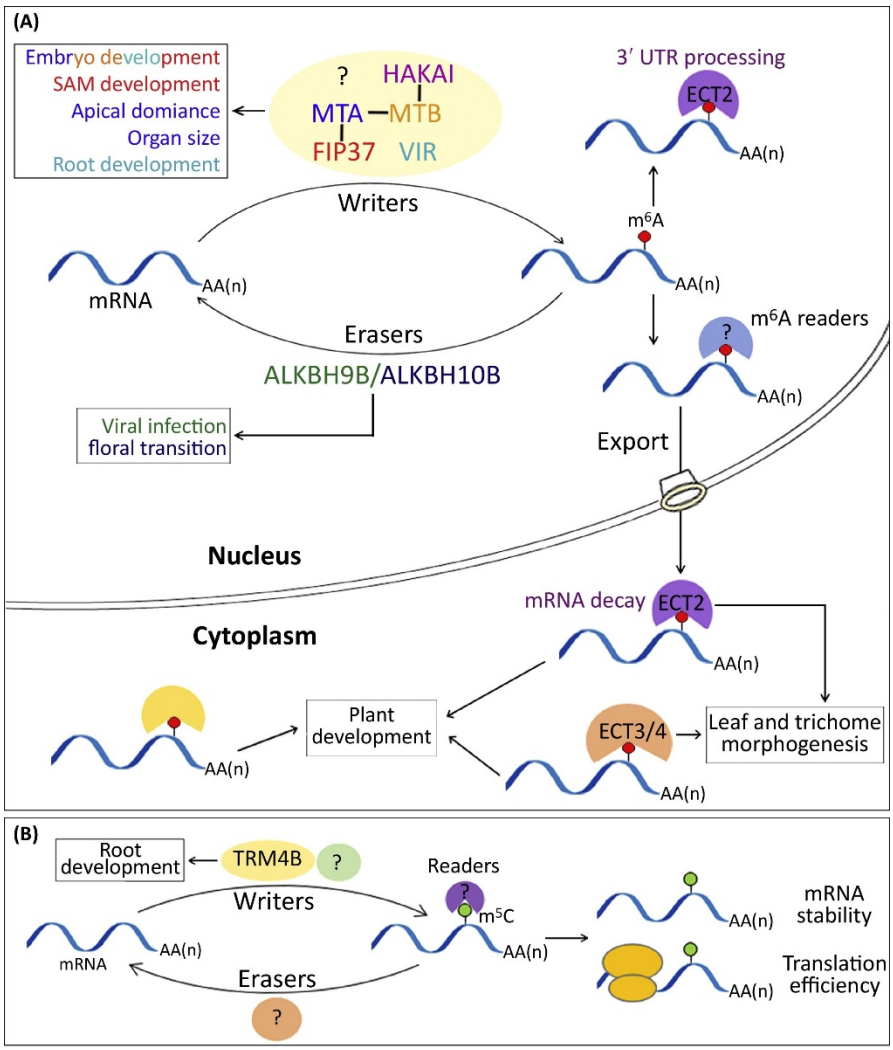

Figure 1.4: *N*^{6}-Methyladenosine (m^{6}A) and 5-Methylcytosine (m^{5}C) modifications in *A. thaliana.*

(A) Major players involved in m^{6}A regulation in *A. thaliana* and their effects on plant development. The methyltransferase complex (writers) and demethylases (erasers) dynamically sculpt the reversible m^{6}A mRNA modification landscape in the nucleus. The methyltransferase complex consists of MTA, MTB, FIP37, VIR, HAKAI, and possibly other components, while the demethylases include ALKBH9B and ALKBH10B. m^{6}A-methylated mRNAs are specifically bound by m^{6}A readers, such as three YTH domain-containing proteins (ECT2, ECT3, and ECT4), in both the nucleus and cytoplasm. "**-**" indicates direct protein interaction observed *in vivo* or *in vitro* between two proteins. A biological process affected by the loss of function of individual components of the writer complex or erasers is colour-coded accordingly. Overall, m^{6}A-methylated mRNAs are involved in a wide range of plant developmental processes. **(B)** m^{5}C modification and its function in *A. thaliana*. m^{5}C modification is catalyzed by TRM4B, and modules root development. m^{5}C is involved in mRNA decay and translation. The erasers, readers, and other writers for m^{5}C remain identified in *Arabidopsis*. Figure from [144].

Additionally, current technology could only detect one kind of modification, while interaction between multiple modifications may exist in a given transcript. Therefore, to better understand how mRNA modification modulates translation and gene expression, it will be necessary to update technologies to determine the combinations of modifications in individual transcripts. As for the less abundant chemical modifications, more breakthroughs should be made to better understand its functions in mRNAs. Furthermore, high-throughput sequencing methods coupled with new approaches are needed to reveal more previously unseen mRNA modifications.

1.3. Ribosomal RNA modifications and functions

In eukaryotic cells, roughly 2% of rRNA nucleotides are modified [145]. Ψ and 2'-O-ribose-methylations are the most abundant rRNA modification and they were installed through small nucleolar ribonucleoprotein complexes (snoRNPs) consisting of multiple conserved proteins and a small nucleolar RNA (snoRNA), which guides RNA to direct protein enzymes to the site of modification [124].

2'-*O*-methylation is accomplished by the rRNA methylation complex, which contains the methyltransferase NOP1 (yeast)/Fibrillarin (human) in combination with scaffolding proteins, the RNA binding protein NHP2L1 and a single snoRNA from the C/D box snoRNA family, which guide the ribose to be methylated [146], [147]. While H/ACA box RNPs install ψ, each consisting of one H/ACA snoRNA and four core proteins, namely GAR1, NHP2, NOP10 and the pseudouridine synthase dyskerin (DKC1) [148], [149].

The Ψ and 2'-O-ribose methylations sites are now mapped in multiple organisms. In human rRNAs, 95 ψ sites and more than 106 2'-O-ribose-methylations were identified, and the number is still increasing [150], [151]. In yeast, 55 2'-O-methylation sites and 45 ψ sites have been mapped on rRNAs [145]. In *A. thaliana*, a total of 117 2'-O-ribose-methylation sites were mapped by the Illumina-based RiboMethSeq approach, 38 in the 18S rRNA, 2 in the 5.8S rRNA and 77 in the 25S rRNA sequences [152]. After the rRNA modifications were mapped, numerous studies have focused on the rRNA modifying enzymes and phenotypes associated with their loss. Three genes homologous to the yeast and human Fibrillarin 2'-O-ribose methyltransferase were identified in *A. thaliana*, *AtFib1* (*At5g52470*), *AtFib2* (*At4g2563*0) and *AtFib3* (*At5g52490*) [153]. Both the AtFIB1 and AtFIB2 could partially complement a conditional yeast NOP1/Fibrillarin mutant [154]. Surprisingly, six novels C/D snoRNA co-precipitated with AtFIB2 and don't appear to bind rRNA targets, suggesting that the AtFIB2 might function in other coding and/or non-coding RNA(s) [152]. The altered expression level of C/D box HIDDEN TREASURE 2 (*HID2*) snoRNA results in pleiotropic developmental defects, showing leaf polarity and slow growth in *A. thaliana* [155]. Moreover, depletion of rRNA Ψ is lethal to yeast [156]. Additionally, SUPPRESSOR OF VARIAGATION1 (SVR1, At2g39140), encoding a chloroplast Ψ synthase, is required for proper chloroplast rRNA processing and protein translation [157]. Also, disordered of *SVR1* leads to growth defects and decreased sensitivity to phosphorous starvation in *A. thaliana* [158], [159].

The base methylations are also prevalent in rRNA. The m^5C, being the best-understood base methylation in rRNA, is catalysed by two RNA

methyltransferases, NOP2 and RCM1 [36], [39]. In yeast, NOP2 and RCM1 were demonstrated as a 25S rRNA methyltransferase at positions C2870 and C2278. The presence of m^5C methylated sites is required to synthesise the large subunit of the ribosome and is anisomycin sensitive in the yeast [160]. Sequence alignment shows three paralogs of *NOP2* in the *A. thaliana* genome, *OLI2 (NOP2A)*, *NOP2B* and *NOP2C* [161]. The published data from our laboratory shows there is no difference in the m^5C level at nuclear LSU 25S rRNA C2860 in single mutants of *nop2a, nop2b,* or *nop2c* and wild type [36]. Recently, the reduced m^5C level was observed at 25S rRNA C2860 in nop2a/NOP2B RNAi plants [38]. Interestingly, a homozygous double mutant of *nop2a nop2b* could not be obtained from the segregating population in our previous study and is fully investigated in chapter 2 of my thesis. Besides m^5C, other methylated bases are also enriched in rRNAs. N4-methylcytidine (m^4C) formed by RSMH was found at 16S rRNA C1402 and 12S rRNA C839 in *E. coli* and humans [162], [163]. Also, CMAL (Chloroplast MraW- Like), an ortholog of RSMH in *A. thaliana*, methylates the C1352 in chloroplast 16S rRNA. The depletion of CMAL causes chloroplast function defects, showing abnormal leaf and root development and overall plant morphology [164]. Another base modification, $N^{6,6}$-dimethyladenosine (m_2^6A), is catalysed by dimethyladenosine transferase 1 (DIMT1), and its substrates are A1850 and A1851 in human 18S rRNA are vital for protein synthesis and translation fidelity [165]. Three dimethyladenosine transferase homologs (DIM1A, DIM1B, DIM1C) have been characterised in *A. thaliana*. The point mutation in the *dim1A* mutant leads to the lack of two m_2^6A at the 3′ end of 18S rRNA (A1785 and A1786), exhibiting root epidermal defects, abnormal root meristem division, leaf development, and trichome branching [166]. DIM1B was found in the 18S rRNA of *A. thaliana* mitochondria, and it could substitute the *E. coli* rRNA dimethylase activity of KsgA [167]. Surprisingly, it is reported that the catalytic activity of DIMT1 is not necessary for the rRNA processing [168]. In yeast, the variants had no obvious growth defects when the catalytical function of DIMT1 was inactive [169]. Also, the study referring to human DIMT1 influences 18S rRNA processing indicated that ribosome biogenesis requires the presence of the DIMT1 rather than its RNA-modifying catalytic activity, demonstrating the

functions of m_2^6A is still somewhat elusive [168]. Whether this finding exists in plants is still unknown.

The absence of single modification has no apparent effects on growth or ribosome activity in yeast, while altered multiple modification sites lead to reduced growth rates and translation rate [170]. Therefore, it is not yet clear how different rRNA modification patterns affect ribosome function. Furthermore, the rRNA is modified at various stages during the maturation of ribosomal subunits. Specifically, the 2'-O-methylations and Ψ are extensively installed during the early stages of ribosomal subunit maturation, the base methylation commonly occur a little bit later, while little is known about the precise timing of most of them so far [145]. It will be essential to clarify the precise timing of rRNA modifications to understand better the interaction between different modifications and the complex functions in the organism. This will pave the way for understanding the role of rRNA modifications in regulating translation to adapt the cellular proteome.

1.4. Transfer RNA modifications and functions

Cellular tRNAs are the most heavily modified RNA concerning both number, density and diversity, which contains up to 17% of the cells modified nucleotides (Fig 1.5) [171], [172]. By now, more than 90 chemical modifications have been found on tRNAs, including the most prevalent and abundant methylation modifications, adenosine to inosine (A-I), acetylation of RNA bases, and isomerisation of uridine to Ψ or dihydrouridine (D) [5], [154], [173]. Specifically, the functional roles of these modifications are dependent on their chemical properties and the site on the second cloverleaf structure of the tRNAs [154]. Modifications on the anticodon loop have crucial roles in translation by preventing frameshifting, expanding codon recognition, and strengthening the codon-anticodon interaction. Thus, these bases are indispensable for effective translational control [174]. Position 34 or 37 or both are heavily modified on every tRNA and impact the tRNA-mRNA Watson Crick base-pairing [175].

Furthermore, outside of the anticodon loop, modifications occur in the D-loop, T-loop and variable loop, influencing structural stability, translational efficiency and tRNA recognition [176]. The modified sites, the modification types and the specific enzyme introducing the modification will be discussed below.

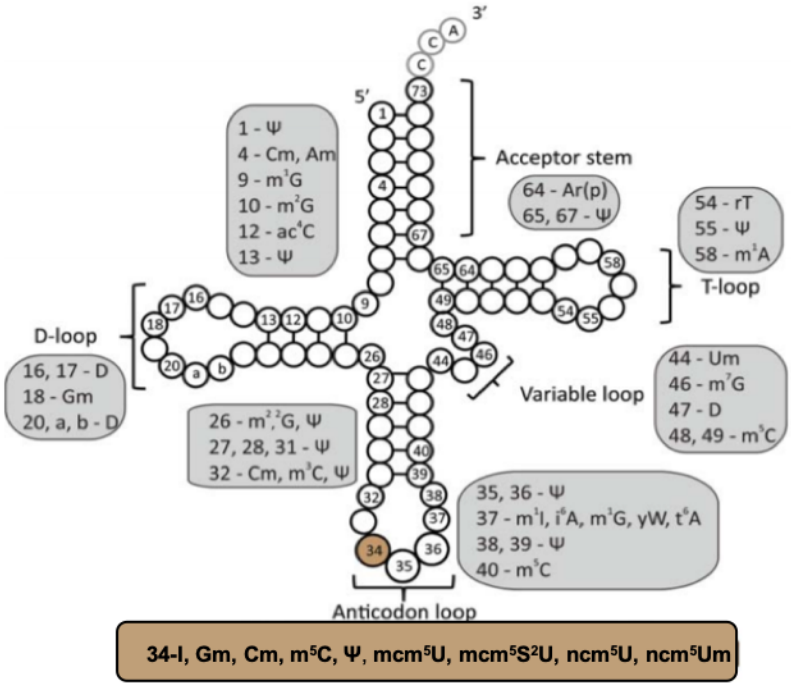

Figure 1.5: Modifications in cytoplasmic tRNAs in *S. cerevisiae*.

Summary of tRNA positions modified on tRNAs. Nucleotides are shown as circles, the residues 34, 35, and 36 in the anticodon are labelled. Figure from [177].

Numerous tRNAs modifications have been discovered in plants, and the fundamental roles of these modifications on plant growth and the response to environmental stress have previously been discussed [178], [179]. In *A. thaliana*, a total of 26 tRNA modifications were mapped through chromatography combined with mass spectroscopy techniques [180], [181]. Among them, the m^1G and m^1I methylation at position 37 on tRNAs are indispensable for vegetative and reproductive growth [182], the m^1A modification at position 58 of tRNA is required for embryo development [183], the high level of m^5C and its corresponding tRNA methyltransferase were necessary for root development [11]. Similarly, loss of 2´-*O*-ribose methylation at positions 32 and 34 of the tRNAs anticodon loop was linked to the immune response to *Pseudomonas syringae* infection [178]. In rice, four kinds of tRNA

modifications, Am, Cm, m^1A and m^7G are important in stress responses, while the Gm, m^5U and m^5C were demonstrated to involve in the plant development [179]. Furthermore, the pattern of tRNA modifications may be dramatically variable during stress conditions and some stress-induced modification sites were found in multiple organisms [184], [185]. For example, the level of 2′-*O*-methyladenosine (Am) increases 10 times during salt stress and ABA treatment in the rice [186]. In *E. coli*, some tRNA 2′-O-methylated positions, particularly several Gm18 sites, are dynamically modulated under starvation and stress conditions [187]. In summary, tRNA modifications not only play a vital role in plant growth but also are involved in plant adaptation to stress conditions by regulating the expression of crucial stress-related proteins [188], [189].

The formation and maintenance of various tRNA modifications are accomplished by the tRNA methyltransferases (TRMs), and these TRMs play an indispensable role in plant growth. m^1A, the most prominent tRNA modification in eukaryotes, is formed by the nuclear localized complex AtTRM61(At5g14600)/AtTRM6(At2g45730) in *A. thaliana* [190]. The knockout of either AtTRM61 or AtTRM6 results in embryo arrest and seed abortion [183]. Strikingly, m^1A is reversible in tRNAs, the ALKBH3 and ALKBH1 catalyse the demethylation of m^1A on the target tRNAs in humans [191], [192]. The m^1G, medication is mainly enriched at the 5′ half of tRNA in all confirmed plants, is added by the TRM5 at position 37. Also, TRM10 in humans and *A. thaliana* are required to modify m^1G in tRNA at position 9 [179], [193]. Interestingly, both in yeast and *A. thaliana,* TRM5 produces not only m^1G, but also the modification m^1I [190], [194]. Dysregulation of AtTRM5 (At3g56120) impedes m^1G and m^1I modifications, causing abnormal translation, disturbed hormone homeostasis, reducing shoot and root biomass and delaying the flowering time [194], [195]. Furthermore, the 2’-O-ribose methyltransferase TRM7 (At5g01230) targeting the anticodon loop is crucial for resistance to *Pseudomonas syringae* in *A. thaliana* [196]. Knockdown mutants *AtTad2* (*At1g48175*) and *AtTad3* (*At5g24670*) exhibit a decreased level of adenosine-to-inosine editing at six nucleus-encoded tRNA species, resulting in arrested embryo development at the globular stage [197]. TRDMT1 methylates three tRNAs at position C38 in animals ($tRNA^{Asp(GTC)}$, $tRNA^{Gly(GCC)}$ and $tRNA^{Val(AAC)}$), however, only one m^5C

at position C38 in $tRNA^{Asp}$ in plants [36], [42] . Another two TRDMT1 dependent tRNAs at position C38 ($tRNA^{Gly(GCC)}$ and $tRNA^{Gly(CCC)}$) were subsequently characterised in plants. Also, TRM4B (At2g22400) methylates tRNA cytosines at positions C48, C49 and C50 in plants. In *A. thaliana* trm4b mutants, show decreased m^5C levels on tRNAs and reduced cell division in the root meristem which leads to shorter primary roots. Both the *trm4b* and *trdmt1 trm4b* are highly sensitive to the antibiotic hygromycin, and this is likely due to altered tRNA structures and hence reduced translation [11], [36].

1.5. tRNA fragments, tRNA-derived sRNAs and functions

Typically, mature tRNAs are 76 to 90 nucleotides in length, forming a secondary cloverleaf structure with a D-loop, a T-loop, an anticodon loop, a variable loop, and an acceptor stem. Over the last decade, high-throughput sequencing demonstrated tRNAs can give rise to sRNAs across all domains of life. These sRNAs are often referred to as tRNA-derived small RNAs (tsRNAs). First assumed to be random tRNA degradation products, it is now clear that tsRNAs are enzymatically cleaved from tRNAs by specific nucleases (Fig 1.6), and accumulation in multiple organisms and tissues is induced by stress conditions [198], [199]. The functional importance of tsRNAs are still mounting. tsRNAs are frequently divided into two sub-classes, tRFs and tRNA halves, based on their relative length and cleavage sites [200].

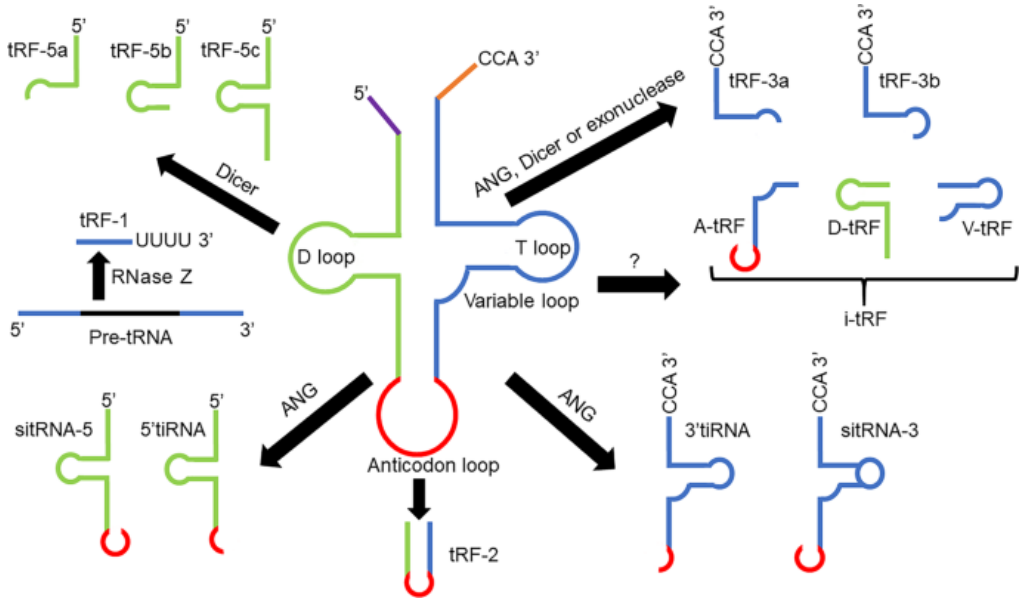

Figure 1.6: Categories of tRNA-derived fragments (tRFs) and tRNA halves (tiRNAs).

tRFs are classified into five subclasses, i-tRF, tRF-1, tRF-2, tRF-3, and tRF-5. i-tRF, tRF-2, tRF-3, and tRF-5 are derived from mature tRNAs digested by Angiogenin (ANG), Dicer, or other RNases at different sites, while tRF-1 is derived from pre-tRNA digested by RNase Z. tiRNAs are divided into two major subtypes, 5′tiRNA and 3′tiRNA, which are derived from mature tRNAs cleaved by ANG at the anticodon ring. Fragments that are longer than tiRNAs are called stress-induced tRNA-5 (sitRNA-5) or sitRNA-3. Figure from [201].

1.5.1. The production of tRFs

One type of tsRNAs are tRNA-derived fragments (tRFs) that are derived from full-length tRNAs cleaved at either the T-loop (tRF-5s) or D-loop (tRF-3s) and are about 19-30 nt in length. The majority of tRFs are derived from cleaved mature tRNAs. Interestingly, tRFs were not only identified from nuclear encoded tRNAs but also from mitochondrial and plastid genomes in plants [202]–[204]. Ribonuclease cleavage of tRNAs to produce the tRFs is mediated by DICER or DICER-like proteins (DCL) or Rnase T2 proteins although DCL involvement is still controversial [205], [206]. For instance, DCL1 was reported to be necessary for the production of specific 19 nt tRF-5s in the pollen of *A. thaliana* [205], but *Arabidopsis* Dicer-like proteins, DCL1-4, do not play a major role in the production of tRFs in another publication [206]. In mammals, tRFs derived from $tRNA^{Gln}$ are DICER-dependent [207], [208] and in *A. thaliana,*

Rnase T2 was shown to be necessary for tRFs production, and did involve DICER-like proteins, DCL1-4 [206]. Additionally, multiple reports in humans show the biogenesis of tRFs requires RNase A protein ANGIOGENIN (ANG) [209], [210]. The multiple ribonucleases required for tRF biogenesis may reflect enzyme-modified tRNA specificity that occurs as a result of heterogeneous tRNA modification patterns across cells and time that are still to be elucidated [211].. In summary, DCL, RNase T2 and RNase A proteins are required for tRF biogenesis however some questions remain to be clarified.

1.5.2. The production of tRNA halves

Another group of tRNA derived sRNAs are tRNA-halves, and these are generated by cleavage at the anticodon loop, forming a corresponding 5'-half or 3'-half tRNA that are about 31-40 nt in length [212]. In lower and higher organisms, the production of tRNA halves is induced by cellular stresses, including oxidative stress, heat shock, phosphate starvation, amino acid starvation, ultraviolent irradiation or virus infection [213]–[215]. In some studies, tRNA halves are also called tRNA-derived stress-induced RNAs [216]. To date, the ribonuclease, Rny1p, required for tRNA cleavage to produce tRNA-halves has only been identified in yeast and mammals. Rny1p, is a member of the RNase T2 family (RNT2) and is conserved amongst eukaryotes [217]. Yeast, *Saccharomyces cerevisiae, rny1Δ* mutants do not cleave tRNAs into t-RNA halves under stress conditions, demonstrating that Rny1p is required to produce tRNA halves [218]. In humans, tRF-5s $tRNA^{Gly(GCC)}$ and tRF-5s $tRNA^{Glu(CTC)}$ were up-regulated in ANGIOGENIN-treated cells [219]. Additionally, it was discovered that DICER also produces the 5'-half $tRNA^{Ala(CGC)}$ under arsenite treatment in mammalian cells [220]. In *A. thaliana*, RNase T2 proteins, namely RNS1, RNS2 and RNS3 are essential endoribonucleases. When the yeast *rny1* strain was complemented by one of the three RNS resulted in the production of tRFs and 5-half from $tRNA^{His(GTG)}$ and $tRNA^{Arg(ACG)}$ *in vitro* and *in vivo*, which also supports the notion that the yeast RNase T2, Rny1p, is able to produce both the tRFs and tRNA halves [206]. As the current investigation of plant RNase T2 only focus on one of the members of plant RNase T2 or is just confirmed in specific one tRNA, the second topic of my

thesis will comprehensively elucidate the cleavage characteristics of plant RNase T2 on multiple tRNAs.

Collectively, DICER, RNS and ANGIOGENIN can produce both tRFs and tRNA halves, which indicates sophisticated processing of tRNAs. It is possible that tRNA halves accumulate first, then further cleaved into shorter tRFs. This question will be answered in Chapter 4 of my thesis.

1.5.3. Distribution of tRFs and tRNA halves

Deep sequencing has led to the characterization of tRFs and tRNA halves in various organisms, especially under stress conditions [221], [222]. In humans, a surprising number of tRF-3s but not tRF-5s accumulate after ANGIOGENIN-mediated cleavage [210]. In yeast, northern blotting showed that tRNA halves increase in abundance when cells are subjected to heat shock, methionine starvation, nitrogen starvation or oxidative starvation [223]. tRFs and tRNA halves populations have also been characterized in various plants, and relative accumulation of individual tRFs or tRNA halves are produced in a developmentally modulated manner and become dominant in tissue-specific [224], [225]. For example, in *A. thaliana*, a 19nt tRF-5s $tRNA^{Gly(TCC)}$, representing over 80% of tRFs and accounting for up to 28% of the total root sRNAs, was observed in the phosphate-starved roots but much less in the shoots. The 5'-half of $tRNA^{His(GTG)}$, $tRNA^{Arg(CCT)}$ and $tRNA^{Trp(CCA)}$ were confirmed through northern blotting in seedlings upon oxidative stress, while the 5'-half $tRNA^{Glu(CTC)}$ was only observed in *A. thaliana* flowers [223]. Alongside, the tRFs ranging from the size of 18 to 25 nt were found in sRNA libraries from leaf, inflorescence and pollen, the 19nt tRFs specifically accumulates to a higher level in the pollen grains, especially the $tRNA^{Ala(AGC)}$ [205]. In rice, tRFs were detected in embryogenic callus in which apart from tRFs-5s $tRNA^{Pro(CGG)}$, the tRFs-5s $tRNA^{Ala(AGC)}$, accounting for 82% of the total tRF reads, is the highest level [226]. Similarly, a 19-nt tRFs-5s $tRNA^{Arg(CCT)}$ enriches at high pattern in seedlings under cold stress, as well in *A. thaliana* under drought stress [227]. In barley, the tRF-5s $tRNA^{Gly(TCC)}$ is the most abundant in shoots under phosphorous-deficient condition, followed by $tRNA^{Arg(CCT)}$ and $tRNA^{Ala(AGC)}$

[228]. Besides the tRFs and tRNA halves, a longer group of tsRNAs were detected in *Giardia lamblia*, which was 46 nt in length and was encystation-induced [229].

Taken together, the reported studies outline that the tRNA halves could be induced by stress, also the abundance shares the character of being tissue-specific. Moreover, the majority of identified tRFs or tRNA halves are from the 5 sides, tRF-3s and 3 halves detection is sparse. Therefore, there is still a long way to elucidate the abundance of tRFs and tRNA halves in multiple species.

1.5.4. The biological functions of tRFs and tRNA halves

The biological functions of tRFs and tRNA halves have gradually been disclosed in recent years (Fig 1.7). Among the functions attributed to tRFs and tRNA halves, the regulation of translation seems to be the most prominent. For instance, a part of tRF-5s $tRNA^{Ala(AGC)}$ from *A. thaliana* was observed in active polyribosomal fractions, suggesting tRFs are translation modulators in land plants [230]. Also, in mammals, the synthetic $tRNA^{Ala}$ repress translation through an eIF4G:RNA interactions, and in this report, the terminal oligo-guanine (TOG) motifs (4–5 guanine residues) at 5′-half $tRNA^{Ala}$ and 5′-half $tRNA^{Cys}$ were the key elements for suppressing translation through interacting with YB-1 and displacing eIF4F [231]. While in *A. thaliana*, the tRNA halves absence of TOG still could impede translation *in vitro* in the wheat germ extracts [232]. Interestingly, translational silencer YB-1 is vital for 5'-half $tRNA^{Ala}$-mediated stress granule formation, while it has no influence on translation repression [233]. Furthermore, some tRFs are proved to have similar miRNA functions. tRF-3s $tRNA^{Leu(CAG)}$ in cancer cells could decrease translation through miRNA-like pathway [201], [234]. Also, in the miRBase database, miR-1274b and miR-1274a have an identical 18 nt with tRF-3s $tRNA^{Lys}$ and tRF-5s $tRNA^{Lys}$, respectively, and there is a positive correlation between the ratio of the miR-1274b:miR-1274a and the known tRF-3s $tRNA^{lys}$:tRF-5s-$tRNA^{lys}$ ratio in the cell [235], [236].

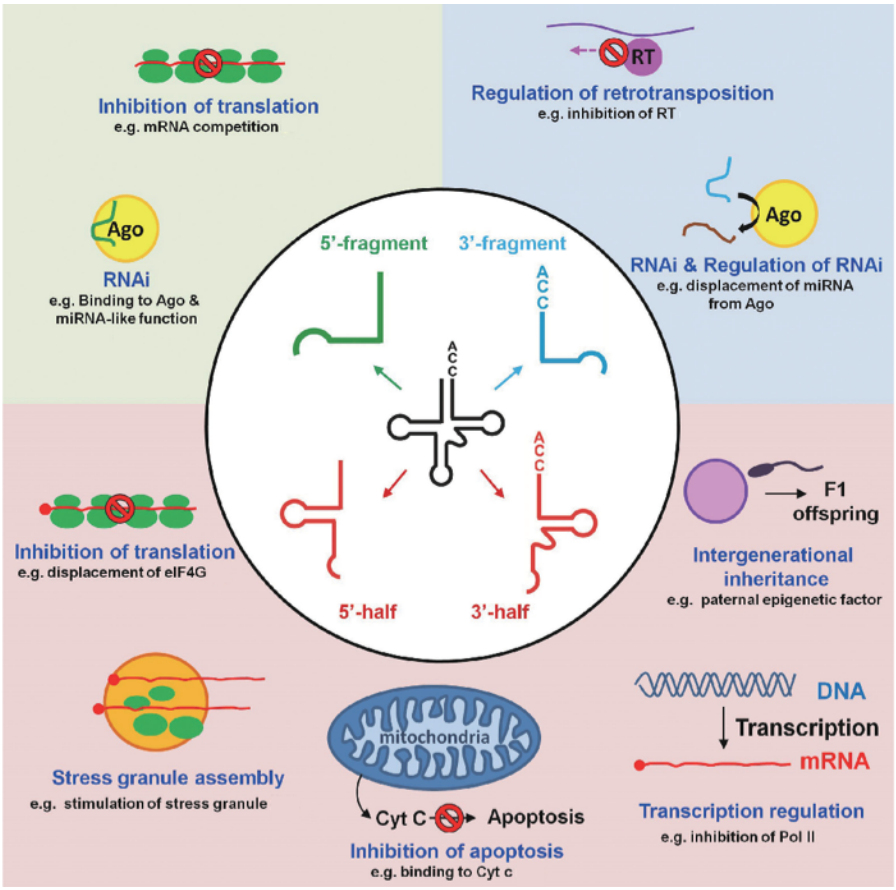

Fig 1.7: The multifaceted regulatory potential of tRNA-derived fragments.

Under certain growth conditions full-length tRNAs (center) can be processed into smaller tRNA-derived RNA fragments (tdRs), such as 5'- and 3'-fragments (green and blue, respectively). Cleavage in the anti-codon loop yields 5'- and 3'-tRNA halves (red). Examples for validated or suspected tdR regulatory functions and/or mechanisms for each tdR class are given in the respective colored section. Figure from [237].

The other regulatory functions of tRFs and tRNA in molecular process halves have been documented in plants and animals. Recently, researchers have reported tRFs and tRNA halves were linked with various diseases, including chronic lymphocytic leukemia (CLL), lung cancer, colon cancer, prostate cancer, breast cancer ovarian cancer, infectious diseases and neurodegenerative diseases [201], [238]. Some tRFs from nuclear have the ability to regulate chromatin structure due to its interaction with ARGONAUTE (AGO) protein [239]. In addition, tRNA halves involve in the cell cycle process and then modulate the cell proliferation, especially tumour cell growth [240]. It was

demonstrated that tiRNAs are able to bind to cytochrome C, and further inhibit apoptosis [241]. Of note, some DCL1-dependent and AGO1-associated tRFs target transposable elements (TEs) and maintain genome stability, specifically retrotransposons [205], [242]. Furthermore, tRFs from rhizobial were confirmed as signal molecules that modulate host nodulation [243].

tRFs and tRNA halves have roles in regulating gene expression through interacting with RNA silencing component ARGONAUTE. Data from deep sequencing libraries of immunoprecipitated ARGONAUTE proteins (AGO-IP) and bioinformatics approaches showed that tRF-5s are mainly present in the AGO1/3/4-IP fractions, for example the most abundant AGO1-associated tRF was tRF-5s $tRNA^{Arg(CCT)}$. In contrast, the tRF-3s were associated with AGO2 in mammals, examples including tRF-3s $tRNA^{Leu(CAG)}$ and tRF-3s $tRNA^{His(GTC)}$. [244]–[247]. Interestingly, the association between AGO and tRFs is regulated by stress, for example AGO1-associated tRF-5s $tRNA^{Gly(TCC)}$ was strongly increased under UV treatment [202]. Moreover, some specific plant tRFs may function in DNA and chromatin modifications as a portion of 24 nt tRFs were assocaited with AGO4 [227]. The target gene of tRFs could be find through prediction based on the tRFs sequences. Transposable elements or long terminal repeats containing have been identified to be the putative tRFs targets in mice, rats, humans, and *A. thaliana* [248]. Although the targets of these AGO-associated tRFs have been predicted, the confirmation still needs to proceed in the future.

1.5.5. Regulation of tRNA cleavage through modifications

A link between RNA modifications and tsRNAs formation is only starting to be elucidated. Until now, tRNA cleavage was only reported to be regulated by m^1A and m^5C abundance in either tRNA methyltransferase or demethylase mutants [249]. ALKBH1, a cytosolic and mitochondrial m^1A demethylase, effects tRNA cleavage in a stress-specific manner [250]. Two m^5C methyltransferases, DNMT2 and NSUN2 protect tRNAs from stress-induced cleavage as mutants

have increased tRNA halve formation [43], [44]. After exposure to either heat shock or oxidative stress, mutant *dnmt2* flies showed increased stress-induced cleavage of tRNAs, and overexpression of *Dnmt2* reduced $tRNA^{Asp(GTC)}$ and $tRNA^{Gly(GCC)}$ tRNA half formation [43]. Also, increased tRNA cleavage catalyzed by ANGIOGENIN occurs in *nsun2* mutant mice, resulting in an enrichment of tRNA halves from the NSUN2 substrate tRNAs ($tRNA^{Asp(GTC)}$, $tRNA^{Gly(GCC)}$ and $tRNA^{Val(AAC)}$) [251]. In *A. thaliana*, decreased $tRNA^{Asp(GTC)}$ stability was observed in *trm4b* mutants however tRNA-hlave abundance was not reported [11]. Together, these findings suggest that methylation protects tRNAs from stress-induced cleavage.

1.6. Conclusion

To date, many covalent chemical modifications were mapped on the epitranscriptome of mRNAs, rRNAs and tRNAs by high-throughput sequencing in various species and cell types. The enzymes regulating these modifications, distribution and regulatory roles have been partially elucidated in plants and animals. However, we are only at the beginning of developing a comprehensive understanding of the epitranscriptome and biological functions for plant growth, development, stress tolerance and plant-pathogen interactions.

1.7. Research aims

RNA m^5C has been implicated to have multiple biological and molecular roles in various organisms, including regulating mRNA translation and plant growth. However, there are still many questions waiting to be answered about RNA m^5C. One of those questions I addressed was understanding the activity and inheritance of rRNA methyltransferase NOP2, as previously *nop2a nop2b* mutants were not obtained from a segregating population. An additional question I addressed was understanding tRNA cleavage under oxidative stress and the role of TRM4B and T2 ribonucleases as previously we observed increased tRNA cleavage in *trm4b* plants. I finally addressed the question of the function of cleaved tRNA halves originated from $tRNA^{Asp(GTC)}$.

The aims of my research are:

(1) To investigate the importance of rRNA methyltransferase NOP2 in gametophyte development,
(2) To investigate the oxidative stress-induced tRNA cleavage regulated by the plant T2 RNases and m^5C, and
(3) To investigate the processing and targets of 5'-half $tRNA^{Asp(GTC)}$.

1.8. References

[1] "DNA Methylation and Epigenetic Inheritance on JSTOR." https://www.jstor.org/stable/2398698 (accessed Aug. 26, 2022).

[2] A. Bird, “Perceptions of epigenetics,” *Nature 2007 447:7143*, vol. 447, no. 7143, pp. 396–398, May 2007, doi: 10.1038/nature05913.

[3] E. E. by Vincenzo Russo and A. D. Riggs, “Epigenetic Mechanisms of Gene Regulation Monograph 32,” 1997, Accessed: Aug. 26, 2022. [Online]. Available: http://www.cshl.org

[4] P. Boccaletto *et al.*, “MODOMICS: A database of RNA modification pathways. 2017 update,” *Nucleic Acids Res*, vol. 46, no. D1, pp. D303–D307, Jan. 2018, doi: 10.1093/nar/gkx1030.

[5] M. A. Machnicka *et al.*, “MODOMICS: A database of RNA modification pathways - 2013 update,” *Nucleic Acids Res*, vol. 41, no. D1, p. D262, Jan. 2013, doi: 10.1093/nar/gks1007.

[6] J. W. Wei, K. Huang, C. Yang, and C. S. Kang, “Non-coding RNAs as regulators in epigenetics (Review),” *Oncol Rep*, vol. 37, no. 1, pp. 3–9, Jan. 2017, doi: 10.3892/or.2016.5236.

[7] H. Covelo-Molares, M. Bartosovic, and S. Vanacova, “RNA methylation in nuclear pre-mRNA processing,” *Wiley Interdisciplinary Reviews: RNA*, vol. 9, no. 6. Blackwell Publishing Ltd, Nov. 01, 2018. doi: 10.1002/wrna.1489.

[8] N. Liu and T. Pan, “N6-methyladenosine-encoded epitranscriptomics,” *Nature Structural and Molecular Biology*, vol. 23, no. 2. Nature Publishing Group, pp. 98–102, Feb. 03, 2016. doi: 10.1038/nsmb.3162.

[9] R. D. HOTCHKISS, “The quantitative separation of purines, pyrimidines, and nucleosides by paper chromatography,” *J Biol Chem*, vol. 175, no. 1, pp. 315–332, Aug. 1948, doi: 10.3891/acta.chem.scand.06-1030.

[10] H. Amos and M. Korn, “5-Methyl cytosine in the RNA of Escherichia coli,” *BBA - Biochimica et Biophysica Acta*, vol. 29, no. 2, pp. 444–445, 1958, doi: 10.1016/0006-3002(58)90214-2.

[11] R. David *et al.*, “Transcriptome-wide mapping of RNA 5-methylcytosine in arabidopsis mRNAs and noncoding RNAs,” *Plant Cell*, vol. 29, no. 3, pp. 445–460, 2017, doi: 10.1105/tpc.16.00751.

[12] M. Schaefer, “RNA 5-Methylcytosine Analysis by Bisulfite Sequencing,” in *Methods in Enzymology*, vol. 560, Academic Press Inc., 2015, pp. 297–329. doi: 10.1016/bs.mie.2015.03.007.

[13] M. Frommer *et al.*, “A genomic sequencing protocol that yields a positive display of 5- methylcytosine residues in individual DNA strands,” *Proc Natl Acad Sci U S A*, vol. 89, no. 5, pp. 1827–1831, 1992, doi: 10.1073/pnas.89.5.1827.

[14] M. Schaefer, “RNA 5-Methylcytosine Analysis by Bisulfite Sequencing,” in *Methods in Enzymology*, vol. 560, Academic Press Inc., 2015, pp. 297–329. doi: 10.1016/bs.mie.2015.03.007.

[15] X. Cui *et al.*, “5-Methylcytosine RNA Methylation in Arabidopsis Thaliana,” *Mol Plant*, vol. 10, no. 11, pp. 1387–1399, Nov. 2017, doi: 10.1016/j.molp.2017.09.013.

[16] K. D. Meyer, Y. Saletore, P. Zumbo, O. Elemento, C. E. Mason, and S. R. Jaffrey, “Comprehensive analysis of mRNA methylation reveals enrichment in 3′ UTRs and near stop codons,” *Cell*, vol. 149, no. 7, pp. 1635–1646, Jun. 2012, doi: 10.1016/j.cell.2012.05.003.

[17] D. Dominissini *et al.*, “Topology of the human and mouse m6A RNA methylomes revealed by m6A-seq,” *Nature*, vol. 485, no. 7397, pp. 201–206, May 2012, doi: 10.1038/nature11112.

[18] L. Meng, Q. Zhang, and X. Huang, “Comprehensive Analysis of 5-Methylcytosine Profiles of Messenger RNA in Human High-Grade Serous Ovarian Cancer by MeRIP Sequencing,” *Cancer Manag Res*, vol. 13, p. 6005, 2021, doi: 10.2147/CMAR.S319312.

[19] L. Yang *et al.*, “m5C Methylation Guides Systemic Transport of Messenger

RNA over Graft Junctions in Plants," *Current Biology*, vol. 29, no. 15, pp. 2465-2476.e5, Aug. 2019, doi: 10.1016/j.cub.2019.06.042.

[20] M. Weber *et al.*, "Chromosome-wide and promoter-specific analyses identify sites of differential DNA methylation in normal and transformed human cells," *Nat Genet*, vol. 37, no. 8, pp. 853–862, Aug. 2005, doi: 10.1038/ng1598.

[21] S. Edelheit, S. Schwartz, M. R. Mumbach, O. Wurtzel, and R. Sorek, "Transcriptome-Wide Mapping of 5-methylcytidine RNA Modifications in Bacteria, Archaea, and Yeast Reveals m5C within Archaeal mRNAs," *PLoS Genet*, vol. 9, no. 6, Jun. 2013, doi: 10.1371/JOURNAL.PGEN.1003602.

[22] V. Khoddami and B. R. Cairns, "Transcriptome-wide target profiling of RNA cytosine methyltransferases using the mechanism-based enrichment procedure Aza-IP," *Nature Protocols 2014 9:2*, vol. 9, no. 2, pp. 337–361, Jan. 2014, doi: 10.1038/nprot.2014.014.

[23] H. George, J. Ule, and S. Hussain, "Illustrating the epitranscriptome at nucleotide resolution using methylation-iCLIP (miCLIP)," *Methods in Molecular Biology*, vol. 1562, pp. 91–106, 2017, doi: 10.1007/978-1-4939-6807-7_7/FIGURES/1.

[24] E. Flatau, F. A. Gonzales, L. A. Michalowsky, and P. A. Jones, "DNA methylation in 5-aza-2'-deoxycytidine-resistant variants of C3H 10T1/2 C18 cells.," *Mol Cell Biol*, vol. 4, no. 10, pp. 2098–2102, Oct. 1984, doi: 10.1128/mcb.4.10.2098.

[25] V. Khoddami and B. R. Cairns, "Identification of direct targets and modified bases of RNA cytosine methyltransferases," *Nat Biotechnol*, vol. 31, no. 5, pp. 458–464, May 2013, doi: 10.1038/nbt.2566.

[26] S. Hussain *et al.*, "NSun2-mediated cytosine-5 methylation of vault noncoding RNA determines its processing into regulatory small RNAs," *Cell Rep*, vol. 4, no. 2, pp. 255–261, Jul. 2013, doi: 10.1016/j.celrep.2013.06.029.

[27] C. Xue, Y. Zhao, and L. Li, “Advances in RNA cytosine-5 methylation: Detection, regulatory mechanisms, biological functions and links to cancer,” *Biomarker Research*, vol. 8, no. 1. BioMed Central Ltd, p. 43, Sep. 14, 2020. doi: 10.1186/s40364-020-00225-0.

[28] O. Begik, J. S. Mattick, and E. M. Novoa, “Exploring the epitranscriptome by native RNA sequencing,” Cold Spring Harbor Laboratory Press.

[29] A. Leger *et al.*, “RNA modifications detection by comparative Nanopore direct RNA sequencing,” *Nat Commun*, vol. 12, no. 1, Dec. 2021, doi: 10.1038/s41467-021-27393-3.

[30] J. S. Abebe, R. Verstraten, and D. P. Depledge, “Nanopore-Based Detection of Viral RNA Modifications,” *mBio*, vol. 13, no. 3. American Society for Microbiology, Jun. 01, 2022. doi: 10.1128/mbio.03702-21.

[31] O. Begik *et al.*, “Quantitative profiling of pseudouridylation dynamics in native RNAs with nanopore sequencing,” *Nat Biotechnol*, vol. 39, no. 10, pp. 1278–1291, Oct. 2021, doi: 10.1038/s41587-021-00915-6.

[32] A. Pavlopoulou and S. Kossida, “Phylogenetic analysis of the eukaryotic RNA (cytosine-5)-methyltransferases,” *Genomics*, vol. 93, no. 4, pp. 350–357, 2009, doi: 10.1016/j.ygeno.2008.12.004.

[33] R. Reid, P. J. Greene, and D. V. Santi, “Exposition of a family of RNA m5C methyltransferases from searching genomic and proteomic sequences,” *Nucleic Acids Res*, vol. 27, no. 15, pp. 3138–3145, Aug. 1999, doi: 10.1093/nar/27.15.3138.

[34] Y. Motorin and H. Grosjean, “Multisite-specific tRNA:m5C-methyltransferase (Trm4) in yeast Saccharomyces cerevisiae: Identification of the gene and substrate specificity of the enzyme,” *RNA*, vol. 5, no. 8, pp. 1105–1118, Aug. 1999, doi: 10.1017/S1355838299982201.

[35] T. Sibbritt, H. R. Patel, and T. Preiss, “Mapping and significance of the

mRNA methylome," *Wiley Interdiscip Rev RNA*, vol. 4, no. 4, pp. 397–422, Jul. 2013, doi: 10.1002/wrna.1166.

[36] A. L. Burgess, R. David, and I. R. Searle, "Conservation of tRNA and rRNA 5-methylcytosine in the kingdom Plantae," *BMC Plant Biol*, vol. 15, no. 1, pp. 1–17, 2015, doi: 10.1186/s12870-015-0580-8.

[37] B. Hong, J. S. Brockenbrough, P. Wu, and J. P. Aris, "Nop2p is required for pre-rRNA processing and 60S ribosome subunit synthesis in yeast.," *Mol Cell Biol*, vol. 17, no. 1, pp. 378–388, Jan. 1997, doi: 10.1128/mcb.17.1.378.

[38] H. Wu *et al.*, "WUSCHEL triggers innate antiviral immunity in plant stem cells," *Science (1979)*, vol. 370, no. 6513, pp. 227–231, Oct. 2020, doi: 10.1126/science.abb7360.

[39] S. Sharma, J. Yang, P. Watzinger, P. Kötter, and K. D. Entian, "Yeast Nop2 and Rcm1 methylate C2870 and C2278 of the 25S rRNA, respectively," *Nucleic Acids Res*, vol. 41, no. 19, pp. 9062–9076, Oct. 2013, doi: 10.1093/nar/gkt679.

[40] M. Okano, S. Xie, and E. Li, "Cloning and characterization of a family of novel mammalian DNA (cytosine-5) methyltransferases [1]," *Nature Genetics*, vol. 19, no. 3. Nat Genet, pp. 219–220, 1998. doi: 10.1038/890.

[41] Y. Motorin and M. Helm, "TRNA stabilization by modified nucleotides," *Biochemistry*, vol. 49, no. 24. Biochemistry, pp. 4934–4944, Jun. 22, 2010. doi: 10.1021/bi100408z.

[42] V. Khoddami and B. R. Cairns, "Identification of direct targets and modified bases of RNA cytosine methyltransferases," *Nat Biotechnol*, vol. 31, no. 5, pp. 458–464, May 2013, doi: 10.1038/nbt.2566.

[43] M. Schaefer *et al.*, "RNA methylation by Dnmt2 protects transfer RNAs against stress-induced cleavage," *Genes Dev*, vol. 24, no. 15, pp. 1590–1595, Aug. 2010, doi: 10.1101/gad.586710.

[44] F. Tuorto *et al.*, “RNA cytosine methylation by Dnmt2 and NSun2 promotes tRNA stability and protein synthesis,” *Nat Struct Mol Biol*, vol. 19, no. 9, pp. 900–905, Sep. 2012, doi: 10.1038/nsmb.2357.

[45] M. G. Goll *et al.*, “Methylation of tRNAAsp by the DNA methyltransferase homolog Dnmt2,” *Science (1979)*, vol. 311, no. 5759, pp. 395–398, Jan. 2006, doi: 10.1126/science.1120976.

[46] X. Cui *et al.*, “5-Methylcytosine RNA Methylation in Arabidopsis Thaliana,” *Mol Plant*, vol. 10, no. 11, pp. 1387–1399, Nov. 2017, doi: 10.1016/j.molp.2017.09.013.

[47] T. Amort *et al.*, “Distinct 5-methylcytosine profiles in poly(A) RNA from mouse embryonic stem cells and brain,” *Genome Biol*, vol. 18, no. 1, Jan. 2017, doi: 10.1186/s13059-016-1139-1.

[48] X. Yang *et al.*, “5-methylcytosine promotes mRNA export-NSUN2 as the methyltransferase and ALYREF as an m 5 C reader,” *Cell Res*, vol. 27, no. 5, pp. 606–625, May 2017, doi: 10.1038/cr.2017.55.

[49] A. Gigova, S. Duggimpudi, T. Pollex, M. Schaefer, and M. Koš, “A cluster of methylations in the domain IV of 25S rRNA is required for ribosome stability,” *RNA*, vol. 20, no. 10, pp. 1632–1644, Oct. 2014, doi: 10.1261/rna.043398.113.

[50] J. E. Squires *et al.*, “Widespread occurrence of 5-methylcytosine in human coding and non-coding RNA,” *Nucleic Acids Res*, vol. 40, no. 11, pp. 5023–5033, 2012, doi: 10.1093/nar/gks144.

[51] L. Trixl and A. Lusser, “The dynamic {RNA} modification 5-methylcytosine and its emerging role as an epitranscriptomic mark.,” *Wiley Interdiscip Rev RNA*, vol. 10, no. 1, p. e1510, Jan. 2019, doi: 10.1002/wrna.1510.

[52] T. P. Hoernes *et al.*, “Nucleotide modifications within bacterial messenger RNAs regulate their translation and are able to rewire the genetic code,” *Nucleic Acids Res*, vol. 44, no. 2, pp. 852–862, Jan. 2016, doi: 10.1093/nar/gkv1182.

[53] N. Khosronezhad, A. Hosseinzadeh Colagar, and S. M. Mortazavi, “The Nsun7 (A11337)-deletion mutation, causes reduction of its protein rate and associated with sperm motility defect in infertile men,” *J Assist Reprod Genet*, vol. 32, no. 5, pp. 807–815, May 2015, doi: 10.1007/s10815-015-0443-0.

[54] S. Blanco and M. Frye, “Role of RNA methyltransferases in tissue renewal and pathology,” *Current Opinion in Cell Biology*, vol. 30, no. 1. Elsevier Ltd, pp. 1–7, 2014. doi: 10.1016/j.ceb.2014.06.006.

[55] A. Chellamuthu and S. G. Gray, “The RNA Methyltransferase NSUN2 and Its Potential Roles in Cancer,” *Cells*, vol. 9, no. 8. NLM (Medline), Jul. 22, 2020. doi: 10.3390/cells9081758.

[56] A. Gigova, S. Duggimpudi, T. Pollex, M. Schaefer, and M. Koš, “A cluster of methylations in the domain IV of 25S rRNA is required for ribosome stability,” *Rna*, vol. 20, no. 10, pp. 1632–1644, 2014, doi: 10.1261/rna.043398.113.

[57] T. Amort *et al.*, “Long non-coding RNAs as targets for cytosine methylation,” *RNA Biol*, vol. 10, no. 6, pp. 1002–1008, 2013, doi: 10.4161/rna.24454.

[58] F. Aguilo *et al.*, “Deposition of 5-Methylcytosine on Enhancer RNAs Enables the Coactivator Function of PGC-1α,” *Cell Rep*, vol. 14, no. 3, pp. 479–492, Jan. 2016, doi: 10.1016/j.celrep.2015.12.043.

[59] S. Hussain *et al.*, “NSun2-mediated cytosine-5 methylation of vault noncoding RNA determines its processing into regulatory small RNAs,” *Cell Rep*, vol. 4, no. 2, pp. 255–261, Jul. 2013, doi: 10.1016/j.celrep.2013.06.029.

[60] B. Moss, A. Gershowitz, J. R. Stringer, L. E. Holland, and E. K. Wagner, “5’-Terminal and internal methylated nucleosides in herpes simplex virus type 1 mRNA.,” *J Virol*, vol. 23, no. 2, pp. 234–239, 1977, doi: 10.1128/jvi.23.2.234-239.1977.

[61] L.-H. Wei *et al.*, “The {m6A} Reader {ECT2} Controls Trichome Morphology by Affecting {mRNA} Stability in Arabidopsis.,” *Plant Cell*, vol. 30, no. 5, pp.

968–985, Apr. 2018, doi: 10.1105/tpc.17.00934.

[62] D. Dominissini *et al.*, “Topology of the human and mouse m6A RNA methylomes revealed by m6A-seq,” *Nature*, vol. 485, no. 7397, pp. 201–206, May 2012, doi: 10.1038/nature11112.

[63] R. C. Desrosiers, K. H. Friderici, and F. M. Rottman, “Characterization of Novikoff Hepatoma Mrna Methylation and Heterogeneity in the Methylated 5′ Terminus,” *Biochemistry*, vol. 14, no. 20, pp. 4367–4374, Oct. 1975, doi: 10.1021/bi00691a004.

[64] J. Hu, S. Manduzio, and H. Kang, “Epitranscriptomic RNA methylation in plant development and abiotic stress responses,” *Frontiers in Plant Science*, vol. 10. Frontiers Media S.A., p. 500, Apr. 16, 2019. doi: 10.3389/fpls.2019.00500.

[65] X. L. Ping *et al.*, “Mammalian WTAP is a regulatory subunit of the RNA N6-methyladenosine methyltransferase,” *Cell Res*, vol. 24, no. 2, pp. 177–189, Feb. 2014, doi: 10.1038/cr.2014.3.

[66] J. Liu *et al.*, “A METTL3-METTL14 complex mediates mammalian nuclear RNA N6-adenosine methylation.,” *Nat Chem Biol*, vol. 10, no. 2, pp. 93–95, 2014, doi: 10.1038/nchembio.1432.

[67] T. Lan *et al.*, “KIAA1429 contributes to liver cancer progression through N6-methyladenosine-dependent post-transcriptional modification of GATA3,” *Mol Cancer*, vol. 18, no. 1, Dec. 2019, doi: 10.1186/s12943-019-1106-z.

[68] A. S. Warda *et al.*, “ Human METTL16 is a N 6 -methyladenosine (m 6 A) methyltransferase that targets pre-mRNAs and various non-coding RNAs ,” *EMBO Rep*, vol. 18, no. 11, pp. 2004–2014, Nov. 2017, doi: 10.15252/embr.201744940.

[69] X. Wang *et al.*, “Structural basis of N6-adenosine methylation by the METTL3-METTL14 complex,” *Nature*, vol. 534, no. 7608, pp. 575–578, 2016,

doi: 10.1038/nature18298.

[70] J. Liu *et al.*, “VIRMA mediates preferential m6A mRNA methylation in 3′UTR and near stop codon and associates with alternative polyadenylation,” *Cell Discov*, vol. 4, no. 1, Dec. 2018, doi: 10.1038/s41421-018-0019-0.

[71] A. S. Warda *et al.*, “ Human METTL16 is a N 6 -methyladenosine (m 6 A) methyltransferase that targets pre-mRNAs and various non-coding RNAs ,” *EMBO Rep*, vol. 18, no. 11, pp. 2004–2014, Nov. 2017, doi: 10.15252/embr.201744940.

[72] H. Ma *et al.*, “N 6-Methyladenosine methyltransferase ZCCHC4 mediates ribosomal RNA methylation,” *Nat Chem Biol*, vol. 15, no. 1, pp. 88–94, Jan. 2019, doi: 10.1038/s41589-018-0184-3.

[73] J. Wen *et al.*, “Zc3h13 Regulates Nuclear RNA m6A Methylation and Mouse Embryonic Stem Cell Self-Renewal,” *Mol Cell*, vol. 69, no. 6, pp. 1028-1038.e6, Mar. 2018, doi: 10.1016/j.molcel.2018.02.015.

[74] K. Růžička *et al.*, “Identification of factors required for m6A mRNA methylation in Arabidopsis reveals a role for the conserved E3 ubiquitin ligase HAKAI,” *New Phytologist*, vol. 215, no. 1, pp. 157–172, Jul. 2017, doi: 10.1111/nph.14586.

[75] G. Zheng *et al.*, “ALKBH5 Is a Mammalian RNA Demethylase that Impacts RNA Metabolism and Mouse Fertility,” *Mol Cell*, vol. 49, no. 1, pp. 18–29, Jan. 2013, doi: 10.1016/j.molcel.2012.10.015.

[76] G. Jia *et al.*, “N6-Methyladenosine in nuclear RNA is a major substrate of the obesity-associated FTO,” *Nat Chem Biol*, vol. 7, no. 12, pp. 885–887, 2011, doi: 10.1038/nchembio.687.

[77] G. Jia *et al.*, “Oxidative demethylation of 3-methylthymine and 3-methyluracil in single-stranded DNA and RNA by mouse and human FTO,” *FEBS Lett*, vol. 582, no. 23–24, pp. 3313–3319, Oct. 2008, doi:

10.1016/j.febslet.2008.08.019.

[78] N. Liu, K. I. Zhou, M. Parisien, Q. Dai, L. Diatchenko, and T. Pan, “N6-methyladenosine alters RNA structure to regulate binding of a low-complexity protein,” *Nucleic Acids Res*, vol. 45, no. 10, pp. 6051–6063, 2017, doi: 10.1093/nar/gkx141.

[79] X. Wang *et al.*, “N 6-methyladenosine-dependent regulation of messenger RNA stability,” *Nature*, vol. 505, no. 7481, pp. 117–120, 2014, doi: 10.1038/nature12730.

[80] C. Tang *et al.*, “ALKBH5-dependent m6A demethylation controls splicing and stability of long 3’-UTR mRNAs in male germ cells,” *Proc Natl Acad Sci U S A*, vol. 115, no. 2, pp. E325–E333, Jan. 2017, doi: 10.1073/pnas.1717794115.

[81] H. Zhu, X. Gan, X. Jiang, S. Diao, H. Wu, and J. Hu, “ALKBH5 inhibited autophagy of epithelial ovarian cancer through miR-7 and BCL-2,” *Journal of Experimental and Clinical Cancer Research*, vol. 38, no. 1, Apr. 2019, doi: 10.1186/s13046-019-1159-2.

[82] Y. Ueda *et al.*, “AlkB homolog 3-mediated tRNA demethylation promotes protein synthesis in cancer cells,” *Sci Rep*, vol. 7, Feb. 2017, doi: 10.1038/srep42271.

[83] D. Mielecki *et al.*, “Novel AlkB dioxygenases-alternative models for in silico and in vivo studies,” *PLoS One*, vol. 7, no. 1, Jan. 2012, doi: 10.1371/journal.pone.0030588.

[84] H. C. Duan *et al.*, “ALKBH10B is an RNA N6-methyladenosine demethylase affecting arabidopsis floral transition,” *Plant Cell*, vol. 29, no. 12, pp. 2995–3011, Dec. 2017, doi: 10.1105/tpc.16.00912.

[85] M. Martínez-Pérez, F. Aparicio, M. P. López-Gresa, J. M. Bellés, J. A. Sánchez-Navarro, and V. Pallás, “Arabidopsis m6A demethylase activity modulates viral infection of a plant virus and the m6A abundance in its genomic

RNAs," *Proc Natl Acad Sci U S A*, vol. 114, no. 40, pp. 10755–10760, Oct. 2017, doi: 10.1073/pnas.1703139114.

[86] C. Xu *et al.*, "Structural basis for selective binding of m6A RNA by the YTHDC1 YTH domain," *Nat Chem Biol*, vol. 10, no. 11, pp. 927–929, Nov. 2014, doi: 10.1038/nchembio.1654.

[87] X. Wang *et al.*, "N 6-methyladenosine-dependent regulation of messenger RNA stability," *Nature*, vol. 505, no. 7481, pp. 117–120, 2014, doi: 10.1038/nature12730.

[88] H. Du *et al.*, "YTHDF2 destabilizes m 6 A-containing RNA through direct recruitment of the CCR4-NOT deadenylase complex," *Nat Commun*, vol. 7, Aug. 2016, doi: 10.1038/ncomms12626.

[89] X. Wang *et al.*, "N6-methyladenosine modulates messenger RNA translation efficiency," *Cell*, vol. 161, no. 6, pp. 1388–1399, Jun. 2015, doi: 10.1016/j.cell.2015.05.014.

[90] H. Shi *et al.*, "YTHDF3 facilitates translation and decay of N 6-methyladenosine-modified RNA," *Cell Res*, vol. 27, no. 3, pp. 315–328, Mar. 2017, doi: 10.1038/cr.2017.15.

[91] I. A. Roundtree *et al.*, "YTHDC1 mediates nuclear export of N6-methyladenosine methylated mRNAs," *Elife*, vol. 6, Oct. 2017, doi: 10.7554/eLife.31311.

[92] P. J. Hsu *et al.*, "Ythdc2 is an N6 -methyladenosine binding protein that regulates mammalian spermatogenesis," *Cell Res*, vol. 27, no. 9, pp. 1115–1127, Sep. 2017, doi: 10.1038/cr.2017.99.

[93] N. Liu, K. I. Zhou, M. Parisien, Q. Dai, L. Diatchenko, and T. Pan, "N6-methyladenosine alters RNA structure to regulate binding of a low-complexity protein," *Nucleic Acids Res*, vol. 45, no. 10, pp. 6051–6063, 2017, doi: 10.1093/nar/gkx141.

[94] H. Huang *et al.*, “Recognition of RNA N 6 -methyladenosine by IGF2BP proteins enhances mRNA stability and translation,” *Nat Cell Biol*, vol. 20, no. 3, pp. 285–295, Mar. 2018, doi: 10.1038/s41556-018-0045-z.

[95] K. D. Meyer *et al.*, “5′ UTR m6A Promotes Cap-Independent Translation,” *Cell*, vol. 163, no. 4, pp. 999–1010, Nov. 2015, doi: 10.1016/j.cell.2015.10.012.

[96] L. H. Wei *et al.*, “The m6A reader ECT2 controls trichome morphology by affecting mRNA stability in arabidopsis,” *Plant Cell*, vol. 30, no. 5, pp. 968–985, May 2018, doi: 10.1105/tpc.17.00934.

[97] J. Scutenaire *et al.*, “The YTH domain protein ECT2 is an m6A reader required for normal trichome branching in arabidopsis,” *Plant Cell*, vol. 30, no. 5, pp. 986–1005, May 2018, doi: 10.1105/tpc.17.00854.

[98] L. Arribas-Hernández, S. Bressendorff, M. H. Hansen, C. Poulsen, S. Erdmann, and P. Brodersen, “An m6A-YTH module controls developmental timing and morphogenesis in arabidopsis,” *Plant Cell*, vol. 30, no. 5, pp. 952–967, May 2018, doi: 10.1105/tpc.17.00833.

[99] L. Arribas-Hernández *et al.*, “Recurrent requirement for the m6A-ECT2/ECT3/ECT4 axis in the control of cell proliferation during plant organogenesis,” *Development (Cambridge)*, vol. 147, no. 14, Jul. 2020, doi: 10.1242/dev.189134.

[100] Y. Yue *et al.*, “VIRMA mediates preferential m6A mRNA methylation in 3′UTR and near stop codon and associates with alternative polyadenylation,” *Cell Discov*, vol. 4, no. 1, p. 10, Dec. 2018, doi: 10.1038/s41421-018-0019-0.

[101] X. Zhao *et al.*, “FTO-dependent demethylation of N6-methyladenosine regulates mRNA splicing and is required for adipogenesis,” *Cell Res*, vol. 24, no. 12, pp. 1403–1419, Dec. 2014, doi: 10.1038/cr.2014.151.

[102] X. Wang *et al.*, “N 6-methyladenosine-dependent regulation of messenger RNA stability,” *Nature*, vol. 505, no. 7481, pp. 117–120, 2014, doi:

10.1038/nature12730.

[103] B. M. Edens *et al.*, “FMRP Modulates Neural Differentiation through m6A-Dependent mRNA Nuclear Export,” *Cell Rep*, vol. 28, no. 4, pp. 845-854.e5, Jul. 2019, doi: 10.1016/j.celrep.2019.06.072.

[104] H. Zhu, X. Gan, X. Jiang, S. Diao, H. Wu, and J. Hu, “ALKBH5 inhibited autophagy of epithelial ovarian cancer through miR-7 and BCL-2,” *Journal of Experimental and Clinical Cancer Research*, vol. 38, no. 1, Apr. 2019, doi: 10.1186/s13046-019-1159-2.

[105] X. Wang *et al.*, “FTO is required for myogenesis by positively regulating mTOR-PGC-1α pathway-mediated mitochondria biogenesis,” *Cell Death Dis*, vol. 8, no. 3, 2017, doi: 10.1038/cddis.2017.122.

[106] S. Lin, J. Choe, P. Du, R. Triboulet, and R. I. Gregory, “The m6A Methyltransferase METTL3 Promotes Translation in Human Cancer Cells,” *Mol Cell*, vol. 62, no. 3, pp. 335–345, May 2016, doi: 10.1016/j.molcel.2016.03.021.

[107] H. Huang, H. Weng, and J. Chen, “The Biogenesis and Precise Control of RNA m6A Methylation,” *Trends in Genetics*, vol. 36, no. 1. Elsevier Ltd, pp. 44–52, Jan. 01, 2020. doi: 10.1016/j.tig.2019.10.011.

[108] S. Zhong *et al.*, “MTA is an Arabidopsis messenger RNA adenosine methylase and interacts with a homolog of a sex-specific splicing factor,” *Plant Cell*, vol. 20, no. 5, pp. 1278–1288, May 2008, doi: 10.1105/tpc.108.058883.

[109] L. Shen *et al.*, “N6-Methyladenosine RNA Modification Regulates Shoot Stem Cell Fate in Arabidopsis,” *Dev Cell*, vol. 38, no. 2, pp. 186–200, Jul. 2016, doi: 10.1016/j.devcel.2016.06.008.

[110] H. C. Duan *et al.*, “ALKBH10B is an RNA N6-methyladenosine demethylase affecting arabidopsis floral transition,” *Plant Cell*, vol. 29, no. 12, pp. 2995–3011, Dec. 2017, doi: 10.1105/tpc.16.00912.

[111] M. Martínez-Pérez, F. Aparicio, M. P. López-Gresa, J. M. Bellés, J. A. Sánchez-Navarro, and V. Pallás, “Arabidopsis m6A demethylase activity modulates viral infection of a plant virus and the m6A abundance in its genomic RNAs,” *Proc Natl Acad Sci U S A*, vol. 114, no. 40, pp. 10755–10760, Oct. 2017, doi: 10.1073/pnas.1703139114.

[112] M. Charette and M. W. Gray, “Pseudouridine in RNA: What, where, how, and why,” *IUBMB Life*, vol. 49, no. 5. Taylor and Francis Inc., pp. 341–351, 2000. doi: 10.1080/152165400410182.

[113] X. Li *et al.*, “Chemical pulldown reveals dynamic pseudouridylation of the mammalian transcriptome,” *Nat Chem Biol*, vol. 11, no. 8, pp. 592–597, Aug. 2015, doi: 10.1038/nchembio.1836.

[114] H. Adachi, M. D. De Zoysa, and Y. T. Yu, “Post-transcriptional pseudouridylation in mRNA as well as in some major types of noncoding RNAs,” *Biochimica et Biophysica Acta - Gene Regulatory Mechanisms*, vol. 1862, no. 3. Elsevier B.V., pp. 230–239, Mar. 01, 2019. doi: 10.1016/j.bbagrm.2018.11.002.

[115] T. M. Carlile, M. F. Rojas-Duran, B. Zinshteyn, H. Shin, K. M. Bartoli, and W. V. Gilbert, “Pseudouridine profiling reveals regulated mRNA pseudouridylation in yeast and human cells,” *Nature*, vol. 515, no. 7525, pp. 143–146, Nov. 2014, doi: 10.1038/nature13802.

[116] S. H. Boo and Y. K. Kim, “The emerging role of RNA modifications in the regulation of mRNA stability,” *Experimental and Molecular Medicine*, vol. 52, no. 3. Springer Nature, pp. 400–408, Mar. 01, 2020. doi: 10.1038/s12276-020-0407-z.

[117] S. Schwartz *et al.*, “Transcriptome-wide mapping reveals widespread dynamic-regulated pseudouridylation of ncRNA and mRNA,” *Cell*, vol. 159, no. 1, pp. 148–162, Sep. 2014, doi: 10.1016/j.cell.2014.08.028.

[118] M. A. Nakamoto, A. F. Lovejoy, A. M. Cygan, and J. C. Boothroyd, “MRNA pseudouridylation affects RNA metabolism in the parasite Toxoplasma gondii,” *RNA*, vol. 23, no. 12, pp. 1834–1849, Dec. 2017, doi: 10.1261/rna.062794.117.

[119] W. A. Decatur and M. J. Fournier, “rRNA modifications and ribosome function,” *Trends in Biochemical Sciences*, vol. 27, no. 7. Trends Biochem Sci, pp. 344–351, Jul. 01, 2002. doi: 10.1016/S0968-0004(02)02109-6.

[120] T. H. King, B. Liu, R. R. McCully, and M. J. Fournier, “Ribosome structure and activity are altered in cells lacking snoRNPs that form pseudouridines in the peptidyl transferase center,” *Mol Cell*, vol. 11, no. 2, pp. 425–435, Feb. 2003, doi: 10.1016/S1097-2765(03)00040-6.

[121] X. hai Liang, Q. Liu, and M. J. Fournier, “rRNA Modifications in an Intersubunit Bridge of the Ribosome Strongly Affect Both Ribosome Biogenesis and Activity,” *Mol Cell*, vol. 28, no. 6, pp. 965–977, Dec. 2007, doi: 10.1016/j.molcel.2007.10.012.

[122] F. Lecointe, O. Namy, I. Hatin, G. Simos, J. P. Rousset, and H. Grosjean, “Lack of Pseudouridine 38/39 in the anticodon arm of yeast cytoplasmic tRNA decreases in vivo recoding efficiency,” *Journal of Biological Chemistry*, vol. 277, no. 34, pp. 30445–30453, Aug. 2002, doi: 10.1074/jbc.M203456200.

[123] L. Fu *et al.*, “Tet-mediated formation of 5-hydroxymethylcytosine in RNA,” *J Am Chem Soc*, vol. 136, no. 33, pp. 11582–11585, Aug. 2014, doi: 10.1021/ja505305z.

[124] I. A. Roundtree, M. E. Evans, T. Pan, and C. He, “Dynamic RNA Modifications in Gene Expression Regulation,” *Cell*, vol. 169, no. 7. Cell Press, pp. 1187–1200, Jun. 15, 2017. doi: 10.1016/j.cell.2017.05.045.

[125] B. Delatte *et al.*, “Transcriptome-wide distribution and function of RNA hydroxymethylcytosine,” *Science (1979)*, vol. 351, no. 6270, pp. 282–285, Jan. 2016, doi: 10.1126/science.aac5253.

[126] P. J. McCown *et al.*, “Naturally occurring modified ribonucleosides,” *Wiley Interdisciplinary Reviews: RNA*, vol. 11, no. 5. Blackwell Publishing Ltd, p. e1595, Sep. 01, 2020. doi: 10.1002/wrna.1595.

[127] M. Tajaddod, M. F. Jantsch, and K. Licht, “The dynamic epitranscriptome: A to I editing modulates genetic information,” *Chromosoma*, vol. 125, no. 1. Springer Science and Business Media Deutschland GmbH, pp. 51–63, Mar. 01, 2016. doi: 10.1007/s00412-015-0526-9.

[128] L. F. Grice and B. M. Degnan, “The origin of the ADAR gene family and animal RNA editing,” *BMC Evol Biol*, vol. 15, no. 1, 2015, doi: 10.1186/s12862-015-0279-3.

[129] C. X. Chen, D. S. C. Cho, Q. Wang, F. Lai, K. C. Carter, and K. Nishikura, “A third member of the RNA-specific adenosine deaminase gene family, ADAR3, contains both single- and double-stranded RNA binding domains,” *RNA*, vol. 6, no. 5, pp. 755–767, May 2000, doi: 10.1017/S1355838200000170.

[130] J. E. Heraud-Farlow and C. R. Walkley, “What do editors do? Understanding the physiological functions of A-to-I RNA editing by adenosine deaminase acting on RNAs,” *Open Biol*, vol. 10, no. 7, p. 200085, Jul. 2020, doi: 10.1098/rsob.200085.

[131] E. Picardi, C. Manzari, F. Mastropasqua, I. Aiello, A. M. D’Erchia, and G. Pesole, “Profiling RNA editing in human tissues: Towards the inosinome Atlas,” *Sci Rep*, vol. 5, Oct. 2015, doi: 10.1038/srep14941.

[132] G. Nigita, D. Veneziano, and A. Ferro, “A-to-I RNA editing: Current knowledge sources and computational approaches with special emphasis on non-coding RNA molecules,” *Frontiers in Bioengineering and Biotechnology*, vol. 3, no. MAR. Frontiers Media S.A., 2015. doi: 10.3389/fbioe.2015.00037.

[133] Y. Notsu *et al.*, “The complete sequence of the rice (Oryza sativa L.) mitochondrial genome: Frequent DNA sequence acquisition and loss during the

evolution of flowering plants," *Molecular Genetics and Genomics*, vol. 268, no. 4, pp. 434–445, 2002, doi: 10.1007/s00438-002-0767-1.

[134] J. M. Gott and R. B. Emeson, "Functions and mechanisms of RNA editing," *Annual Review of Genetics*, vol. 34. Annu Rev Genet, pp. 499–531, Jan. 01, 2000. doi: 10.1146/annurev.genet.34.1.499.

[135] I. Anreiter, Q. Mir, J. T. Simpson, S. C. Janga, and M. Soller, "New Twists in Detecting mRNA Modification Dynamics," *Trends in Biotechnology*, vol. 39, no. 1. Elsevier Ltd, pp. 72–89, Jan. 01, 2021. doi: 10.1016/j.tibtech.2020.06.002.

[136] S. J. Anderson *et al.*, "N6-Methyladenosine Inhibits Local Ribonucleolytic Cleavage to Stabilize mRNAs in Arabidopsis," *Cell Rep*, vol. 25, no. 5, pp. 1146-1157.e3, Oct. 2018, doi: 10.1016/j.celrep.2018.10.020.

[137] Y. Li, X. Wang, C. Li, S. Hu, J. Yu, and S. Song, "Transcriptome-wide N6-methyladenosine profiling of rice callus and leaf reveals the presence of tissue-specific competitors involved in selective mRNA modification," *RNA Biol*, vol. 11, no. 9, pp. 1180–1188, Sep. 2014, doi: 10.4161/rna.36281.

[138] L. Zhou, S. Tian, and G. Qin, "RNA methylomes reveal the m6A-mediated regulation of DNA demethylase gene SlDML2 in tomato fruit ripening," *Genome Biol*, vol. 20, no. 1, Aug. 2019, doi: 10.1186/s13059-019-1771-7.

[139] X. Cui *et al.*, "5-Methylcytosine RNA Methylation in Arabidopsis Thaliana," *Mol Plant*, vol. 10, no. 11, pp. 1387–1399, Nov. 2017, doi: 10.1016/j.molp.2017.09.013.

[140] Y. Zhou *et al.*, "Telobox motifs recruit {CLF}/{SWN}-{PRC2} for {H3K27me3} deposition via {TRB} factors in Arabidopsis.," *Nat Genet*, vol. 50, no. 5, pp. 638–644, May 2018, doi: 10.1038/s41588-018-0109-9.

[141] H.-C. Duan *et al.*, "{ALKBH10B} Is an {RNA} N6-Methyladenosine Demethylase Affecting Arabidopsis Floral Transition.," *Plant Cell*, vol. 29, no. 12, pp. 2995–3011, Dec. 2017, doi: 10.1105/tpc.16.00912.

[142] F. Zhang *et al.*, “The subunit of RNA n6-methyladenosine methyltransferase OsFIP regulates early degeneration of microspores in rice,” *PLoS Genet*, vol. 15, no. 5, May 2019, doi: 10.1371/journal.pgen.1008120.

[143] X. Yang *et al.*, “5-methylcytosine promotes mRNA export-NSUN2 as the methyltransferase and ALYREF as an m 5 C reader,” *Cell Res*, vol. 27, no. 5, pp. 606–625, May 2017, doi: 10.1038/cr.2017.55.

[144] L. Shen, Z. Liang, C. E. Wong, and H. Yu, “Messenger RNA Modifications in Plants,” *Trends in Plant Science*, vol. 24, no. 4. Elsevier Ltd, pp. 328–341, Apr. 01, 2019. doi: 10.1016/j.tplants.2019.01.005.

[145] K. E. Sloan, A. S. Warda, S. Sharma, K. D. Entian, D. L. J. Lafontaine, and M. T. Bohnsack, “Tuning the ribosome: The influence of rRNA modification on eukaryotic ribosome biogenesis and function,” *RNA Biology*, vol. 14, no. 9. Taylor and Francis Inc., pp. 1138–1152, Sep. 02, 2017. doi: 10.1080/15476286.2016.1259781.

[146] N. J. Watkins and M. T. Bohnsack, “The box C/D and H/ACA snoRNPs: key players in the modification, processing and the dynamic folding of ribosomal RNA,” *Wiley Interdiscip Rev RNA*, vol. 3, no. 3, pp. 397–414, May 2012, doi: 10.1002/wrna.117.

[147] S. Sharma and D. L. J. Lafontaine, “‘View From A Bridge’: A New Perspective on Eukaryotic rRNA Base Modification,” *Trends in Biochemical Sciences*, vol. 40, no. 10. Elsevier Ltd, pp. 560–575, Oct. 01, 2015. doi: 10.1016/j.tibs.2015.07.008.

[148] N. D. Venezia, A. Vincent, V. Marcel, F. Catez, and J. J. Diaz, “Emerging role of eukaryote ribosomes in translational control,” *International Journal of Molecular Sciences*, vol. 20, no. 5. MDPI AG, p. 1226, Mar. 01, 2019. doi: 10.3390/ijms20051226.

[149] J. Ge and Y. T. Yu, “RNA pseudouridylation: New insights into an old

modification," *Trends in Biochemical Sciences*, vol. 38, no. 4. Trends Biochem Sci, pp. 210–218, Apr. 2013. doi: 10.1016/j.tibs.2013.01.002.

[150] M. Penzo and L. Montanaro, "Turning uridines around: Role of rRNA pseudouridylation in ribosome biogenesis and ribosomal function," *Biomolecules*, vol. 8, no. 2. MDPI AG, Jun. 05, 2018. doi: 10.3390/biom8020038.

[151] P. Lo Monaco, V. Marcel, J. J. Diaz, and F. Catez, "2′-O-methylation of ribosomal RNA: Towards an epitranscriptomic control of translation?," *Biomolecules*, vol. 8, no. 4. MDPI AG, Dec. 01, 2018. doi: 10.3390/biom8040106.

[152] J. Azevedo-Favory *et al.*, "Mapping rRNA 2'-O-methylations and identification of C/D snoRNAs in Arabidopsis thaliana plants," *RNA Biol*, pp. 1–18, Feb. 2021, doi: 10.1080/15476286.2020.1869892.

[153] F. Barneche, F. Steinmetz, and M. Echeverria, "Fibrillarin genes encode both a conserved nucleolar protien and a novel small nucleolar RNA involved in ribosomal RNA methylation in Arabidopsis thaliana," *Journal of Biological Chemistry*, vol. 275, no. 35, pp. 27212–27220, Sep. 2000, doi: 10.1074/jbc.M002996200.

[154] A. Burgess, R. David, and I. R. Searle, "Deciphering the epitranscriptome: A green perspective," *Journal of Integrative Plant Biology*, vol. 58, no. 10. Blackwell Publishing Ltd, pp. 822–835, Oct. 01, 2016. doi: 10.1111/jipb.12483.

[155] P. Zhu *et al.*, "Arabidopsis small nucleolar RNA monitors the efficient pre-rRNA processing during ribosome biogenesis," *Proc Natl Acad Sci U S A*, vol. 113, no. 42, pp. 11967–11972, Oct. 2016, doi: 10.1073/pnas.1614852113.

[156] I. Lermontova, V. Schubert, F. Börnke, J. Macas, and I. Schubert, "Arabidopsis CBF5 interacts with the H/ACA snoRNP assembly factor NAF1," *Plant Mol Biol*, vol. 65, no. 5, pp. 615–626, Nov. 2007, doi: 10.1007/s11103-

007-9226-z.

[157] F. Yu, X. Liu, M. Alsheikh, S. Park, and S. Rodermel, “Mutations in suppressor of variegation1, a factor required for normal chloroplast translation, suppress var2-mediated leaf variegation in Arabidopsis,” *Plant Cell*, vol. 20, no. 7, pp. 1786–1804, Jul. 2008, doi: 10.1105/tpc.107.054965.

[158] L. Sun *et al.*, “Transcriptome-wide analysis of pseudouridylation of mRNA and non-coding RNAs in Arabidopsis,” *J Exp Bot*, vol. 70, no. 19, pp. 5089–5600, Oct. 2019, doi: 10.1093/jxb/erz273.

[159] S. Lu, C. Li, Y. Zhang, Z. Zheng, and D. Liu, “Functional disruption of a chloroplast pseudouridine synthase desensitizes arabidopsis plants to phosphate starvation,” *Front Plant Sci*, vol. 8, Aug. 2017, doi: 10.3389/fpls.2017.01421.

[160] S. Sharma, J. Yang, P. Watzinger, P. Kötter, and K. D. Entian, “Yeast Nop2 and Rcm1 methylate C2870 and C2278 of the 25S rRNA, respectively,” *Nucleic Acids Res*, vol. 41, no. 19, pp. 9062–9076, 2013, doi: 10.1093/nar/gkt679.

[161] P. Chen, G. Jäger, and B. Zheng, “Transfer RNA modifications and genes for modifying enzymes in Arabidopsis thaliana,” *BMC Plant Biol*, vol. 10, pp. 1–19, 2010, doi: 10.1186/1471-2229-10-201.

[162] S. Kimura and T. Suzuki, “Fine-tuning of the ribosomal decoding center by conserved methyl-modifications in the Escherichia coli 16S rRNA,” *Nucleic Acids Res*, vol. 38, no. 4, pp. 1341–1352, Dec. 2009, doi: 10.1093/nar/gkp1073.

[163] H. Chen *et al.*, “ARTICLE the human mitochondrial 12S rRNA m4C methyltransferase METTL15 is required for mitochondrial function,” *Journal of Biological Chemistry*, vol. 295, no. 25, pp. 8505–8513, Jun. 2020, doi: 10.1074/jbc.ra119.012127.

[164] M. Zou *et al.*, “The critical function of the plastid rRNA methyltransferase,

CMAL, in ribosome biogenesis and plant development," *Nucleic Acids Res*, vol. 48, no. 6, pp. 3195–3210, Apr. 2020, doi: 10.1093/nar/gkaa129.

[165] H. Shen, J. Stoute, and K. F. Liu, "Structural and catalytic roles of the human 18S rRNA methyltransferases DIMT1 in ribosome assembly and translation," *Journal of Biological Chemistry*, vol. 295, no. 34, pp. 12058–12070, Aug. 2020, doi: 10.1074/jbc.ra120.014236.

[166] Y. Wieckowski and J. Schiefelbein, "Nuclear ribosome biogenesis mediated by the DIM1A rRNA dimethylase is required for organized root growth and epidermal patterning in Arabidopsis," *Plant Cell*, vol. 24, no. 7, pp. 2839–2856, Jul. 2012, doi: 10.1105/tpc.112.101022.

[167] U. Richter, K. Kühn, S. Okada, A. Brennicke, A. Weihe, and T. Börner, "A mitochondrial rRNA dimethyladenosine methyltransferase in Arabidopsis," *Plant Journal*, vol. 61, no. 4, pp. 558–569, Feb. 2010, doi: 10.1111/j.1365-313X.2009.04079.x.

[168] C. Zorbas, E. Nicolas, L. Wacheul, E. Huvelle, V. Heurgué-Hamard, and D. L. J. Lafontaine, "The human 18S rRNA base methyltransferases DIMT1L and WBSCR22-TRMT112 but not rRNA modification are required for ribosome biogenesis," *Mol Biol Cell*, vol. 26, no. 11, pp. 2080–2095, Jun. 2015, doi: 10.1091/mbc.E15-02-0073.

[169] J. G. Tokuhisa, P. Vijayan, K. A. Feldmann, and J. A. Browse, "Chloroplast development at low temperatures requires a homolog of DIM1, a yeast gene encoding the 18S rRNA dimethylase," *Plant Cell*, vol. 10, no. 5, pp. 699–711, May 1998, doi: 10.1105/tpc.10.5.699.

[170] X. H. Liang, Q. Liu, and M. J. Fournier, "Loss of rRNA modifications in the decoding center of the ribosome impairs translation and strongly delays pre-rRNA processing," *RNA*, vol. 15, no. 9, pp. 1716–1728, Sep. 2009, doi: 10.1261/rna.1724409.

[171] S. Kirchner and Z. Ignatova, “Emerging roles of tRNA in adaptive translation, signalling dynamics and disease,” *Nature Reviews Genetics*, vol. 16, no. 2. Nature Publishing Group, pp. 98–112, Jan. 01, 2015. doi: 10.1038/nrg3861.

[172] J. E. Jackman and J. D. Alfonzo, “Transfer RNA modifications: Nature’s combinatorial chemistry playground,” *Wiley Interdisciplinary Reviews: RNA*, vol. 4, no. 1. Wiley Interdiscip Rev RNA, pp. 35–48, Jan. 2013. doi: 10.1002/wrna.1144.

[173] H. Hori, “Methylated nucleosides in tRNA and tRNA methyltransferases,” *Frontiers in Genetics*, vol. 5, no. MAY. Frontiers Research Foundation, 2014. doi: 10.3389/fgene.2014.00144.

[174] Y. Nakai *et al.*, “tRNA Wobble Modification Affects Leaf Cell Development in Arabidopsis thaliana,” *Plant Cell Physiol*, vol. 60, no. 9, pp. 2026–2039, Sep. 2019, doi: 10.1093/pcp/pcz064.

[175] P. F. Agris, “Bringing order to translation: The contributions of transfer RNA anticodon-domain modifications,” *EMBO Rep*, vol. 9, no. 7, pp. 629–635, Jul. 2008, doi: 10.1038/embor.2008.104.

[176] E. M. Phizicky and J. D. Alfonzo, “Do all modifications benefit all tRNAs?,” *FEBS Letters*, vol. 584, no. 2. FEBS Lett, pp. 265–271, Jan. 21, 2010. doi: 10.1016/j.febslet.2009.11.049.

[177] N. Ranjan and M. V. Rodnina, “TRNA wobble modifications and protein homeostasis,” *Translation*, vol. 4, no. 1, Jan. 2016, doi: 10.1080/21690731.2016.1143076.

[178] V. Ramírez *et al.*, “Loss of a Conserved tRNA Anticodon Modification Perturbs Plant Immunity,” *PLoS Genetics*, vol. 11, no. 10. Public Library of Science, 2015. doi: 10.1371/journal.pgen.1005586.

[179] Y. Wang *et al.*, “Identification of tRNA nucleoside modification genes

critical for stress response and development in rice and Arabidopsis," *BMC Plant Biol*, vol. 17, no. 1, p. 261, Dec. 2017, doi: 10.1186/s12870-017-1206-0.

[180] P. Chen, G. Jäger, and B. Zheng, "Transfer RNA modifications and genes for modifying enzymes in Arabidopsis thaliana," *BMC Plant Biol*, vol. 10, p. 201, Sep. 2010, doi: 10.1186/1471-2229-10-201.

[181] A. Hienzsch, C. Deiml, V. Reiter, and T. Carell, "Total synthesis of the hypermodified RNA bases wybutosine and hydroxywybutosine and their quantification together with other modified RNA bases in plant materials," *Chemistry - A European Journal*, vol. 19, no. 13, pp. 4244–4248, Mar. 2013, doi: 10.1002/chem.201204209.

[182] X. Jin *et al.*, "AtTrm5a catalyses 1-methylguanosine and 1-methylinosine formation on tRNAs and is important for vegetative and reproductive growth in Arabidopsis thaliana," *Nucleic Acids Res*, vol. 47, no. 2, pp. 883–898, Jan. 2019, doi: 10.1093/nar/gky1205.

[183] J. Tang, P. Jia, P. Xin, J. Chu, D. Q. Shi, and W. C. Yang, "The Arabidopsis TRM61/TRM6 complex is a bona fide tRNA N1-methyladenosine methyltransferase," *J Exp Bot*, vol. 71, no. 10, pp. 3024–3036, May 2020, doi: 10.1093/jxb/eraa100.

[184] C. T. Y. Chan *et al.*, "Reprogramming of tRNA modifications controls the oxidative stress response by codon-biased translation of proteins," *Nat Commun*, vol. 3, p. 937, 2012, doi: 10.1038/ncomms1938.

[185] P. C. Dedon and T. J. Begley, "A system of RNA modifications and biased codon use controls cellular stress response at the level of translation," *Chemical Research in Toxicology*, vol. 27, no. 3. American Chemical Society, pp. 330–337, Mar. 17, 2014. doi: 10.1021/tx400438d.

[186] Y. Wang *et al.*, "The 2′-O-methyladenosine nucleoside modification gene OsTRM13 positively regulates salt stress tolerance in rice," *J Exp Bot*, vol. 68,

no. 7, pp. 1479–1491, Mar. 2017, doi: 10.1093/jxb/erx061.

[187] A. Galvanin *et al.*, “Bacterial tRNA 2’-O-methylation is dynamically regulated under stress conditions and modulates innate immune response,” *Nucleic Acids Res*, vol. 48, no. 22, pp. 12833–12844, Dec. 2020, doi: 10.1093/nar/gkaa1123.

[188] C. Gu, T. J. Begley, and P. C. Dedon, “TRNA modifications regulate translation during cellular stress,” *FEBS Letters*, vol. 588, no. 23. Elsevier, pp. 4287–4296, Nov. 28, 2014. doi: 10.1016/j.febslet.2014.09.038.

[189] L. Pollo-Oliveira and V. De Crécy-Lagard, “Can Protein Expression Be Regulated by Modulation of tRNA Modification Profiles?,” *Biochemistry*, vol. 58, no. 5. American Chemical Society, pp. 355–362, Feb. 05, 2019. doi: 10.1021/acs.biochem.8b01035.

[190] X. Ma, F. Si, X. Liu, and W. Luan, “PRMdb: A Repository of Predicted RNA Modifications in Plants,” *Plant Cell Physiol*, vol. 61, no. 6, pp. 1213–1222, Jun. 2020, doi: 10.1093/pcp/pcaa042.

[191] C. Zhang and G. Jia, “Reversible RNA Modification N1-methyladenosine (m1A) in mRNA and tRNA,” *Genomics, Proteomics and Bioinformatics*, vol. 16, no. 3. Beijing Genomics Institute, pp. 155–161, Jun. 01, 2018. doi: 10.1016/j.gpb.2018.03.003.

[192] F. Liu *et al.*, “ALKBH1-Mediated tRNA Demethylation Regulates Translation,” *Cell*, vol. 167, no. 3, pp. 816-828.e16, Oct. 2016, doi: 10.1016/j.cell.2016.09.038.

[193] R. Jordan Ontiveros *et al.*, “Coordination of mRNA and tRNA methylations by TRMT10A,” *Proc Natl Acad Sci U S A*, vol. 117, no. 14, pp. 7782–7791, Apr. 2020, doi: 10.1073/pnas.1913448117.

[194] Q. Guo *et al.*, “Arabidopsis TRM5 encodes a nuclear-localised bifunctional tRNA guanine and inosine-N1-methyltransferase that is important

for growth," *PLoS One*, vol. 14, no. 11, p. e0225064, Nov. 2019, doi: 10.1371/journal.pone.0225064.

[195] X. Jin *et al.*, "{AtTrm5a} catalyses 1-methylguanosine and 1-methylinosine formation on {tRNAs} and is important for vegetative and reproductive growth in Arabidopsis thaliana.," *Nucleic Acids Res*, vol. 47, no. 2, pp. 883–898, Jan. 2019, doi: 10.1093/nar/gky1205.

[196] V. Ramírez *et al.*, "A 29-O-methyltransferase responsible for transfer RNA anticodon modification is pivotal for resistance to pseudomonas syringae DC3000 in arabidopsis," *Molecular Plant-Microbe Interactions*, vol. 31, no. 12, pp. 1323–1336, Dec. 2018, doi: 10.1094/MPMI-06-18-0148-R.

[197] W. Zhou, D. Karcher, and R. Bock, "Identification of enzymes for adenosine-to-inosine editing and discovery of cytidine-to-uridine editing in nucleus-encoded transfer RNAs of arabidopsis," *Plant Physiol*, vol. 166, no. 4, pp. 1985–1997, Dec. 2014, doi: 10.1104/pp.114.250498.

[198] P. Schimmel, "RNA Processing and Modifications: The emerging complexity of the tRNA world: Mammalian tRNAs beyond protein synthesis," *Nature Reviews Molecular Cell Biology*, vol. 19, no. 1. Nature Publishing Group, pp. 45–58, Jan. 01, 2018. doi: 10.1038/nrm.2017.77.

[199] E. J. Park and T.-H. Kim, "Fine-Tuning of Gene Expression by {tRNA}-Derived Fragments during Abiotic Stress Signal Transduction.," *Int J Mol Sci*, vol. 19, no. 2, Feb. 2018, doi: 10.3390/ijms19020518.

[200] S. Li, Z. Xu, and J. Sheng, "tRNA-derived small RNA: A novel regulatory small non-coding RNA," *Genes*, vol. 9, no. 5. MDPI AG, May 01, 2018. doi: 10.3390/genes9050246.

[201] Y. Xie, L. Yao, X. Yu, Y. Ruan, Z. Li, and J. Guo, "Action mechanisms and research methods of tRNA-derived small RNAs," *Signal Transduction and Targeted Therapy*, vol. 5, no. 1. Springer Nature, pp. 1–9, Dec. 01, 2020. doi:

10.1038/s41392-020-00217-4.

[202] V. Cognat *et al.*, “The nuclear and organellar {tRNA}-derived {RNA} fragment population in Arabidopsis thaliana is highly dynamic.,” *Nucleic Acids Res*, vol. 45, no. 6, pp. 3460–3472, Apr. 2017, doi: 10.1093/nar/gkw1122.

[203] L. Wang *et al.*, “A novel class of heat-responsive small RNAs derived from the chloroplast genome of Chinese cabbage (Brassica rapa),” *BMC Genomics*, vol. 12, p. 289, Jun. 2011, doi: 10.1186/1471-2164-12-289.

[204] Y. Hirose, K. T. Ikeda, E. Noro, K. Hiraoka, M. Tomita, and A. Kanai, “Precise mapping and dynamics of tRNA-derived fragments (tRFs) in the development of Triops cancriformis (tadpole shrimp),” *BMC Genet*, vol. 16, no. 1, Jul. 2015, doi: 10.1186/s12863-015-0245-5.

[205] G. Martinez, S. G. Choudury, and R. K. Slotkin, “TRNA-derived small RNAs target transposable element transcripts,” *Nucleic Acids Res*, vol. 45, no. 9, pp. 5142–5152, May 2017, doi: 10.1093/nar/gkx103.

[206] C. Megel *et al.*, “Plant RNases T2, but not Dicer-like proteins, are major players of tRNA-derived fragments biogenesis,” *Nucleic Acids Res*, vol. 47, no. 2, pp. 941–952, 2019, doi: 10.1093/nar/gky1156.

[207] C. Cole *et al.*, “Filtering of deep sequencing data reveals the existence of abundant Dicer-dependent small RNAs derived from tRNAs,” *RNA*, vol. 15, no. 12, pp. 2147–2160, Dec. 2009, doi: 10.1261/rna.1738409.

[208] R. Magee and I. Rigoutsos, “On the expanding roles of tRNA fragments in modulating cell behavior,” *Nucleic Acids Res*, vol. 48, no. 17, pp. 9433–9448, Sep. 2020, doi: 10.1093/nar/gkaa657.

[209] S. P. Thomas, T. T. Hoang, V. T. Ressler, and R. T. Raines, “Human angiogenin is a potent cytotoxin in the absence of ribonuclease inhibitor,” *RNA*, vol. 24, no. 8, pp. 1018–1027, Aug. 2018, doi: 10.1261/rna.065516.117.

[210] Z. Li, C. Ender, G. Meister, P. S. Moore, Y. Chang, and B. John, “Extensive terminal and asymmetric processing of small RNAs from rRNAs, snoRNAs, snRNAs, and tRNAs,” *Nucleic Acids Res*, vol. 40, no. 14, pp. 6787–6799, Aug. 2012, doi: 10.1093/nar/gks307.

[211] S. Dou, Y. Wang, and J. Lu, “Metazoan tsRNAs: Biogenesis, evolution and regulatory functions,” *Non-coding RNA*, vol. 5, no. 1. MDPI AG, 2019. doi: 10.3390/ncrna5010018.

[212] P. Kumar, J. Anaya, S. B. Mudunuri, and A. Dutta, “Meta-analysis of tRNA derived RNA fragments reveals that they are evolutionarily conserved and associate with AGO proteins to recognize specific RNA targets,” *BMC Biol*, vol. 12, no. 1, p. 78, Dec. 2014, doi: 10.1186/s12915-014-0078-0.

[213] M. M. Emara *et al.*, “Angiogenin-induced {tRNA}-derived stress-induced {RNAs} promote stress-induced stress granule assembly.,” *J Biol Chem*, vol. 285, no. 14, pp. 10959–10968, Apr. 2010, doi: 10.1074/jbc.M109.077560.

[214] Q. Wang, I. Lee, J. Ren, S. S. Ajay, Y. S. Lee, and X. Bao, “Identification and functional characterization of tRNA-derived RNA fragments (tRFs) in respiratory syncytial virus infection,” *Molecular Therapy*, vol. 21, no. 2, pp. 368–379, 2013, doi: 10.1038/mt.2012.237.

[215] S. R. Lee and K. Collins, “Starvation-induced cleavage of the tRNA anticodon loop in Tetrahymena thermophila,” *Journal of Biological Chemistry*, vol. 280, no. 52, pp. 42744–42749, Dec. 2005, doi: 10.1074/jbc.M510356200.

[216] M. Saikia and M. Hatzoglou, “The many virtues of tRNA-derived stress-induced RNAs (tiRNAs): Discovering novel mechanisms of stress response and effect on human health,” *Journal of Biological Chemistry*, vol. 290, no. 50. American Society for Biochemistry and Molecular Biology Inc., pp. 29761–29768, Dec. 11, 2015. doi: 10.1074/jbc.R115.694661.

[217] L. Ambrosio, S. Morriss, A. Riaz, R. Bailey, J. Ding, and G. C. MacIntosh,

"Phylogenetic analyses and characterization of RNase X25 from Drosophila melanogaster suggest a conserved housekeeping role and additional functions for RNase T2 enzymes in protostomes," *PLoS One*, vol. 9, no. 8, Aug. 2014, doi: 10.1371/journal.pone.0105444.

[218] D. M. Thompson and R. Parker, "The RNase Rny1p cleaves tRNAs and promotes cell death during oxidative stress in Saccharomyces cerevisiae," *Journal of Cell Biology*, vol. 185, no. 1, pp. 43–50, Apr. 2009, doi: 10.1083/jcb.200811119.

[219] S. P. Thomas, T. T. Hoang, V. T. Ressler, and R. T. Raines, "Human angiogenin is a potent cytotoxin in the absence of ribonuclease inhibitor," *RNA*, vol. 24, no. 8, pp. 1018–1027, Aug. 2018, doi: 10.1261/rna.065516.117.

[220] S. Liu *et al.*, "A tRNA-derived RNA Fragment Plays an Important Role in the Mechanism of Arsenite -induced Cellular Responses," *Sci Rep*, vol. 8, no. 1, Dec. 2018, doi: 10.1038/s41598-018-34899-2.

[221] T. Gogakos, M. Brown, A. Garzia, C. Meyer, M. Hafner, and T. Tuschl, "Characterizing Expression and Processing of Precursor and Mature Human tRNAs by Hydro-tRNAseq and PAR-CLIP," *Cell Rep*, vol. 20, no. 6, pp. 1463–1475, Aug. 2017, doi: 10.1016/j.celrep.2017.07.029.

[222] M. Shigematsu, S. Honda, P. Loher, A. G. Telonis, I. Rigoutsos, and Y. Kirino, "YAMAT-seq: An efficient method for high-throughput sequencing of mature transfer RNAs," *Nucleic Acids Res*, vol. 45, no. 9, p. e70, May 2017, doi: 10.1093/nar/gkx005.

[223] D. M. Thompson, C. Lu, P. J. Green, and R. Parker, "tRNA cleavage is a conserved response to oxidative stress in eukaryotes," *RNA*, vol. 14, no. 10, pp. 2095–2103, Oct. 2008, doi: 10.1261/rna.1232808.

[224] G. C. MacIntosh and B. Castandet, "Organellar and secretory ribonucleases: Major players in plant RNA homeostasis1[OPEN]," *Plant Physiol*,

vol. 183, no. 4, pp. 1438–1452, Aug. 2020, doi: 10.1104/pp.20.00076.

[225] K. L. Andersen and K. Collins, “Several RNase T2 enzymes function in induced tRNA and rRNA turnover in the ciliate Tetrahymena,” *Mol Biol Cell*, vol. 23, no. 1, pp. 36–44, Jan. 2012, doi: 10.1091/mbc.E11-08-0689.

[226] C. J. Chen, Q. Liu, Y. C. Zhang, L. H. Qu, Y. Q. Chen, and D. Gautheret, “Genome-wide discovery and analysis of microRNAs and other small RNAs from rice embryogenic callus,” *RNA Biol*, vol. 8, no. 3, pp. 538–547, 2011, doi: 10.4161/rna.8.3.15199.

[227] C. S. Alves, R. Vicentini, G. T. Duarte, V. F. Pinoti, M. Vincentz, and F. T. S. Nogueira, “Genome-wide identification and characterization of {tRNA}-derived {RNA} fragments in land plants.,” *Plant Mol Biol*, vol. 93, no. 1–2, pp. 35–48, Jan. 2017, doi: 10.1007/s11103-016-0545-9.

[228] M. Hackenberg, P. J. Huang, C. Y. Huang, B. J. Shi, P. Gustafson, and P. Langridge, “A Comprehensive expression profile of microrna and other classes of non-coding small RNAs in barley under phosphorous-deficient and-sufficient conditions,” *DNA Research*, vol. 20, no. 2, pp. 109–125, Apr. 2013, doi: 10.1093/dnares/dss037.

[229] Y. Li *et al.*, “Stress-induced tRNA-derived RNAs: A novel class of small RNAs in the primitive eukaryote Giardia lamblia,” *Nucleic Acids Res*, vol. 36, no. 19, pp. 6048–6055, 2008, doi: 10.1093/nar/gkn596.

[230] S. Lalande, R. Merret, T. Salinas-Giegé, and L. Drouard, “Arabidopsis tRNA-derived fragments as potential modulators of translation,” *RNA Biol*, vol. 17, no. 8, pp. 1137–1148, 2020, doi: 10.1080/15476286.2020.1722514.

[231] P. Ivanov, M. M. Emara, J. Villen, S. P. Gygi, and P. Anderson, “Angiogenin-induced {tRNA} fragments inhibit translation initiation.,” *Mol Cell*, vol. 43, no. 4, pp. 613–623, Aug. 2011, doi: 10.1016/j.molcel.2011.06.022.

[232] M. Nowacka, P. M. Strozycki, P. Jackowiak, A. Hojka-Osinska, M.

Szymanski, and M. Figlerowicz, “Identification of stable, high copy number, medium-sized {RNA} degradation intermediates that accumulate in plants under non-stress conditions.,” *Plant Mol Biol*, vol. 83, no. 3, pp. 191–204, Oct. 2013, doi: 10.1007/s11103-013-0079-3.

[233] S. M. Lyons, C. Achorn, N. L. Kedersha, P. J. Anderson, and P. Ivanov, “YB-1 regulates tiRNA-induced Stress Granule formation but not translational repression,” *Nucleic Acids Res*, vol. 44, no. 14, pp. 6949–6960, Aug. 2016, doi: 10.1093/nar/gkw418.

[234] Y. Shao, Q. Sun, X. Liu, P. Wang, R. Wu, and Z. Ma, “tRF-Leu-CAG promotes cell proliferation and cell cycle in non-small cell lung cancer,” *Chem Biol Drug Des*, vol. 90, no. 5, pp. 730–738, Nov. 2017, doi: 10.1111/cbdd.12994.

[235] R. D. Morin *et al.*, “Application of massively parallel sequencing to microRNA profiling and discovery in human embryonic stem cells,” *Genome Res*, vol. 18, no. 4, pp. 610–621, Apr. 2008, doi: 10.1101/gr.7179508.

[236] N. C. T. Schopman, S. Heynen, J. Haasnoot, and B. Berkhout, “A miRNA-tRNA mix-up: tRNA origin of proposed miRNA,” *RNA Biology*, vol. 7, no. 5. Taylor and Francis Inc., pp. 573–576, 2010. doi: 10.4161/rna.7.5.13141.

[237] M. Cristodero and N. Polacek, “The multifaceted regulatory potential of tRNA-derived fragments,” *Noncoding RNA Investig*, vol. 1, no. 3, pp. 7–7, Sep. 2017, doi: 10.21037/ncri.2017.08.07.

[238] V. Balatti *et al.*, “tsRNA signatures in cancer,” *Proc Natl Acad Sci U S A*, vol. 114, no. 30, pp. 8071–8076, Jul. 2017, doi: 10.1073/pnas.1706908114.

[239] A. Boskovic, X. Y. Bing, E. Kaymak, and O. J. Rando, “Control of noncoding RNA production and histone levels by a 5’ tRNA fragment,” *Genes Dev*, vol. 34, no. 1–2, pp. 118–131, Jan. 2020, doi: 10.1101/gad.332783.119.

[240] D. Veneziano, S. di Bella, G. Nigita, A. Laganà, A. Ferro, and C. M. Croce, “Noncoding RNA: Current Deep Sequencing Data Analysis Approaches and

Challenges," *Human Mutation*, vol. 37, no. 12. John Wiley and Sons Inc., pp. 1283–1298, Dec. 01, 2016. doi: 10.1002/humu.23066.

[241] M. Saikia *et al.*, "Angiogenin-Cleaved tRNA Halves Interact with Cytochrome c, Protecting Cells from Apoptosis during Osmotic Stress," *Mol Cell Biol*, vol. 34, no. 13, pp. 2450–2463, Jul. 2014, doi: 10.1128/mcb.00136-14.

[242] A. J. Schorn, M. J. Gutbrod, C. LeBlanc, and R. Martienssen, "{LTR}-Retrotransposon Control by {tRNA}-Derived Small {RNAs}.," *Cell*, vol. 170, no. 1, pp. 61-71.e11, Jun. 2017, doi: 10.1016/j.cell.2017.06.013.

[243] B. Ren, X. Wang, J. Duan, and J. Ma, "Rhizobial tRNA-derived small RNAs are signal molecules regulating plant nodulation.," *Science*, p. eaav8907, Jul. 2019, doi: 10.1126/science.aav8907.

[244] Z. Li, C. Ender, G. Meister, P. S. Moore, Y. Chang, and B. John, "Extensive terminal and asymmetric processing of small RNAs from rRNAs, snoRNAs, snRNAs, and tRNAs," *Nucleic Acids Res*, vol. 40, no. 14, pp. 6787–6799, Aug. 2012, doi: 10.1093/nar/gks307.

[245] D. Haussecker, Y. Huang, A. Lau, P. Parameswaran, A. Z. Fire, and M. A. Kay, "Human tRNA-derived small RNAs in the global regulation of RNA silencing," *RNA*, vol. 16, no. 4, pp. 673–695, Apr. 2010, doi: 10.1261/rna.2000810.

[246] G. Loss-Morais, P. M. Waterhouse, and R. Margis, "Description of plant tRNA-derived RNA fragments (tRFs) associated with argonaute and identification of their putative targets," *Biology Direct*, vol. 8, no. 1. Biol Direct, Feb. 12, 2013. doi: 10.1186/1745-6150-8-6.

[247] C. S. Alves, R. Vicentini, G. T. Duarte, V. F. Pinoti, M. Vincentz, and F. T. S. Nogueira, "Genome-wide identification and characterization of tRNA-derived RNA fragments in land plants," *Plant Mol Biol*, vol. 93, no. 1–2, pp. 35–48, Jan. 2017, doi: 10.1007/s11103-016-0545-9.

[248] E. J. Park and T.-H. Kim, “Fine-Tuning of Gene Expression by tRNA-Derived Fragments during Abiotic Stress Signal Transduction,” 2018, doi: 10.3390/ijms19020518.

[249] S. Rashad, T. Tominaga, and K. Niizuma, “The cell and stress-specific canonical and noncanonical tRNA cleavage,” *J Cell Physiol*, vol. 236, no. 5, pp. 3710–3724, May 2021, doi: 10.1002/jcp.30107.

[250] S. Rashad *et al.*, “The stress specific impact of ALKBH1 on tRNA cleavage and tiRNA generation,” *RNA Biol*, vol. 17, no. 8, pp. 1092–1103, Aug. 2020, doi: 10.1080/15476286.2020.1779492.

[251] S. Blanco *et al.*, “Aberrant methylation of {tRNAs} links cellular stress to neuro-developmental disorders.,” *EMBO J*, vol. 33, no. 18, pp. 2020–2039, Sep. 2014, doi: 10.15252/embj.201489282.

Chapter 2. The RNA 5-methylcytosine methyltransferase NOP2 is essential for ovule development in *Arabidopsis thaliana*

2.1. Abstract

RNA 5-methylcytosine (m^5C) is a wide-spread post-transcriptional modification present on mRNA and non-coding RNAs. Ribsomal RNA m^5C is important for fine-tuning translational efficiency and ribosomal fidelity. Here, we focus on NOP2, a putative rRNA 5-methylcytosine methyltransferase, and show NOP2 is genetically redundant and is essential for ovule development in *A. thaliana*. Three NOP2 homologues, *NOP2A, NOP2B* and *NOP2C* are present in the *A. thaliana* genome and we demonstrated genetic redundancy by generating double mutants. We showed *nop2a nop2b* mutants were lethal and aborted at the two to eight-nucleate stage during female gametophyte development. Gene expression analysis using a GUS reporter assay showed that *NOP2A* was expressed at all tested stages of plant growth. Mutant *NOP2a* plants were smaller, with shorter roots and pointed rosette leaves. Reduction of *NOP2A* in *nop2b nop2c* mutants using an artificial miRNA led a range of phenotypes from abortion at the globular stage of embryo development through to viable, slower growing seedlings. We also showed that all three *NOP2* genes contribute to m^5C methylation of C2268 on 25S rRNA. Finally, we demonstrated that *nop2* mutants have increased sensitivity to antibiotics suggesting impaired ribosome activity. Taken together, our findings highlight the importance of *NOP2* during ovule and vegetative development.

2.2. Introduction

More than 150 distinct post-transcriptional modifications have been discovered on eukaryotic RNAs, and these modifications expand the functional space of RNA [1]. Ribosomal RNAs (rRNAs) modifications are involved in diverse biological processes including conformational stability, fine-tuning translational efficiency and ribosomal fidelity [2]–[4]. Ribosomal RNA modifications vary between prokaryotes and eukaryotes [5], collectively over 100 modifications were identified on yeast rRNAs and over 200 modifications on invertebrate rRNAs [6]. The most common RNA modifications involve methylation or pseudouridylation, and are located in functionally conserved RNA regions from bacteria to plants.

Typically, mature ribosomes are formed by two ribosomal subunits, the large ribosomal subunit (LSU) and the small ribosomal subunit (SSU). In prokaryotic ribosomes, 23S and 5S rRNAs are in the LSU and 16S rRNA is in the SSU. In eukaryotes, 5S, 5.8S and 28S rRNAs are in LSU and 18S rRNA is in the SSU [7], [8]. RNA cytosine methylation at the fifth carbon atom (m^5C) is highly abundant on cellular rRNAs [9]. Advancements in high-throughput sequencing led to the identification of m^5C on rRNAs in various species. For example, the yeast LSU 25S rRNA is methylated at C2278 and C2870 [10], [11]. Apart from yeast, *Escherichia coli* contains two m^5C sites in the SSU 16S rRNA at C965 and C1407, and one single in LSU 23S rRNA m^5C site at C1962 [12], [13]. In humans, LSU 28S rRNA have two m^5C sites at C3782 and C4447, and the LSU 5S rRNA is only methylated at C92 [14]–[16]. Additionally, one m^5C site was identified in hamster mitochondrial SSU 13S rRNA [17], which corresponds to C911 in mouse SSU 12S rRNA [18]. In plants, a total of seven m^5C sites were identified in the nuclear LSU 25S, chloroplast SSU 16S, LSU 23S and mitochondrial SSU 18S and LSU 26S rRNAs, and six of these m^5C sites were highly conserved in position and methylation percentage across all tested species [10].

In eukaryotes, two RNA methyltransferases were characterized with a Rossmann-like fold SAM binding domain [19], NOP2 (nuclear protein 2) and RCM1 (rRNA cytosine methyltransferase 1) and demonstrated to methylate

rRNAs [10], [20]. In yeast, NOP2 and RCM1 are rRNA methyltransferases acting on C2870 and C2278 positions of LSU 25S. NOP2 is essential for the synthesis of the large subunit of the ribosome [9], [20]. Yeast *rcm1* mutants exhibit hypersensitivity to azinomycin, which suggests the structure of 25S rRNA was altered due to the lack of m^5C modification at position C2278. More broadly, *NOP2* expression increases in various cancerous tissues and has the potential to be used as a tumour marker [21]. Also, NOP2 is required for nucleolar and blastocyst formation [22], [23]. The RCM1 homology, NSUN5 in *A. thaliana*, methylates C2268 in the 25S rRNA [10]. Genome sequence analysis of *A. thaliana* identified three paralogs of *NOP2*, *NOP2A* (also known as *OLI2*), *NOP2B* and *NOP2C* [24]. Polypeptide sequence alignment of NOP2A, NOP2B and NOP2C showed that NOP2B has no motif IV, which is predicted to be involved in the release of methylated RNA from the enzyme [25], [26]. NOP2C has an altered motif N1, which is involved in RNA binding but is not essential for RMTase activity [27]. Our previous research shows that there was no difference in the m^5C level at nuclear LSU 25S rRNA C2860 in single mutants *nop2a, nop2b, nop2c* compared to wild type (WT) [10]. However recently, reduced m^5C level was observed at 25S rRNA C2860 in nop2a/NOP2B RNAi plants [28]. From a biological perspective, NOP2A is involved leaf cell proliferation, especially during leaf development [29]. Recently, repression of NOP2A was linked with viral penetration of plant shoot apical meristems [28]. In our previous data, we could not obtain *nop2a nop2b* double mutants in a F_2 segregating population, which suggesting that NOP2A and NOP2B may act redundantly and are essential for plant viability [10].

In *A. thaliana,* ovules are indispensable reproductive organs consisting of the outer integument, the nucellus and the female gametophyte in the center. The female gametophyte, or megagametophyte, undergoes meiosis to produce four haploid cells and then a round of mitosis to produce 8 haploid cells of which one cell is the egg cell and the other is the central cell [30], [31]. A number of studies have shown that there are numerous genes involved in ovule development including those that function in polarity establishment, cell division, floral organ determination, ovule identity, and structure specification [32]–[34]. In this study, we discovered a putative RNA methyltransferase, NOP2, which is

essential for female gametophyte development. Understanding the factors that influence the ovule development is of great importance from an agricultural and economical point of view, as the ovule will determine the number of seeds that develop in fruit, and thus crop yield.

In this study, we explored the function of three paralogs of NOP2 in *A. thaliana*, NOP2A, NOP2B and NOP2C. We found that the *nop2a nop2b* mutants was lethal due to female gametophyte abortion at the two to eight-nucleate stages. However, by knocking down *NOP2A* using an artificial miRNA in either *nop2b* or *nop2b nop2c* mutants, we were able to recover T_1 seeds (namely *amiR_NOP2A nop2b* and *amiR_NOP2A nop2b nop2c*). Illumina sequencing of bisulphite-treated RNA from *amiR_NOP2A nop2b* and *amiR_NOP2A nop2b nop2c* plants showed that all three *NOP2* genes contribute to m^5C methylation of rRNA. Furthermore, we observed *amiR_NOP2A nop2b nop2c* seedlings were more sensitive than wild type controls when treated with antibiotics suggesting reduced rRNA methylation interferes with translational activity. Finally, results from northern blotting and RT-qPCR analysis for rRNA intermediates suggested that *NOP2* methylation might be involved in modulating rRNA activity and not rRNA biogenesis.

2.3. Material and methods

2.3.1. Plant materials and growth conditions

A. thaliana (Columbia ecotype) were grown in Phoenix Biosystem controlled environment rooms at 21°C under metal halide lights that provided a level of photosynthetic active radiation (PRA) of 110 µmol of photos/m^2/s [10]. For *in vitro* plant growth, *A. thaliana* seeds were surface sterilized in a solution containing one part 10% sodium hypochlorite and nine parts 100% ethanol and plated on ½ Murashige and Skoog (MS) medium supplemented with 1% sucrose as previous described [35]. Plants were grown under long day photoperiod conditions of 16 hrs light. Seeds of *A. thaliana* mutants *nop2a* (salk_129648), *nop2b* (salk_054685) and *nop2c* (sail_1263_B04) were obtained from *A. thaliana* Biological Resource Center (ABRC).

Characterization of the mutant alleles, *nop2a*, *nop2b* and *nop2c* and double mutants *nop2a nop2b*, *nop2a nop2c*, *nop2b nop2c* are as described previously [10], [36]. Primers to detect *nop2* mutants were generated using the SIGnAL iSect Primer Design program. The PCR thermal cycling conditions were: 95°C for 3 min followed by 35 cycles of 95°C for 15 sec, 55 °C for 20 sec, 73°C for 45 sec and the final elongation step at 73°C for 5 min.

The reciprocal crossing was performed for *nop2a* and *nop2b*, *nop2a* and *nop2c*, *nop2b* and *nop2c*. Flowers were emasculated before anthesis and then pollinated 48 hrs later. The segregation ratio for each *nop2* was undertaken using PCR analysis in the F_1 population.

Nucleotide sequence data for the following genes are available from The Arabidopsis Information Resource (TAIR) database under the following accession numbers: NOP2A (At5g55920), NOP2B (At4g26600), NOP2C (At1g06560).

2.3.2. Plasmid construction and generation of transgenic plants

MicroRNA targeting NOP2A was designed as the Web MicroRNA Designer (WMD3) tools instruction (http://wmd3.weigelworld.org/cgi-bin/webapp.cgi?page=Designer;project=stdwmd). The transcription library was set to "TAIR9_cdna_20090619", the minimum number of included targets is 1 and accepted off-target was 0. Micro RNA sequence was synthesized in Integrated DNA Technologies (IDT) company and ligated into modified pMDC111 vector which contains Actin2 (Act2) promoter (Supplementary_Vectors). The construct was transformed into *nop2b* and *nop2bnop2c* mutant plants by *Agrobacterium tumefaciens*-mediated floral dipping method [37]. Transgenic plants were selected on ½ MS media supplemented with 50 µg/ml kanamycin [38].

The full-length genomic promoter regions of *NOP2A* (2638 bp), *NOP2B* (2153 bp) and *NOP2C* (401 bp) were amplified from Col-0 genomic DNA template with primers provided in the Supplemental Data. The amplified PCR products were gel purified, A-tailed and cloned into Gateway entry vector PCR8 (Invitrogen). The inserts were sequenced and then cloned into the destination vector pMDC163, using the Gateway cloning system following the manufacturer's protocol (Invitrogen) [39], resulting in the pMDC163:NOP2A_promoter:GUS, pMDC163:NOP2B_promoter:GUS, and pMDC163:NOP2C_promoter:GUS (Supplementary Vectors). The construct was transformed into *A. thaliana* WT Col-0 plants by the *A. tumefaciens* -mediated floral dipping method [37].

2.3.3. Seed sterilization and antibiotic stress treatments

A. thaliana seeds were surface sterilized for 4 hrs by gas produced from a mixed solution containing 1.5 mL of 32% HCl and 50 mL 12.5% NaClO. The sterilized seeds were plated on ½ MS medium supplemented with 1% sucrose on petri dishes, then stratified at 4°C in the dark for four days before placing under fluorescent light (110 µmol of photos/m^2/s) with a long-day photoperiod

condition of 16 hrs light. To measure the root growth, seedlings on plates were grown vertically and photos of the roots were taken at 10 DAG for root length measurement using ImageJ software. In antibiotic stress experiments, seedlings were grown horizontally on media supplemented with different antibiotics, 100 µg/mL spiramycin, 50 ng/mL cycloheximide, 50 µg/mL streptomycin, 50 µg/mL erythromycin or 20 µg/mL spectinomycin, and plant phenotypes were recorded after six days.

2.3.4. Microscopic observation of *A. thaliana* ovules development

Fresh *A. thaliana* pistils were collected, and the carpels were removed to expose the ovules before immediately placing in a bottle containing 4% glutaraldehyde in phosphate buffer pH 6.8. Slight vacuum (~5 Torr) was applied to the samples in glutaraldehyde for 30 mins and left-over night at room temperature. Samples were then dehydrated through an ethanol series (20%, 40%, 60%, 70%, 80%, 95% and 100% ethanol) before clearing using benzyl benzoate : benzyl alcohol (2:1 v/v) (BABB) series (BABB : EtOH (1:1 v/v), BABB : EtOH (3:1 v/v) and BABB) [40]. Samples in BABB solution were viewed under the FV300 confocal microscope (Olympus) using oil immersion. The excitation beam was set at 488nm and the collection range from 488nm to 700nm.

2.3.5. Histochemical β-glucuronidase (GUS) expression assay

GUS expression tissues were incubated with substrate solution, 2 mM XGluc, 0.5 mM $K_3Fe(CN)_6$, 0.5 mM $K_4Fe(CN)_6$, 50 mM Na_2HPO_4 pH 7.2 and 0.1 % (v/v) Triton X-100 at 37 ^oC overnight. The tissues were then washed with 100 % EtOH three times and incubated in EtOH for at least 1 hr before observation under a stereomicroscope (Olympus SZ2_ILST). At least 10 independent transgenic lines harbouring NOP2A_promoter:GUS, NOP2B_promoter:GUS and NOP2C_promoter:GUS were tested for GUS activity.

2.3.6. RNA bisulfite sequencing

Total RNA was isolated from ten-day-old WT and *nop2* seedlings using the Spectrum Plant total RNA kit (Sigma-Aldrich), and contaminating DNA was removed using DNase I (Sigma-Aldrich). For each sample, 4 µg of total RNA was bisulfite treated as previous described [10], [14], [41] and then 100 ng of bisulfite treated RNA was used to prepare library using NEBNext Ultra Ditrectional RNA library Prep Kit for Illumina (NEB). As bisulfite-treated RNA is sheared, the fragmentation step of the library preparation was omitted, and samples were quickly processed for first-strand cDNA synthesis after the addition of the fragmentation buffer. 15 cycles PCR was performed at the enrichment step. The libraries were sequenced on the Illumina HiSeq 2500 platform at ACRF, Adelaide. Detection of m^5C level in samples were as previously described [42].

2.3.7. Northern blotting

Total RNA was extracted from ten-day-old WT and *amiR_NOP2A_nop2b nop2c* seedlings and 20-30 ug of RNA was loaded into each lane of a native 1% agarose gel in 0.5X TBE buffer for electrophoresis. After electrophoresis, RNA was then transferred onto a Hybond-N+ membrane and the membrane was incubated with either a gamma-dATP32P labeled 5'ETS, ITS1, or ITS2 probes for rRNA intermediate detection before being scanned using Phosphorimager (Typhoon 3410) [43].

2.3.8. Real-time quantitative PCR (RT-qPCR)

Total RNA was extracted from the leaves of ten-day-old WT and *amiR_NOP2A nop2b nop2c* seedlings using Trizol reagent (Invitrogen). cDNA was synthesized using the gene-specific primers for 25S rRNA, PDF2 and SAND (Supplementary, Table 2) using SuperscriptIII reverse transcriptase (Invitrogen). The abundance of rRNA intermediate products (5′-ETS, ITS1, ITS2, 5.8S, 18S and 25S) was determined using quantitative real-time PCR (qPCR) with primers from (Supplementary, Table 2), the LightCycler® 480 SYBR Green I Master mix and Roche Lightcycler 480 system. Three biological replicates were carried out

for each sample set. The relative expression was corrected using reference genes PDF2 and SAND and calculated using the $2^{-\Delta CT}$ method as described previously [35], [44].

2.4. Results

2.4.1 NOP2A and NOP2B are required for the early stages of seed development

Our previous study showed that *nop2a nop2b* mutant plants could not be recovered in a segregating population derived from self-pollinating F_1 *nop2a* -/+ *nop2b* -/+ plant suggesting the double mutant was lethal, perhaps at an early stage of development [10]. Therefore, we asked the question if NOP2A and NOP2B are required during seed development. First, we investigated seed development from reciprocal crosses between *nop2a* -/+ *nop2b* -/+ and WT. Siliques were collected from each plant before desiccation, the seed pods opened and the total number of developed and aborted seeds for each silique were recorded. Interestingly, a significant portion of aborted seeds, ~25%, was observed only in the *nop2a* -/+ *nop2b* -/+ (♀) x WT (♂) cross (Fig 2.1A, B). However, no aborted seeds in the reciprocal cross WT (♀) x *nop2a* -/+ *nop2b* -/+ (♂) were observed. In the F_1 *nop2a* -/+ *nop2b* -/+ (♀) x WT (♂) population, we did not identify any *nop2a* -/+ *nop2b* -/+ seedlings by PCR screening (Table 1). In contrast, *nop2a* -/+ *nop2b* -/+ seedlings were identified at the expected frequency in the F_1 WT (♀) x *nop2a* -/+ *nop2b* -/+ (♂) population by PCR (Supplementary Table 1). Together this data suggested *nop2a nop2b* alleles were not inherited through the female germline. To reassure ourselves of this inference, we tested pollen grain viability of pollen derived from *nop2* single mutants, *nop2a, nop2b and nop2c*, and double heterozygous *nop2* mutants, *nop2a* -/+ *nop2b* -/+, *nop2a* -/+ *nop2c* -/+ and *nop2b* -/+ *nop2c* -/+, using Lugol's stain [45] We did not observe any significant difference in pollen viability in the mutants compared to the WT control (Fig 2.1C). Next, we the tested if the viable pollen could germinate using an *in vitro* assay and we observed no difference in the pollen germination of pollen derived from *nop2a* -/+ *nop2b* -/+ or WT (Fig 2.1D, E). Collectively, the pollen viability, pollen germination data and the aborted seeds only in the *nop2a* -/+ *nop2b* -/+ (♀) x WT (♂) cross indicated that *NOP2A* and *NOP2B* are vital for the early stage of seed development when inherited through the female germline line.

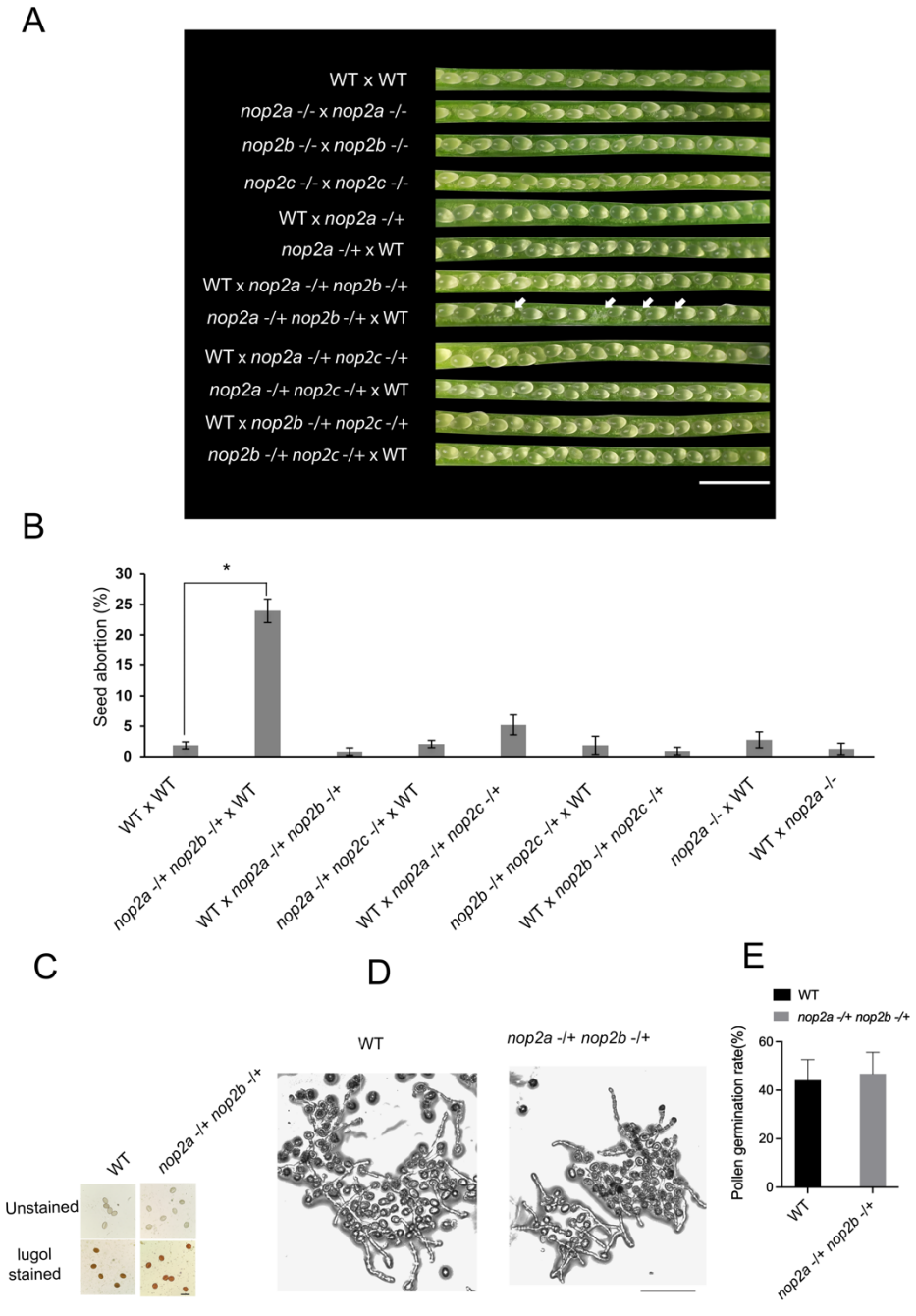
A
WT x WT
nop2a -/- x nop2a -/-
nop2b -/- x nop2b -/-
nop2c -/- x nop2c -/-
WT x nop2a -/+
nop2a -/+ x WT
WT x nop2a -/+ nop2b -/+
nop2a -/+ nop2b -/+ x WT
WT x nop2a -/+ nop2c -/+
nop2a -/+ nop2c -/+ x WT
WT x nop2b -/+ nop2c -/+
nop2b -/+ nop2c -/+ x WT
B
Seed abortion (%)
30
25
20
15
10
5
0
*
WT x WT
nop2a -/+ nop2b -/+ x WT
WT x nop2a -/+ nop2b -/+
nop2a -/+ nop2c -/+ x WT
WT x nop2a -/+ nop2c -/+
nop2b -/+ nop2c -/+ x WT
WT x nop2b -/+ nop2c -/+
nop2a -/- x WT
WT x nop2a -/-
C
WT
nop2a -/+ nop2b -/+
Unstained
lugol stained
D
WT
nop2a -/+ nop2b -/+
E
WT
nop2a -/+ nop2b -/+
Pollen germination rate(%)
60
40
20
0
WT
nop2a -/+ nop2b -/+

Figure 2.1: Functional *NOP2a NOP2b* are required in the female germline for seed development.

(A) Seed development in five-day-old siliques from reciprocal crosses between *nop2* mutants and WT. The siliques were collected at five days after the pollination, seed pods were removed, and images were taken under a stereo microscope. Seed development is normal for self-pollinated WT (WT x WT), self-pollinated *nop2* (*nop2a* -/- x *nop2a* -/-, *nop2b* -/- x *nop2b* -/- and *nop2c* -/- x *nop2c* -/-), reciprocal crosses between WT and heterozygous *nop2a* (WT x nop2a -/+ and nop2a -/+ x WT) , and reciprocal crosses between WT and heterozygous *nop2* double *mutants* (WT x nop2a -/+ nop2c-/+, *nop2a* -/+ *nop2c* -/+ x WT, WT x *nop2b* -/+ *nop2c* -/+ and *nop2b* -/+ *nop2c* -/+ x WT). However, while the cross WT (♀) x *nop2a* -/+ *nop2b* -/+ (♂) showed normal seed development, the reciprocal cross *nop2a* -/+ *nop2b* -/+ (♀) x WT (♂) showed some seeds were aborted at the early stage of development (arrows). Scale bar = 2 mm. **(B)** Seed abortion of different *nop2* crosses. Aborted seed up to 25% was recorded for *nop2a* -/+ *nop2b* -/+ x WT. All results were not significantly different from the control cross except the cross shown with an asterix. * P<0.01, Student's t-test, Error bars = SE. **(C)** Pollen viability test using Lugol's stain for pollen from WT, and *nop2a* -/+ *nop2b* -/+. The top panels show unstained pollen. The bottom panels show viable pollen that uptake iodine from the stain and are subsequently brown. Scale bar = 40 μm. **(D)** and **(E)** Matured pollen grains were collected from WT and *nop2a* -/+ *nop2b* -/+ flowers and then germinated on a glass slide at 25 ºC for 6 hrs with light [46]. Pollen germination was observed under a microscope and imaged for the data analysis. Scale bar = 100 um. Error bars = SE, * P<0.01 (Student's t-test),

Table 1. PCR detection of *nop2* alleles in F_1 plants derived from *nop2a* -/+ *nop2b* -/+ x WT cross

F_1 population	Expected segregation (%)	Segregation results (%, n=61)
nop2a +/+ nop2b +/+	25	39
nop2a -/+ nop2b +/+	25	19
nop2a +/+ nop2b -/+	25	40
nop2a -/+ nop2b -/+	25	0*
Total	100	100

* Statistical difference from the expected ratio as determined by the χ^2 test.

2.4.2. *nop2a -/+ nop2b -/+* female gametophyte aborts at the two to eight-nucleate stage

The female gametophyte referred to as megagametophyte develops within the ovule and has a critical role during the reproductive process. Female gametophyte development occurs through several stages and includes three rounds of mitosis to produce eight-nucleate cells and subsequent double fertilization that gives rise to a mature seed [47], [48]. To elucidate whether *nop2a nop2b* female gametes are involve in the seed abortion phenotype described earlier, flowers from *nop2a* -/+ *nop2b* -/+ plants were emasculated, the stigma wrapped in plastic to prevent cross-fertilisation. Two days after emasculation, the siliques were collected, fixed in glutaraldehyde, and cleared using benzyl benzoate: benzyl alcohol (BABB) before the ovules were observed using a confocal microscope. Two days after the emasculation, all the female gametophytes in the ovule of the WT control had completely undergone three rounds of mitosis, and all of them were at the eight-nucleate stage (Fig 2.2 A-C). After the eight-nucleate stage, the female gametophyte will finally develop into the three-celled stage containing one egg cell, one fused central cell and one synergid cell (Supplementary Fig 1). However, in *nop2a* -/+ *nop2b* -/+, the female gametophytes failed to progress past the two to the eight- nucleate stage (Fig 2.2 D-F) [49]. Therefore, it is likely that failure to develop egg cells during *nop2a nop2b* female gametophyte underpins later seed abortion.

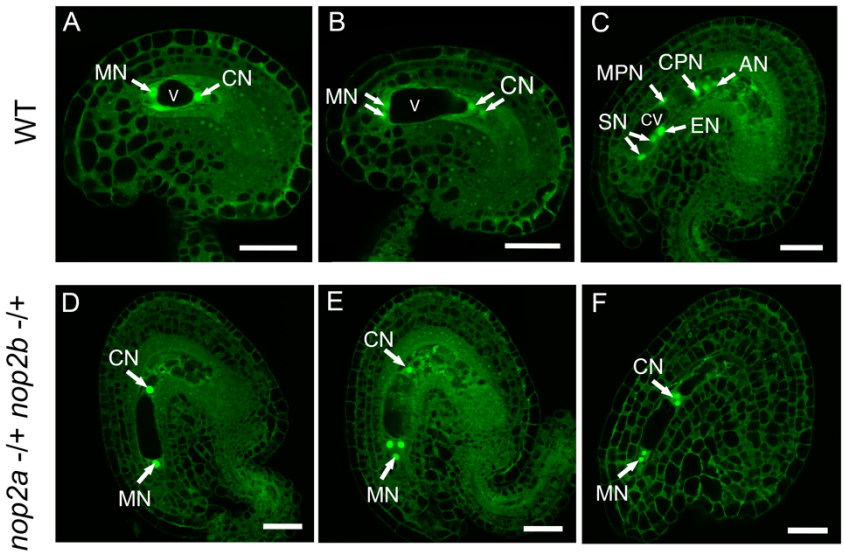

Figure 2.2: Female gametophyte development of WT and *nop2a* -/+ *nop2b* -/+ plants.

WT gametophytes (A-C) and *nop2a* -/+ *nop2b* -/+ gametophytes (D-E) two days after emasculation are shown. Gametophytes were fixed and imaged using a confocal microscopy. **(A)** Two-nucleate female gametophyte (FG) with a vacuole at FG3 stage. **(B)** Four-nucleate female gametophyte at FG4 stage. **(C)** Eight-nucleate/seven-celled female gametophyte at FG5 stage. **(D**) The ovule of the seed aborted *nop2a* -/+ *nop2b* -/+ mutant at two-nucleate female gametophyte (FG3 stage). **(E**) **(F**) The ovule of the seed aborted *nop2a* -/+ *nop2b* -/+ mutant at eight-nucleate female gametophyte (FG5 stage). CN, central cell nucleus; MN, micropylar nucleus; CV, central vacuole; DAN, degenerated antipodal nucleus; DS, degenerated synergid; EN, egg cell nucleus; EV, egg cell vacuole; SEN, secondary endosperm nucleus. Scale bar = 25 μm.

2.4.3. MicroRNA knockdown of NOP2A in nop2b nop2c mutants reduces vegetative growth and increases seed abortion

Generating a null NOP2 for functional analysis was impossible, as *nop2a nop2b* mutants were lethal. Therefore, we used an artificial microRNA (Supplementary Vectors) approach to knockdown *NOP2A* in either *nop2b* or *nop2b nop2c* mutants, and the transgenic plants were referred to as amiR_NOP2A *nop2b* or amiR_NOP2A *nop2b nop2c*, respectively. Previously, we observed that *nop2a* seedlings had a pointed leaf phenotype at early two to four-leaf stages (Fig 2.3

A). The same leaf phenotype was also observed in amiR_NOP2A *nop2b nop2c* seedlings (Fig 2.3B), suggesting that the microRNA successfully reduced NOP2A, and therefore these plants were selected for further molecular analysis. Both the amiR_NOP2A *nop2b* mutant plants and the amiR_NOP2A *nop2b nop2c* mutant plants showed a reduced plant growth 10 days after germination with significantly shorter roots compared to WT (Fig 2.3C and D). Furthermore, seeds in siliques isolated from independent amiR_NOP2A *nop2b nop2c* lines aborted at various stages of development (Fig 2.3E, F). Similar observations in amiR_NOP2A *nop2b* lines were also made (Supplementary Fig 2).

To explore the expression pattern of *NOP2A*, *NOP2B* and *NOP2C*, promoter fusions to the visual report β-Glucuronidase (GUS) were constructed and transformed into *Arabidopsis* (Supplementary Vectors, Fig 2.3G). Broad expression of all three GUS reporters was observed in the roots and rosette leaves of seedlings. Due to time constraints, reporter gene expression was not recorded in the reproductive tissues. Taken together, our results show that *NOP2* genes are crucial for plant development and are broadly expressed throughout plant development.

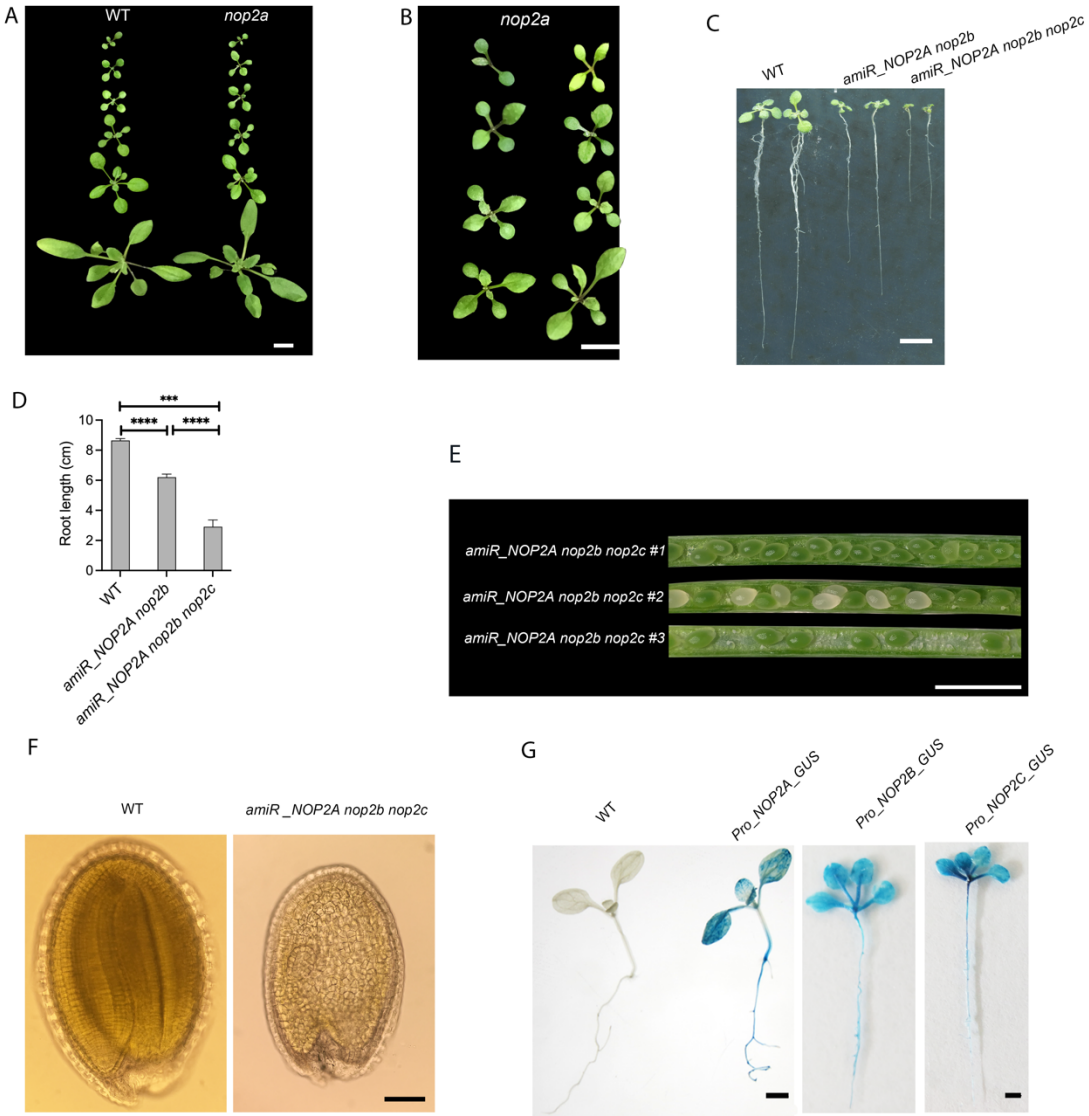
A
WT
nop2a
B
nop2a
C
WT
amiR_NOP2A nop2b
amiR_NOP2A nop2b nop2c
D
Root length (cm)
10
8
6
4
2
0
***
****
****
WT
amiR_NOP2A nop2b
amiR_NOP2A nop2b nop2c
E
amiR_NOP2A nop2b nop2c #1
amiR_NOP2A nop2b nop2c #2
amiR_NOP2A nop2b nop2c #3
F
WT
amiR _NOP2A nop2b nop2c
G
WT
Pro_NOP2A_GUS
Pro_NOP2B_GUS
Pro_NOP2C_GUS

Figure 2.3: Phenotypic defects caused by knock-down of *NOP2A*

(A) The pointed leaf phenotype was present in plants up to the four-leaf stage of *nop2a* (right) compared to WT (left). Scale bar = 1 cm. **(B)** The pointed leaf phenotype was also observed in *amiR_NOP2A nop2b nop2c* plants. The WT control is shown in panel A (left). Scale bar = 1cm. **(C)** Transgenic *amiR_NOP2A nop2b* and *amiR_NOP2A nop2b nop2c* seedlings have a short root compared to WT at 10 days after germination. Scale bar =1 cm. **(D)** Quantification of the root length data shown in panel (E). Error bars = SE (*P<0.01, Student's t-test, n= 20). **(E)** Opened siliques from three transgenic *amiR_NOP2A nop2b nop2c* lines. Line 1 had no seed abortion, line 2 had seed abortion at globular stage (white seeds) and line 3 had abortion at the early ovule development stage. Scale bar = 2 mm. **(F)** Microscopy of a translucent seed from line 2 (right) in panel E appeared to abort at the globular stage compared to WT (left) seed that developed to the two-cotyledon embryo stage. Scale bar = 25 μm. **(G)** Expression patterns of β-Glucuronidase (GUS) reporters driven by the *NOP2A* (2638 bp upstream of *NOP2A*), *NOP2B* (2153 bp upstream of *NOP2A*), or *NOP2C* (401 bp upstream of *NOP2A*) promoters in *A. thaliana* seedlings. Scale bar = 1 mm.

2.4.4. NOP2A, B & C contribute to m^5C methylation of C2268 on 25S rRNA

Previously, NOP2 was demonstrated to methylate the 25S rRNA C2870 in yeast [9], [20]. In *Arabidopsis*, there are three paralogs of NOP2, NOP2A, NOP2B and NOP2C, and research about their methylation activity or target m^5C sites is sparse. In this study, the methylation levels at candidate m^5C sites of rRNAs were analysed for WT, *nop2b nop2c*, *amiR_NOP2A*, *amiR_NOP2A nop2b* and *amiR_NOP2A nop2b nop2c* through RNA bisulphite sequencing. A total of eight m^5C sites in rRNA from nuclear, chloroplast and mitochondrial rRNAs, 18S rRNA C960, 26S rRNA C1586, 16S rRNA C105, 16S rRNA C916, 23S rRNA C1940, 23S rRNA C1977, 25S rRNA C2268 and 25S rRNA C2860, were investigated. While there was little difference in the methylation levels of chloroplast and mitochondrial m^5C sites from all the investigated lines (Fig 2.4), there was a clear reduction in methylation level at C2268 of the nuclear 25S rRNA when NOP2 function was inhibited in amiRNA lines (Fig 2.4). A reduction in methylation at 25S rRNA C2268 was detected in *amiR_NOP2A nop2b* to 50%, and was even lower in *amiR_NOP2A nop2b nop2c* at 30% when compared to WT levels of 70%. As expected, all the other examined rRNA m^5C

sites had similar methylation levels to WT. Taken together, NOP2A, NOP2B and NOP2C contribute to the methylation of 25S rRNA C2268.

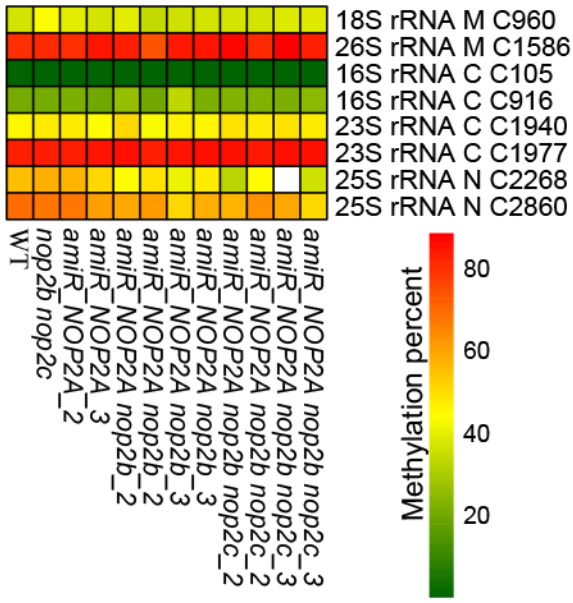

Figure 2.4: Ribosomal RNA m^{5}C analysis in WT and NOP2 amiRNA lines.

The RNA from the ten-day-old seedlings were bisulphite-treated and then prepared for sequencing library construction. The data were aligned to the *Arabidopsis* references and the numbering was based on the nucleotide position of the corresponding *Arabidopsis* rRNA reference sequence. A heatmap showing methylation percentage of measured cytosines in nuclear (N), chloroplast (C) and mitochondrial (M) rRNAs in WT and knock-down *NOP2* lines. Cytosine positions are indicated next to rRNA (1 biological replicate).

2.4.5. *NOP2* rRNA methylation may modulate ribosome activity

Reduced NOP2 function in *amiR_NOP2A nop2b nop2c* plants reduced methylation of nuclear 25S rRNA C2268. The 25S rRNA is a component of the large subunit of the ribosome. Therefore, we investigated if ribosomal activity was impaired by using several well described antibiotics that impair ribosome activity. Seeds of WT and *amiR_NOP2A nop2b nop2c* were sown on agar plates containing different antibiotics and the seedling phenotype was observed six days after germination (Fig 2.5). On the control media, no germination or cotyledon expansion differences were observed between WT and *amiR_NOP2A nop2b nop2c* seedlings (Fig 2.5A). However, when cycloheximide or erythromycin was added to the media, the germination of

amiR_NOP2A_nop2bnop2c was significantly inhibited compared to WT (Fig 2.5A). The addition of spiramycin delayed the germination of *amiR_NOP2A nop2b nop2c* compared to the WT (Fig 2.5A). Interestingly, the addition of streptomycin caused photobleaching in WT but not in *amiR_NOP2A nop2b nop2c* seedlings but adding spectinomycin caused photobleaching for both lines. Finally, cycloheximide was previously demonstrated as a protein synthesis inhibitor [50]. Overall, our result suggests that ribosomal activity is partially impaired in seedlings with reduced 25S rRNA C2268 methylation.

To determine whether NOP2 plays a role in 25S rRNA biogenesis, we next investigated the level of rRNA intermediates in *amiR_NOP2A nop2b nop2c*. RT-qPCR analysis showed that the rRNA intermediates, 5′-ETS, ITS1, ITS2, 5.8S, 18S and 25S have the same abundance as in WT [51] (Fig 2.5B). In addition, detection of rRNA intermediates accumulation in *amiR_NOP2A nop2b nop2c* by northern blotting detected no difference between *amiR_NOP2A nop2b nop2c* and WT (Fig 2.5C). Therefore, it is possible that NOP2 is involved in modulating rRNA activity but not rRNA biogenesis.

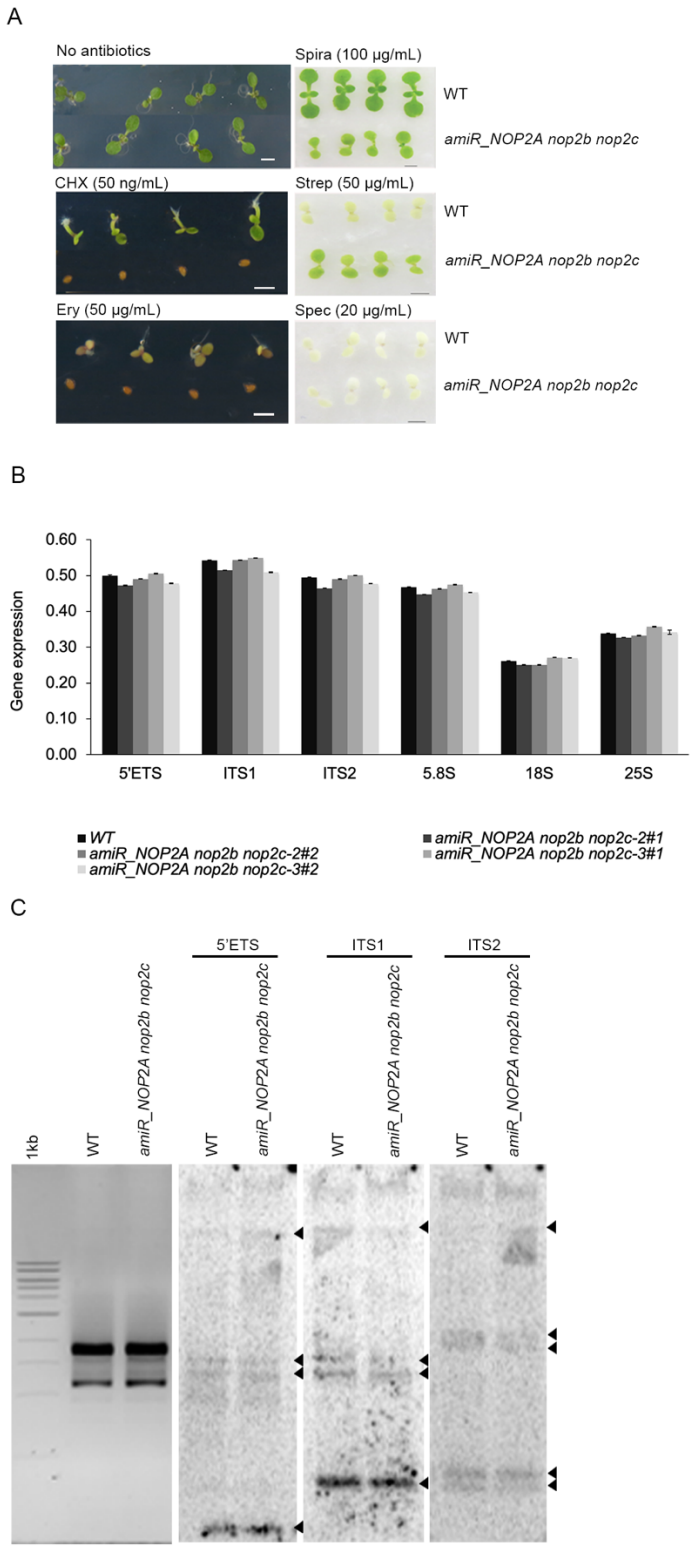

Fig 2.5: 25S rRNA methylation modulates ribosome activity but not rRNA biogenesis.

The ribosome activity in WT and *amiR_NOP2A nop2b nop2c* seedlings were

investigated by the response to antibiotics. The rRNA intermediates were examined through RT-qPCR and northern blotting on the leaves of WT and *amiR_NOP2A nop2b nop2c* to investigate the rRNA biogenesis. **(A)** Seeds of WT and *amiR_NOP2A nop2b nop2c* were grown on media containing either cycloheximide, CHX; or antibiotics erythromycin, Ery; spiramycin, Spira; streptomycin, Strep; or spectinomycin, Spec. The seedlings were photographed 6 days after germination. Scale bar = 2mm. **(B)** RT-qPCR analysis of rRNAs and processing intermediates in WT and *amiR_NOP2A nop2b nop2c* lines. For each line, 10 leaves from 10 individual plants showing the *nop2a* leaf phenotype were harvested and bulked together before RNA extraction. The data from three technical RT-qPCR replicates is shown. **(C)** Detection of rRNA intermediates in WT and *amiR_NOP2A nop2b nop2c* total-RNA by northern blotting. 5'ETS, ITS1, ITS2 probes were labelled with gamma-dATP32P.

2.5. Discussion and conclusion

The function of NOP2 is best understood in yeast and mammals, while in other organisms, like *Arabidopsis,* it is only starting to be investigated [52]. In yeast, NOP2 is necessary for the function of the large ribosome subunit [9] and in mammals, NOP2 was shown to be necessary for nucleolar and blastocyst formation [22]. Here, three paralogs of NOP2, NOP2A NOP2B and NOP2C, in *Arabidopsis* were investigated.

In this study, we showed that *NOP2A* and *NOP2B* are essential in early female gametophyte development and explains why in an earlier report *nop2a nop2b* mutants could not be recovered [10]. About 25% of aborted seeds were observed in the crossing between *nop2a* -/+ *nop2b* -/+ (♀) and WT (♂), while seed development in the reciprocal cross was normal. Besides *NOP2A* and *NOP2B*, the auxin efflux carrier *PIN1*, the type I MADS-box gene *AGL23* and transcription factor *MYB98* were also functionally characterized in female gametophyte development [53]–[55]. The embryos homozygous of the *agl23-1* allele are albino and fail to give rise to viable plants, which is due to the *agl23-1* mutant embryo being unable to develop beyond the one-nucleate stage [54]. *PIN1* downregulation leads to embryo sacs arrest at the one-nucleate and two-nucleate stage [55]. While the female gametophyte cells of *myb98* mutant showed aberrant morphology after the eight-nucleate stage [53]. In our results, why not all female gametophytes aborted at the two-nucleate stage, and some progressed to the four and eight-cell stage is unclear. It is likely that the developmental synchrony of female gametophytes was impaired by the loss of *NOP2*.

To study NOP2 function post fertilization, we used artificial miRNAs targeting NOP2 mRNA. Recovered transgenic lines had a range of phenotypes allowing us to study ribosome function at the post embryo stage. An alternative approach could have been driving NOP2 expression by a cell or organ specific promoter, like ABI3, in the *nop2* mutant that expresses predominantly in the female gametophyte and early seed development, and is lowly expressed in tissues developed post germination. Other approaches that could be used include

Cas9-genome editing to generate a *nop2* allelic series or cell-specific mutant alleles, or BRAINBOW-NOP2 complementation and Cre-Lox recombination to study cell autonomous and non- autonomous effects [56]–[58].

NOP2A positively regulates seedling growth. Previously reported phenotypes of pointed early-stage rosette leaves and shorter roots in *nop2a* mutants were confirmed in our study [59]. The pointed leaves of *nop2a* mutants, namely leaf abaxialization phenotype, was reported to be because of a cell proliferation defect [29]. The pointed rosette leaves were exclusively observed at the two to four leaf stage only in our study and later recovered to a wild type-type shape. This may result from different *NOP2*-induced methylation levels at different stages of plant growth, for example juvenile and adult leaves. This speculation is worthwhile testing in future research.

The importance of the methylation activity of three NOP2 paralogs, NOP2A, NOP2B and NOP2C was elucidated. Our previous research suggested that NSUN5 and NOP2A were required for methylation of C2268 and C2860 in nuclear LSU 25S rRNA in *A. thaliana* [10]. I explored eight candidate m^5C sites in this study on WT, *nop2b nop2c*, *amiR_NOP2A*, *amiR_NOP2A nop2b* and *amiR_NOP2A nop2b nop2c*. The methylation in chloroplast and mitochondrial rRNAs remained unchanged in WT and all *nop2* mutant lines. Likely another RNA methyltransferases, for example bacterial Fmu, contributes to the methylation [60]. It may be possible that the rRNA was demethylated before being exported into the chloroplast and mitochondria and hence not detected in our analysis. For the nuclear 25S rRNA rRNA methylation site C2268, the methylation level significantly reduced in the *amiR_NOP2A nop2b nop2c* mutant compared to other single or double mutants and WT. While for nuclear rRNA methylation sites C2860 at 25S rRNA, the difference between double and triple mutants is not very clear, which indicates the redundant activity among *NOP2A, NOP2B* and *NOP2C* in methylation process at some sites.

The absence of NOP2 was previously shown to corelate with a reduction of ribosomal subunits in multiple species. Data in yeast demonstrated that Nop2p depletion impairs the processing of the 35S pre-rRNA and processing of the 27S pre-rRNA is greatly reduced, resulting in lower steady-state levels of the

25S and 5.8S rRNAs [61]. Additionally, six temperature sensitive *nop2* mutants exhibited dramatic reductions in levels of 60S ribosome subunits, as well the 25S rRNA defection under non-permissive conditions in *S. cerevisiae* [62]. In mammals, RNAi-mediated NOP2 depletion leads to reduced developmental potential and decreased abundance of ribosome RNA in bovine early embryos [22]. Our study also analysed the influence of NOP2 on the rRNA biogenesis. In our *Arabidopsis* experiments, rRNA intermediates were investigated by RT-qPCR and northern blotting, and we observed no difference between WT and the *nop2* mutants, which indicates that *Nop2* deletion did not exert an influence on the rRNA biogenesis. Surprisingly, when the *amiR_NOP2A nop2b nop2c* mutants were treated with antibiotics known to target ribosomal function, the distinct response of *amiR_NOP2A_nop2b nop2c* mutants suggests that the structure of ribosome may be changed [63]. The seeds of *amiR_NOP2A nop2b nop2c* cannot germinate on medium supplemented with cycloheximide, suggesting a defect in protein synthesis, possibly due to altered ribosome functions [50], [64]. It is conceivable that the depletion of *nop2* in *Arabidopsis* alters ribosome activity and therefore translation. Surprisingly, recently it was reported NOP2A plays a role in modulating the telomere length in *Arabidopsis* this may contribute to the abnormal cell proliferation in *nop2* mutants [65].

The role of three *Arabidopsis* NOP2 paralogs, NOP2A, NOP2B and NOP2C, in ribosomal methylation and plant growth and development are beginning to be illustrated. In this study, we elucidated that *NOP2* is essential for the early stages of ovule development in *Arabidopsis*, and functions as an rRNA methyltransferase and mutants substantially influence growth. It appears likely that the other rRNA methyltransferase also plays vital role in growth regulation and remain to be explored.

2.6. References

[1] P. Boccaletto *et al.*, “MODOMICS: A database of RNA modification pathways. 2017 update,” *Nucleic Acids Res*, vol. 46, no. D1, pp. D303–D307, 2018, doi: 10.1093/nar/gkx1030.

[2] C. S. Chow, T. N. Lamichhane, and S. K. Mahto, “Expanding the nucleotide repertoire of the ribosome with post-transcriptional modifications,” ACS Chemical Biology, vol. 2, no. 9. ACS Chem Biol, pp. 610–619, Sep. 2007. doi: 10.1021/cb7001494.

[3] A. Gigova, S. Duggimpudi, T. Pollex, M. Schaefer, and M. Koš, “A cluster of methylations in the domain IV of 25S rRNA is required for ribosome stability,” *RNA*, vol. 20, no. 10, pp. 1632–1644, Oct. 2014, doi: 10.1261/rna.043398.113.

[4] Y. Motorin, F. Lyko, and M. Helm, “5-methylcytosine in RNA: Detection, enzymatic formation and biological functions,” *Nucleic Acids Res*, vol. 38, no. 5, pp. 1415–1430, 2009, doi: 10.1093/nar/gkp1117.

[5] D. D. Piekna-Przybylska, W. A. Decatur, and M. J. Fournier, “The 3D rRNA modification maps database: With interactive tools for ribosome analysis,” *Nucleic Acids Res*, vol. 36, no. SUPPL. 1, pp. 178–183, 2008, doi: 10.1093/nar/gkm855.

[6] D. Piekna-Przybylska, W. A. Decatur, and M. J. Fournier, “New bioinformatic tools for analysis of nucleotide modifications in eukaryotic rRNA,” *Rna*, vol. 13, no. 3, pp. 305–312, 2007, doi: 10.1261/rna.373107.

[7] E. Emmott, M. Jovanovic, and N. Slavov, “Ribosome Stoichiometry: From Form to Function,” *Trends Biochem Sci*, vol. 44, no. 2, pp. 95–109, Feb. 2019, doi: 10.1016/J.TIBS.2018.10.009.

[8] S. Granneman and S. J. Baserga, “Ribosome biogenesis: of knobs and RNA processing,” *Exp Cell Res*, vol. 296, no. 1, pp. 43–50, May 2004, doi: 10.1016/J.YEXCR.2004.03.016.

[9] S. Sharma, J. Yang, P. Watzinger, P. Kötter, and K. D. Entian, “Yeast Nop2

and Rcm1 methylate C2870 and C2278 of the 25S rRNA, respectively," *Nucleic Acids Res*, vol. 41, no. 19, pp. 9062–9076, 2013, doi: 10.1093/nar/gkt679.

[10] A. L. Burgess, R. David, and I. R. Searle, "Conservation of tRNA and rRNA 5-methylcytosine in the kingdom Plantae," *BMC Plant Biol*, vol. 15, no. 1, pp. 1–17, 2015, doi: 10.1186/s12870-015-0580-8.

[11] G. M. Veldman *et al.*, "The primary and secondary structure of yeast 26S rRNA," *Nucleic Acids Res*, vol. 9, no. 24, pp. 6935–6952, 1981, doi: 10.1093/nar/9.24.6935.

[12] J. A. Kowalak, S. C. Pomerantz, P. F. Crain, and J. A. Mccloskey, "A novel method for the determination of posttranscriptional modification in RNA by mass spectrometry," *Nucleic Acids Res*, vol. 21, no. 19, pp. 4577–4585, 1993, doi: 10.1093/nar/21.19.4577.

[13] N. M. Andersen and S. Douthwaite, "YebU is a m5C Methyltransferase Specific for 16 S rRNA Nucleotide 1407," *J Mol Biol*, vol. 359, no. 3, pp. 777–786, Jun. 2006, doi: 10.1016/J.JMB.2006.04.007.

[14] J. E. Squires *et al.*, "Widespread occurrence of 5-methylcytosine in human coding and non-coding RNA," *Nucleic Acids Res*, vol. 40, no. 11, pp. 5023–5033, 2012, doi: 10.1093/nar/gks144.

[15] V. Khoddami and B. R. Cairns, "Identification of direct targets and modified bases of RNA cytosine methyltransferases," *Nat Biotechnol*, vol. 31, no. 5, pp. 458–464, May 2013, doi: 10.1038/nbt.2566.

[16] S. Hussain *et al.*, "NSun2-mediated cytosine-5 methylation of vault noncoding RNA determines its processing into regulatory small RNAs," *Cell Rep*, vol. 4, no. 2, pp. 255–261, Jul. 2013, doi: 10.1016/j.celrep.2013.06.029.

[17] "Methylated regions of hamster mitochondrial ribosomal RNA: structural and functional correlates." https://www.ncbi.nlm.nih.gov/pmc/articles/PMC326695/ (accessed Apr. 26, 2020).

[18] M. D. Metodiev *et al.*, “NSUN4 Is a Dual Function Mitochondrial Protein Required for Both Methylation of 12S rRNA and Coordination of Mitoribosomal Assembly,” *PLoS Genet*, vol. 10, no. 2, Feb. 2014, doi: 10.1371/journal.pgen.1004110.

[19] A. Pavlopoulou and S. Kossida, “Phylogenetic analysis of the eukaryotic RNA (cytosine-5)-methyltransferases,” *Genomics*, vol. 93, no. 4, pp. 350–357, 2009, doi: 10.1016/j.ygeno.2008.12.004.

[20] G. Bourgeois et al., “Eukaryotic rRNA modification by yeast 5-methylcytosine-methyltransferases and human proliferation-associated antigen p120,” PLoS One, vol. 10, no. 7, pp. 1–16, 2015, doi: 10.1371/journal.pone.0133321.

[21] Y. Gao *et al.*, “NOP2/Sun RNA methyltransferase 2 promotes tumor progression via its interacting partner RPL6 in gallbladder carcinoma,” *Cancer Sci*, vol. 110, no. 11, pp. 3510–3519, Nov. 2019, doi: 10.1111/cas.14190.

[22] H. Wang *et al.*, “The nucleolar protein NOP2 is required for nucleolar maturation and ribosome biogenesis during preimplantation development in mammals,” *The FASEB Journal*, vol. 34, no. 2, pp. 2715–2729, Feb. 2020, doi: 10.1096/fj.201902623R.

[23] W. Cui, J. Pizzollo, Z. Han, C. Marcho, K. Zhang, and J. Mager, “Nop2 is required for mammalian preimplantation development,” *Mol Reprod Dev*, vol. 83, no. 2, pp. 124–131, Feb. 2016, doi: 10.1002/mrd.22600.

[24] P. Chen, G. Jäger, and B. Zheng, “Transfer RNA modifications and genes for modifying enzymes in Arabidopsis thaliana,” *BMC Plant Biol*, vol. 10, pp. 1–19, 2010, doi: 10.1186/1471-2229-10-201.

[25] M. Y. King and K. L. Redman, “RNA methyltransferases utilize two cysteine residues in the formation of 5-methylcytosine,” *Biochemistry*, vol. 41, no. 37, pp. 11218–11225, 2002, doi: 10.1021/bi026055q.

[26] Y. Liu and D. v. Santi, “m5C RNA and m5C DNA methyl transferases use different cysteine residues as catalysts,” *Proc Natl Acad Sci U S A*, vol. 97, no.

15, pp. 8263–8265, 2000, doi: 10.1073/pnas.97.15.8263.

[27] P. G. Foster, C. R. Nunes, P. Greene, D. Moustakas, and R. M. Stroud, “The First Structure of an RNA m5C Methyltransferase, Fmu, Provides Insight into Catalytic Mechanism and Specific Binding of RNA Substrate,” *Structure*, vol. 11, no. 12, pp. 1609–1620, 2003, doi: 10.1016/j.str.2003.10.014.

[28] H. Wu *et al.*, “WUSCHEL triggers innate antiviral immunity in plant stem cells,” *Science (1979)*, vol. 370, no. 6513, pp. 227–231, Oct. 2020, doi: 10.1126/science.abb7360.

[29] K. Kojima, J. Tamura, H. Chiba, K. Fukada, H. Tsukaya, and G. Horiguchi, “Two nucleolar proteins, GDP1 and OLI2, function as ribosome biogenesis factors and are preferentially involved in promotion of leaf cell proliferation without strongly affecting leaf adaxial–abaxial patterning in Arabidopsis thaliana,” *Front Plant Sci*, vol. 8, p. 2240, Jan. 2018, doi: 10.3389/fpls.2017.02240.

[30] A. Capron, S. Chatfield, N. Provart, and T. Berleth, “Embryogenesis: Pattern Formation from a Single Cell,” *Arabidopsis Book*, vol. 7, p. e0126, Jan. 2009, doi: 10.1199/tab.0126.

[31] T. Laux and G. Jürgens, “Embryogenesis: A new start in life,” *Plant Cell*, vol. 9, no. 7. American Society of Plant Physiologists, pp. 989–1000, Jul. 01, 1997. doi: 10.1105/tpc.9.7.989.

[32] D. Q. Shi and W. C. Yang, “Ovule development in Arabidopsis: Progress and challenge,” *Curr Opin Plant Biol*, vol. 14, no. 1, pp. 74–80, 2011, doi: 10.1016/j.pbi.2010.09.001.

[33] V. Sundaresan and M. Alandete-Saez, “Pattern formation in miniature: The female gametophyte of flowering plants,” *Development*, vol. 137, no. 2. Oxford University Press for The Company of Biologists Limited, pp. 179–189, Jan. 15, 2010. doi: 10.1242/dev.030346.

[34] J. Liu and L. J. Qu, “Meiotic and mitotic cell cycle mutants involved in gametophyte development in arabidopsis,” *Molecular Plant*, vol. 1, no. 4. Oxford

University Press, pp. 564–574, Jul. 01, 2008. doi: 10.1093/mp/ssn033.

[35] H. L. Tsai, W. L. Lue, K. J. Lu, M. H. Hsieh, S. M. Wang, and J. Chen, “Starch Synthesis in Arabidopsis Is Achieved by Spatial Cotranscription of Core Starch Metabolism Genes,” *Plant Physiol*, vol. 151, no. 3, p. 1582, 2009, doi: 10.1104/PP.109.144196.

[36] L. Fan, Y. Wang, H. Wang, and W. Wu, “In vitro Arabidopsis pollen germination and characterization of the inward potassium currents in Arabidopsis pollen grain protoplasts,” *J Exp Bot*, vol. 52, no. 361, pp. 1603–1614, Aug. 2001, doi: 10.1093/JEXBOT/52.361.1603.

[37] R. Yadegari and G. N. Drews, “Female gametophyte development,” *Plant Cell*, vol. 16, no. SUPPL. American Society of Plant Biologists, pp. S133–S141, Jun. 01, 2004. doi: 10.1105/tpc.018192.

[38] C. A. Christensen, E. J. King, J. R. Jordan, and G. N. Drews, “Megagametogenesis in Arabidopsis wild type and the Gf mutant,” *Sex Plant Reprod*, vol. 10, no. 1, pp. 49–64, 1997, doi: 10.1007/s004970050067.

[39] D. Q. Shi, J. Liu, Y. H. Xiang, D. Ye, V. Sundaresan, and W. C. Yang, “Slow walker1, essential for gametogenesis in Arabidopsis, encodes a WD40 protein involved in 18S ribosomal RNA biogenesis,” *Plant Cell*, vol. 17, no. 8, pp. 2340–2354, Aug. 2005, doi: 10.1105/tpc.105.033563.

[40] N. Abbasi *et al.*, “{APUM23}, a nucleolar Puf domain protein, is involved in pre-ribosomal {RNA} processing and normal growth patterning in Arabidopsis.,” *Plant J*, vol. 64, no. 6, pp. 960–976, Dec. 2010, doi: 10.1111/j.1365-{313X}.2010.04393.x.

[41] I. Ohbayashi, M. Konishi, K. Ebine, and M. Sugiyama, “Genetic identification of Arabidopsis RID2 as an essential factor involved in pre-rRNA processing,” *Plant Journal*, vol. 67, no. 1, pp. 49–60, 2011, doi: 10.1111/j.1365-313X.2011.04574.x.

[42] Q. Guo *et al.*, “Arabidopsis TRM5 encodes a nuclear-localised bifunctional tRNA guanine and inosine-N1-methyltransferase that is important for growth,”

PLoS One, vol. 14, no. 11, p. e0225064, Nov. 2019, doi: 10.1371/journal.pone.0225064.

[43] J. M. Alonso *et al.*, “Genome-wide insertional mutagenesis of Arabidopsis thaliana,” *Science*, vol. 301, no. 5633, pp. 653–657, Aug. 2003, doi: 10.1126/SCIENCE.1086391.

[44] S. J. Clough and A. F. Bent, “Floral dip: a simplified method for Agrobacterium-mediated transformation of Arabidopsis thaliana,” *Plant J*, vol. 16, no. 6, pp. 735–743, Dec. 1998, doi: 10.1046/J.1365-313X.1998.00343.X.

[45] S. J. Harrison, E. K. Mott, K. Parsley, S. Aspinall, J. C. Gray, and A. Cottage, “A rapid and robust method of identifying transformed Arabidopsis thaliana seedlings following floral dip transformation,” *Plant Methods*, vol. 2, no. 1, pp. 1–7, Nov. 2006, doi: 10.1186/1746-4811-2-19/FIGURES/4.

[46] M. D. Curtis and U. Grossniklaus, “A Gateway Cloning Vector Set for High-Throughput Functional Analysis of Genes in Planta,” *Plant Physiol*, vol. 133, no. 2, pp. 462–469, Oct. 2003, doi: 10.1104/pp.103.027979.

[47] D. Maruyama, T. Sugiyama, T. Endo, and S. I. Nishikawa, “Multiple BiP Genes of Arabidopsis thaliana are Required for Male Gametogenesis and Pollen Competitiveness,” *Plant Cell Physiol*, vol. 55, no. 4, pp. 801–810, Apr. 2014, doi: 10.1093/PCP/PCU018.

[48] M. Schaefer, T. Pollex, K. Hanna, and F. Lyko, “RNA cytosine methylation analysis by bisulfite sequencing,” *Nucleic Acids Res*, vol. 37, no. 2, p. 12, 2008, doi: 10.1093/nar/gkn954.

[49] R. David *et al.*, “Transcriptome-wide mapping of RNA 5-methylcytosine in arabidopsis mRNAs and noncoding RNAs,” *Plant Cell*, vol. 29, no. 3, pp. 445–460, 2017, doi: 10.1105/tpc.16.00751.

[50] I. Ohbayashi, M. Konishi, K. Ebine, and M. Sugiyama, “Genetic identification of Arabidopsis RID2 as an essential factor involved in pre-rRNA processing,” *Plant J*, vol. 67, no. 1, pp. 49–60, Jul. 2011, doi: 10.1111/J.1365-313X.2011.04574.X.

[51] T. Czechowski, M. Stitt, T. Altmann, M. K. Udvardi, and W. R. Scheible, “Genome-Wide Identification and Testing of Superior Reference Genes for Transcript Normalization in Arabidopsis,” *Plant Physiol*, vol. 139, no. 1, p. 5, 2005, doi: 10.1104/PP.105.063743.

[52] K. E. Bohnsack, C. Höbartner, and M. T. Bohnsack, “Eukaryotic 5-methylcytosine (M 5 C) RNA methyltransferases: Mechanisms, cellular functions, and links to disease,” *Genes*, vol. 10, no. 2. MDPI AG, Feb. 01, 2019. doi: 10.3390/genes10020102.

[53] D. Susaki, T. Suzuki, D. Maruyama, M. Ueda, T. Higashiyama, and D. Kurihara, “Dynamics of the cell fate specifications during female gametophyte development in Arabidopsis,” *PLoS Biol*, vol. 19, no. 3, p. e3001123, Mar. 2021, doi: 10.1371/JOURNAL.PBIO.3001123.

[54] M. Colombo, S. Masiero, S. Vanzulli, P. Lardelli, M. M. Kater, and L. Colombo, “AGL23, a type I MADS-box gene that controls female gametophyte and embryo development in Arabidopsis,” *The Plant Journal*, vol. 54, no. 6, pp. 1037–1048, Jun. 2008, doi: 10.1111/J.1365-313X.2008.03485.X.

[55] L. Ceccato *et al.*, “Maternal Control of PIN1 Is Required for Female Gametophyte Development in Arabidopsis,” *PLoS One*, vol. 8, no. 6, p. e66148, Jun. 2013, doi: 10.1371/JOURNAL.PONE.0066148.

[56] J. X. Tang, A. Pyle, R. W. Taylor, and M. Oláhová, “Interrogating Mitochondrial Biology and Disease Using CRISPR/Cas9 Gene Editing,” *Genes (Basel)*, vol. 12, no. 10, p. 1604, Oct. 2021, doi: 10.3390/GENES12101604.

[57] L. Gilbertson, “Cre-lox recombination: Cre-ative tools for plant biotechnology,” *Trends Biotechnol*, vol. 21, no. 12, pp. 550–555, Dec. 2003, doi: 10.1016/j.tibtech.2003.09.011.

[58] T. A. Weissman and Y. A. Pan, “Brainbow: New Resources and Emerging Biological Applications for Multicolor Genetic Labeling and Analysis,” *Genetics*, vol. 199, no. 2, p. 293, Feb. 2015, doi: 10.1534/GENETICS.114.172510.

[59] U. Fujikura, G. Horiguchi, M. R. Ponce, J. L. Micol, and H. Tsukaya,

“Coordination of cell proliferation and cell expansion mediated by ribosome-related processes in the leaves of Arabidopsis thaliana,” *Plant J*, vol. 59, no. 3, pp. 499–508, Aug. 2009, doi: 10.1111/J.1365-313X.2009.03886.X.

[60] C. Hébrard *et al.*, “Identification of differentially methylated regions during vernalization revealed a role for RNA methyltransferases in bolting,” *J Exp Bot*, vol. 64, no. 2, pp. 651–663, Jan. 2013, doi: 10.1093/jxb/ers363.

[61] B. Hong, J. S. Brockenbrough, P. Wu, and J. P. Aris, “Nop2p is required for pre-rRNA processing and 60S ribosome subunit synthesis in yeast.,” *Mol Cell Biol*, vol. 17, no. 1, pp. 378–388, 1997, doi: 10.1128/mcb.17.1.378.

[62] B. Hong, K. Wu, J. S. Brockenbrough, P. Wu, and J. P. Aris, “Temperature sensitive nop2 alleles defective in synthesis of 25S rRNA and large ribosomal subunits in Saccharomyces cerevisiae,” *Nucleic Acids Res*, vol. 29, no. 14, pp. 2927–2937, Jul. 2001, doi: 10.1093/nar/29.14.2927.

[63] P. Zhu *et al.*, “Arabidopsis small nucleolar {RNA} monitors the efficient pre-{rRNA} processing during ribosome biogenesis.,” *Proc Natl Acad Sci U S A*, vol. 113, no. 42, pp. 11967–11972, Oct. 2016, doi: 10.1073/pnas.1614852113.

[64] L. Rajjou, K. Gallardo, I. Debeaujon, J. Vandekerckhove, C. Job, and D. Job, “The effect of α-amanitin on the arabidopsis seed proteome highlights the distinct roles of stored and neosynthesized mRNAs during germination,” *Plant Physiol*, vol. 134, no. 4, pp. 1598–1613, Apr. 2004, doi: 10.1104/pp.103.036293.

[65] L. R. Abdulkina *et al.*, “Components of the ribosome biogenesis pathway underlie establishment of telomere length set point in Arabidopsis”, doi: 10.1038/s41467-019-13448-z.

2.7. Supplementary data

Table 1. PCR detection of *nop2* alleles in F_1 plants derived from WT x *nop2a -/+ nop2b -/+*

F_1 population	Expected segregation (%)	Segregation results (%, n=71)
nop2a+/+ *nop2b* +/+	25	32
nop2a -/+ *nop2b* +/+	25	28
nop2a +/+ *nop2b* -/+	25	37
nop2a -/+ *nop2b* -/+	25	2
Total	100	100

* Statistical difference from the expectation as determined by the χ^2 test.

Table 2. Primers used in this chapter

Primers	Sequence (5'-3')
salk_129648_LP	GCCTACGTCCATCCGAACTA
salk_129648_RP	AGGTGAAGAAAAGGGAAAGACA
salk_054685_LP	AGGCAACAACATACCTTTTGC
salk_054685_RP	AATCTACATCGCATGGGAGTG

sail_1263_B04_LP	TGAGATGGGCTTATTCATTGC
sail_1263_B04_RP	AGCTAAATGCGCCTAAAGGAG
Pro_NOP2A_F	TGAGCCCAATAACTATATGGTGCCTTG
Pro_NOP2A_R	ACCAGCATTTAGGTTTAGTGGCTTTC
5'ETS_F	CTCATCCGTCCGTCCTTCGGGCAA
5'ETS_R	GCATTCATCGATCACGGCAA
ITS1_F	TCGATACCTGTCCAAAACAG
ITS1_R	AGACTTCAGTTCGCAGC
ITS2_F	ATCGTCGTCCCTCACCATCC
ITS2_R	GGGGTCGCTATATGGACTTTG
5.8S_F	CGACTCTCGGCAACGGATAT
5.8S_R	TTGTGACACCCAGGCAGACG
18S_F	GACTCAACACGGGGAAACTTAC
18S_R	GTAGCTAGTTAGCAGGCTGAGGTC
25S_F	GTAAACGGCGGGAGTAACTATG
25S_R	GGACTAGAGTCAAGCTCAACAGG
PDF2_F	GGGCAATGCAGCATATAGTTC

PDF2_R	TGGGTCTTCACTTAGCTCCAC
SAND (At2g28390)_F	CAGACAAGGCGATGGCGATA
SAND (At2g28390)_R	GCTTTCTCTCAAGGGTTTCTGGGT
Pro_NOP2B_F	TCACTTTACTTCTCTGGTTTGAAAGA
Pro_NOP2B_R	GAATCTAGTAAAGATGGAGGATGAGC
Pro_NOP2C_F	TAAACAAGCAGATGAATATGATGGA
Pro_NOP2C_R	AGGAGACTGGAGAGATAGAGAGAGC

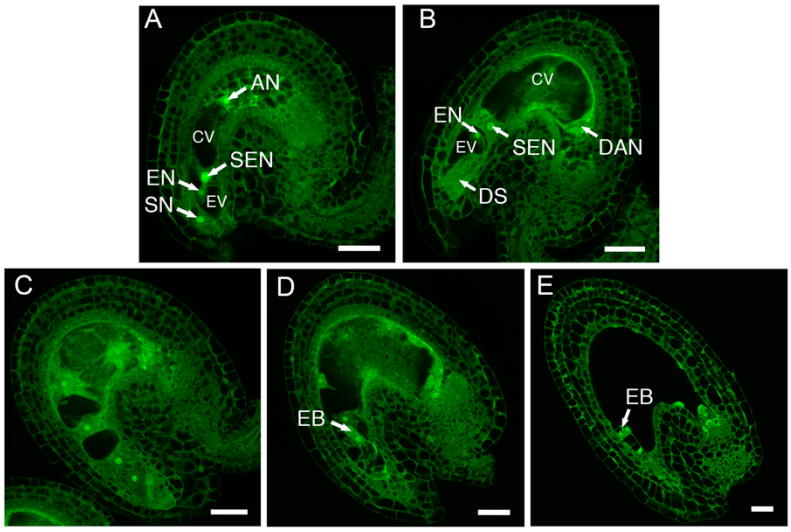

Fig 1. Female gametophyte development of WT after FG5 stage.

(A) Seven-celled female gametophyte at FG6 stage. **(B)** FG8 stage showing the three-celled female gametophyte. The female gametophyte consists of the egg cell, central cell, and one persistent synergid cell. **(C)-(E)** Development of an embryo from the zygote to early globular stages. Images were taken using a confocal microscope with an excitation beam at 488nm. AN, antipodal nucleus; CN, central cell nucleus; CPN, chalazal polar nucleus; CV, central vacuole; DAN, degenerated antipodal nucleus; DS, degenerated synergid; EB,

embryo; EN, egg cell nucleus; EV, egg cell vacuole; MPN, micropylar polar nucleus; SEN, secondary endosperm nucleus; SN, synergid nucleus; V, vacuole. Scale bar, 25 μm.

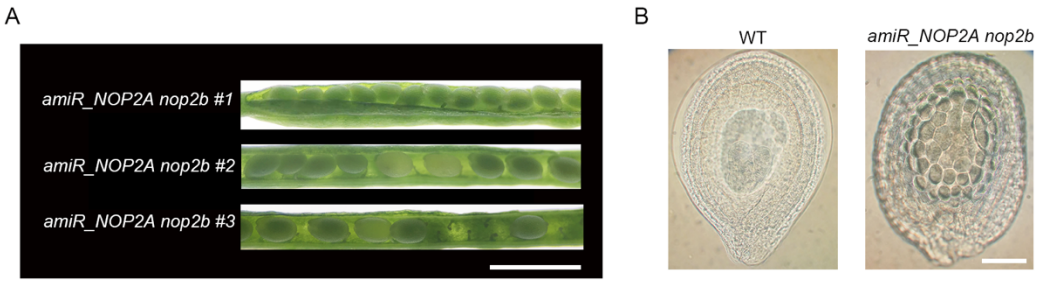

Fig 2. Seeds in independent *amiR_NOP2A nop2b* lines aborted at various stages of development.

(A) Opened siliques from three transgenic *amiR_NOP2A nop2b* lines. Line 1 had no seed abortion, line 2 had seed abortion at globular stage (white seeds) and line 3 had abortion at the early ovule development stage. Scale bar = 2 mm. **(B)** Microscopy of a translucent seed from line 2 (left) in panel A appeared to abort at the globular stage compared to WT (left) seed that developed to the two-cotyledon embryo stage. Scale bar = 25 μm.

The plasmid structures used in this chapter

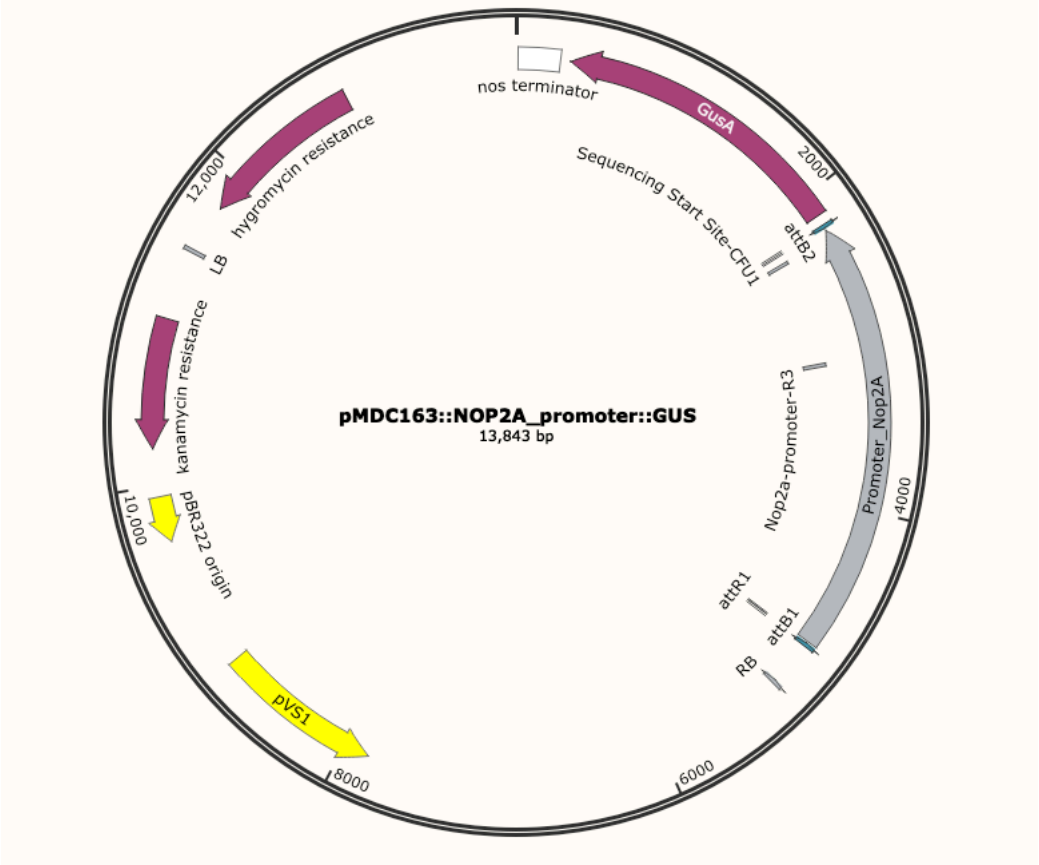

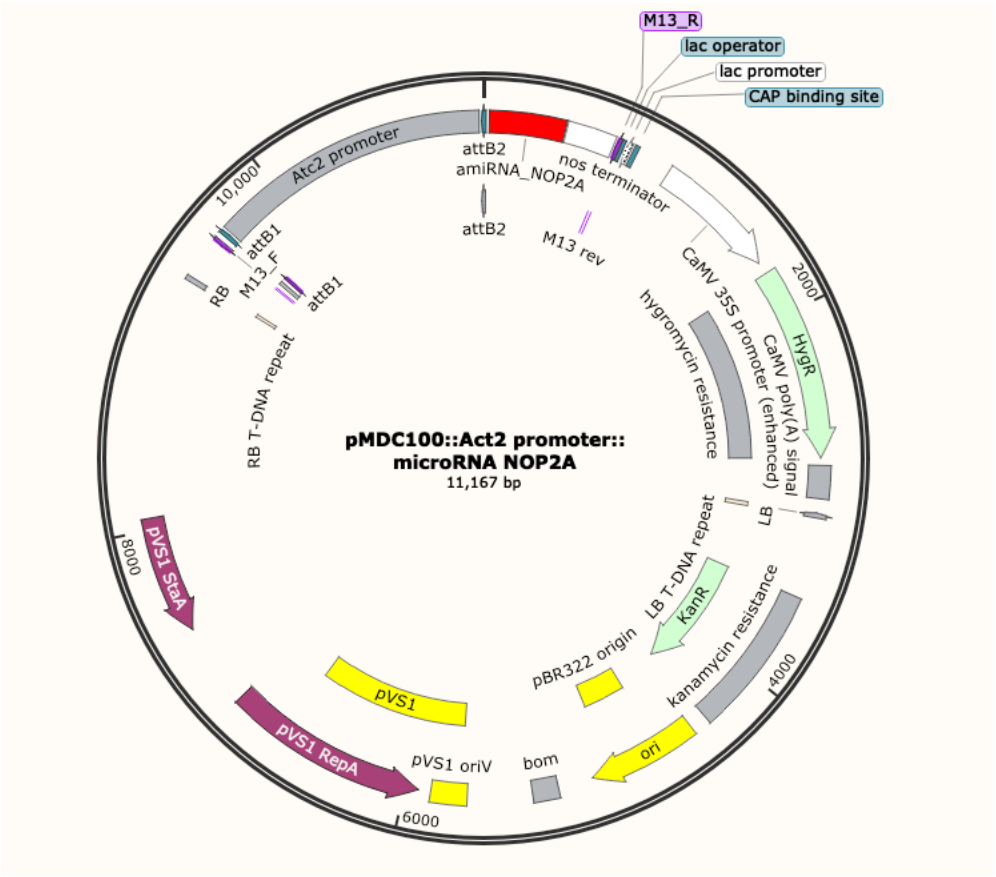
M13_R
lac operator
lac promoter
CAP binding site
attB2
amiRNA_NOP2A
attB2
nos terminator
M13 rev
Atc2 promoter
10,000
attB1
M13_F
attB1
RB
RB T-DNA repeat
pMDC100::Act2 promoter::
microRNA NOP2A
11,167 bp
CaMV 35S promoter (enhanced)
hygromycin resistance
CaMV poly(A) signal
HygR
2000
LB
LB T-DNA repeat
KanR
kanamycin resistance
4000
pBR322 origin
ori
bom
pVS1 oriV
pVS1
pVS1 RepA
6000
8000
pVS1 StaA

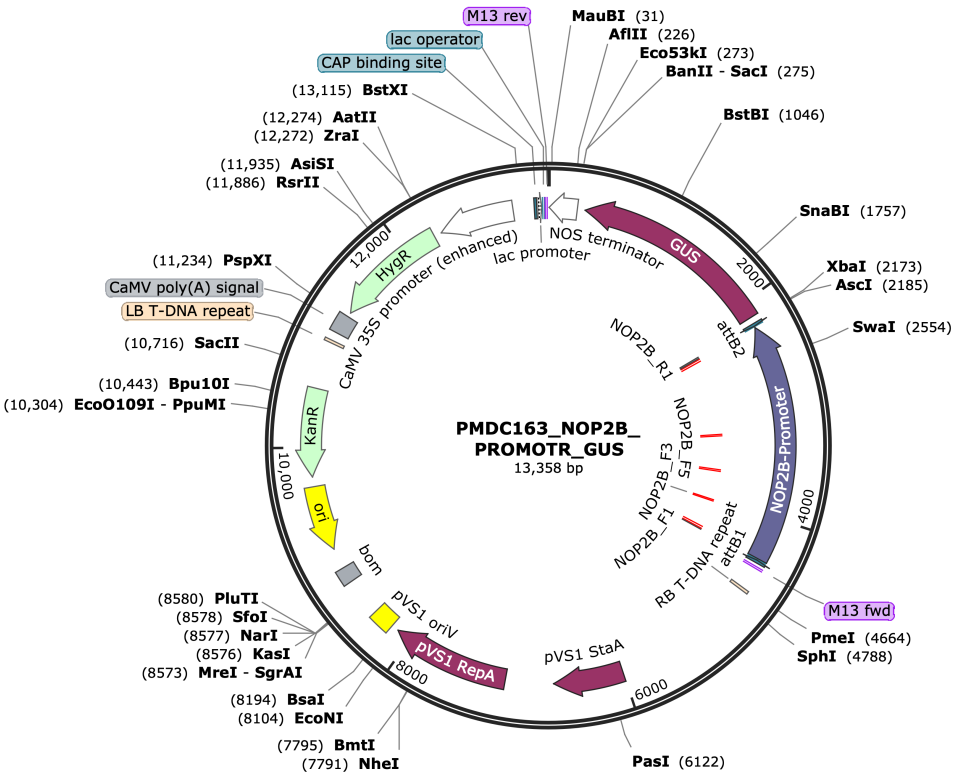
Created with SnapGene®
M13 rev
lac operator
CAP binding site
(13,115) BstXI
(12,274) AatII
(12,272) ZraI
(11,935) AsiSI
(11,886) RsrII
(11,234) PspXI
CaMV poly(A) signal
LB T-DNA repeat
(10,716) SacII
(10,443) Bpu10I
(10,304) EcoO109I - PpuMI
(8580) PluTI
(8578) SfoI
(8577) NarI
(8576) KasI
(8573) MreI - SgrAI
(8194) BsaI
(8104) EcoNI
(7795) BmtI
(7791) NheI
MauBI (31)
AflII (226)
Eco53kI (273)
BanII - SacI (275)
BstBI (1046)
SnaBI (1757)
XbaI (2173)
AscI (2185)
SwaI (2554)
M13 fwd
PmeI (4664)
SphI (4788)
PasI (6122)
PMDC163_NOP2B_
PROMOTR_GUS
13,358 bp
NOS terminator
lac promoter
CaMV 35S promoter (enhanced)
HygR
12,000
GUS
2000
attB2
NOP2B_R1
NOP2B_F3
NOP2B_F5
NOP2B_F1
NOP2B-Promoter
4000
RB T-DNA repeat
attB1
KanR
ori
bom
pVS1 oriV
pVS1 RepA
pVS1 StaA
8000
6000
10,000

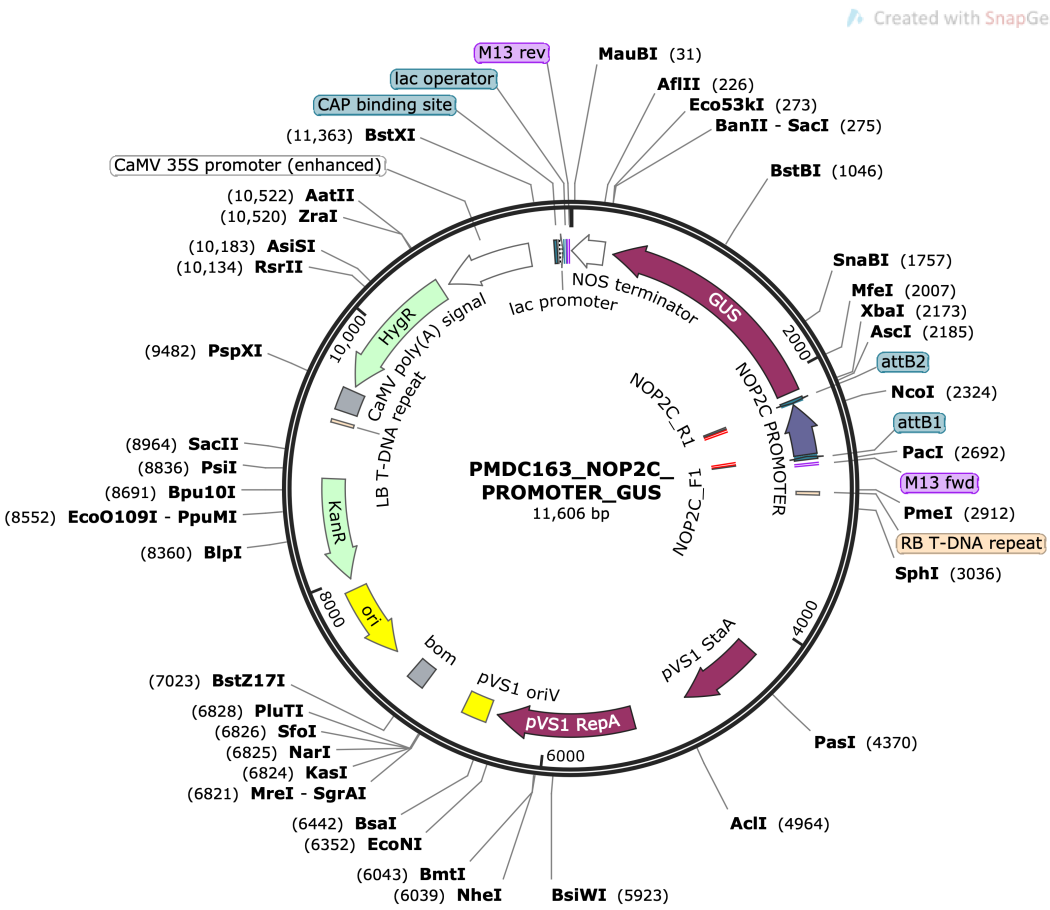
Created with SnapGene®
M13 rev
MauBI (31)
lac operator
AflII (226)
CAP binding site
Eco53kI (273)
(11,363) BstXI
BanII - SacI (275)
CaMV 35S promoter (enhanced)
BstBI (1046)
(10,522) AatII
(10,520) ZraI
(10,183) AsiSI
(10,134) RsrII
SnaBI (1757)
MfeI (2007)
XbaI (2173)
AscI (2185)
(9482) PspXI
attB2
NcoI (2324)
attB1
(8964) SacII
PacI (2692)
(8836) PsiI
M13 fwd
(8691) Bpu10I
PmeI (2912)
(8552) EcoO109I - PpuMI
RB T-DNA repeat
(8360) BlpI
SphI (3036)
PMDC163_NOP2C_
PROMOTER_GUS
11,606 bp
NOS terminator
lac promoter
GUS
NOP2C PROMOTER
NOP2C_R1
NOP2C_F1
HygR
CaMV poly(A) signal
LB T-DNA repeat
KanR
ori
bom
pVS1 oriV
pVS1 RepA
pVS1 StaA
10,000
2000
4000
6000
8000
(7023) BstZ17I
(6828) PluTI
(6826) SfoI
(6825) NarI
(6824) KasI
(6821) MreI - SgrAI
PasI (4370)
AclI (4964)
(6442) BsaI
(6352) EcoNI
(6043) BmtI
(6039) NheI
BsiWI (5923)

Chapter 3. Functional roles of plant RNases T2 and RNA modification 5-methylcytosine on oxidative stress-induced tRNA halves in *Arabidopsis thaliana*

3.1. Abstract

Transfer RNA cleavage triggered by stress is a conserved molecular process. tRNA halves originating from cleavage of the anticodon loop of the mature tRNA in response to stress is now recognised as important, although the ribonucleases required for producing the tRNA halves are only beginning to be uncovered in plants. Furthermore, the roles of tRNA modifications in tRNA cleavage are starting to be elucidated. This study aimed to elucidate the mechanism of tRNA cleavage in response to oxidative stress and explore the link between RNA 5-methylcytosine and *Arabidopsis* ribonuclease RNS2 in *A. thaliana*. Northern blotting and small RNA sequencing demonstrated that RNS1, RNS2 and RNS4 may be involved in tRNA cleavage into halves under oxidative stress. In RNS2 mutants, changes in pre-tRNA and mature tRNA profiles under oxidative stress were observed. Northern blotting data of *trm4b* and *rns2 trm4b* seedlings indicated that the 5-methylcytosine protects $tRNA^{Asp(GTC)}$ from cleavage by RNS2. Using a ribosome integrity assay, both *trm4b* and *rns2 trm4b* mutants exhibit the same hypersensitivity to hygromycin. Overall, the results in our study provide an understanding of tRNA cleavage in response to oxidative stress and establish a role for RNS proteins. Future work still needs to be conducted to disclose the complex link between m^5C modification and RNS2.

3.2. Introduction

Functionally being a connection between the mRNA and the polypeptide sequence of proteins, transfer RNAs (tRNAs) are present across all branches of life. Typically, the mature tRNAs are 76-90 nucleotides in length, forming a secondary cloverleaf structure with a D-loop, T-loop, anticodon loop, variable loop, and an acceptor stem [1]. In eukaryotes, the production of tRNAs is formed by transcription of a pre-tRNA by RNA polymerase III, removal of 5' and 3' sequences by RNase P and RNase Z, and finally the addition of CCA terminal nucleotides to the 3' end [2]. Apart from tRNAs canonical role in translation, tRNA abundance and processing into smaller functional RNA fragments in response to stimuli is now well established [3]–[5]. These observations were first observed in high-throughput sRNA sequencing data sets originating from various cellular non-coding RNAs. Initially thought of as random tRNA degradation products, sRNAs derived from tRNAs now appear to be modulated by specific biological processes and accumulated in multiple organisms and tissues [6], [7]. These tRNA-derived sRNAs are frequently separated into two main sub-classes based on their relative length and cleavage sites [8].

One kind of tRNA-derived RNAs are tRNA-derived fragments (tRFs) that are 19-30 nt in length and are formed from cleavage at either the T-loop to give so-called tRF-5s, or D-loop to give so-called tRF-3s. In *Arabidopsis,* tRFs production can be DICER-like dependent or DICER-like independent [9]. For example, DICER-like enzymes produce specific tRFs in the pollen of *Arabidopsis*, maize and rice [10], [11]. Deep sequencing data in mammalian cells revealed tRFs biogenesis is DICER dependent [12], [13]. The mechanism for tRFs biogenesis still needs to be fully elucidated.

tRNA halves are 31-40 nucleotides in length and are produced from tRNAs cleaved at the anticodon loop [14]. Accumulation of tRNA halves occurs under various cellular stresses, including oxidative stress, heat shock, phosphate starvation, amino acid starvation, ultraviolent irradiation or virus infection in diverse organisms. tRNA halves were first described in the bacterium

Escherichia coli and required the nuclease PrrC in 1990 [15], and are now described in yeast, mammalian cells, fruit flies, and plants by using high-throughput sequencing and northern blotting [16]–[19]. Several papers demonstrated the increased abundance of stress-induced tRNA halves are one of the protein synthesis regulatory pathways in response to stimuli. For example, the tRNA halves from ANGIOGENIN induction promote stress granule assembly in mammalian cells [20]. Recently, the 3 halves of $tRNA^{Thr}$ produced under nutrient deprivation interact with ribosomes and polysomes and then stimulate translation by facilitating mRNA loading during stress recovery [21].

As of yet, the investigation of ribonucleases cleaving the tRNA within the anticodon-loop is still waiting to be fully discovered. Yeast *Saccharomyces cerevisiae rny1Δ* strain does not produce tRNA halves under stress conditions, demonstrating that RNY1, the RNase T2 ribonuclease family member, isinvolved in tRNA cleavage [16]. In mammalian cells, the ANGIOGENIN, belonging to the RNase A family, mediates the production of tRFs and tRNA halves in response to stress [22]. Furthermore, it was discovered that DICER is required for processing tRNA halves under the condition of arsenite treatment in mammalian cells [23]. While the ribonucleases necessary for the tRNA cleavage in plants are still poorly understood. In *A. thaliana*, it is shown that RNS1, RNS2 and RNS3, the RNase T2 ribonuclease family member, are able to complement the yeast *rny1Δ* mutant strain, producing tRFs and 5' halves from $tRNA^{His(GTG)}$ and $tRNA^{Arg(ACG)}$ *in vitro* [9]. In addition, the RNS1 was reported to produce specific tRFs and tRNA halves in *A. thaliana* [5], [10]. In this paper, we systematically characterize the ribonucleases cleaving the tRNAs in *A. thaliana* under oxidative stress and explore the profile of tRNA halves with and without oxidative stress.

The link between RNA modifications has been gradually disclosed in multiple organisms. Modifications within the anti-codon loop of tRNAs have crucial roles in translation by preventing frameshifting, expanding codon recognition, and strengthening the codon-anticodon interaction [24]. By now, more than 90 chemical modifications have been found on tRNAs [25]. Among the identified

tRNA modifications, 5-methylcytosine (m^5C) plays a role in regulating tRNA cleavage. For example, in NSUN2 mutant mice subjected to stress, increased tRNAs cleavage mediated by the ribonuclease angiogenin was observed, resulting in an increased abundance of tRNA halves [26]. Furthermore, in tRNA methyltransferase DNMT2 mutant flies exposed to heat shock or oxidative stress, increased tRNA cleavage was observed, and in contrast, overexpression of DNMT2 reduced $tRNA^{Asp(GTC)}$ and $tRNA^{Gly(GCC)}$ cleavage [27]. Overall, compelling evidence shows tRNA m^5C sites prevents tRNAs cleavage by ribonuclease under stress. TRM4B, one of the paralogs of RNA-specific methyltransferase 4 (TRM4) in *Arabidopsis*, methylates some nuclear tRNAs and mRNAs as shown in our previous research [28]. *Arabidopsis trm4b* seedlings display increased sensitivity to oxidative stress, and genes in the oxidative response pathway are constitutively activated, suggesting a role of TRM4B in regulating oxidative stress responses. Furthermore, the abundance of some TRM4B methylated tRNAs was reduced in *trm4b* [29]. Many questions arise from these observations including the role of tRNA cleavage by TRM4B and RNase T2 ribonucleases.

3.3. Materials and methods

3.3.1. Plant materials and growth conditions

A. thaliana (Columbia ecotype) were grown in Phoenix Biosystem controlled environment rooms at 21°C under metal halide lights that provided a level of photosynthetic active radiation (PAR) of 110 µmol of photos/m^2/s [28]. For *in vitro* plant growth, seeds were gas-sterilized using 50 ml 12.5 % sodium hypochlorite and 1.25 ml 32% hydrochloric acid overnight and plated on ½ Murashige and Skoog (MS) medium supplemented with 1% sucrose, and then incubate at 4°C for three days. Plants were grown under long-day photoperiod conditions of 16 hrs light. Seeds of *A. thaliana* mutants *rns1* (SALKseq_078116.1), *rns2* (SALK_069588), *rns4* (SALKseq_055304.0) and *trm4b* (SALK_318_G04) were obtained from Arabidopsis Biological Resource Center (ABRC). Characterisation of the mutant alleles, *rns1*, *rns2*, *rns4, trm4b* and derived double mutants *rns2 trm4b* were previously described [1], [2]. Primers to detect *nop2* mutants were generated using the SIGnAL iSect Primer Design program (Supplementary Table 1).

Nucleotide sequence data for the following genes are available from The Arabidopsis Information Resource (TAIR) database under the following accession numbers: RNS1 (At2g02990), RNS2 (At2g39780), RNS3 (At1g26820), RNS4 (At1g14210) and TRM4B (At2g22400).

3.3.2. RNA extraction, library construction and sequencing

Total RNA was isolated from ten-day-old WT and *rns2* seedlings using TRIZOL Reagent. 20 ug of total RNA mixed with RNA gel loading buffer was loaded onto a 15% polyacrylamide gel and separated for 2 hrs at 100V, along with the microRNA ladder. An estimated gel slice corresponding to 30-40 nucleotides (nt) was transferred into a shredder column and spun at 13K rpm for 2 min into

a clean tube. Sterilised 0.3 M NaCl was added to the shredded gel fragments and rotated overnight and then the gel-purified RNA was precipitated using isopropanol and glycogen. 6 ul of the resuspended small RNA was used for library construction using the NEXTflex® Small RNA Sequencing Kit v3 for Illumina® Platform (Perkin Elmer) following the manufacturer's instructions. The small RNAs were sequenced on Illumina® Nextseq^{500} in single read mode of 75 cycles at the Australian Cancer Research Foundation (ACRF, Adelaide). A total of three replicates were sequenced for WT and *rns2*.

3.3.3. Small RNA sequencing data processing, alignment, clustering, and annotation

The quality of sRNA sequencing data was checked by ngsReports (https://github.com/UofABioinformaticsHub/ngsReports). The Illumina small RNA sequence adapter was trimmed by Trim Galore!, then the NEXTflex® Small RNA 3' adapter and the four random bases in both 3' and 5' adapters trimmed by the cutadapt (https://cutadapt.readthedocs.io/en/stable/installation.html). Redundant sequence reads were removed by seqcluster and the raw counts of unique reads were used for clustering analysis. The seqcluster prepare function was used to assign the ID to unique reads (https://github.com/lpantano/seqcluster), followed by alignment to *A. thaliana* TAIR10 (https://www.arabidopsis.org/) reference genome using the STAR aligner v2.5.3 [31], with the parameter --alignIntronMax 1 to disable soft-clipping during the alignment process. Next, the reads aligned were clustered using the cluster function and annotated using the Araport11 annotation [32]. Aligned short reads were clustered under metaclusters by regions of the alignment. For global sRNA profile detection, reads were normalised as recommended in BEDtools genomecov function (https://bedtools.readthedocs.io/en/latest/content-content/tools/genomecov.html) (Pei et al, unpublished).

3.3.4. Differential expression and Gene ontology (GO) analysis

The Trimmed Mean Method (TMM) was adopted to normalize the raw counts of the sRNA sequence data after being clustered [33], [34]. Differential expression analysis was performed using the ExactTest method within edgeR [33]. The p-value was corrected using Benjamin Hochberg correction. Differentially expressed tRNA loci were filtered by using the following criteria: logFC > 1.5, False Discovery Rate (FDR) < 0.01, and adjusted p-value < 0.01.

3.3.5. Oxidative treatment for seedlings

Gas-sterilized seeds were plated on ½ MS medium supplemented with 1% sucrose. After stratification at 4°C for three days, the plates were moved to the Phoenix Biosystem controlled environment rooms and were put vertically. Four days after germination, the seedlings were transferred to the ½ MS medium supplemented with 1% sucrose and 10 mM hydrogen peroxide for 4 hrs. Oxidative treated seedlings were collected and snap frozen in liquid nitrogen for subsequent RNA extraction.

3.3.6. Northern blotting for tRNA halves abundance detection

Total RNA was isolated from ten-days-old WT, *rns1*, *rns2, rns4, trm4b, rns1 rns2, rns2 rns4* and *rns2 trm4b* mutant using TRIZOL reagent. 10 ug of the total RNA was proceeded to separate the different sizes of RNA on 12.5% urea-polyacrylamide gel. After being transferred on the Amersham Hybond-N+membrance for 3.5 hrs, the gel was stained in SYBR gold, and the RNA was cross-linked on the membrane with a Stratalinker UV crosslinker. Prehybridization could be conducted for up to several hours at 68°C in 20 ul of the DIG easy Hyb Granules (Roche). 60 pmol of the 5-end Digoxin labelled oligonucleotides Hybridization was added into 6 ml DIG easy Hyb Granules to hybridise overnight at 40 °C (Supplementary Table 2). The membrane was

washed in low-stringency buffer (2X SSC, 0.1% SDS) twice and high-stringency buffer (0.1X SSC, 0.1% SDS) twice. The probe-target hybrid was localised with the anti-DIG-alkaline phosphatase antibody (Roche). The membrane was put into washing and blocking and detection buffer to visualise using the CDP-Star, ready to use (Roche). Finally, the membrane was imaged by the Bio-Rad Chemi-Doc MP Imaging System.

3.4. Results

3.4.1. Identification of *Arabidopsis* RNase T2 homologues

When I commenced my PhD, numerous experiments showed evidence that ribonucleases RNY1 and ANGIOGENIN are required for stress-induced tRNA cleavage in yeast and mammalian cells and no evidence was published in plants for a role of RNY1-like proteins [16], [22]. However, in 2019 Megel *et al* showed roles for RNS1 and RNS3 in tRNA half cleavage in *Arabidopsis*. Nevertheless, I will describe my experiments.

As the genome of the members of the RNase T2 family is highly conserved in all eukaryotic organisms, five ribonuclease paralogue members (RNS1, 2, 3, 4 and 5) in *A. thaliana* were identified [35], [36]. In this study, the amino acid sequence of yeast RNY 1 and *A. thaliana* RNS1, 2, 3, 4 and 5 were collected separately from the TAIR and the Saccharomyces Genome Database. Firstly, as we can see from Fig 3.1A, the analysis of evolutionary relationships among the RNase T2 ribonuclease showed that the RNS2 was clustered into a high-homology branch of *ScRny1*, the following are RNS4 and RNS1. Furthermore, two active histidine sites were identified in the multiple alignments (Fig 3.1B), which have been characterised to be a conserved RNaseT2 catalytic activity and are vital for the nuclease activity of *ScRny1* [37]. Finally, the data of the percent identity matrix from Clustal Omega shows that the RNS2, RNS4 and RNS1 share 24%, 23% and 27% sequence similarity with *ScRny1*. Therefore, this paper focuses on the RNS1, RNS2 and RNS4 in *A. thaliana*.

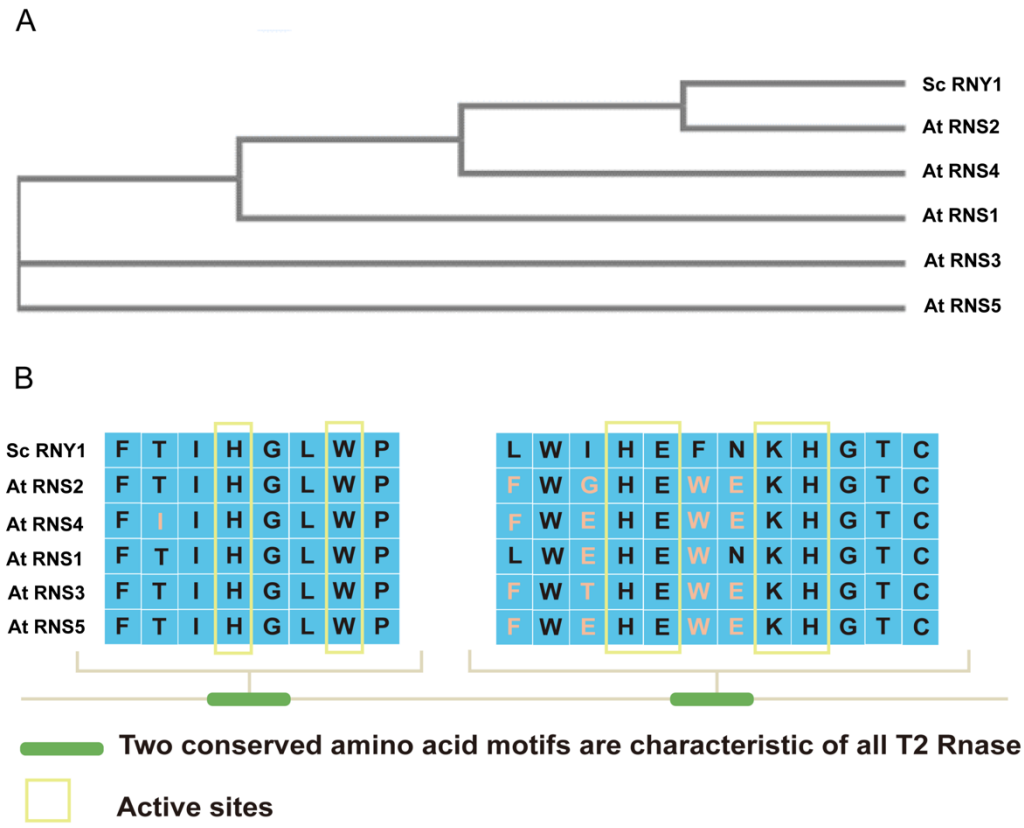

Figure 3.1: RNS1, RNS2 and RNS4 may be the main homologues of ribonucleases identified in *A. thaliana*.

(A) The phylogenetic tree was constructed by using the amino acid sequences of RNS1-5 (RNS1: At2g02990, RNS2: At2g39780, RNS3: At1g26820, RNS4: At1g14210, RNS5: At1g14220) in *Arabidopsis* and RNY1 of *S. cerevisiae*. The alignments and phylogenetic tree were performed by implementing Clustal Omega (EMBL-EBI, UK). **(B)** Multiple amino acid sequence alignment of *Arabidopsis* RNS domain and *S. cerevisiae* RNY1. The alignment was carried out by using Clustal Omega. Two T2 Rnase conserved amino acid motifs were identified. The yellow box represents active sites.

To confirm the function of RNS1, RNS2 and RNS4, the T-DNA insertion lines SALKseq_078116.1, SALK_069588, and SALKseq_055304.0, were chosen and screened for homozygous. We measured the mRNA abundance of *RNS1*, *RNS2* and *RNS4* and found almost no mRNA abundance in the homozygous T-DNA insertion mutants (Fig 3.2B). The insertion sites of each allele mutant were labelled as indicated in Fig 3.2A. The double mutants *rns1 rns2* and *rns2 rns4* were also made and screened for homozygous.

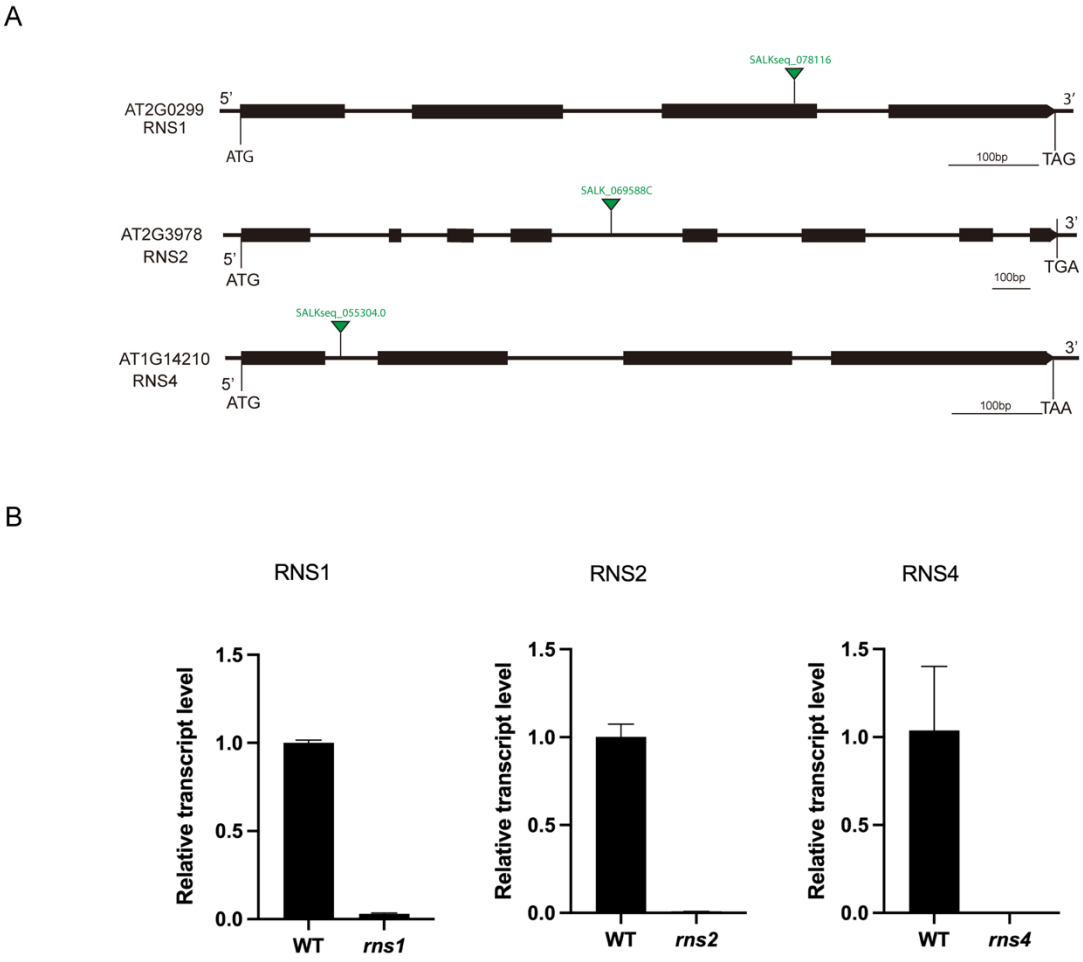

Figure 3.2: Identification of *rns* mutants in *A. thaliana*.

(A) Genomic structure of *RNS* and T-DNA insertion sites. Black shaded boxes show exons and intervening line lines are introns. ATG is initiating methionine, TAA, TGA and TAG are stop codons. **(B)** Relative transcript levels of *RNS1*, RNS2, and *RNS4* were quantified by reverse transcription PCR.

3.4.2. *Arabidopsis* RNS1, RNS2 and RNS4 all cleave tRNA into halves under oxidative stress

As outlined in the introduction, tRNA cleavage is a conserved response to oxidative stress in yeast, *A. thaliana* and mammalian [17]. RNS1 was reported to possibly have roles in the processing and/or degradation of tRFs in land plants [5]. Also, the RNS1, RNS2 and RNS3 of *A. thaliana* were documented to complement *rny1δ* yeast and generate the tRNA halves *in vitro* [9]. To better understand the cleavage activity of RNS on tRNA halves for *A. thaliana*, we

measured the accumulation of 5'-half tRNA fragments in single mutants *rns1*, *rns2*, *rns4*, and double mutants *rns1 rns2* and *rns2 rns4* by Northern blotting.

As detailed in Fig 3.3, in all hydrogen peroxide treated *rns* mutants and wild type seedlings, the abundance of the 5'-half tRNA fragments of $tRNA^{Asp(GTC)}$, $tRNA^{Arg(CCT)}$ and $tRNA^{His(GTG)}$ all dramatically increases, which indicates that the oxidative stress efficiently intensifies the tRNA cleavage. The highest abundance of 5'-half tRNA fragments was observed in $tRNA^{Arg(CCT))}$ (Fig 3.3A) and the lowest abundance of 5'-half tRNA fragments was observed in $tRNA^{Asp(GTC)}$ (Fig 3.3C, D), which reflects that not every tRNA could be cleaved at the same efficiency. Furthermore, the reduced 5'-half $tRNA^{Arg(CCT)}$ fragments were only observed in *rns1*, the reduced 5'-half $tRNA^{Asp(GTC)}$ fragments were just detected in *rns2*, and the absence of RNS4 cause the reduced 5'-half tRNA fragments in $tRNA^{Asp(GTC)}$ and $tRNA^{His(GTG)}$. It seems that not every RNS is able to cleave all the tRNAs. Of note, there are two more bands between the full-length and 5'-half $tRNA^{Arg(GTC)}$ in *rns1* with hydrogen peroxide treatment. Apart from checking the tRNA cleavage in *rns* single mutants, we also detected the abundance of 5'-half $tRNA^{Asp(GTC)}$ fragments in double mutants *rns1 rns2* and *rns2 rns4* (Fig 3.3C, D). For *rns1 rns2*, the decreased abundance of 5'-half $tRNA^{Asp(GTC)}$ fragments is not very obvious compared to wild type with hydrogen peroxide treatment. While the cleavage of $tRNA^{Asp(GTC)}$ decreased by 20% in *rns2 rns4* mutants when compared to wild type. These findings suggest that the RNS1, RNS2 and RNS4 all could cleave the tRNA under oxidative stress in *A. thaliana*.

Of note, in all the *rns* mutants without hydrogen peroxide treatment, decreased abundance of all 5'-half tRNA fragments was observed in *rns1* in comparison to wild type. In contrast, the absence of RNS2 increased the abundance of 5'-half tRNA fragments. It is possible that the RNS2 may involve in other processing and causes RNA degradation or cleavage.

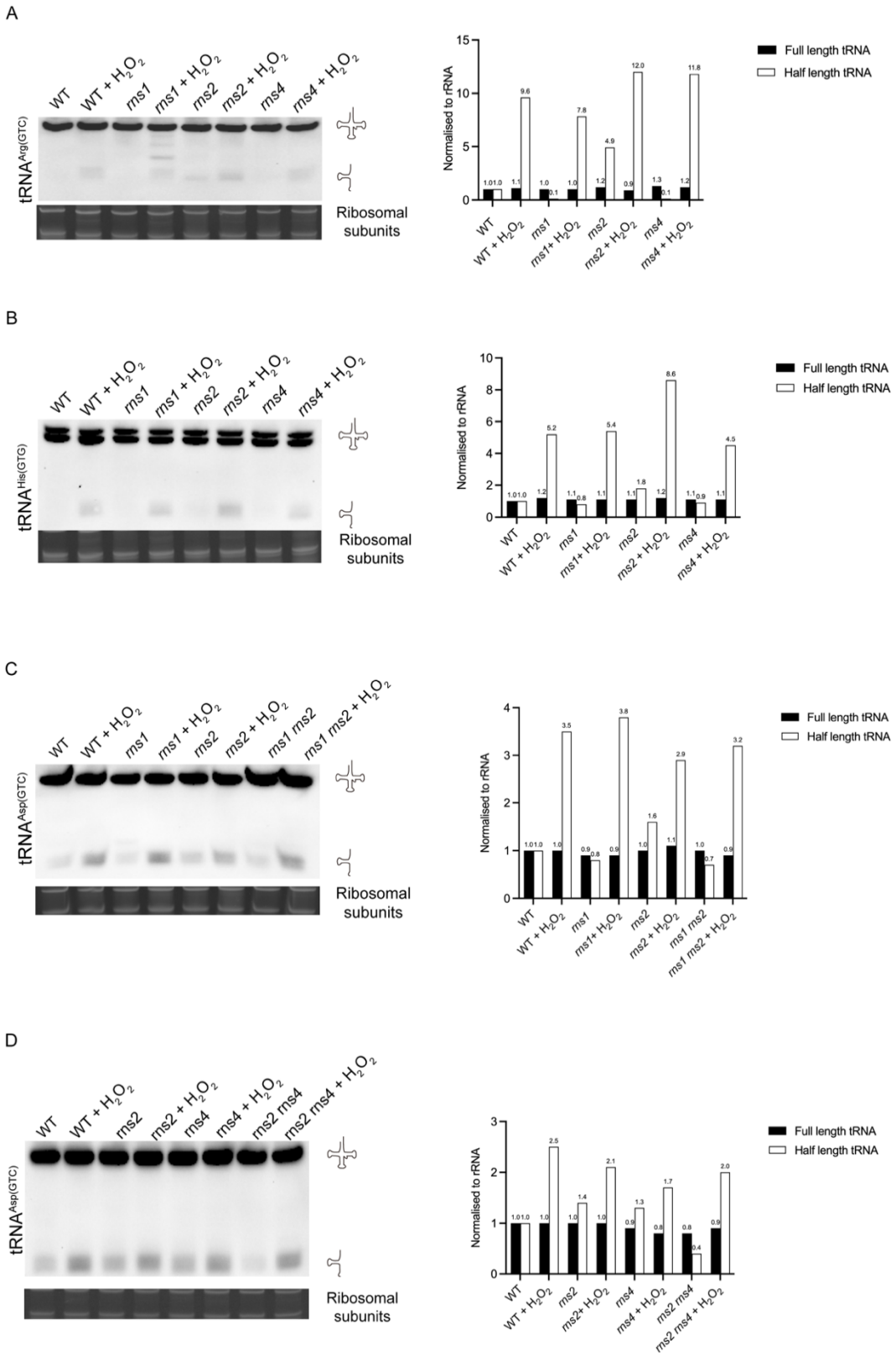
A
WT
WT + H2O2
rns1
rns1 + H2O2
rns2
rns2 + H2O2
rns4
rns4 + H2O2
tRNAArg(GTC)
Ribosomal subunits
Normalised to rRNA
Full length tRNA
Half length tRNA
B
tRNAHis(GTG)
C
rns1 rns2
rns1 rns2 + H2O2
tRNAAsp(GTC)
D
rns2
rns2 + H2O2
rns4
rns4 + H2O2
rns2 rns4
rns2 rns4 + H2O2

Figure 3.3: RNS1, RNS2 and RNS4 all cleave the tRNAs under oxidative stress in *A. thaliana*.

Ten-old-day wild type, *rns 1*, *rns2*, *rns4*, *rns1 rns2* and *rns2 rns4* seedlings were treated with 0 and 10 mM hydrogen peroxide for 4 hrs. **(A)(B)** Left: representative northern blotting analysis of $tRNA^{Arg(CCT)}$ and $tRNA^{His(GTG)}$ for wild type, *rns1*, *rns2*, and *rns4*. The bottom is the ribosomal band staining after transferring. Right: quantitative analysis of RNS substrate $tRNA^{Arg(CCT)}$ and $tRNA^{His(GTG)}$. The signal intensities were normalised to ribosomal subunits and were also chosen to indicate the cleavage efficiency. **(C)** Left: representative northern blotting analysis of $tRNA^{Asp(GTC)}$ for wild type, *rns1*, *rns2*, and double mutant *rns1 rns2*. The bottom is the ribosomal band staining after transferring. Right: quantitative analysis of RNS substrate $tRNA^{Asp(GTC)}$. The signal intensities were normalised to ribosomal subunits and were used (?) to indicate the cleavage efficiency. **(D)** Left: representative northern blotting analysis of $tRNA^{Asp(GTC)}$ for wild type, *rns2*, *rns4*, and double mutant *rns2 rns4*. The bottom is the ribosomal band staining after transferring. Right: quantitative analysis of RNS substrate $tRNA^{Asp(GTC)}$. The signal intensities were normalised to ribosomal subunits and were used to indicate the cleavage efficiency.

3.4.3. The variation in the accumulation of tRNA half fragments caused by the absence of RNS2

Due to the increased abundance of 5'-half tRNA fragments in *rns2* before hydrogen peroxide treatment and the high sequence similarity with *ScRny1*, we explored the variation of tRNA halves accumulation caused by RNS2 through sequencing. The length of sequenced small RNA is roughly about 30-42 nt, nearly the same size as the tRNA half. The differential expression analysis of mapped tRNA halves reads between wild type and *rns2* mutants under non-oxidative and oxidative stress was conducted using the exactTest in edgeR. As shown in Fig 3.4A, B, there are more upregulated tRNA half loci in both WT and *rns2*, which suggests more tRNA are cleaved under oxidative stress. However, there is no remarkable count difference between the upregulated and downregulated tRNA half loci caused by oxidative stress in *rns2* and WT (Fig 3.4C). This result is in line with our northern blotting analysis that RNS2 is not the only ribonuclease cleaving for the tRNAs. Only one upregulated tRNA loci in the *rns2* compared to WT without oxidative stress. Apart from being mapped to the mature tRNA, the differential expressed tRNA halves were also mapped to pre-tRNA. The percentage of pre-tRNA and the corresponding mature tRNAs in the up-regulated and downregulated tRNA loci are presented in Fig 3.4E.

Overall, it is evident from the sequencing results that the loss of RNS2 could not only influence the population of mature tRNA under oxidative stress, but also the pre-tRNA.

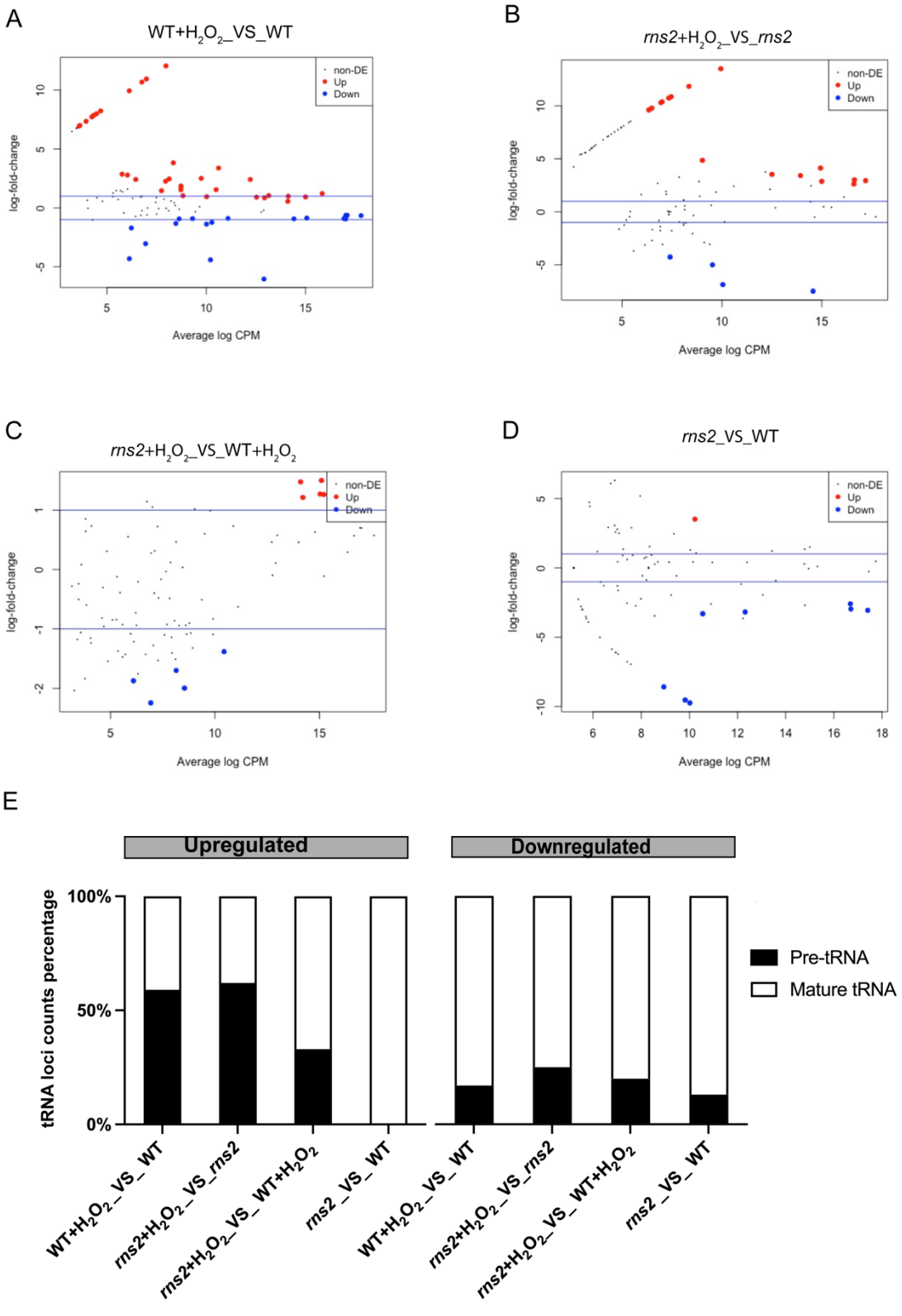

Figure 3.4: The accumulation of tRNA halves varies due to the loss of RNS2 in *A. thaliana*.

Ten-old-day wild type, *rns2* seedlings were treated with 0 and 10 mM hydrogen peroxide for 4 hrs. The tRNAs were separated and purified for library construction. **(A-D)** The upregulated and downregulated tRNA loci were identified in the compared groups, including wild type with oxidative relative to nonoxidative stress, *rns2* with oxidative relative to nonoxidative stress, *rns2 relative to* wild type under oxidative stress and *rns2* relative to wild type under nonoxidative stress. **(E)** Histogram of pre-tRNA and the corresponding mature tRNA percentage identified in the upregulated and downregulated tRNA loci in the compared groups, including wild type with oxidative relative to nonoxidative stress, *rns2* with oxidative relative to nonoxidative stress, *rns2* relative to wild type under oxidative stress and *rns2* relative to wild type under nonoxidative stress.

3.4.4. Correlation with methyltransferase TRM4B and ribonucleases RNS2 in *A. thaliana*

Previously, it was reported in mouse and flies subjected to oxidative stress that the methylation by DNMT2 and NSUN2 could inhibit the tRNA from being cleaved, suggesting that m^5C may interfere with the interaction between tRNA cleavage and ribonucleases [26], [27]. In our previous work, the TRM4B has been proved to be necessary for three m^5C sites (C48, C49, and C50) in nuclear $tRNA^{Asp(GTC)}$, and the decreased full-length $tRNA^{Asp(GTC)}$ fragments were observed in *trm4b* [29]. Therefore, to further test whether the TRM4B-mediated methylation could prevent the ribonuclease RNS2 catalyzed tRNA cleavage in *A. thaliana*, we identified the homozygous double mutant *rns2 trm4b* and subjected them to oxidative stress, then measured the abundance of 5'-half $tRNA^{Asp(GTC)}$ fragments by northern blotting. It was shown in Fig 3.5A that the full-length $tRNA^{Asp(GTC)}$ decreased in *trm4b* and *rns2 trm4b* mutants under nonoxidative and oxidative stress conditions compared to wild type and *rns2* mutants, which indicates that more $tRNA^{Asp(GTC)}$ has been cleaved without the protection of m^5C modification, or less $tRNA^{Asp(GTC)}$ were synthesized. However, the decreased full length of $tRNA^{Asp(GTC)}$ in *trm4b* and *rns2 trm4b* mutants resulted in the unexpected decreased abundance of 5'-half $tRNA^{Asp(GTC)}$ fragments. We suspected that the cleaved 5'-half tRNA without m^5C modification might be processed into small non-coding RNAs or be degraded,

which could also explain the much more 5'-half tRNA$^{Asp(GTC)}$ fragments in *rns2* than the *trm4b* under oxidative stress. As expected, the 5'-half tRNA$^{Asp(GTC)}$ fragments are much less in *rns2 trm4b* than the *trm4b* response to oxidative stress. These results provide important confirmation that m^{5}C modification could partially protect the tRNA$^{Asp(GTC)}$ from the cleavage by RNS2 in *A. thaliana* under oxidative stress.

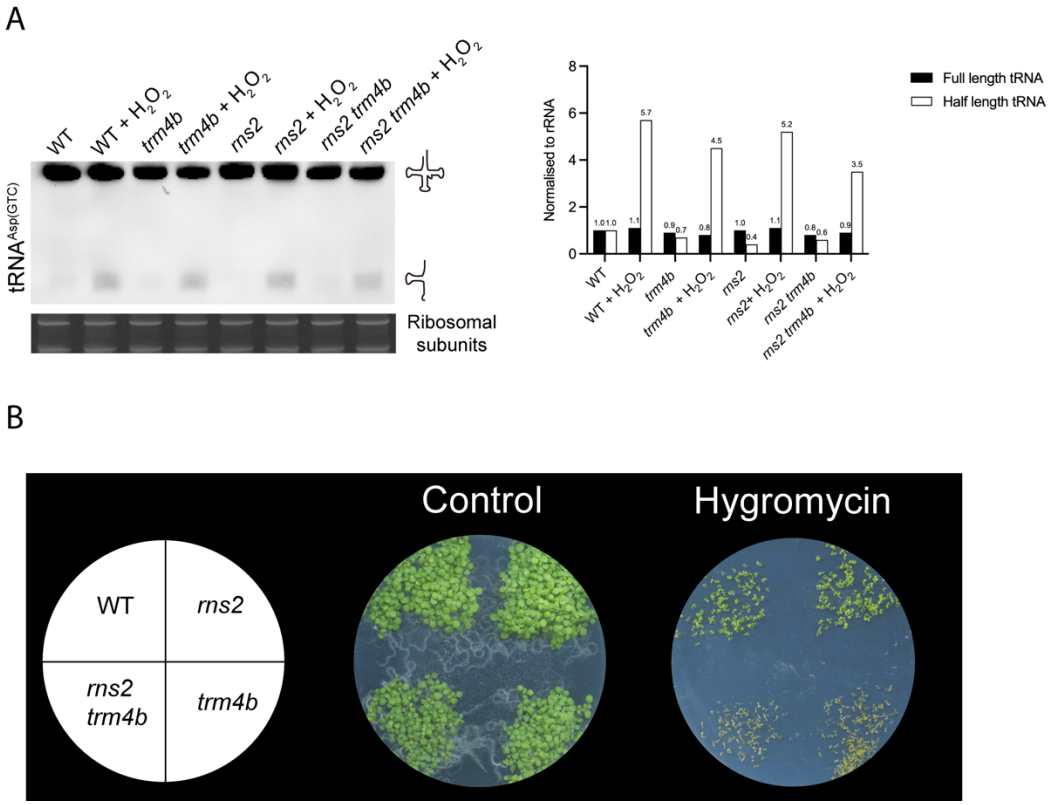

Figure 3.5: Correlation with m^{5}C modification and ribonucleases RNS2 in *A. thaliana*.

(A) TRM4B could partially protect the tRNAA$^{sp(GTC)}$ from the cleavage from RNS2. Ten-old-day wild type, *rns2*, *trm4b* and *rns2 trm4b* seedlings were treated with 0 and 10 mM hydrogen peroxide for 4 hrs. Left: representative northern blotting analysis of tRNA$^{Asp(GTC)}$, *rns2*, *trm4b*, and *rns2 trm4b*. The bottom is the ribosomal band staining after transferring. Right: quantitative analysis of RNS and TRM4B substrate tRNA$^{Asp(GTC)}$. The signal intensities were normalised to ribosomal subunits. **(B)** The response of wild type, *rns2*, *trm4b* and *rns2 trm4b* to hygromycin. The sterilized seeds were placed on a 0 and 15 ug/ml medium for ten days after germination.

Beyond the function of methylating the tRNAs, the TRM4B is also crucial for

mRNAs and non-coding RNAs [29]. Loss of the TMR4B caused changes in global small RNA profiles in *A. thaliana* (Pei et al, unpublished data). RNS2 has been demonstrated to mediate the accumulation of rRNA intracellularly [38]. The short primary root phenotype in *trm4b* caused by the reduced cell division in the root apical meristem was restored in *rns2 trm4b* [29] (Pei et al, unpublished data), which may be due to the accumulated rRNA in vacuole caused by loss of RNS2 [39]. Hygromycin was thought to alter the conformation of the A-site in the ribosome, resulting in inhibiting translocation and reducing translational fidelity [40]. As this correlation between TRM4B and RNS2, we wonder whether the absence of both TRM4B and RNS2 could affect the translation. We placed seeds of wild type, *rns2*, *trm4b* and *rns2 trm4b* on the medium containing 15 ug/ml of antibiotic hygromycin B. The sensitivity of *rns2* to hygromycin is the same as wild type, which could be found in Fig 3.5B. It is likely that the accumulated rRNA caused by lacking RNS2 activity did not influence the translation [39]. As expected, the *trm4b* mutants exhibited increased sensitivity to hygromycin after germination, which is consistent with our previous study [28]. Also, we observe from Fig 3.5B that the double mutant *rns2 trm4b* showed increased sensitivity to hygromycin. Therefore, it could be inferred that an unknown interaction between reduced methylation in *trm4b* and increased rRNA accumulation in *rns2* led to translation reduction.

3.5. Discussion and Conclusion

Prior research documented the biogenesis of tRNA halves in *A. thaliana*. For example, Megel et al. (2018) demonstrated that the production of 5'-half $tRNA^{Ala(TGC)}$ and the tRF-5s of $tRNA^{Ala(TGC)}$ could be restored *in vivo* and *in vitro* in the yeast *rny1Δ* mutant strain complemented with either *Arabidopsis* RNS1, RNS2 or RNS3. Alves et al. (2016) provided evidence that some specific tRFs that were 19 or 20 nts are dependent on RNS1. However, these studies were either conducted to check the change of tRNA derived fragments caused by one of the RNase T2 ribonuclease family members or were designed to explore the cleavage activities of *Arabidopsis* RNS on specific one tRNA. Furthermore, published data from our laboratory supported the idea that the additional m^5C sites on tRNAs play a role to strengthen the tRNA stability in *A. thaliana*, and the decreased tRNA stability may contribute to the hypersensitivity to oxidative stress in *trm4b* mutants and reduce translational efficiency [28], [29]. Also, the depletion of TRM4B leads to the upregulation of some chromosome specific sRNA expression (Pei et al, unpublished). Nevertheless, the alteration in the accumulation of tRNA halves regulated by m^5C and the RNase T2 ribonuclease under oxidative stress in *A. thaliana* still has not been elucidated. In this study, we combined northern blotting and small RNA sequencing to investigate the cleavage activity of different *Arabidopsis* RNS under oxidative stress compared to wild type, to disclose the variation of tRNA halves caused by mutation of RNS2. At the same time, the co-regulatory function of TRM4B and RNS2 on tRNA cleavage and the translation were also tested.

We found in *A. thaliana* that RNS2 may be the highest homology branch of ScRny1, the following are RNS4 and RNS1. The increased abundance of three 5'-half tRNA fragments in all *rns* mutants and wild type treated with hydrogen peroxide demonstrates that the RNase T2 ribonucleases RNS are induced under oxidative stress, which indicates that all the *Arabidopsis* RNS are able to cleave tRNAs into halves. Strikingly, the cleavage efficiency of all RNS on the three different tRNAs varies, with the highest on $tRNA^{Asp(GTC)}$ and lowest on $tRNA^{Arg(CCT)}$. It seems very probable that the m^5C provides protection for the

tRNAs for specific tRNA molecules from cleavage, as there are three TRM4B-dependent m^5C sites in nuclear $tRNA^{Asp(GTC)}$, one TRM4B-dependent m^5C site in nuclear $tRNA^{His(GTG)}$ and none in $tRNA^{Arg(CCT)}$[28]. Meanwhile, it was found that not all three intact tRNAs could be cleaved by each RNS, which may be due to the differentially tissue-specific expression of *Arabidopsis* RNS during plant development [9]. The cleavage of $tRNA^{Asp(GTC)}$ is modest less in double mutant *rns2 rns4* than *rns1 rns2*, demonstrating that the cleavage function of RNS4 may be more obvious for ten-days-old seedlings exposed to oxidative stress. Of note, the increased 5'-half fragments of all three tRNAs were observed in *rns2* mutants without oxidative stress treatment, which suggests the loss of RNS2 may trigger RNA degradation through other unknown mechanisms. Furthermore, the small RNA sequencing data disclosed that the loss of RNS2 could not only influence the population of mature tRNA under oxidative stress, but also the pre-tRNA. While, it is mentioned in one publication that the decreased tRFs from $tRNA^{Ala(AGC)}$ is not attributed to the downregulation of RNS1 and RNS3 in *Botrytis* cinerea-affected *A. thaliana*, which may provide a new hint for investigating the coorelation with the enzyme activity of *Arabidopsis* RNS and tRNA cleavage [41].

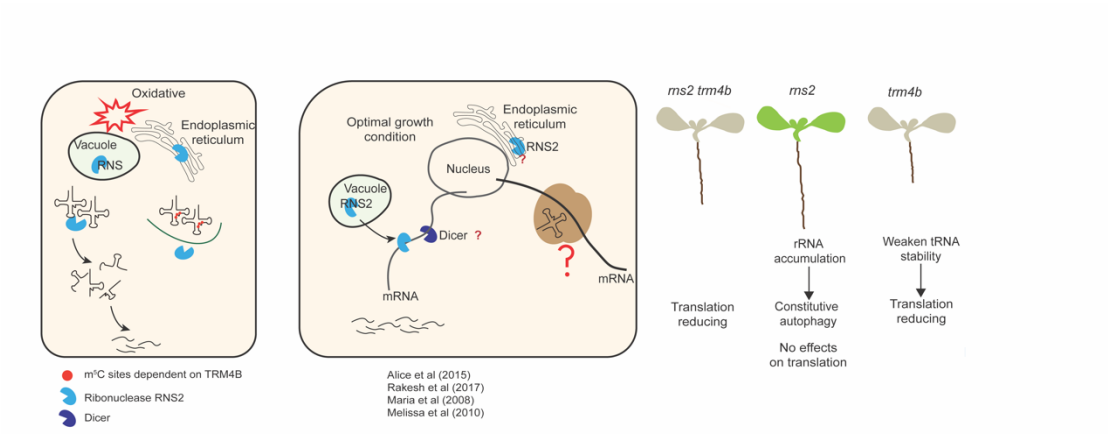

Figure 3.6: Proposed model for the interaction between TRM4B and RNS2.

Under oxidative stress conditions, the *Arabidopsis* RNS exit from the vacuole and endoplasmic reticulum to the cytoplasm to cleave the tRNAs without the m^5C site, and the cleaved tRNA halves might be processed into the sRNAs. While under the optimal growth condition, on the one hand, the mRNAs absence of TRM4B might be cut by RNS2 exit from the vacuole and endoplasmic reticulum and diced into small RNAs, on the other hand, the tRNAs without the m^5C cooperated with the accumulated rRNA may reduce the translation.

As the seeds of *trm4b* and *rns2 trm4b* exhibited hypersensitivity to hygromycin compared to WT and *rns2*, we are reasonable to assume that a subtle interaction between reduced methylation in *trm4b* and increased rRNA accumulation in *rns2* might lead to the translation reduction. Furthermore, under oxidative stress, the decreased full-length $tRNA^{Asp(GTC)}$ in *trm4b* mutants indicates that the protective function of m^5C is abolished. Compared to wild type and *rns2*, the decreased 5'-half $tRNA^{Asp(GTC)}$ fragments in *trm4b* seem likely that the cleaved tRNA halves are further processed into a smaller fragment. This explanation could be supported by unpublished data in our laboratory that the absence of m^5C sites in *trm4b* leads to the upregulation of sRNAs (Pei et al, unpublished). Moreover, only a slight decrease of 5'-half $tRNA^{Asp(GTC)}$ fragments could be detected in double mutant *rns2 trm4b* compared to *trm4b* exposed to oxidative stress, which suggests that other plant RNase T2 ribonucleases also have the cleavage efficiency. Therefore, investigating the change of tRNA halves and sRNAs (18 to 21 nt in length) in wild type, *rns2*, *trm4b* and *rns2 trm4b* through small RNA sequencing is very necessary for future work. Also, making other double mutant *rns1 trm4b*, *rns4 trm4b* and then examining the accumulation of $tRN^{Asp(GTC)}$ through northern blotting will be needed to validate the cleavage role of other *Arabidopsis* RNS in *trm4b* mutants.

Overall, the insights gained from this study broaden our understanding of the cleavage feature of *Arabidopsis* RNS on tRNAs under oxidative stress. Furthermore, the reduced translation in double mutants *rns2 trm4b*, and the unpublished data in our labarotary referring to the upregulated sRNAs in *trm4b* provide compelling evidence that the RNAs without the m^5C sites might

proceed into small RNAs catalysed by RNS or DICER and then modulate the translation (Figure 3.6).

3.6. References

[1] S. J. Sharp, J. Schaack, L. Cooley, D. J. Burke, and D. Soil, “Structure and transcription of eukaryotic tRNA gene,” *Crit Rev Biochem Mol Biol*, vol. 19, no. 2, pp. 107–144, 1985, doi: 10.3109/10409238509082541.

[2] M. Sprinzl and F. Cramer, “The -C-C-A End of tRNA and Its Role in Protein Biosynthesis,” *Prog Nucleic Acid Res Mol Biol*, vol. 22, no. C, pp. 1–69, Jan. 1979, doi: 10.1016/S0079-6603(08)60798-9.

[3] Y. Mei *et al.*, “tRNA Binds to Cytochrome c and Inhibits Caspase Activation,” *Mol Cell*, vol. 37, no. 5, pp. 668–678, Mar. 2010, doi: 10.1016/j.molcel.2010.01.023.

[4] C. Zhu, B. Sun, A. Nie, and Z. Zhou, “The tRNA-associated dysregulation in immune responses and immune diseases,” *Acta Physiologica*, vol. 228, no. 2. Blackwell Publishing Ltd, Feb. 01, 2020. doi: 10.1111/apha.13391.

[5] C. S. Alves, R. Vicentini, G. T. Duarte, V. F. Pinoti, M. Vincentz, and F. T. S. Nogueira, “Genome-wide identification and characterization of tRNA-derived RNA fragments in land plants,” *Plant Mol Biol*, vol. 93, no. 1–2, pp. 35–48, Jan. 2017, doi: 10.1007/s11103-016-0545-9.

[6] P. Schimmel, “RNA Processing and Modifications: The emerging complexity of the tRNA world: Mammalian tRNAs beyond protein synthesis,” *Nature Reviews Molecular Cell Biology*, vol. 19, no. 1. Nature Publishing Group, pp. 45–58, Jan. 01, 2018. doi: 10.1038/nrm.2017.77.

[7] E. J. Park and T.-H. Kim, “Fine-Tuning of Gene Expression by {tRNA}-Derived Fragments during Abiotic Stress Signal Transduction.,” *Int J Mol Sci*, vol. 19, no. 2, Feb. 2018, doi: 10.3390/ijms19020518.

[8] S. Li, Z. Xu, and J. Sheng, “tRNA-derived small RNA: A novel regulatory small non-coding RNA,” *Genes*, vol. 9, no. 5. MDPI AG, p. 246, May 01, 2018.

doi: 10.3390/genes9050246.

[9] C. Megel *et al.*, “Plant RNases T2, but not Dicer-like proteins, are major players of tRNA-derived fragments biogenesis,” *Nucleic Acids Res*, vol. 47, no. 2, pp. 941–952, 2019, doi: 10.1093/nar/gky1156.

[10] C. S. Alves and F. T. S. Nogueira, “Plant Small RNA World Growing Bigger: tRNA-Derived Fragments, Longstanding Players in Regulatory Processes,” *Front Mol Biosci*, vol. 8, Jun. 2021, doi: 10.3389/FMOLB.2021.638911.

[11] G. Martinez, S. G. Choudury, and R. K. Slotkin, “TRNA-derived small RNAs target transposable element transcripts,” *Nucleic Acids Res*, vol. 45, no. 9, pp. 5142–5152, May 2017, doi: 10.1093/nar/gkx103.

[12] P. Zhu, J. Yu, and P. Zhou, “Role of tRNA-derived fragments in cancer: novel diagnostic and therapeutic targets tRFs in cancer.,” *Am J Cancer Res*, vol. 10, no. 2, pp. 393–402, 2020, Accessed: Oct. 12, 2020. [Online]. Available: http://www.ncbi.nlm.nih.gov/pubmed/32195016

[13] C. Cole *et al.*, “Filtering of deep sequencing data reveals the existence of abundant Dicer-dependent small RNAs derived from tRNAs,” *RNA*, vol. 15, no. 12, pp. 2147–2160, Dec. 2009, doi: 10.1261/rna.1738409.

[14] P. Kumar, J. Anaya, S. B. Mudunuri, and A. Dutta, “Meta-analysis of tRNA derived RNA fragments reveals that they are evolutionarily conserved and associate with AGO proteins to recognize specific RNA targets,” *BMC Biol*, vol. 12, no. 1, p. 78, Dec. 2014, doi: 10.1186/s12915-014-0078-0.

[15] R. Levitz, D. Chapman, M. Amitsur, R. Green, L. Snyder, and G. Kaufmann, “The optional E. coli prr locus encodes a latent form of phage T4-induced anticodon nuclease.,” *EMBO J*, vol. 9, no. 5, pp. 1383–1389, May 1990, doi: 10.1002/J.1460-2075.1990.TB08253.X.

[16] D. M. Thompson and R. Parker, “The RNase Rny1p cleaves tRNAs and promotes cell death during oxidative stress in Saccharomyces cerevisiae,”

Journal of Cell Biology, vol. 185, no. 1, pp. 43–50, Apr. 2009, doi: 10.1083/jcb.200811119.

[17] D. M. Thompson, C. Lu, P. J. Green, and R. Parker, “tRNA cleavage is a conserved response to oxidative stress in eukaryotes,” *RNA*, vol. 14, no. 10, pp. 2095–2103, Oct. 2008, doi: 10.1261/rna.1232808.

[18] A. A. Aravin *et al.*, “The Small RNA Profile during Drosophila melanogaster Development,” *Dev Cell*, vol. 5, no. 2, pp. 337–350, Aug. 2003, doi: 10.1016/S1534-5807(03)00228-4.

[19] R. Peng, H. J. Santos, and T. Nozaki, “Transfer RNA-Derived Small RNAs in the Pathogenesis of Parasitic Protozoa,” *Genes (Basel)*, vol. 13, no. 2, Feb. 2022, doi: 10.3390/GENES13020286.

[20] M. M. Emara *et al.*, “Angiogenin-induced {tRNA}-derived stress-induced {RNAs} promote stress-induced stress granule assembly.,” *J Biol Chem*, vol. 285, no. 14, pp. 10959–10968, Apr. 2010, doi: 10.1074/jbc.M109.077560.

[21] R. Fricker *et al.*, “A tRNA half modulates translation as stress response in Trypanosoma brucei,” *Nat Commun*, vol. 10, no. 1, Dec. 2019, doi: 10.1038/S41467-018-07949-6.

[22] S. Yamasaki, P. Ivanov, G.-F. Hu, and P. Anderson, “Angiogenin cleaves {tRNA} and promotes stress-induced translational repression.,” *J Cell Biol*, vol. 185, no. 1, pp. 35–42, Apr. 2009, doi: 10.1083/jcb.200811106.

[23] S. Liu *et al.*, “A tRNA-derived RNA Fragment Plays an Important Role in the Mechanism of Arsenite -induced Cellular Responses,” *Scientific Reports 2018 8:1*, vol. 8, no. 1, pp. 1–9, Nov. 2018, doi: 10.1038/s41598-018-34899-2.

[24] Y. Nakai *et al.*, “tRNA Wobble Modification Affects Leaf Cell Development in Arabidopsis thaliana,” *Plant Cell Physiol*, vol. 60, no. 9, pp. 2026–2039, Sep. 2019, doi: 10.1093/pcp/pcz064.

[25] M. A. Machnicka *et al.*, “MODOMICS: A database of RNA modification pathways - 2013 update,” *Nucleic Acids Res*, vol. 41, no. D1, p. D262, Jan. 2013, doi: 10.1093/nar/gks1007.

[26] S. Blanco *et al.*, “Aberrant methylation of tRNAs links cellular stress to neuro-developmental disorders,” *EMBO J*, vol. 33, no. 18, p. 2020, Sep. 2014, doi: 10.15252/EMBJ.201489282.

[27] M. Schaefer *et al.*, “RNA methylation by Dnmt2 protects transfer RNAs against stress-induced cleavage,” *Genes Dev*, vol. 24, no. 15, pp. 1590–1595, Aug. 2010, doi: 10.1101/gad.586710.

[28] A. L. Burgess, R. David, and I. R. Searle, “Conservation of tRNA and rRNA 5-methylcytosine in the kingdom Plantae,” *BMC Plant Biol*, vol. 15, no. 1, pp. 1–17, 2015, doi: 10.1186/s12870-015-0580-8.

[29] R. David *et al.*, “Transcriptome-wide mapping of RNA 5-methylcytosine in arabidopsis mRNAs and noncoding RNAs,” *Plant Cell*, vol. 29, no. 3, pp. 445–460, 2017, doi: 10.1105/tpc.16.00751.

[30] J. M. Alonso *et al.*, “Genome-wide insertional mutagenesis of Arabidopsis thaliana,” *Science*, vol. 301, no. 5633, pp. 653–657, Aug. 2003, doi: 10.1126/SCIENCE.1086391.

[31] A. Dobin *et al.*, “STAR: ultrafast universal RNA-seq aligner,” *Bioinformatics*, vol. 29, no. 1, pp. 15–21, Jan. 2013, doi: 10.1093/BIOINFORMATICS/BTS635.

[32] C. Y. Cheng, V. Krishnakumar, A. P. Chan, F. Thibaud-Nissen, S. Schobel, and C. D. Town, “Araport11: a complete reannotation of the Arabidopsis thaliana reference genome,” *The Plant Journal*, vol. 89, no. 4, pp. 789–804, Feb. 2017, doi: 10.1111/TPJ.13415.

[33] M. D. Robinson, D. J. McCarthy, and G. K. Smyth, “edgeR: a Bioconductor package for differential expression analysis of digital gene expression data,” *Bioinformatics*, vol. 26, no. 1, pp. 139–140, Nov. 2010, doi:

10.1093/BIOINFORMATICS/BTP616.

[34] M. D. Robinson and A. Oshlack, “A scaling normalization method for differential expression analysis of RNA-seq data,” *Genome Biol*, vol. 11, no. 3, pp. 1–9, Mar. 2010, doi: 10.1186/GB-2010-11-3-R25/FIGURES/3.

[35] B. Igic and J. R. Kohn, “Evolutionary relationships among self-incompatibility RNases,” *Proc Natl Acad Sci U S A*, vol. 98, no. 23, pp. 13167–13171, Nov. 2001, doi: 10.1073/PNAS.231386798/SUPPL_FILE/3867TABDELIMITED.TSV.

[36] C. B. Taylor and P. J. Green, “Genes with Homology to Fungal and S-Gene RNases Are Expressed in Arabidopsis thaliana,” *Plant Physiol*, vol. 96, no. 3, pp. 980–984, 1991, doi: 10.1104/PP.96.3.980.

[37] N. Luhtala and R. Parker, “Structure-Function Analysis of Rny1 in tRNA Cleavage and Growth Inhibition,” *PLoS One*, vol. 7, no. 7, p. e41111, Jul. 2012, doi: 10.1371/JOURNAL.PONE.0041111.

[38] D. K. St Clair, S. M. Rybak, J. F. Riordan, and B. L. Vallee, “Angiogenin abolishes cell-free protein synthesis by specific ribonucleolytic inactivation of ribosomes.,” *Proc Natl Acad Sci U S A*, vol. 84, no. 23, p. 8330, 1987, doi: 10.1073/PNAS.84.23.8330.

[39] M. S. Hillwig, A. L. Contento, A. Meyer, D. Ebany, D. C. Bassham, and G. C. MacIntosha, “RNS2, a conserved member of the RNase T2 family, is necessary for ribosomal RNA decay in plants,” *Proc Natl Acad Sci U S A*, vol. 108, no. 3, pp. 1093–1098, Jan. 2011, doi: 10.1073/PNAS.1009809108/SUPPL_FILE/PNAS.201009809SI.PDF.

[40] M. A. Borovinskaya, S. Shoji, K. Fredrick, and J. H. D. Cate, “Structural basis for hygromycin B inhibition of protein biosynthesis,” *RNA*, vol. 14, no. 8, pp. 1590–1599, Aug. 2008, doi: 10.1261/RNA.1076908.

[41] H. Gu *et al.*, “A 5′ tRNA-Ala-derived small RNA regulates anti-fungal

defense in plants," vol. 65, no. 1, pp. 1–15, 2022, doi: 10.1007/s11427-021-2017-1.

3.7. Supplementary data

Table 1. Oligonucleotide primer sequences

Primer	Sequence
SALKseq_078116.1-LP	AAGGGAATTCGATCTCAGCTC
SALKseq_078116.1-RP	AATGAAGAAGAGCTGGCCAAC
SALK_069588-LP	CTCGATGAAGACTTACCGTGAC
SALK_069588-RP	CTGGCCTAGTCTCAGTTGTGG
SAILseq_389_A06.1-LP	ATCATGCATGAACAGGCTAGG
SAILseq_389_A06.1-RP	CATGATGTAGGGATCAAACCG
SAILseq_286_A12.1-LP	ATAGCCAAAAAGGATGTTGCC
SAILseq_286_A12.1-RP	TCTGCATAATTGTTTCCACAGG
SALKseq_055304.0-LP	ACACAGGTGCCATGCTTATTC
SALKseq_055304.0-RP	ACAGAGCCTTGTCGTGTCTTC
SAIL_318_G04-LP	AACAGTTTCCTGGTTGCCGTTTG
SAIL_318_G04-RP	CAAACAGACATATTTACGATAGGCGGA

Table 2: Probes used for northern blotting

tRNA	Probe sequence
$tRNA^{Asp(GTC)}$	GACAGGCGGGAATACTTACCACTATACTACAACGAC
$tRNA^{Arg(CCT)}$	AGGAAACAGACGCTCTATCCACTGAGCTACAGGCGC
$tRNA^{His(GTG)}$	AACGTGGAATTCTAACCACTAAACTACAGCCAC

Chapter 4. Towards understanding the lethal effect of transgene expressed 5'-half $tRNA^{Asp}$, *Killer*, in *Arabidopsis thaliana*

4.1. Abstract

Besides the canonical role of tRNAs in protein synthesis, tRNAs are cleaved at different positions, particularly under stress conditions, to produce tRNA halves and tRNA-derived fragments (tRFs) in numerous organisms. Mounting evidence supports roles of tRFs in transcriptional and translational regulation, stress granule assembly, ribosome biogenesis, and apoptosis. tRNA halves are 35-40 nucleotides in length and whether the tRNA halves are further cleaved and their biological function is still unclear in plants. Herein, we show that a transgene expressed 5'-half $tRNA^{Asp}$ ($tRNA^{Asp5'}$), so-called *Killer*, results in seedling or embryo death in *A. thaliana*. Interestingly, transformation of mutagenized nucleotides at 16 th, 17 th, 21 th, 22 th, 26 th, 27 th positions of *Killer* resulted in recovered transgenic plants for all nucleotides suggesting that all *Killer* nucleotides were important. Both small RNA sequencing data and mutants isolated from a genetic suppressor screen indicate that *Killer* was processed into several sRNAs involving RDR6, DCL2, DCL3, DCL4, AGO1, AGO3, AGO4, AGO5, AGO7, AGO9 and AGO10, resembling a sRNA-like mechanism. Further investigation illustrated that two sRNAs derived from $tRNA^{Asp5'}$ that may silence the expression of embryo-defective genes, At1g67490 and At1g3249, thereby leading to death. Our results suggest a sRNA-like processing of $tRNA^{Asp5'}$/*Killer* after being transformed into *A. thaliana*.

4.2. Introduction

The application of high-throughput sequencing technology offers an excellent opportunity for researchers to gain a deeper insight into the small RNAs (sRNAs) originating from various cellular non-coding RNAs. Currently, two rising sorts of sRNAs named tRNA-derived small RNAs (tsRNAs) are gaining particular attention in all branches of life, tRFs in 19-30 nucleotides (nt) in length and tRNA halves that are 31-40 nt in length. The biogenesis of tRFs and tRNA halves in yeast, plants and mammalian cells was clarified in an increasing list of research (Chapter 3). However, the functional significance of them is only beginning to be uncovered.

Before the understanding the diverse biological roles of tsRNAs, it is also crucial to gain insight into the population of tsRNAs. Generally, tRNAs are thought to be the most heavily modified cellular RNAs concerning the number, density and diversity, containing up to 17% modified nucleotides [1], which challenges the characterization of tsRNAs through sequencing approaches. The developed tRNA-seq, hydro-tRNAseq and YAMAT-seq have been widely adopted to quantify tsRNAs [2]–[4]. Meanwhile, there is debate whether the sequenced tsRNAs data should be only aligned to the mature tRNAs database because the genome could produce the tsRNAs [5]. In a few recent studies, the sequenced data was only either mapped to mature tRNA or genome sequence, while Thompson et al. (2018) determined to map the sequenced reads to tRNAs and *A. thaliana* genome [5]–[7].

Advanced sequencing techniques and the application of bioinformatics extensively facilitated the profiling and abundance of tsRNAs in numerous plants and tissues. For instance, in *A. thaliana*, a 19 nt tRF-5s from $tRNA^{Gly(TCC)}$, representing over 80% of tRFs and accounting for up to 28% of the total root sRNAs reads, were observed in the phosphate-starved roots library but were much less in the shoots library; the tRF-5s from $tRNA^{Asp(GTC)}$ was also detected much more in roots libraries than shoots, which is consistent with the northern blotting data. The author proposed that it is difficult for the tRFs to move from

root to shoots because of the long-distance [8]. Upon oxidative stress, 5'-half of $tRNA^{His(GTG)}$, $tRNA^{Arg(CCT)}$ and $tRNA^{Trp(CCA)}$ were accumulated in *A. thaliana* seedlings, while the 5'-half of $tRNA^{Glu(CTC)}$ was just observed in flowers [9]. Specific tRFs ranging from 18 to 25 nt were found in sRNA libraries from *Arabidopsis* leaf, inflorescence and pollen, the tRF-5s of $tRNA^{Ala(AGC)}$ in 19 nt distinctively accumulated to a higher level in the pollen grains [10]. Besides, a 19-nt tRF-5s of $tRNA^{Arg(CCT)}$ was found at a high pattern in *A. thaliana* seedlings under drought stress, as well in rice under cold stress [7]. A study conducted on the pumpkin suggested tRNA halves in the phloem sap were thought to be a potential long-distance signal [11]. tRFs were also elucidated in rice embryogenic callus in which the tRF-5s from $tRNA^{Ala(AGC)}$ accounting for 82% of the total tRF reads are the most abundant [12]. In addition, it is reported the tRF-5s are accumulated in barley under the phosphorous-deficient condition, with $tRNA^{Gly(TCC)}$ being the most abundant in shoots, followed by $tRNA^{Arg(CCT)}$ and $tRNA^{Ala(AGC)}$ [13]. Apart from the tRFs and tRNA halves, a longer group of sRNAs derived from tRNAs were detected in Giardia lamblia, which was 46 nt in length and was encystation-induced [14]. Taken together, the reported studies revealed the tRNA cleaved fragments could be induced by stress, and the abundance shares the character of being tissue specific. Moreover, the majority of identified tRFs or tRNA halves are originated from the 5 side, study concerning tRF-3s and 3 halves is sparse. In addition, only numbers of tRFs or tRNA halves are related to the specific stress in limited reports. Therefore, there is still a long way to elucidate the abundance of tRFs and tRNA halves in multiple species.

The biological function of tRFs and tRNA halves has been gradually disclosed in many studies in recent years. Among the functions attributed to tRFs and tRNA halves, although the regulation of translation seems to be the most studied, the patterns of action appear to vary based on the organism and the category of tRF [15]. For instance, the 5'- half of $tRNA^{Ala}$ and $tRNA^{Cys}$ with the terminal oligo-guanine (TOG) motifs (4–5 guanine residues) at 5′ ends have the ability to suppress translation through displacing eIF4F in human [16]. While in *A. thaliana*, it was observed that there is no correlation between the tRNA halves with TOG and the translation inhibition *in vitro* [17]. Furthermore, a small

part of tRF-5s derived from $tRNA^{Ala(AGC)}$ in young leaves of *A. thaliana* under normal conditions was observed to associate with actively elongating polyribosomal fractions, which demonstrates the tRFs may be slightly and regularly modulate translation in land plants [15]. Intriguingly, whether the tRFs are interacting with ARGONAUTE (AGO) and are dependent on mRNA sequence to repress translation through the canonical silencing pathway is still inconclusive. Some studies on human and plants implicated that tRF-5s can inhibit protein translation through association with polyribosomes rather than ribosomal subunits [15], [18]. This is different to what has been described in deep sequencing libraries of immunoprecipitated Argonaute proteins (AGO-IP) and bioinformatics approaches in *A. thaliana* where the tRF-5s are mainly present in the AGO1/3/4-IP fractions [19]. Meanwhile, the association between AGO and tRFs could be regulated by stress, like, AGO1-associated tRF-5s from $tRNA^{Gly(TCC)}$ population were enormously increased under UV treatment [20]. Although the targets of these AGO-associated tRFs have been predicted, the confirmation still needs to proceed in the future.

Apart from being a translational regulator, the tsRNAs were elucidated to be vital in other various cellular processes. Such as, the specific tRF-5s from $tRNA^{Gly(GCC)}$ in mammalian cells was documented to be a regulator of noncoding RNA and the subsequent global chromatin organization [21]. And increasing studies unveiled the tRFs in mammals involved in the cell cycle process and then modulate the cell proliferation, especially the tumour cell growth [22]. Of note, some DCL1-dependent and AGO1-associated tRFs were reported to target transposable elements (TEs) and maintain genome stability, specifically retrotransposons, in both plants and mammals [10], [23]. Furthermore, tRFs from rhizobial were confirmed as signal molecules that modulate host nodulation [24].

However, the functional investigation of tRNA halves is challenging due to their structure and length. In Chapter 2, we proposed that tRNA halves were cleaved into sRNAs and then involved in cellular regulation. In this Chapter, T-DNA constructs expressing either full-length or tRNA halves were transformed into *A. thaliana* to identify their possible cellular function, but unexpectedly we did not

obtain transgenic plants for the 5'-half tRNA construct, $tRNA^{Asp5'}$, suggesting expressing this RNA leads to egg cell, embryo or seedling death. Hence, we called this construct, *Killer*. Next, we performed mutagenesis of specific nucleotides sequence in *Killer* and recovered transgenic plants for all tested positions. Small RNA sequencing of *Nicotiana benthamiana* leaves infiltrated expressing *Killer* indicated the 35 nt $tRNA^{Asp5'}$ was processed into sRNAs. Short Tandem Target Mimics (STTM) and psRNATarget analysis suggests *Killer*-derived sRNAs target two embryo essential genes.

4.3. Materials and methods

4.3.1. Plant materials and growth conditions

A. thaliana (Columbia ecotype) were grown in Phoenix Biosystem controlled environment rooms at 21°C under metal halide lights that provided a level of photosynthetic active radiation (PRA) of 110 µmol of photos/m^2/s [25]. For *in vitro* plant growth, seeds were gas-sterilized (50 ml 12.5 % sodium hypochlorite and 1.25 ml 32% hydrochloric acid) overnight and plated on ½ Murashige and Skoog (MS) medium supplemented with 1% sucrose, then were put 4°C for three days. Plants were grown under long-day photoperiod conditions of 16 hrs light and 8 hrs darkness. When screening for transgenic plants, the corresponding antibiotics was added into the media MS medium without sucrose. The seeds in the plate underwent a 2-day stratification period, a 4–6 hrs light regime, 48 hrs dark and 24 hrs light [26].

Seeds of *A. thaliana* mutants *ago1-27* [27], *ago2-1* (Salk_003380), *ago3-1* (SM_3_31520), *ago4-3* (WiscDsLox338A06), *ago5-3* (SALK_063806), *ago7-1* (Salk_037458), *ago9-1* (Salk_127358), *ago10* (*zll-3*), *dcl2-1* (Salk_064627), *dcl3-1* (Salk_005512), *dcl4-2* (GK_160G05), *rdr2-2* (Salk_059661), *rdr6-15* (SAIL_617) were obtained from Arabidopsis Biological Resource Center (ABRC).

The crossing was performed for WT X WT, *ago 1-27 ($tRNA^{Asp(GTC)\ 5'}$) (-/+)* X *ago 1-27 ($tRNA^{Asp(GTC)\ 5'}$) (-/+)*, *ago 1-27 ($tRNA^{Asp(GTC)\ 5'}$) (-/+)* X WT and WT X *ago 1-27 ($tRNA^{Asp(GTC)\ 5'}$) (-/+)*. Flowers were emasculated before anthesis and then pollinated after 48 hrs.

4.3.2. Transient infiltration of *N. benthamiana* and the GFP detection

Electroporation was used to transform the plasmids into *Agrobacterium tumefaciens*. The cells were cultured in the Luria-Bertani broth supplemented

with 50 ug/mL kanamycin, 50 ug/mL rifampicin, 25 uM acetosyringone and 20 mM MES at 30 °C for 48 hrs. The cultured cells were centrifuged and then resuspended in infiltration buffer (1x MS salt, 10 mM MES, 200 μM acetosyringone, 2% sucrose) to an OD of 0.6. All suspensions were left in the dark for 2 hrs before being infiltrated into the abaxial side of *N. benthamiana* pBin-35S-mGFP5 leaves using a 1 mL needle-less syringe. After being infiltrated for four days, the leaves were cut into small sections to observe the GFP signal using an epifluorescence microscope.

4.3.3. Northern blotting for tRNA halves abundance detection

Total RNA was isolated from ten-days-old seedlings using TRIZOL Reagent. 10 ug of the total RNA was proceeded to separate the different sizes of RNA on 12.5% urea-polyacrylamide gel. After being transferred on the Amersham Hybond-N+membrance for 3.5 hrs, the gel was stained in SYBR gold, and the RNA was cross-linked on the membrane with a Stratalinker UV crosslinker. Prehybridization could be conducted for up to several hours at 68°C in 20 ul of the DIG easy Hyb Granules (Roche). 60 pmol of the 5-end Digoxin labelled oligonucleotides Hybridization was added into 6 ml DIG easy Hyb Granules to hybridise overnight at 40°C. The membrane was washed in low-stringency buffer (2X SSC, 0.1% SDS) twice and high-stringency buffer (0.1X SSC, 0.1% SDS) twice. The probe-target hybrid was localised with the anti-DIG-alkaline phosphatase antibody (Roche). The membrane was put into washing and blocking and detection buffer to visualise using the CDP-Star, ready to use (Roche). The membrane was imaged by the Bio-Rad Chemi-Doc MP Imaging System.

4.3.4. Plasmid construction and generation of transgenic plants

For different tRNA fragments expression constructs, a gene block flanked by AscI and SacI restriction sites was constructed containing the AtU3b promoter,

full-length *A. thaliana* $tRNA^{Asp(GTC)}$ and polyT sequence (Supplementary Table 2). The top and bottom strand sequences containing AscI and SacI restriction sites were synthesised and annealed for the other tRNA fragments to produce dsDNA. Gene block and other synthesised tRNA fragments are provided (Supplementary Table 3). Then, 25 ng of the gene block was used for the A-tailing reaction and ligated into Gateway entry vector pCR8 TOPO TA (Thermo Fisher Scientific). After being confirmed by PCR and sequence, the plasmid of pCR8:TOPO:AtU3b:$tRNA^{Asp(GTC)}$:polyT was enzyme digested by AscI and SacI to replace the other tRNA fragments (Oligos for PCR and sequence are provided in Supplementary Table 1). All the regenerated constructs were also sequenced for verification. Finally, all the constructs were cloned into the destination vector pMDC100 through the LR Gateway cloning system following the manufacturer's protocol, resulting in the pMDC100:AtU3b:$tRNA^{NNN(NNN)}$:polyT construct (Supplementary vectors) [28]. The constructs were transformed into *A. thaliana* wild type by *Agrobacterium*-mediated floral dip[29]. The T_1 seeds were screened on ½ MS medium supplemented with 1% sucrose and 60 ug/mL Kanamycin [26].

For the four STTM expression constructs, vectors pUC57 containing the STTM sequence flanked by SpeI and SacI restriction sites was synthesized (GenScript). The sequence of four STTM is provided (Supplementary Table 4). pUC57 vectors were enzyme digested by enzymes SpeI and SacI, and the sticky ends of STTM were ligated to the linear expression vector, resulting in the circular vector pGreen:Act2_pro:STTM:Act2_ter (Supplementary vectors). After being confirmed by PCR and the sequence (Oligos for PCR and sequence are provided in Supplementary Table 1), the four different STTM expression constructs were co-transformed with construct pMDC100:Atu3b:$tRNA^{Asp(GTC)}$ $^{5'}$:polyT into *A. thaliana* wild type by *Agrobacterium*-mediated floral dip [29]. Also the four pGreen:Act2_pro:STTM:Act2_ter constructs were transformed into *A. thaliana* wild type by *Agrobacterium*-mediated floral dip [4]. The T_1 seeds of co-transformation were screened on ½ MS medium supplemented with 1% sucrose and 60 ug/mL Kanamycin [26]. The T_1 seeds of pGreen:Act2_pro:STTM:Act2_ter were sown in seed raising superior germinating soil (Debco, Australia), then the 10 ug/mL Basta (Ammonium

Glufosinate) were sprayed onto the young seedlings for screening

4.3.5. Small RNA sequencing data processing, alignment, clustering, and annotation

The quality of sRNA sequencing data was firstly checked by ngsReports (https://github.com/UofABioinformaticsHub/ngsReports). The Illumina small RNA Adapter for sequence data was first trimmed by Trim Galore, then the NEXTflex® Small RNA 3' adapter and the four random bases in both 3' and 5' adapters trimmed by the cutadapt (https://cutadapt.readthedocs.io/en/stable/installation.html). The redundant reads of sequence data were removed by seqcluster and the raw counts of unique reads were used for clustering analysis. The seqcluster prepare function was used to assign the ID to unique reads (https://github.com/lpantano/seqcluster), followed by alignment to *A. thaliana* TAIR10 (https://www.arabidopsis.org/) reference genome through STAR aligner v2.5.3 with the parameter --alignIntronMax 1 to disable soft-clipping during the alignment process. Next, the reads aligned were clustered through cluster function and annotated with Araport11 annotation [30]. Aligned short reads were clustered under metaclusters by regions of the alignment. For global sRNA profile detection, reads were normalised as recommended in BEDtools genomecov function (https://bedtools.readthedocs.io/en/latest/content/tools/genomecov.html) (Pei et al, unpublished).

4.4. Results

4.4.1. Failure to isolate transgenic lines expressing the *Killer* construct/5'-half of tRNA$^{Asp(GTC)}$

As first documented by Thompson *et al.,* (2008), tRNA cleavage is a conserved molecular response to oxidative stimulus in yeast, human cell lines and plants. Sequence data showed that the accumulated tRNA halves are often tissue-specific. Therefore, it is necessary to clarify the function of specific tRNA halves in *A. thaliana*. Therefore, either the full-length sequence, 5'-half from nucleotides 1 to 36 or 3'-half from nucleotides 36 to 72 of both tRNA$^{Asp(GTC)}$ and tRNA$^{Gln(CTG)}$ were chemically synthesized as dsDNA and inserted into a transgene vector containing the polymerase III AtU3b promoter a PolyT terminator, and plant selectable kanamycin marker gene (Figure 4.1A, B). An obvious difference between our transgene expressed tRNA halves and the cellular tRNA halves is that the transgene derived tRNA halves would not have RNA modifications as these are thought to be added to full-length, folded tRNAs [1]. Nevertheless, the engineered constructs were transformed into *A. thaliana* via floral dipping [29]. Unexpectedly, no kanamycin resistance T_1 seedlings were recovered for the 5'-half of tRNA^{Asp} (labelled tRNA^{Asp} 5' in Figure 4.1) compared to either full-length, 3'-half tRNA^{Asp} or the corresponding constructs of tRNA^{Gln} (Figure 4.1C, D). We then screened about 10 times more seed to recover transgenic 5'-half of tRNA^{Asp} plant, however none were recovered. To determine if this observation was specific to the 5'-half of tRNA$^{Asp5'}$, we generated and transformed four control 5' half tRNA constructs of tRNA$^{Gly(GCC)}$, tRNA$^{Arg(CCT)}$, tRNA$^{His(GTG)}$ and tRNA$^{Tyr(GTA)}$. Transgenic plants were recovered of all four controls (Figure 4.1B, C). Therefore, we proposed that the tRNA$^{Asp5'}$ construct might cause egg, embryo or seedling death when transformed into *A. thaliana*. We called the 5'-half tRNA^{Asp}/tRNA^{Asp} 5' construct, *Killer*.

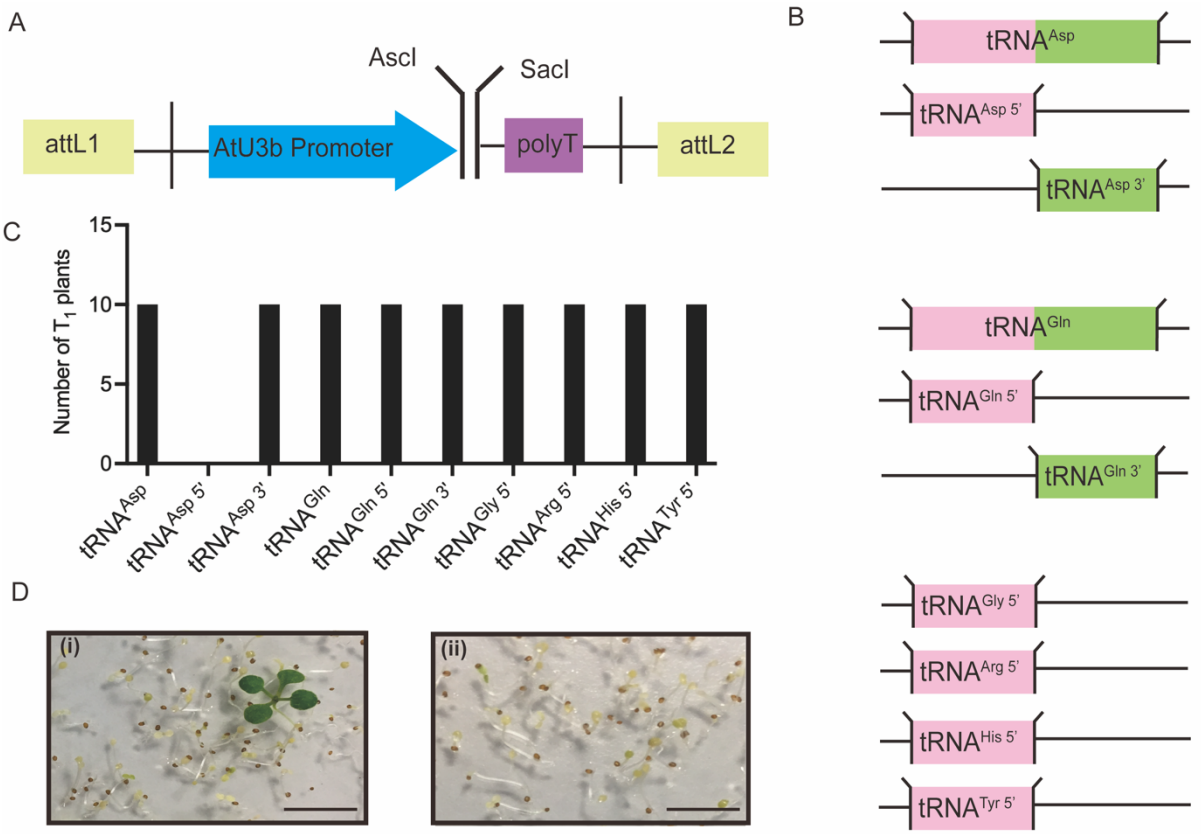

Figure 4.1: Transgenic plants expressing 5'-half tRNA^{Asp} (tRNA$^{Asp5'}$) are not recovered after transformation into *A. thaliana.*

(A) T-DNA region of pMDC100_AtU3b::polyT. The kanamycin gene that confers resistance to kanamycin in planta is not shown. AtU3b is the *Arabidopsis* U3b polymerase III promoter. AscI and SacI restriction enzyme sites were used to clone either full-length or tRNA halves. polyT is the polIII terminator sequence. attL1 and attL2 are GateWay recombination sequences. **(B)** Cartoon representation of ten tRNA sequences that were cloned into pMDC100_AtU3b::polyT. Pink indicates the 5' tRNA region and green indicates the 3' region of the selected tRNAs. **(C)** After *Agrobacterium* mediated floral dipping transformation of the ten transgenes, transgenic plants were recovered after kanamycin selection of approximately 1,000 harvested seeds as determined by seed mass except for tRNA$^{Asp5'}$. About 10,000 seeds were screened in an attempt to recover a single tRNA$^{Asp5'}$ transgenic plant however were recovered. Recovered seeldings were confirmed to contain the transformed cassettes by PCR (data not shown). **(D)** Left, an example of a tRNA^{Asp} T_1 transgenic, kanamycin resistant T_1 seedling and right, examples of kanamycin sensitive seedlings after transforming tRNA$^{Asp5'}$.

4.4.2. Transgenic lines recovered after mutagenesis of nucleotides in tRNA$^{Asp5'}$/*Killer*

To ascertain which specific nucleotide sequence(s) were vital for egg cell, embryo or seedling death caused by *Killer*, we performed mutagenesis of single or double nucleotides. Considering canonical cleavage of mRNA is interfered with ARGONAUTE (AGO) and guided by sRNAs, which normally happens in the 10th and 11th nucleotide of complementarity relative to the sRNAs. Therefore, the 10th and 11th nucleotides from the 5' end of tRNA$^{Asp5'}$ were replaced by other nucleotides, as well as the 16 th, 17 th, 21 th, 22 th, 26 th, 27 th (Fig 4.2A). These ten different constructs containing the mutagenesis sequence of tRNA$^{Asp5'}$ were transformed into *A. thaliana*. Surprisingly, transgenic lines could be screened from the seeds in each of the transformed plants (Fig 4.2B). It shows that nearly every nucleotide chosen is important for the tRNA$^{Asp5'}$ to kill the transgenic lines.

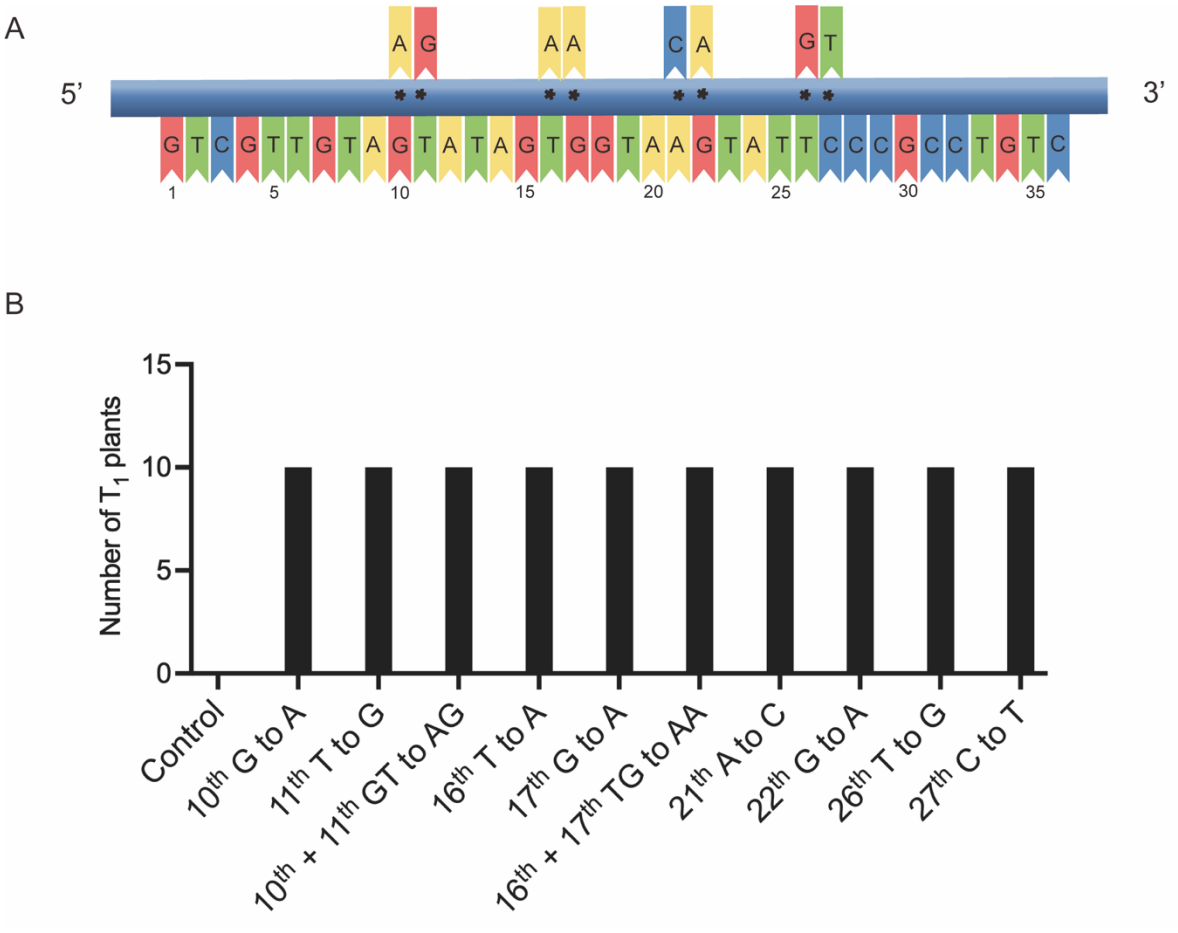

Figure 4.2: Identification of nucleotides necessary for the lethal effect of *Killer*/tRNA$^{Asp5'}$

(A) Specific sites of tRNA$^{Asp\ 5'}$ were mutagenized as indicated by an asterisk. The nucleotide above the blue line is the new base. Ten different mutagenized fragments were cloned into vector pMDC100:AtU3b::polyT to produce recombinant plasmids. **(B)** The number of transgenic plants obtained from the ten vectors and the control plasmid, *Killer*. The number of ten-day-old antibiotics resistant seedlings are shown and were subsequently PCR confirmed (data not shown). The modified nucleotide position is shown in the x-axis ranging from position 10-27.

4.4.3. Identification of genetic suppressors required for the lethal phenotype of *Killer*

Generally, the double-stranded RNA (dsRNA) is cut by DICER-LIKE (DCL) proteins to generate small interfering RNAs (siRNAs) normally in 20-24 nt length; next, the ARGONAUTE (AGO) proteins proceed with the loading of one strand of these siRNAs to get the RNA-induced silencing complex (RISC) to lead the posttranscriptional gene silencing (PTGS) or transcriptional gene silencing (TGS) of the target RNA [31]. Considering the size and the secondary structure, we made the hypothesis that the tRNA$^{Asp5'}$ was firstly synthesized into double-stranded by the RNA-DEPENDENT RNA POLYMERASE (RDR) due to the structure instability, then was cut into several sRNAs by DCL and subsequently processed into siRNAs for gene silencing (Fig 4.3A). Therefore, we ask the question of which genetic suppressors incorporate into the processing of the tRNA$^{Asp5'}$. We transformed the construct pMDC100:AtU3b:tRNA$^{Asp5'}$:polyT into the *Arabidopsis* genetic suppressors background mutants (*ago1-27*, *ago2-1*, *ago3-1*, *ago4-3*, *ago5-3*, *ago7-1*, *ago9-1*, *ago10*, *dcl2-1*, *dcl3-1*, *dcl4-2*, *rdr2-2*, *rdr6-15*), the transformation of pMDC100:AtU3b:tRNA^{Asp}:polyT was used as the comparison. As expected, the transformation of pMDC100:AtU3b:tRNA^{Asp}:polyT in mutants could get the kanamycin-resistance seedlings (Fig 4.3B). While for the transformation of pMDC100:AtU3b:tRNA$^{Asp5'}$:polyT, the majority of transformed mutants could get kanamycin-resistance seedlings apart from the mutants *ago2-1* and *rdr2-2* (Fig 4.3B), which suggests that the tRNA$^{Asp5'}$ might be processed into several fragments of sRNAs in which most of the genetic suppressors are incorporated.

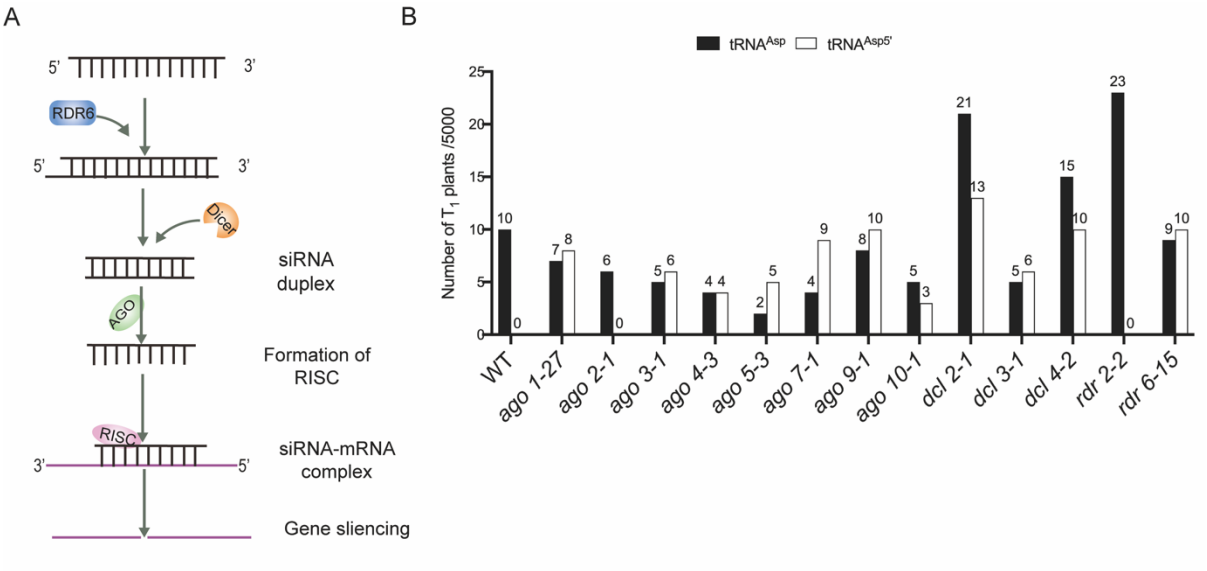

Figure 4.3: Identification of genetic suppressors of *Killer*/tRNA$^{Asp5'}$ in *A. thaliana.*

(A) The predicted mechanism of *Killer*/tRNA$^{Asp\ 5'}$ processing and mRNA targeting. After the transgene expressing the 5 half tRNA fragment was transformed into *Arabidopsis*, double-stranded RNA is formed, processed via a RNA silencing RNA pathway involving a RNA dependent RNA polymerase (RDR), Dicer-like ribonuclease (DCL) and Argonaute effector protein (AGO). **(B)** The number of transgenic plants obtained after transformation of either full-length tRNA^{Asp} (control) or *Killer* constructs into various mutants. WT is wild type *A. thaliana*. Ten-day-old antibiotic resistant seedlings were identified and confirmed by PCR (data not shown).

4.4.4. Observation of seed development in the genetic suppressor mutant transformed with tRNA$^{Asp5'}$

The dysregulation of genetic suppressors like AGO1, DCL2 and RDR6 contribute to the obtaining of transgenic lines having tRNA$^{Asp5'}$. Subsequently, we performed the crossing between genetic suppressors mutants transformed with tRNA$^{Asp5'}$ and wild type to check if the crossing seeds could be developed normally. We selected one of tRNA$^{Asp5'}$ transformed mutant *ago1-27* (*ago1-27 (tRNA$^{Asp5'}$)*) for assay. The self-crossing of WT and *ago1-27 (tRNA$^{Asp5'}$)* was conducted for control. As we can see from the Fig 4.4A, aborted seeds in the siliques could be observed in the F_1 cross between *ago1-27 (tRNA$^{Asp5'}$)* (♀) x WT (♂) and WT (♀) x *ago1-27 (tRNA$^{Asp5'}$)* (♂). The aborted seeds in the F_1 cross were counted and shown in Fig 4.4B. Overall, it has been again

evidenced that the AGO1 is associated with the processing of tRNA$^{Asp5'}$, as well other genetic suppressors besides the AGO2 and RDR2 in *A. thaliana*.

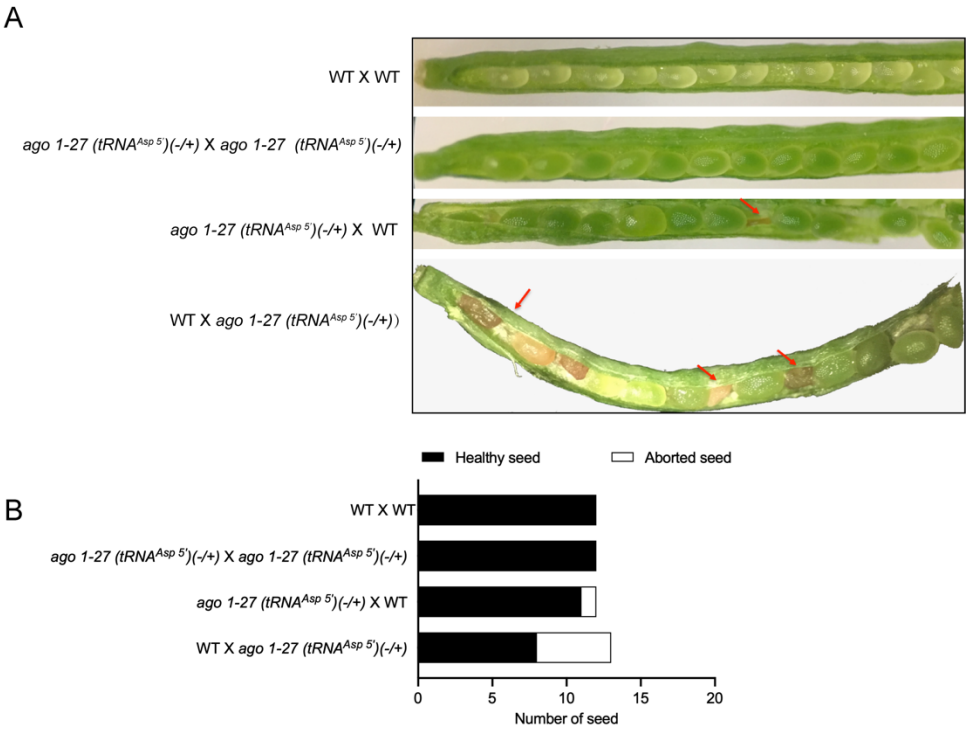

Figure 4.4: Seed abortion occurred in translation inhibitor mutant *ago1-27* seedlings transformed by pMDC100:AtU3b:tRNA^{Asp}:polyT.

(A) Observation of seed development in F_1 crosses of WT X WT, *ago1-27(tRNA $^{Asp5'}$) (-/+)* X *ago1-27(tRNA $^{Asp5'}$) (-/+)*, *ago1-27(tRNA $^{Asp5'}$) (-/+)* X WT and WT X *ago1-27(tRNA $^{Asp5'}$) (-/+)*. **(B)** The number of healthy/green or aborted seeds per silique from different crosses. Green or healthy seed numbers are shown in black and aborted seeds are shown in white. The pollen donor is written second.

4.4.5. Identification of the tRNA$^{Asp5'}$ derived sRNAs after transient expression in *N. benthamiana*

To further test our hypothesis that the tRNA$^{Asp5'}$ was processed into sRNAs and then influence the translation in *A. thaliana*, we infiltrated the plasmid containing pMDC100:AtU3b: tRNA$^{Asp5'}$:polyT (tRNA$^{Asp5'}$) into the leaves of transgenic *N. benthamiana* having pBin-35S-mGFP5, the plasmid containing pMDC100:AtU3b: tRNA^{Asp}:polyT (tRNA^{Asp}) and the *Agrobacterium tumefaciens*

without the plasmid was used as control (Fig 4.5A). Five days later, either the GFP fluorescence signal under microscope or the qPCR on GFP relative abundance on *N. benthamiana* leaves shown that infiltrated plasmid having both the $tRNA^{Asp5'}$ and $tRNA^{Asp}$ lead to the decreased GFP expression (Fig 4.5B, C). Furthermore, the transient infiltrated leaves on fifth days were collected for sRNAs extraction prepared for northern blotting and library construction. As we can see from the Fig 4.5D, E, the infiltration of plasmid having the $tRNA^{Asp5'}$ results in the increased 5'-half of $tRNA^{Asp(GTC)}$ abundance, in comparison to the no plasmid and $tRNA^{Asp}$ infiltration, which indicates the plasmids were successfully infiltrated into the leaves of *N. benthamiana*. As proposed the $tRNA^{Asp5'}$ was processed into sRNAs shorter than 35 nt, so the sRNAs on the gel windows were roughly about 35 nt and the corresponding 18-25 nt were cut and purified for small RNA sequencing. The sequencing data analysis of the *N. benthamiana* leaves infiltrated with the plasmid having the pMDC100:AtU3b: $tRNA^{Asp5'}$:polyT demonstrated that the several sRNAs from the $tRNA^{Asp5'}$ in a different range of size were mapped to the genome (Fig 4.5F), which supports our hypothesis and consistent with the genetic suppressors results. Among these sRNAs, a 19 nt sRNAs from the $tRNA^{Asp}$ is the most abundant.

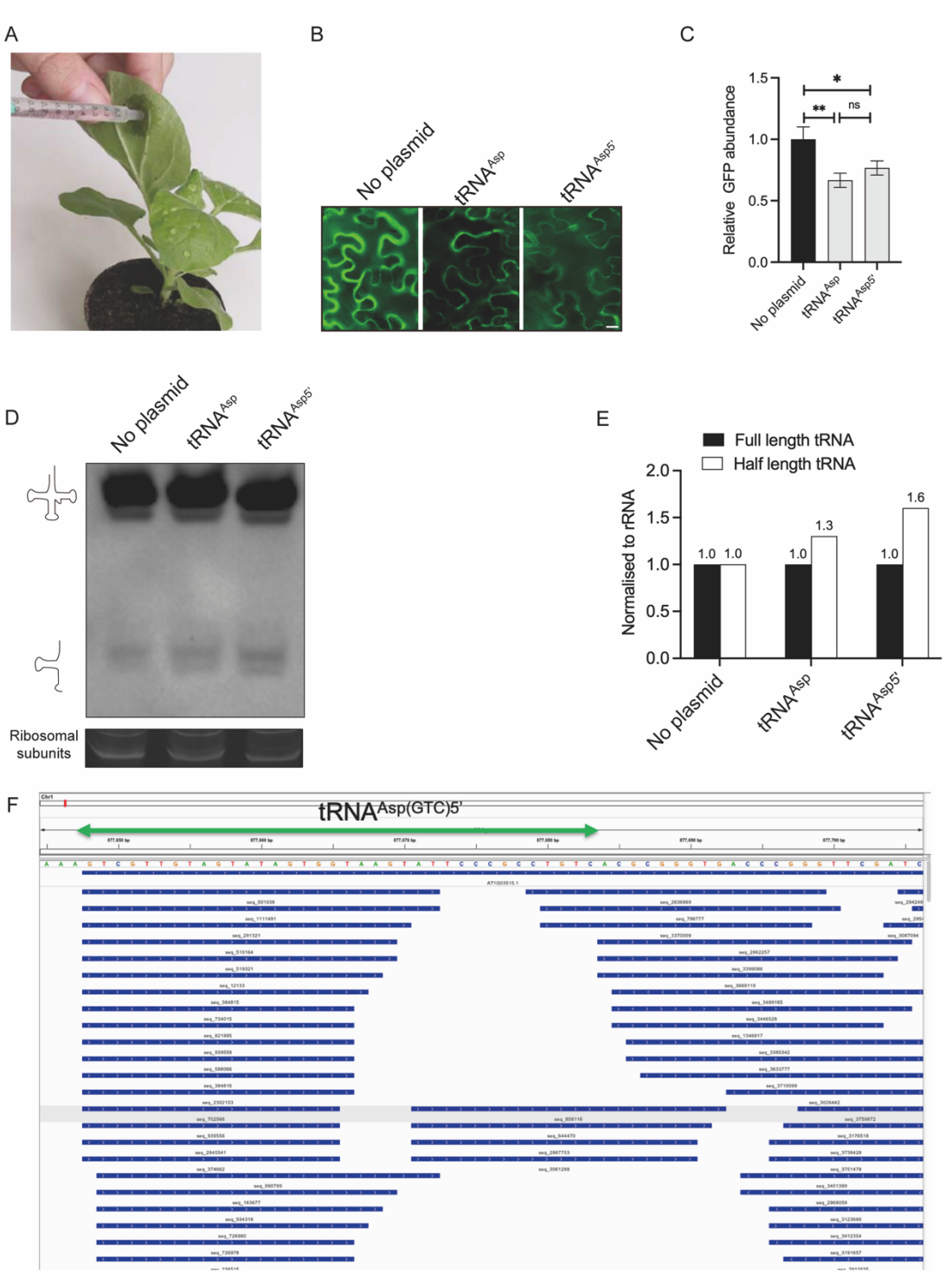
A
B
No plasmid
tRNA^Asp
tRNA^Asp5'
C
Relative GFP abundance
1.5
1.0
0.5
0.0
*
**
ns
No plasmid
tRNA^Asp
tRNA^Asp5'
D
No plasmid
tRNA^Asp
tRNA^Asp5'
Ribosomal subunits
E
Full length tRNA
Half length tRNA
Normalised to rRNA
2.0
1.5
1.0
0.5
0.0
1.0 1.0
1.0 1.3
1.0 1.6
No plasmid
tRNA^Asp
tRNA^Asp5'
F
tRNA^Asp(GTC)5'

Figure 4.5: sRNAs derived from tRNA$^{Asp5'}$ are different lengths and accumulate in *N. benthamiana*

(A) Transient infiltration of the tRNA$^{Asp5'}$ and tRNA^{Asp} constructs in *N. benthamiana* 35S-mGFP5. No plasmid control were leaves infiltrated with *Agrobacterium* without a binary T-DNA plasmid. **(B)** The GFP signal was observed five days after infiltration by epifluorescence microscopy. **(C)** The mRNA abundance of GFP mRNA in infiltrated leaves was determined by RT-PCR. The error bars show the standard deviation of the mean from three replicates. **(D)** Northern blotting analysis using a tRNA$^{Asp(GTC)}$ probe on RNA purified from the infiltrated *N. benthamiana* leaves. The full-length tRNA is shown as a clover leaf symbol. The RNA loading control was the ethidium bromide stained gel prior to transfer. **(E)** Quantitative analysis of tRNA$^{Asp(GTC)}$ abundance in infiltrated *N. benthamiana* leaves. The signal intensities were normalised to ribosomal subunits. **(F)** Genome browser view of full-length tRNA^{Asp}. Small RNA sequencing data from infiltrated leaves expressing the tRNA$^{Asp5'}$ and tRNA^{Asp} transgene. The green arrow shows the 5' half sequence.

4.4.6. Inhibition of the tRNA$^{Asp5'}$ by STTM in *A. thaliana*

The STTM, an effective technology tool, has been widely designed to simultaneously block the function of sRNAs in plants and animals, in which the sequence of two binding sites at the two sides of the stem-loop is complementary to target sRNAs except for trinucleotide bulge at the 10th or 11th nucleotides [32]. Therefore, to prevent the sRNAs from tRNA$^{Asp5'}$ binding to the mRNA and leading to seedlings death, the STTM construct was introduced into our experiment. Considering the sequence and direction of the double-strand RNA of tRNA$^{Asp5'}$, four STTM constructs, STTM5, STTM3, STTM5 reverse, and STTM3 reverse were designed and co-transformed with pMDC100:AtU3b: tRNA$^{Asp5'}$:polyT into *A. thaliana* (Fig 4.6A, B). The T_1 seeds from co-transformed plants and transformed plants with only STTM were screened with kanamycin and BASTA (Ammonium Glufosinate) separately. Since there are no transformed tRNA$^{Asp5'}$, the transgenic plants only containing the four STTM constructs could all be detected (Fig 4.6C). After normalising to the co-transformation rate [33], [34], we screened three and twelve T_1 transgenic plants from the co-transformation of STTM5 with tRNA$^{Asp5'}$ and STTM3 with tRNA$^{Asp5'}$ (Fig 4.6C), which indicates the bottom strand of tRNA$^{Asp5'}$ is processed into sRNAs and two of them results in the gene silencing. The T_1 plant co-transformed with STTM5 and tRNA$^{Asp5'}$ was further PCR confirmed

(Fig 4.6D). Furthermore, we also check the abundance of tRNA$^{Asp5'}$ in wild type, STTM5 transformant plants and the co-transformant plants of STTM5 and tRNA$^{Asp5'}$ through northern blotting. As we can see from the northern blotting in Fig 4.6E and the quantification data in Fig 4.6F, the abundance of 5'-half in tRNA$^{Asp(GTC)}$ decreases in comparison to wild type and the STTM5 transformant plants. It is likely that the sRNAs from the transformed tRNA$^{Asp5'}$ are bound by the STTM5 construct and prevent its targeting. Because three STTM5 transformant lines are heterozygous or the RNA loading problem, the data of abundance of 5'-half in tRNA$^{Asp(GTC)}$ exhibits fluctuation. Overall, the transgenic plants from the co-transformation of STTM5 and STTM3 with the tRNA$^{Asp5'}$ verify our assumption that the 35 nt single-stranded tRNA$^{Asp5'}$ was firstly synthesised into double-stranded RNA, then it was cut into sRNAs in which two single-stranded sRNAs from the bottom strand of tRNA$^{Asp5'}$ inhibit the target gene expression.

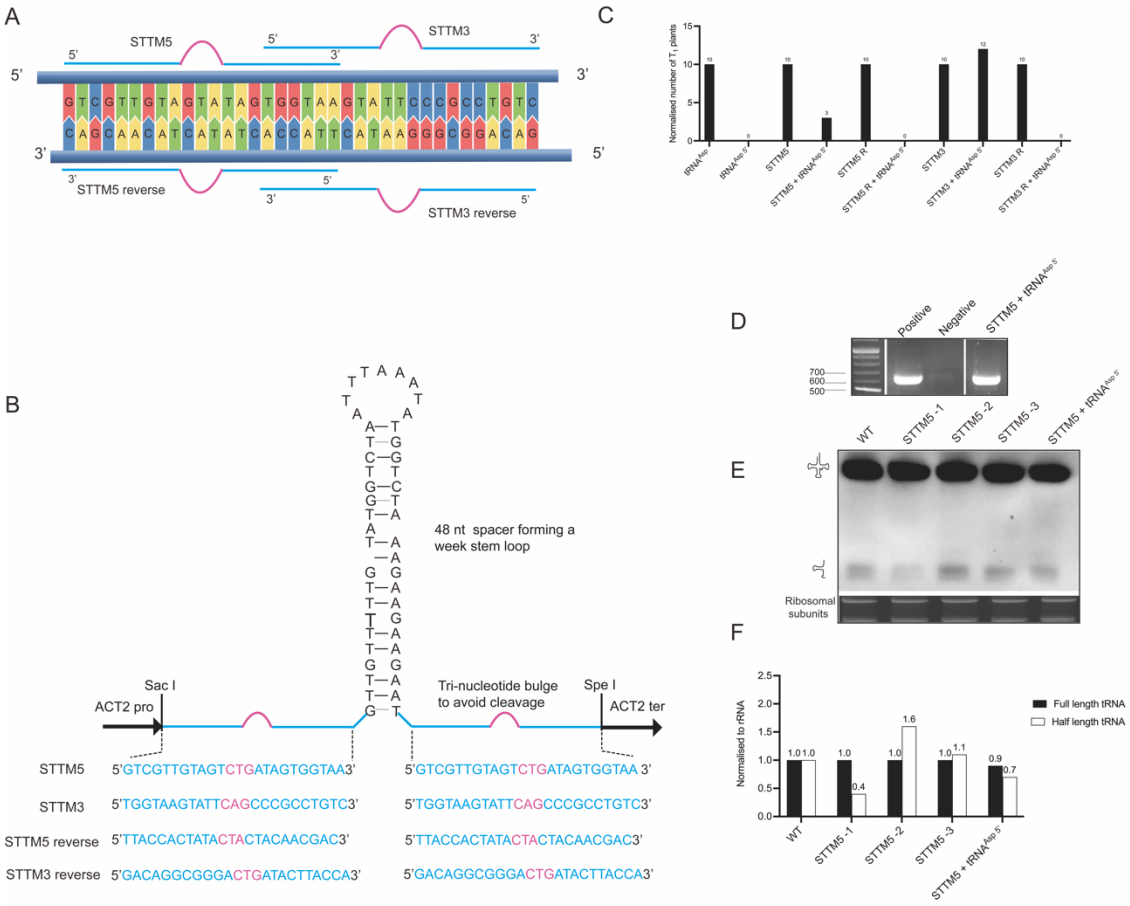

Figure 4.6: STTM constructs alleviate the lethal function of *Killer* in *A. thaliana*.

(A) (B) Based on the direction and sequence of $tRNA^{Asp\ 5'}$, four STTM sequences, STTM 5, STTM3, STTM5 reverse (STTM5 R), or STTM3 reverse (STTM3 R) were constructed in a pGreen vector driven by the ACTIN2 promoter and contained an ACTIN2 terminator. **(C)** The number of transgenic plants obtained after transforming wild type (WT) Columbia with either single or double plasmids (STTM5, STTM5 + $tRNA^{Asp5'}$, STTM5 R, STTM5R + $tRNA^{Asp5'}$, STTM3, STTM3 + $tRNA^{Asp5'}$, STTM3 R and STTM3 R+ $tRNA^{Asp5'}$). **(D)** PCR detection of the kanamycin gene in antibiotic resistant T_1 seedlings after transformation of double plasmids STTM5 + $tRNA^{Asp5'}$. **(E)** Northern blotting analysis using a $tRNA^{Asp(GTC)}$ probe of RNA isolated from wild type (WT) or T_1 seedlings transformed with plasmids STTM5 and double plasmids STTM5 + $tRNA^{Asp5'}$. **(F)** The signal intensities were normalised to ribosomal subunits.

4.4.7. Target prediction of two sRNAs from the $tRNA^{Asp5'}$

The results from the above validation provide compelling evidence that the $tRNA^{Asp5'}$ transformed into *A. thaliana* has been processed into several sRNAs by genetic suppressors, and the recovery of transgenic plants from the co-transformation of STTM5 and $tRNA^{Asp5'}$ also verifies our presumption. Next, the priority is to identify the target gene of these two sRNAs and then proceed with the validation. Currently, the developed psRNATarget is widely adopted to identify the targets of plant sRNA through analyzing complementary matching between the sRNA sequence and target mRNA sequence using a predefined scoring schema and by evaluating target site accessibility [35]. Consequently, we input the corresponding reverse complementary sequence of STTM5 and STTM3 of the $tRNA^{Asp5'}$ into the psRNATarget web server and got a list of candidate genes. Among them, two embryo-defective genes At1g67490 and At1g32490 were found. Therefore, we think two sRNAs from $tRNA^{Asp5'}$ target these two embryo-defective genes and lead to the dysregulation of them, which may explain the non-transgenic lines from the transformation of $tRNA^{Asp5'}$.

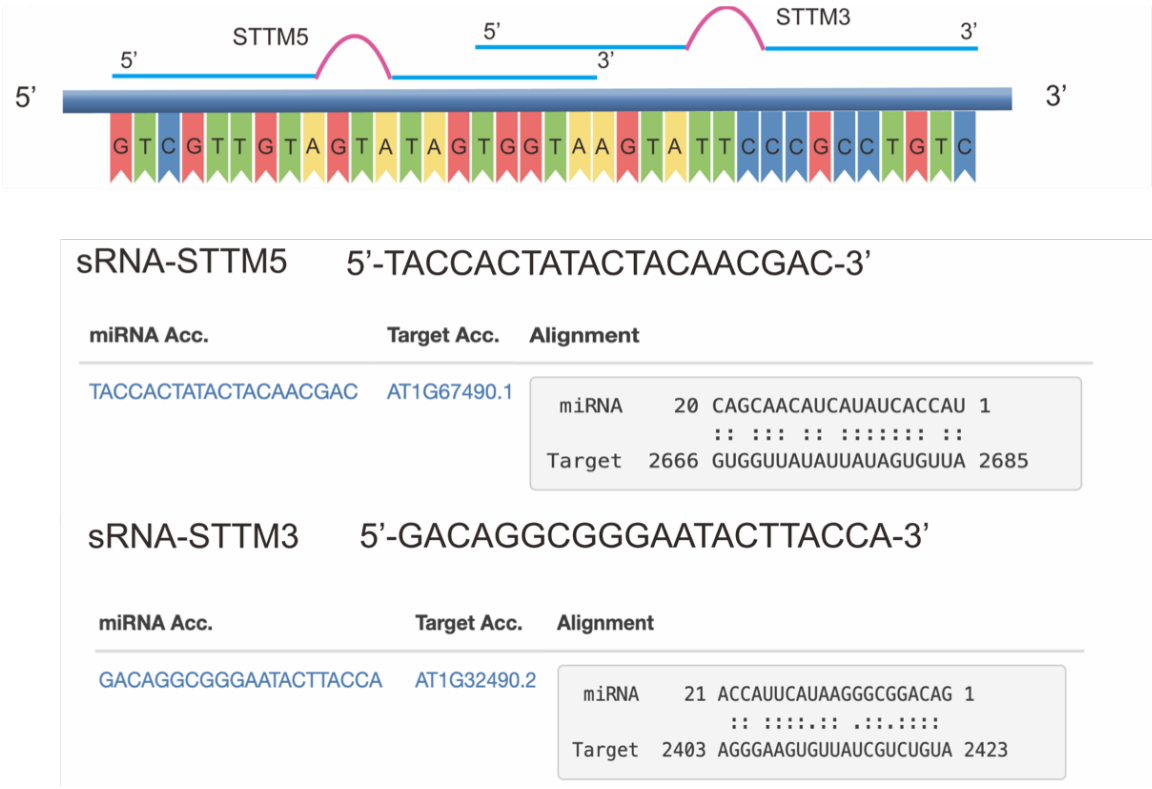

Figure 4.7: Prediction of the target embryo-defective genes of two sRNAs from tRNA$^{Asp5'}$.

Upper panel shows the sequence of of tRNA$^{Asp5'}$ and the sequence of STTM5 and STTM3. Below panel shows predicted micro-RNA sequences derived from tRNA$^{Asp5'}$ and candidate target genes using psRNATarget. Among the list of candidate genes, two embryo-defective genes At1g67490 and At1g32490 were found.

4.5. Discussion and conclusion

Since the beginning of this century, stressed-induced tRNA halves and tRFs discussed in multiple organisms have been recognised as part of the cellular response. As of now, the ribonucleases needed for the tRNA cleavage have been gradually disclosed [36]–[38], and the next focus for the research would be the multi-functionality of the tsRNAs, especially under stress conditions. The potential molecular function of specific tRFs has been broadly deciphered, including regulating protein translation and non-coding RNA activity, modulating gene silencing, and impacting human disease and other cellular activities [39]–[42]. However, very little is known about the physiological function of certain tRNA halves, especially in plants.

Our Northern blotting results and the published data indicated that the abundance of $tRNA^{Asp5'}$ increased upon oxidative stress [9]. Due to the technical difficulty in purifying the certain tRNA halves, we, therefore, attempt to address the impacts of $tRNA^{Asp5'}$on molecular function by using the synthetic tRNA sequence. Interestingly, only the transformation of $tRNA^{Asp5'}$ results in the seedling death in our study, compared to its full length, 3'-half and other 5'-half tRNAs. Taking into consideration the D-loop in secondary structure and the size in 35 nt, the transformed $tRNA^{Asp5'}$ was suggested to be firstly synthesized into double-stranded RNA then processed into the smaller fragments and get involved in the canonical gene silencing pathway.

Our attempts to mutagenesis some specific nucleotides of $tRNA^{Asp5'}$ all obtained the transgenic plants, suggesting the selected nucleotides are vital for the further processing of $tRNA^{Asp5'}$. The sequenced data on $tRNA^{Asp5'}$ transient infiltrated leaves of *N. benthamiana* verified that the 35 nt $tRNA^{Asp5'}$ was processed into a series of sRNAs at different lengths in which the 19 nt is the most dominant, and the genetic suppressors RDR6, most members of the DCL and AGO are all involved. Besides the AGO2, the other members of the AGO were found to be associated with sRNAs from $tRNA^{Asp5'}$, which could be explained by the nucleotides preference of AGO [19]. Specifically, the sRNA

with the uracil at the 5' terminal is preferentially bonded by AGO1 [43], while the AGO4 and AGO5 have a strong preference for adenine and cytosine separately [44]. In addition, the length preference of AGOs is also suggested with the siRNAs, the AGO1 and AGO5 are incorporated with 19 nt siRNAs, and the AGO4 and AGO6 are mostly correlated with 23-26 nt siRNAs [7], [45]. Furthermore, DCL2, DCL3 and DCL4 generate siRNAs in certain sizes respectively, 22, 24 and 21 nt [46]. As of yet, report about the stability of tRFs and tRNA halves is sparse. In general, our results provide compelling evidence that there are sRNAs produced from the tRNA halves, which disclose that the cleaved tRNA halves are not stable and may be the resource of tRFs and sRNAs.

The developed technique STTM and the website psRNATarget are widely adopted to study the function of miRNA. The STTM is designed to silence the miRNA, and the psRNATarget is used to predict the target gene of miRNA [32], [35]. Therefore, we designed four STTM constructs based on the sequence of $tRNA^{Asp5'}$, the co-transformation of four STTM constructs with $tRNA^{Asp5'}$ revealed that the two sRNAs from the bottom strand of $tRNA^{Asp5'}$ lead to the seedling death through canonical gene silencing pathway. Two embryo-defective genes, At1g67490 and At1g32490, were predicted to be the target of these two sRNAs by the psRNATarget. However, confirmation is needed to be conducted in the future.

The tRFs were also suspected to bind to the genetic suppressors AGO to form the RISC to inhibit the target gene expression. Various investigations have been conducted to rationalise this assumption. Specifically, the LTR retrotransposon *Athila6A* was suggested to be targeted and cleaved by a 19 nt tRF-5s from $tRNA^{Met(CAT)}$ in the pollen of *A. thaliana* [10]. Similarly, the tRFs from rhizobial were confirmed to regulate soybean (*Glycine max*) development and nodule formation, thereby exerting a vital impact on the symbiotic regulation between bacteria and root [24]. In addition, the tRF-5s from $tRNA^{Ala(AGC)}$ are indicated to be linked with AGO1 to inhibit the expression of *Cytochrome* (CYP71A13) upon fungal infection [47]. It is noteworthy that tsRNAs may compete with dsRNA precursors and siRNAs for DCL or AGO

binding, respectively under stress conditions [48]. Zeljko et al. (2013) provide evidence that the DCL2 activity on long dsRNA substrates was inhibited by the increased tRFs under heat shock, leading to an inhibition of siRNA pathway-dominated genes [49].

The functional validation of tRFs through the miRNA-like pathway could simplify the investigation of the biological role in some tRFs and the sRNAs from the tRNA halves. Nevertheless, there are still some uncleared questions. Such as the cleavage sites generally are between the 10^{th} and 11^{th} nucleotides of miRNA, while the 13^{th} and 14^{th} nucleotides of tRF-5s from $tRNA^{Ala(AGC)}$ were suggested to cleave the CYP71A13 mRNA [47]. Furthermore, molecular insight into the association between tRF-3s and 3'-half tRNA and microRNA-like gene silencing activities is less.

Overall, our study revealed that the cleaved 5'-half of $tRNA^{Asp}$ could be cleaved into sRNAs and then get involved in gene silencing, which advances our understanding of cleaved tRNA halves. However, whether other tRNA halves experience the processing as $tRNA^{Asp5'}$ is still unclear. Meanwhile, the seedling death caused by the transformation of $tRNA^{Asp5'}$ provides a potential opportunity that the $tRNA^{Asp5'}$ could be developed for the herbicide application.

4.6. References

[1] J. E. Jackman and J. D. Alfonzo, “Transfer RNA modifications: Nature’s combinatorial chemistry playground,” *Wiley Interdisciplinary Reviews: RNA*, vol. 4, no. 1. Wiley Interdiscip Rev RNA, pp. 35–48, Jan. 2013. doi: 10.1002/wrna.1144.

[2] M. Shigematsu, S. Honda, P. Loher, A. G. Telonis, I. Rigoutsos, and Y. Kirino, “YAMAT-seq: An efficient method for high-throughput sequencing of mature transfer RNAs,” *Nucleic Acids Res*, vol. 45, no. 9, p. e70, May 2017, doi: 10.1093/nar/gkx005.

[3] T. Gogakos, M. Brown, A. Garzia, C. Meyer, M. Hafner, and T. Tuschl, “Characterizing Expression and Processing of Precursor and Mature Human tRNAs by Hydro-tRNAseq and PAR-CLIP,” *Cell Rep*, vol. 20, no. 6, pp. 1463–1475, Aug. 2017, doi: 10.1016/j.celrep.2017.07.029.

[4] Y. L. J. Pang, R. Abo, S. S. Levine, and P. C. Dedon, “Diverse cell stresses induce unique patterns of tRNA up- and down-regulation: tRNA-seq for quantifying changes in tRNA copy number,” *Nucleic Acids Res*, vol. 42, no. 22, 2014, doi: 10.1093/nar/gku945.

[5] X. Ma *et al.*, “Extensive profiling of the expressions of tRNAs and tRNA-derived fragments (tRFs) reveals the complexities of tRNA and tRF populations in plants,” *Sci China Life Sci*, 2021, doi: 10.1007/s11427-020-1891-8.

[6] A. Thompson *et al.*, “tRex: A Web Portal for Exploration of tRNA-Derived Fragments in Arabidopsis thaliana,” *Plant Cell Physiol*, vol. 59, no. 1, p. E1, Jan. 2018, doi: 10.1093/PCP/PCX173.

[7] C. S. Alves, R. Vicentini, G. T. Duarte, V. F. Pinoti, M. Vincentz, and F. T. S. Nogueira, “Genome-wide identification and characterization of tRNA-derived RNA fragments in land plants,” *Plant Mol Biol*, vol. 93, no. 1–2, pp. 35–48, Jan. 2017, doi: 10.1007/s11103-016-0545-9.

[8] L. C. Hsieh *et al.*, “Uncovering small RNA-mediated responses to phosphate deficiency in Arabidopsis by deep sequencing,” *Plant Physiol*, vol. 151, no. 4, pp. 2120–2132, Dec. 2009, doi: 10.1104/pp.109.147280.

[9] D. M. Thompson, C. Lu, P. J. Green, and R. Parker, “tRNA cleavage is a conserved response to oxidative stress in eukaryotes,” *RNA*, vol. 14, no. 10, pp. 2095–2103, Oct. 2008, doi: 10.1261/rna.1232808.

[10] G. Martinez, S. G. Choudury, and R. K. Slotkin, “TRNA-derived small RNAs target transposable element transcripts,” *Nucleic Acids Res*, vol. 45, no. 9, pp. 5142–5152, May 2017, doi: 10.1093/nar/gkx103.

[11] S. Zhang, L. Sun, and F. Kragler, “The phloem-delivered RNA pool contains small noncoding RNAs and interferes with translation1[W][OA],” *Plant Physiol*, vol. 150, no. 1, pp. 378–387, May 2009, doi: 10.1104/pp.108.134767.

[12] C. J. Chen, Q. Liu, Y. C. Zhang, L. H. Qu, Y. Q. Chen, and D. Gautheret, “Genome-wide discovery and analysis of microRNAs and other small RNAs from rice embryogenic callus,” *RNA Biol*, vol. 8, no. 3, pp. 538–547, 2011, doi: 10.4161/rna.8.3.15199.

[13] M. Hackenberg, P. J. Huang, C. Y. Huang, B. J. Shi, P. Gustafson, and P. Langridge, “A Comprehensive expression profile of microrna and other classes of non-coding small RNAs in barley under phosphorous-deficient and-sufficient conditions,” *DNA Research*, vol. 20, no. 2, pp. 109–125, Apr. 2013, doi: 10.1093/dnares/dss037.

[14] Y. Li *et al.*, “Stress-induced tRNA-derived RNAs: A novel class of small RNAs in the primitive eukaryote Giardia lamblia,” *Nucleic Acids Res*, vol. 36, no. 19, pp. 6048–6055, 2008, doi: 10.1093/nar/gkn596.

[15] S. Lalande, R. Merret, T. Salinas-Giegé, and L. Drouard, “Arabidopsis tRNA-derived fragments as potential modulators of translation,” *RNA Biol*, vol. 17, no. 8, pp. 1137–1148, 2020, doi: 10.1080/15476286.2020.1722514.

[16] P. Ivanov, M. M. Emara, J. Villen, S. P. Gygi, and P. Anderson, “Angiogenin-Induced tRNA Fragments Inhibit Translation Initiation,” *Mol Cell*, vol. 43, no. 4, pp. 613–623, Aug. 2011, doi: 10.1016/j.molcel.2011.06.022.

[17] M. Nowacka, P. M. Strozycki, P. Jackowiak, A. Hojka-Osinska, M. Szymanski, and M. Figlerowicz, “Identification of stable, high copy number, medium-sized RNA degradation intermediates that accumulate in plants under non-stress conditions,” *Plant Mol Biol*, vol. 83, no. 3, pp. 191–204, Oct. 2013, doi: 10.1007/s11103-013-0079-3.

[18] A. Sobala and G. Hutvagner, “Small RNAs derived from the 5′ end of tRNAs can inhibit protein translation in human cells,” *RNA Biol*, vol. 10, no. 4, pp. 553–563, 2013, doi: 10.4161/RNA.24285/SUPPL_FILE/KRNB_A_10924285_SM0001.ZIP.

[19] G. Loss-Morais, P. M. Waterhouse, and R. Margis, “Description of plant tRNA-derived RNA fragments (tRFs) associated with argonaute and identification of their putative targets,” *Biology Direct*, vol. 8, no. 1. Biol Direct, Feb. 12, 2013. doi: 10.1186/1745-6150-8-6.

[20] V. Cognat *et al.*, “The nuclear and organellar {tRNA}-derived {RNA} fragment population in Arabidopsis thaliana is highly dynamic.,” *Nucleic Acids Res*, vol. 45, no. 6, pp. 3460–3472, Apr. 2017, doi: 10.1093/nar/gkw1122.

[21] A. Boskovic, X. Y. Bing, E. Kaymak, and O. J. Rando, “Control of noncoding RNA production and histone levels by a 5’ tRNA fragment,” *Genes Dev*, vol. 34, no. 1–2, pp. 118–131, Jan. 2020, doi: 10.1101/gad.332783.119.

[22] D. Veneziano, S. di Bella, G. Nigita, A. Laganà, A. Ferro, and C. M. Croce, “Noncoding RNA: Current Deep Sequencing Data Analysis Approaches and Challenges,” *Human Mutation*, vol. 37, no. 12. John Wiley and Sons Inc., pp. 1283–1298, Dec. 01, 2016. doi: 10.1002/humu.23066.

[23] A. J. Schorn, M. J. Gutbrod, C. LeBlanc, and R. Martienssen, “LTR-

Retrotransposon Control by tRNA-Derived Small RNAs," *Cell*, vol. 170, no. 1, pp. 61-71.e11, Jun. 2017, doi: 10.1016/j.cell.2017.06.013.

[24] B. Ren, X. Wang, J. Duan, and J. Ma, "Rhizobial tRNA-derived small RNAs are signal molecules regulating plant nodulation.," *Science*, p. eaav8907, Jul. 2019, doi: 10.1126/science.aav8907.

[25] A. L. Burgess, R. David, and I. R. Searle, "Conservation of tRNA and rRNA 5-methylcytosine in the kingdom Plantae," *BMC Plant Biol*, vol. 15, no. 1, pp. 1–17, 2015, doi: 10.1186/s12870-015-0580-8.

[26] S. J. Harrison, E. K. Mott, K. Parsley, S. Aspinall, J. C. Gray, and A. Cottage, "A rapid and robust method of identifying transformed Arabidopsis thaliana seedlings following floral dip transformation," *Plant Methods*, vol. 2, no. 1, pp. 1–7, Nov. 2006, doi: 10.1186/1746-4811-2-19/FIGURES/4.

[27] J. B. Morel *et al.*, "Fertile Hypomorphic ARGONAUTE (ago1) Mutants Impaired in Post-Transcriptional Gene Silencing and Virus Resistance," *Plant Cell*, vol. 14, no. 3, pp. 629–639, Mar. 2002, doi: 10.1105/TPC.010358.

[28] M. D. Curtis and U. Grossniklaus, "A gateway cloning vector set for high-throughput functional analysis of genes in planta," *Plant Physiol*, vol. 133, no. 2, pp. 462–469, 2003, doi: 10.1104/PP.103.027979.

[29] S. J. Clough and A. F. Bent, "Floral dip: a simplified method for Agrobacterium-mediated transformation of Arabidopsis thaliana," *Plant J*, vol. 16, no. 6, pp. 735–743, Dec. 1998, doi: 10.1046/J.1365-313X.1998.00343.X.

[30] C. Y. Cheng, V. Krishnakumar, A. P. Chan, F. Thibaud-Nissen, S. Schobel, and C. D. Town, "Araport11: a complete reannotation of the Arabidopsis thaliana reference genome," *The Plant Journal*, vol. 89, no. 4, pp. 789–804, Feb. 2017, doi: 10.1111/TPJ.13415.

[31] D. Baulcombe, "RNA silencing in plants," *Nature 2004 431:7006*, vol. 431, no. 7006, pp. 356–363, Sep. 2004, doi: 10.1038/nature02874.

[32] G. Tang *et al.*, “Construction of short tandem target mimic ({STTM}) to block the functions of plant and animal {microRNAs}.,” *Methods*, vol. 58, no. 2, pp. 118–125, Oct. 2012, doi: 10.1016/j.ymeth.2012.10.006.

[33] R. Ghedira, S. de Buck, F. van Ex, and G. Angenon, “T-DNA transfer and T-DNA integration efficiencies upon Arabidopsis thaliana root explant cocultivation and floral dip transformation,” vol. 238, no. 6, pp. 1025–1037, 2013, Accessed: May 04, 2022. [Online]. Available: https://about.jstor.org/terms

[34] B. Damm, R. Schmidt, and L. Willmitzer, “Efficient transformation of Arabidopsis thaliana using direct gene transfer to protoplasts,” *Molecular and General Genetics MGG 1989 217:1*, vol. 217, no. 1, pp. 6–12, May 1989, doi: 10.1007/BF00330935.

[35] X. Dai, Z. Zhuang, and P. X. Zhao, “psRNATarget: a plant small RNA target analysis server (2017 release),” *Nucleic Acids Res*, vol. 46, no. W1, pp. W49–W54, Jul. 2018, doi: 10.1093/NAR/GKY316.

[36] D. M. Thompson and R. Parker, “The RNase Rny1p cleaves tRNAs and promotes cell death during oxidative stress in Saccharomyces cerevisiae,” *Journal of Cell Biology*, vol. 185, no. 1, pp. 43–50, Apr. 2009, doi: 10.1083/jcb.200811119.

[37] M. Saikia *et al.*, “Angiogenin-Cleaved tRNA Halves Interact with Cytochrome c, Protecting Cells from Apoptosis during Osmotic Stress,” *Mol Cell Biol*, vol. 34, no. 13, pp. 2450–2463, Jul. 2014, doi: 10.1128/mcb.00136-14.

[38] C. Megel *et al.*, “Plant RNases T2, but not Dicer-like proteins, are major players of tRNA-derived fragments biogenesis,” *Nucleic Acids Res*, vol. 47, no. 2, pp. 941–952, 2019, doi: 10.1093/nar/gky1156.

[39] S. M. Lyons, C. Achorn, N. L. Kedersha, P. J. Anderson, and P. Ivanov, “YB-1 regulates tiRNA-induced Stress Granule formation but not translational repression,” *Nucleic Acids Res*, vol. 44, no. 14, pp. 6949–6960, Aug. 2016, doi:

10.1093/nar/gkw418.

[40] C. Kuscu, P. Kumar, M. Kiran, Z. Su, A. Malik, and A. Dutta, “tRNA fragments (tRFs) guide Ago to regulate gene expression post-transcriptionally in a Dicer-independent manner,” *RNA*, vol. 24, no. 8, pp. 1093–1105, Aug. 2018, doi: 10.1261/rna.066126.118.

[41] A. Boskovic, X. Y. Bing, E. Kaymak, and O. J. Rando, “Control of noncoding RNA production and histone levels by a 5’ tRNA fragment,” *Genes Dev*, vol. 34, no. 1–2, pp. 118–131, Jan. 2020, doi: 10.1101/GAD.332783.119/-/DC1.

[42] Z. Su, B. Wilson, P. Kumar, and A. Dutta, “Non-canonical roles of tRNAs: tRNA fragments and beyond,” *Annu Rev Genet*, vol. 54, p. 47, Nov. 2020, doi: 10.1146/ANNUREV-GENET-022620-101840.

[43] B. Zhang, X. Pan, C. H. Cannon, G. P. Cobb, and T. A. Anderson, “Conservation and divergence of plant microRNA genes,” *Plant J*, vol. 46, no. 2, pp. 243–259, Apr. 2006, doi: 10.1111/J.1365-313X.2006.02697.X.

[44] S. Mi *et al.*, “Sorting of Small RNAs into Arabidopsis Argonaute Complexes Is Directed by the 5′ Terminal Nucleotide,” *Cell*, vol. 133, no. 1, p. 116, Apr. 2008, doi: 10.1016/J.CELL.2008.02.034.

[45] M. Hackenberg, A. Rueda, P. Gustafson, P. Langridge, and B. J. Shi, “Generation of different sizes and classes of small RNAs in barley is locus, chromosome and/or cultivar-dependent,” *BMC Genomics*, vol. 17, no. 1, Sep. 2016, doi: 10.1186/S12864-016-3023-5.

[46] Z. Xie *et al.*, “Genetic and Functional Diversification of Small RNA Pathways in Plants,” *PLoS Biol*, vol. 2, no. 5, p. e104, 2004, doi: 10.1371/JOURNAL.PBIO.0020104.

[47] H. Gu *et al.*, “A 5′ tRNA-Ala-derived small RNA regulates anti-fungal defense in plants,” vol. 65, no. 1, pp. 1–15, 2022, doi: 10.1007/s11427-021-2017-1.

[48] Z. Durdevic and M. Schaefer, “tRNA modifications: Necessary for correct tRNA-derived fragments during the recovery from stress?,” *BioEssays*, vol. 35, no. 4, pp. 323–327, Apr. 2013, doi: 10.1002/bies.201200158.

[49] Z. Durdevic, M. B. Mobin, K. Hanna, F. Lyko, and M. Schaefer, “The RNA Methyltransferase Dnmt2 Is Required for Efficient Dicer-2-Dependent siRNA Pathway Activity in Drosophila,” *CellReports*, vol. 4, pp. 931–937, 2013, doi: 10.1016/j.celrep.2013.07.046.

4.7. Supplementary data

Table 1. Primers used in this chapter

Primer name	Sequence (5’—3’)
pMDC100:AtU3b-F2	CCTTGACCAATGTTGCTCCC
pMDC100:AtU3b-R2	TCAAACAAATGGCGTCTGGG
pGreen:Act2_pro:STTM-F2	GGCTGATGATATCGCTGAGC
pGreen:Act2_pro:STTM-R2	CAAGTGAAGATGGAGGTAGCA
KAN_F	TAAAGCACGAGGAAGCGGTCAG
KAN_R	CAGACAATCGGCTGCTCTGATG
M13/pUC-F	TGTAAAACGACGGCCAGT

M13/pUC-R	CAGGAAACAGCTATGACC
pGreen:Act2_pro::Act_ter-F	TTGTAGTGTCGTACGTTGAACAG
eGFP-F	AAGGGCGAGGAGCTGTTCAC
eGFP-R	GCCGTTCTTCTGCTTGTCG
mGFP-F	AGTGGAGAGGGTGAAGGTGATG
mGFP-R	GCATTGAACACCATAAGAGAAAGTAGTG
EF-F	CACGCATTGCTTGCTTTCA
EF-R	TCCATCTTGTTACAGCAGCAAATC

Table 2: Probe for northern blotting

Probe	Probe sequence (5'—3')
$tRNA^{Asp(GTC)}$	GACAGGCGGGAATACTTACCACTATACTACAACGAC

Table 3: The sequence of gene block AtU3b_$tRNA^{Asp(GTC)}$_polyT

Sequence (5'—3')
GCGGCCCGTTTACTTTAAATTTTTTCTTATGCAGCCTGTGATGGATAACTGAATCAAACAAATGGCGTCTGGGTTTAAGAAGATCTGTTTTGGCTATGTTGGACGAAACAAGTGAACTTTTAGGATCAACTTCAGTTTATATATGGAGCTTATATCGAGCAATAAGATAAGTGGGCTTTTTATGTAATTTAATGGGCTATCGTCCATAGATTCACTAATACCCATGCCCAGTACCCATGTATGCGTTTCATATAAGCTCCTAATTTCTCCCACATCGCTCAAATCTAAACAAATCTTGTTGTATATATAACACT

GAGGGAGCAACATTGGTCAAGGCGCGCCGTCGTTGTAGTATAG
TGGTAAGTATTCCCGCCTGTCACGCGGGTGACCCGGGTTCGAT
CCCCGGCAACGGCGGAGCTCTTTTTTTTTTAAAGG

Table 4. The synthesized sequences of tRNA fragments used for cloning.

Red letters indicate the nucleotides of $tRNA^{Asp(GTC)}$ that were mutagenized.

tRNA fragment	**Top strand (5'—3')**	**Bottom strand (5'—3')**
$tRNA^{Asp(GTC)}$	CGCGGTCGTTGTAGTATA GTGGTAAGTATTCCCGCCT GTCACGCGGGTGACCCGG GTTCGATCCCCGGCAACG GCGAGCT	CGCCGTTGCCGGGGATCGA ACCCGGGTCACCCGCGTGA CAGGCGGGAATACTTACCAC TATACTACAACGAC
$tRNA^{Asp(GTC)\ 5'}$	CGCGGTCGTTGTAGTATA GTGGTAAGTATTCCCGCCT GTCAGCT	GACAGGCGGGAATACTTACC ACTATACTACAACGAC
$tRNA^{Asp(GTC)\ 3'}$	CGCGACGCGGGTGACCCG GGTTCGATCCCCGGCAAC GGCGAGCT	CGCCGTTGCCGGGGATCGA ACCCGGGTCACCCGCGT
$tRNA^{Gln(CTG)}$	CGCGTATAGCCAAGTGGT AAGGCACCGGTTTTTGGTA CGGCATGCAAAGGTTCGA ATCTTTTACTCCAGAGCT	CTGAGTAAAAGGATTCGAAC CTTTGCATGCCGGTACCAAA AACCGGTGCCTTACCACTTG GCTATA

tRNA$^{Gln(CTG)\ 5'}$	CGCGTATAGCCAAGTGGT AAGGCACCGGTTTTTGGTA CGAGCT	CGTACCAAAAACCGGTGCCT TACCACTTGGCTATA
tRNA$^{Gln(CTG)\ 3'}$	CGCGGCATGCAAAGGTTC GAATCCTTTTACTCCAGAG CT	CTGGAGTAAAAGGATTCGAA CCTTTGCATGC
tRNA$^{Gly(GCC)\ 5'}$	CGCGGCACCAGTGGTCTA GTGGTAGAATAGTACTCTG CCAGCT	GGCAGAGTACTATTCTACCA CTAGACCACTGGTGC
tRNA$^{Arg(CCT)\ 5'}$	CGCGGCGTCTGTAGCTCA GTGGATAGAGCGTCTGTTT CCT AGCT	AGGAAACAGACGCTCTATCC ACTGAGCTACAGACGC
tRNA$^{His(GTG)\ 5'}$	CGCGGTGGCTGTAGTTTA GTGGTAAGAATTCCACGTT GTG AGCT	CACAACGTGGAATTCTTACC ACTAAACTACAGCCAC
tRNA$^{Tyr(GTA)\ 5'}$	CGCGCCGACCTTAGCTCA GTTGGTAGAGCGGAAGAC TGTAGTAGTTAGCT	AACTACTACAGTCTTCCGCT CTACCAACTGAGCTAAGGTC GG
tRNA$^{Asp(GTC)\ 5'}$ 10th G to A	CGCGGTCGTTGTAATATAG TGGTAAGTATTCCCGCCTG TCAGCT	GACAGGCGGGAATACTTACC ACTATATTACAACGAC

$tRNA^{Asp(GTC)}$ 5' 11^{th} T to G	CGCGGTCGTTGTAGGATA GTGGTAAGTATTCCCGCCT GTCAGCT	GACAGGCGGGAATACTTACC ACTATCCTACAACGAC
$tRNA^{Asp(GTC)}$ 5' 10^{th}+11^{th} GT to AG	CGCGGTCGTTGTAAGATA GTGGTAAGTATTCCCGCCT GTC AGCT	GACAGGCGGGAATACTTACC ACTATCTTACAACGAC
$tRNA^{Asp(GTC)}$ 5' 16^{th} T to A	CGCGGTCGTTGTAGTATA GAGGTAAGTATTCCCGCCT GTCAGCT	GACAGGCGGGAATACTTACC TCTATACTACAACGAC
$tRNA^{Asp(GTC)}$ 5' 17^{th} G to A	CGCGGTCGTTGTAGTATA GTAGTAAGTATTCCCGCCT GTC AGCT	GACAGGCGGGAATACTTACT ACTATACTACAACGAC
$tRNA^{Asp(GTC)}$ 5' 16^{th}+17^{th} TG to AA	CGCGGTCGTTGTAGTATA GAAGTAAGTATTCCCGCCT GTC AGCT	GACAGGCGGGAATACTTACT TCTATACTACAACGAC
$tRNA^{Asp(GTC)}$ 5' 21^{th} A to C	CGCGGTCGTTGTAGTATA GTGGTACGTATTCCCGCCT GTC AGCT	GACAGGCGGGAATACGTAC CACTATACTACAACGAC

tRNA$^{Asp(GTC)\ 5'}$ 22th G to A	CGCGGTCGTTGTAGTATA GTGGTAAATATTCCCGCCT GTC AGCT	GACAGGCGGGAATATTTACC ACTATACTACAACGAC
tRNA$^{Asp(GTC)\ 5'}$ 26th T to G	CGCGGTCGTTGTAGTATA GTGGTAAGTATGCCCGCC TGTCAGCT	GACAGGCGGGCATACTTACC ACTATACTACAACGAC
tRNA$^{Asp(GTC)\ 5'}$ 27th C to T	CGCGGTCGTTGTAGTATA GTGGTAAGTATTTCCGCCT GTCAGCT	GACAGGCGGAAATACTTACC ACTATACTACAACGAC

Table 5. The sequences of four STTMs used to suppress tRNA$^{Asp(GTC)}$ biological function.

The green letters indicate the SacI and SpeI enzyme recognition sites, the blue letters indicate the tri-nucleotide bulges. The underlined nucleotides indicate the region forming a week stem-loop.

STTM name	**Sequence (5'—3')**
STTM 5	GAGCTCGTCGTTGTAGTCTGATAGTGGTAAGTTGTTGTTGTTAT GGTCTAATTTAAATATGGTCTAAAGAAGAAGAATGTCGTTGTAG

STTM 3	GAGCTCTGGTAAGTATTCAGCCCGCCTGTCGTTGTTGTTGTTA TGGTCTAATTTAAATATGGTCTAAAGAAGAAGAATTGGTAAGTA
STTM 5	GAGCTCTTACCACTATACTACTACAACGACGTTGTTGTTGTTAT GGTCTAATTTAAATATGGTCTAAAGAAGAAGAATTTACCACTAT
STTM 3	GAGCTCGACAGGCGGGACTGATACTTACCAGTTGTTGTTGTTA TGGTCTAATTTAAATATGGTCTAAAGAAGAAGAATGACAGGCG

The plasmid structures used in this chapter

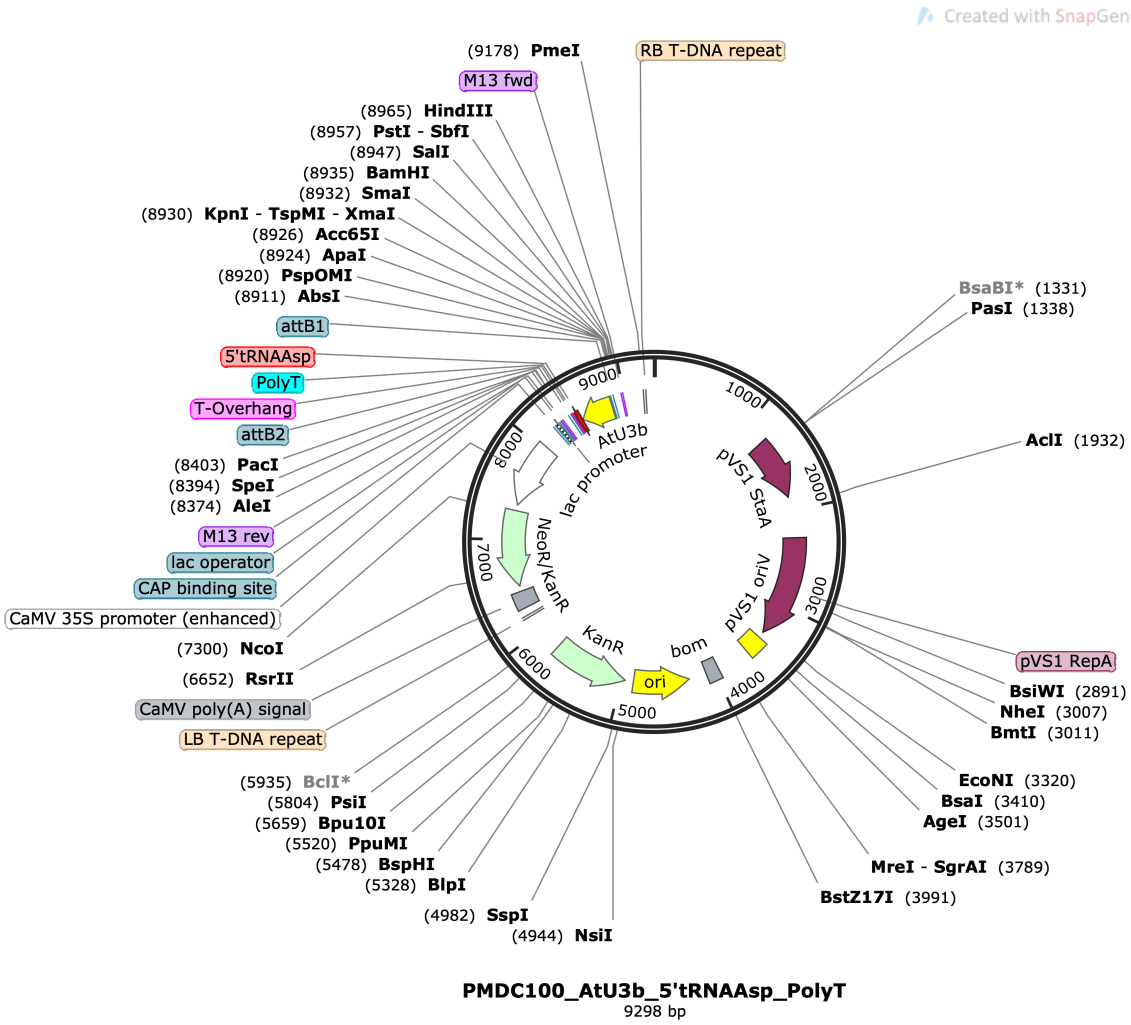

PMDC100_AtU3b_5'tRNAAsp_PolyT
9298 bp

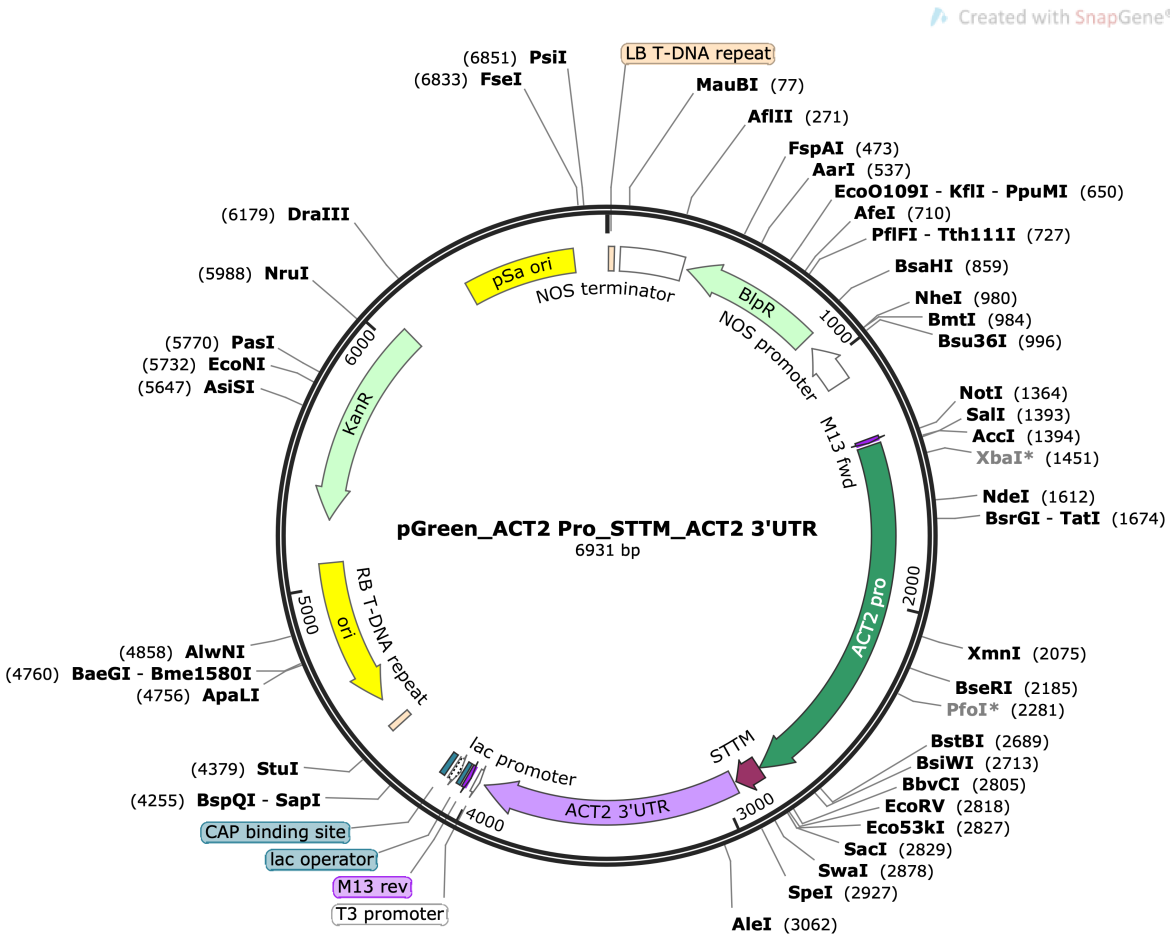
Created with SnapGene®
pGreen_ACT2 Pro_STTM_ACT2 3'UTR
6931 bp
LB T-DNA repeat
MauBI (77)
AflII (271)
FspAI (473)
AarI (537)
EcoO109I - KflI - PpuMI (650)
AfeI (710)
PflFI - Tth111I (727)
BsaHI (859)
NheI (980)
BmtI (984)
Bsu36I (996)
NotI (1364)
SalI (1393)
AccI (1394)
XbaI* (1451)
NdeI (1612)
BsrGI - TatI (1674)
XmnI (2075)
BseRI (2185)
PfoI* (2281)
BstBI (2689)
BsiWI (2713)
BbvCI (2805)
EcoRV (2818)
Eco53kI (2827)
SacI (2829)
SwaI (2878)
SpeI (2927)
AleI (3062)
(6851) PsiI
(6833) FseI
(6179) DraIII
(5988) NruI
(5770) PasI
(5732) EcoNI
(5647) AsiSI
(4858) AlwNI
(4760) BaeGI - Bme1580I
(4756) ApaLI
(4379) StuI
(4255) BspQI - SapI
CAP binding site
lac operator
M13 rev
T3 promoter
pSa ori
NOS terminator
BlpR
NOS promoter
M13 fwd
ACT2 pro
STTM
ACT2 3'UTR
lac promoter
RB T-DNA repeat
ori
KanR
1000
2000
3000
4000
5000
6000

Chapter 5. Discussion and future directions

Amongst the identified 170 cellular RNA modifications, m^5C is one of the most extensively studied modifications occurring on mRNAs, and non-coding rRNAs, tRNAs and lncRNAs [1], [2]. The importance of m^5C is manifested in m^5C RNA methyltransferase mutants, as a short primary root in *Arabidopsis trm4b* seedlings, reduced short-term memory in *nsuns2 Drosophila* flies, and autosomal-recessive intellectual disability in *nsuns2* patients [2]–[4]. While progress has been made in expanding the RNA m^5C field, there is many aspects still to be elucidated. In my thesis, I investigated the molecular and biological role of the putative rRNA methyltransferase NOP2 in *Arabidopsis* in Chapter 2. Then, I explored the regulatory roles of methyltransferase TRM4B and the plant RNase T2 on tRNA cleavage under oxidative stress in Chapter 3. Finally in Chapter 4, I explored the processing and targets of one tRNA half, $tRNA^{Asp(GTC)}$.

The regulatory network of ribosome-biogenesis factors

Ribosome biogenesis is accomplished through pre-rRNA processing, modification and folding, in which ribosome biogenesis factors (RBFs), small nucleolar RNA (snoRNA) species and ribosomal proteins (r-proteins) are involved [5], [6]. Ribosome biogenesis is complicated and the best studied organism is *S. cerevisiae* in which about 250 RBFs have been identified so far. In plants, orthologues of over 80% the yeast RBFs have been bioinformatically identified [6], [7]. Only some of these RBFs have been investigated to date.

The role of ribose base modifications on rRNAs have been gradually uncovered. Being an RBF, NOP2 introduces methyl groups onto cytidine to produce m^5C residues on rRNAs and are described in yeast and plants [8], [9]. As demonstrated in Chapter 2 of my thesis, three NOP2 homologues, NOP2A, NOP2B and NOP2C in the *Arabidopsis* genome all contribute to methylation of C2268 on the 25S rRNA. Apart from m^5C, the rRNAs are highly modified with other modifications, such as 2′-O-methylation and pseudouridylation. Recently the variation of rRNA modifications was shown to be a source of ribosome

heterogeneity [10], thereby extending translation. As I discussed in the Chapter 1 of this thesis, the RNA modification m^5C are dynamic upon environmental stress conditions, and variation in rRNA modifications may assist the ribosome to translate specific mRNAs to adapt to environmental challenges. Furthermore, the benchmark data with known RNA modification sites were used to predict whether novel RNA sequences have RNA modifications through machine learning [11]. Therefore, it is necessary to explore if the specific rRNA modification pattern is related to characterising the ribosome subunits in performing the specific cellular functions, for example in promoting or repressing translation. To fully elucidate the roles of rRNA modifications and translation, single-cell-sequencing to detect rRNA modifications combined with translational assays, like Ribo-seq, will be required. Combining this data with physiological and developmental defects will lead to a great understand of the role of rRNA modifications and organism growth and development.

Dysregulation of RBF in plants is linked to diverse and important molecular and developmental processes. For example, RBF's *SWA1* and *AtRH36* are vital for cell mitotic division during female gametogenesis [12], [13], and *TOZ* is also indispensable for embryo development [14]. In addition, leaf polarity defects were observed in *Arabidopsis* RBFs mutants, including *PUMILIO23* (*PUM23*), *G-PATCH DOMAIN PROTEIN* (*GDP1*) and *RNA HELICASE10* (*RH10*) [15]–[17]. Our *nop2*a mutants have a short root, pointed rosette leaves and abnormal female gametophyte development, which is consistent with previous reports and a role in ribosome-related protein synthesis during cell proliferation [18]. Very recently, NOP2A was shown to have a critical role in telomere length homeostasis in *A. thaliana,* somewhat similar to the role of RBFs in regulation telomeres in yeast [19]. However, the exact molecular role of NOP2A in telomere length homeostasis in *Arabidopsis* remains unclear. It is worth speculating that NOP2A may methylate the telomere RNA component, TERC, and TERC-m^5C is essential for telomere length homeostasis.

The interactions between different RBF were reported to regulate the growth of plants. For example, additive phenotype of enhanced leaf development defects were observed in double mutants of *gdp1 and oli2*. OLI2 was found to interact

with another RBF, BRX, in plants with extended lifespans [17], [20]. These examples illustrate the interactive effects of RBFs. Studies have also shown that climate change can affect phenotypes of these mutants. The benefits and risks of utilising these interactions through promotion of translation of different typoes of mRNAs needs to be carefully considered.

Exploring the biogenesis of tRNA-derived small RNAs

The full repertoire of ribonucleases and related factors that produce tRNA halves remains to be elucidated. Experiments presented in Chapter 3 investigate the role of plant ribonuclease RNases T2 on the production of tRNA halves under oxidative stress in *Arabidopsis*. A growing body of evidence demonstrates that Rny1, angiogenin, and plant Rnases T2 are able to produce both the tRNA halves and tRFs in yeast, mammalian cells and plants under stress conditions [21]–[23]. Whether DICER contributes to the accumulation of tRFs is still controversial in plants. Furthermore, the tRNA halves could also be produced without experimental stress treatment, as demonstrated in results presented in chapter 3. Therefore, further experiments are required to clarify how tRNA halves could be produced under normal conditions and whether these types of tRNA halves are related to biological processes.

Different hypotheses have been put forward to link tRNA cleavage and stress stimulus in plants. For example it has been reported that the ribonuclease Rny1, angiogenin and RNS2 transition from membrane-bound to the cytoplasm under stress [21], [24], [25]. The release of these ribonucleases is assumed to be a result of environmental stress but the mechanism of the transfer of ribonuclease has not been characterised. The cleavage of tRNA triggered by stress-induced ribonucleases should inhibit the translation as a result of the decreased tRNA pool. As is evidenced in this study, the absence of RNS2 under oxidative stress leads to the perturbation of both mature tRNAs and pre-tRNAs. However, the full-length tRNA pool is not significantly affected by the increased abundance of tRFs and tRNA halves [26], [27]. It remains unclear whether the new tRNAs

are synthesised to maintain the translation after sensing a stress-induced tRNA cleavage signal.

The cleavage characteristics of the specific ribonuclease are still unclear. Current research suggests that angiogenin and Rny1 give rise to the specific accumulation of partial types of tRNA halves [21], [28]. Similarly, in our results show that members of plant Rnases T2 family, RNS1, RNS2 and RNS4 only cleavage specific tRNAs, and the cleavage efficiency of each ribonucleases RNS vary among different tRNAs. Future research will clarify whether there is a common feature among the specifically cleaved tRNAs and identify the molecular mechanisms underpinning interaction of the ribonuclease with the specific tRNAs.

The influence of tRNA modifications on cleavage has been implicated in a wide range of research. Evidence provided in this thesis and the literature shows that m^5C sites on tRNAs maintain tRNA stability and reduce the accumulation of tRNA halves [1], [29]. However, the protective effects of tRNA modifications on stress-induced cleavage are only considered for individual modification. It is known that the tRNAs can be subject to a variety of modifications [30], which may act as individual signal or in combination with other modifications. In addition, tRNA modifications can be affected by environmental changes [31], [32]. This can complicate the understanding of tRNA cleavage as it is difficult to determine if tRNA cleavage is a result of altered tRNA modifications level or stress-induced ribonuclease activity. Another open question is the inheritance of tsRNA modification from parental tRNAs. Therefore, purified endogenous tsRNAs should be qualified for modification identification.

The potential function of tRNA-derived small RNAs

Despite our increased understanding of the biogenesis of tRFs and tRNA halves, their specific functional and regulatory targets have not been established yet.

In chapter 4, we describe results on the processing of transformed 5'-half $tRNA^{Asp(GTC)}$ in *A. thaliana.* Specifically, in our study, the artificial synthetic 5'-half $tRNA^{Asp(GTC)}$ sequences were used which ignores RNA modification and the loss of activity, which might fail to explore the interactome of 5'-half $tRNA^{Asp(GTC)}$. Development of effective methods to obtain high purified endogenous single tsRNA from biological sources will facilitate the in-depth molecular functional analysis of single specific tsRNAs. Approaches aimed at deciphering the structure of endogenous tsRNAs have not been developed yet, and it is unclear if the original D-loop in the parent tRNA is still present in the 5'-half tRNA or if the 5'-half tRNA might form a different RNA structure?

The tRFs were reported to be functionally analogous to miRNAs due to their similar size, however it is currently unclear if tRFs act as the canonical miRNA-regulated pathway. Recent work in plants has shown that the tRF-5s from $tRNA^{Ala(AGC)}$ may cleave the CYP71A13 mRNA between nucleotides 13 and 14, rather than the 11 and 12 [33]. In animals, a short seed region complementary to the target mRNA is normally located on the 5' end of the small RNA, while a seed region at the 3' end of a tRF molecule results in mRNA repression [34], [35]. In addition, computational analysis of large-scale datasets demonstrated that the tRFs seem to recognise the mRNAs through multiple seed regions [36]. It is likely that some tRFs require the conserved motif in the seed region for cleavage. Clarifying the mechanism of the seed region for tRFs is vital for the subsequent prediction of the target genes. Development of specific tools for the prediction of target genes of tRFs is urgently needed for plants and animals. A throrough understanding of the role of the seed region in the miRNA-like pathway, accurate target gene predication and experimental validation are imperative for understanding the function of tRFs.

Stress-induced tRFs and tRNA halves have been observed in various cellular processes and are under appreciated to date. In humans, tsRNAs from specific are proposed as biomarkers in cancer progression and disease [37], [38]. However, the regulatory mechanism forming these tRFs in cancer cells and disease development is still unclear. Therefore, it is an urgent need to clarify the tRFs expression, biological function and interactions in cells to realise their

medical application. In plants, the production of tRFs and tRNA halves were linked to both biotic and abiotic stress conditions. In black pepper, tRF-5s $tRNA^{Ala(CGC)}$ was highly expressed after infection with the wilt pathogen, *Phytophthora capsica* although the significance is still to be clarified [39]. In wheat, tRF-5s $tRNA^{Glu(CTC)}$, tRF-5s $tRNA^{Lys(CTT)}$ tRF-5s $tRNA^{Thr(CGT)}$ were linked wheat resistance against Fusarium head blight [40]. Interestingly, *Rhizobium* tRFs from $tRNA^{Val(CAC)}$, $tRNA^{Glyal(TCC)}$ and $tRNA^{Gln(CTG)}$ were demonstrated to modulate nodulation efficiency in legumes [41]. Therefore, tRFs are good candidates to exploit for improving tolerance to abiotic and biotic challenges.

Concluding remarks

In summary, results presented in this thesis advance our understanding of the regulatory roles of RNA m^5C on rRNAs and tRNAs in *Arabidopsis.* The importance of rRNA m^5C methyltransferase, NOP2, was demonstrated initially during ovule and then vegetative development and provides a framework to further explore in crop plants. Investigation of the ribonucleases giving rise to tRNA halves in response to oxidative stress and exploration of the link between tRNA cleavage and tRNA m^5C methyltransferase, TRM4B, expanded our knowledge into tRNA processing and plant growth. I also progressed our understanding of $tRNA^{Asp(GTC)}$ half function, and processing into sRNAs. Given climate change is on our doorstep, novel genetic and epigenetic approaches will need to be utilized to enhance crop yields. The research conducted in this thesis is a step towards a plant biotechnology approach to address this challenge.

References

[1] R. David *et al.*, “Transcriptome-wide mapping of RNA 5-methylcytosine in arabidopsis mRNAs and noncoding RNAs,” *Plant Cell*, vol. 29, no. 3, pp. 445–460, 2017, doi: 10.1105/tpc.16.00751.

[2] A. L. Burgess, R. David, and I. R. Searle, “Conservation of tRNA and rRNA 5-methylcytosine in the kingdom Plantae,” *BMC Plant Biol*, vol. 15, no. 1, pp. 1–17, 2015, doi: 10.1186/s12870-015-0580-8.

[3] S. Blanco and M. Frye, “Role of RNA methyltransferases in tissue renewal and pathology,” *Current Opinion in Cell Biology*, vol. 30, no. 1. Elsevier Ltd, pp. 1–7, 2014. doi: 10.1016/j.ceb.2014.06.006.

[4] L. Abbasi-Moheb *et al.*, “Mutations in NSUN2 Cause Autosomal- Recessive Intellectual Disability,” *The American Journal of Human Genetics*, vol. 90, no. 5, pp. 847–855, May 2012, doi: 10.1016/J.AJHG.2012.03.021.

[5] T. W. Turowski and D. Tollervey, “Cotranscriptional events in eukaryotic ribosome synthesis,” *Wiley Interdiscip Rev RNA*, vol. 6, no. 1, pp. 129–139, Jan. 2015, doi: 10.1002/WRNA.1263.

[6] J. L. Woolford and S. J. Baserga, “Ribosome Biogenesis in the Yeast Saccharomyces cerevisiae,” *Genetics*, vol. 195, no. 3, pp. 643–681, Nov. 2013, doi: 10.1534/GENETICS.113.153197.

[7] I. Ebersberger *et al.*, “The evolution of the ribosome biogenesis pathway from a yeast perspective,” *Nucleic Acids Res*, vol. 42, no. 3, pp. 1509–1523, Feb. 2014, doi: 10.1093/NAR/GKT1137.

[8] H. Wu *et al.*, “WUSCHEL triggers innate antiviral immunity in plant stem cells,” *Science (1979)*, vol. 370, no. 6513, pp. 227–231, Oct. 2020, doi: 10.1126/science.abb7360.

[9] S. Sharma, J. Yang, P. Watzinger, P. Kötter, and K. D. Entian, “Yeast Nop2 and Rcm1 methylate C2870 and C2278 of the 25S rRNA, respectively,” *Nucleic Acids Res*, vol. 41, no. 19, pp. 9062–9076, Oct. 2013, doi: 10.1093/nar/gkt679.

[10] D. Li and J. Wang, “Ribosome heterogeneity in stem cells and development,” *Journal of Cell Biology*, vol. 219, no. 6, Jun. 2020, doi: 10.1083/JCB.202001108/151702.

[11] A. el Allali, Z. Elhamraoui, and R. Daoud, “Machine learning applications in RNA modification sites prediction,” *Comput Struct Biotechnol J*, vol. 19, p. 5510, Jan. 2021, doi: 10.1016/J.CSBJ.2021.09.025.

[12] D. Q. Shi, J. Liu, Y. H. Xiang, D. Ye, V. Sundaresan, and W. C. Yang, “SLOW WALKER1, Essential for Gametogenesis in Arabidopsis, Encodes a WD40 Protein Involved in 18S Ribosomal RNA Biogenesis,” *Plant Cell*, vol. 17, no. 8, p. 2340, 2005, doi: 10.1105/TPC.105.033563.

[13] C. K. Huang, L. F. Huang, J. J. Huang, S. J. Wu, C. H. Yeh, and C. A. Lu, “A DEAD-box protein, AtRH36, is essential for female gametophyte development and is involved in rRNA biogenesis in Arabidopsis,” *Plant Cell Physiol*, vol. 51, no. 5, pp. 694–706, May 2010, doi: 10.1093/PCP/PCQ045.

[14] M. E. Griffith *et al.*, “The TORMOZ Gene Encodes a Nucleolar Protein Required for Regulated Division Planes and Embryo Development in Arabidopsis,” *Plant Cell*, vol. 19, no. 7, p. 2246, 2007, doi: 10.1105/TPC.106.042697.

[15] N. Abbasi *et al.*, “APUM23, a nucleolar Puf domain protein, is involved in pre-ribosomal RNA processing and normal growth patterning in Arabidopsis,” *Plant J*, vol. 64, no. 6, pp. 960–976, Dec. 2010, doi: 10.1111/J.1365-313X.2010.04393.X.

[16] Y. Matsumura *et al.*, “A genetic link between epigenetic repressor AS1-AS2 and a putative small subunit processome in leaf polarity establishment of

Arabidopsis," *Biol Open*, vol. 5, no. 7, p. 942, Jul. 2016, doi: 10.1242/BIO.019109.

[17] K. Kojima, J. Tamura, H. Chiba, K. Fukada, H. Tsukaya, and G. Horiguchi, "Two nucleolar proteins, GDP1 and OLI2, function as ribosome biogenesis factors and are preferentially involved in promotion of leaf cell proliferation without strongly affecting leaf adaxial–abaxial patterning in Arabidopsis thaliana," *Front Plant Sci*, vol. 8, p. 2240, Jan. 2018, doi: 10.3389/fpls.2017.02240.

[18] U. Fujikura, G. Horiguchi, M. R. Ponce, J. L. Micol, and H. Tsukaya, "Coordination of cell proliferation and cell expansion mediated by ribosome-related processes in the leaves of Arabidopsis thaliana," *Plant Journal*, vol. 59, no. 3, pp. 499–508, 2009, doi: 10.1111/j.1365-313X.2009.03886.x.

[19] L. R. Abdulkina *et al.*, "Components of the ribosome biogenesis pathway underlie establishment of telomere length set point in Arabidopsis", doi: 10.1038/s41467-019-13448-z.

[20] S. Maekawa and S. Yanagisawa, "Ribosome biogenesis factor OLI2 and its interactor BRX1-2 are associated with morphogenesis and lifespan extension in Arabidopsis thaliana," *Plant Biotechnology*, vol. 38, pp. 117–125, 2021, doi: 10.5511/plantbiotechnology.20.1224a.

[21] D. M. Thompson and R. Parker, "The RNase Rny1p cleaves tRNAs and promotes cell death during oxidative stress in Saccharomyces cerevisiae," *Journal of Cell Biology*, vol. 185, no. 1, pp. 43–50, Apr. 2009, doi: 10.1083/jcb.200811119.

[22] P. Ivanov, M. M. Emara, J. Villen, S. P. Gygi, and P. Anderson, "Angiogenin-Induced tRNA Fragments Inhibit Translation Initiation," *Mol Cell*, vol. 43, no. 4, pp. 613–623, Aug. 2011, doi: 10.1016/j.molcel.2011.06.022.

[23] C. Megel *et al.*, "Plant RNases T2, but not Dicer-like proteins, are major

players of tRNA-derived fragments biogenesis," *Nucleic Acids Res*, vol. 47, no. 2, pp. 941–952, 2019, doi: 10.1093/nar/gky1156.

[24] M. S. Hillwig, A. L. Contento, A. Meyer, D. Ebany, D. C. Bassham, and G. C. MacIntosha, "RNS2, a conserved member of the RNase T2 family, is necessary for ribosomal RNA decay in plants," *Proc Natl Acad Sci U S A*, vol. 108, no. 3, pp. 1093–1098, Jan. 2011, doi: 10.1073/PNAS.1009809108/SUPPL_FILE/PNAS.201009809SI.PDF.

[25] J. Moroianu and J. F. Riordan, "Nuclear translocation of angiogenin in proliferating endothelial cells is essential to its angiogenic activity," *Proc Natl Acad Sci U S A*, vol. 91, no. 5, pp. 1677–1681, Mar. 1994, doi: 10.1073/PNAS.91.5.1677.

[26] H. Fu *et al.*, "Stress induces tRNA cleavage by angiogenin in mammalian cells," *FEBS Lett*, vol. 583, no. 2, pp. 437–442, Jan. 2009, doi: 10.1016/J.FEBSLET.2008.12.043.

[27] C. Jöchl *et al.*, "Small ncRNA transcriptome analysis from Aspergillus fumigatus suggests a novel mechanism for regulation of protein synthesis," *Nucleic Acids Res*, vol. 36, no. 8, pp. 2677–2689, May 2008, doi: 10.1093/NAR/GKN123.

[28] Z. Su, C. Kuscu, A. Malik, E. Shibata, and A. Dutta, "Angiogenin generates specific stress-induced tRNA halves and is not involved in tRF-3-mediated gene silencing," *Journal of Biological Chemistry*, vol. 294, no. 45, pp. 16930–16941, Nov. 2019, doi: 10.1074/JBC.RA119.009272/ATTACHMENT/76676FEF-349E-40A6-B3B6-2A6C57ABA9D9/MMC1.ZIP.

[29] F. Tuorto *et al.*, "RNA cytosine methylation by Dnmt2 and NSun2 promotes tRNA stability and protein synthesis," *Nat Struct Mol Biol*, vol. 19, no. 9, pp. 900–905, Sep. 2012, doi: 10.1038/nsmb.2357.

[30] P. Boccaletto *et al.*, "MODOMICS: a database of RNA modification

pathways. 2021 update," *Nucleic Acids Res*, vol. 50, no. D1, pp. D231–D235, Jan. 2022, doi: 10.1093/NAR/GKAB1083.

[31] P. C. Dedon and T. J. Begley, "A system of RNA modifications and biased codon use controls cellular stress response at the level of translation," *Chemical Research in Toxicology*, vol. 27, no. 3. American Chemical Society, pp. 330–337, Mar. 17, 2014. doi: 10.1021/tx400438d.

[32] C. T. Y. Chan *et al.*, "Reprogramming of tRNA modifications controls the oxidative stress response by codon-biased translation of proteins," *Nat Commun*, vol. 3, p. 937, 2012, doi: 10.1038/ncomms1938.

[33] H. Gu *et al.*, "A 5′ tRNA-Ala-derived small RNA regulates anti-fungal defense in plants," vol. 65, no. 1, pp. 1–15, 2022, doi: 10.1007/s11427-021-2017-1.

[34] Q. Wang, I. Lee, J. Ren, S. S. Ajay, Y. S. Lee, and X. Bao, "Identification and functional characterization of tRNA-derived RNA fragments (tRFs) in respiratory syncytial virus infection," *Mol Ther*, vol. 21, no. 2, pp. 368–379, 2013, doi: 10.1038/MT.2012.237.

[35] R. L. Maute *et al.*, "TRNA-derived microRNA modulates proliferation and the DNA damage response and is down-regulated in B cell lymphoma," *Proc Natl Acad Sci U S A*, vol. 110, no. 4, pp. 1404–1409, Jan. 2013, doi: 10.1073/PNAS.1206761110/-/DCSUPPLEMENTAL/PNAS.201206761SI.PDF.

[36] L. Guan, S. Karaiskos, and A. Grigoriev, "Inferring targeting modes of Argonaute-loaded tRNA fragments," *RNA Biol*, vol. 17, no. 8, pp. 1070–1080, 2020, doi: 10.1080/15476286.2019.1676633.

[37] S. Yamasaki, M. Nakashima, and H. Ida, "Possible Roles of tRNA Fragments, as New Regulatory ncRNAs, in the Pathogenesis of Rheumatoid Arthritis," *Int J Mol Sci*, vol. 22, no. 17, Sep. 2021, doi: 10.3390/IJMS22179481.

[38] C. Zhao *et al.*, "tRNA-halves are prognostic biomarkers for patients with

prostate cancer," *Urologic Oncology: Seminars and Original Investigations*, vol. 36, no. 11, pp. 503.e1-503.e7, Nov. 2018, doi: 10.1016/J.UROLONC.2018.08.003.

[39] S. Asha and E. v. Soniya, "Transfer RNA derived small RNAs targeting defense responsive genes are induced during phytophthora capsici infection in black pepper (Piper nigrum l.)," *Front Plant Sci*, vol. 7, no. JUNE2016, p. 767, Jun. 2016, doi: 10.3389/FPLS.2016.00767/BIBTEX.

[40] Z. Sun *et al.*, "tRNA-derived fragments from wheat are potentially involved in susceptibility to Fusarium head blight," *BMC Plant Biol*, vol. 22, no. 1, pp. 1–17, Dec. 2022, doi: 10.1186/S12870-021-03393-9/FIGURES/7.

[41] B. Ren, X. Wang, J. Duan, and J. Ma, "Rhizobial tRNA-derived small RNAs are signal molecules regulating plant nodulation.," *Science*, p. eaav8907, Jul. 2019, doi: 10.1126/science.aav8907.

Co-authored publications in addition to this work

PLOS ONE

RESEARCH ARTICLE

Arabidopsis TRM5 encodes a nuclear-localised bifunctional tRNA guanine and inosine-N1-methyltransferase that is important for growth

Qianqian Guo[1‡], Pei Qin Ng[2‡], Shanshan Shi[1], Diwen Fan[1], Jun Li[2], Jing Zhao[2], Hua Wang[3], Rakesh David[4], Parul Mittal[5], Trung Do[2], Ralph Bock[6], Ming Zhao[1], Wenbin Zhou[1]*, Iain Searle[2]*

1 Institute of Crop Sciences, Chinese Academy of Agricultural Sciences, Beijing, China, **2** School of Biological Sciences, School of Agriculture, Food and Wine, The University of Adelaide and Shanghai Jiao Tong University Joint International Centre for Agriculture and Health, The University of Adelaide, Adelaide, Adelaide, Australia, **3** National Key Laboratory of Plant Molecular Genetics, CAS Center for Excellence in Molecular Plant Sciences, Shanghai Institute of Plant Physiology and Ecology, Chinese Academy of Sciences, Shanghai, China, **4** ARC Centre of Excellence in Plant Energy Biology, School of Agriculture, Food and Wine, University of Adelaide, Adelaide, Australia, **5** Adelaide Proteomics Centre, School of Biological Sciences, The University of Adelaide, SA, Australia, **6** Max Planck Institute of Molecular Plant Physiology, Am Mühlenberg, Potsdam-Golm, Germany

‡ These authors are joint first authors on this work.
* Iain.Searle@adelaide.edu.au(LS); zhouwenbin@caas.cn(WZ)

OPEN ACCESS

Citation: Guo Q, Ng PQ, Shi S, Fan D, Li J, Zhao J, et al. (2019) *Arabidopsis* TRM5 encodes a nuclear-localised bifunctional tRNA guanine and inosine-N1-methyltransferase that is important for growth. PLoS ONE 14(11): e0225064. https://doi.org/10.1371/journal.pone.0225064

Editor: Hector Candela, Universidad Miguel Hernández de Elche, SPAIN

Received: June 20, 2019

Accepted: October 28, 2019

Published: November 22, 2019

Peer Review History: PLOS recognizes the benefits of transparency in the peer review process; therefore, we enable the publication of all of the content of peer review and author responses alongside final, published articles. The editorial history of this article is available here: https://doi.org/10.1371/journal.pone.0225064

Data Availability Statement: The data used in this paper is submitted into NCBI with the GEO accession number GSE114898. Proteomics raw data has been deposited on iProX, with under

Abstract

Modified nucleosides in tRNAs are critical for protein translation. N^1-methylguanosine-37 and N^1-methylinosine-37 in tRNAs, both located at the 3'-adjacent to the anticodon, are formed by Trm5. Here we describe *Arabidopsis thaliana AtTRM5* (At3g56120) as a Trm5 ortholog. *Attrm5* mutant plants have overall slower growth as observed by slower leaf initiation rate, delayed flowering and reduced primary root length. In *Attrm5* mutants, mRNAs of flowering time genes are less abundant and correlated with delayed flowering. We show that *AtTRM5* complements the yeast *trm5* mutant, and *in vitro* methylates tRNA guanosine-37 to produce N^1-methylguanosine (m^1G). We also show *in vitro* that AtTRM5 methylates tRNA inosine-37 to produce N^1-methylinosine (m^1I) and in *Attrm5* mutant plants, we show a reduction of both N^1-methylguanosine and N^1-methylinosine. We also show that AtTRM5 is localized to the nucleus in plant cells. Proteomics data showed that photosynthetic protein abundance is affected in *Attrm5* mutant plants. Finally, we show tRNA-Ala aminoacylation is not affected in *Attrm5* mutants. However the abundance of tRNA-Ala and tRNA-Asp 5' half cleavage products are deduced. Our findings highlight the bifunctionality of AtTRM5 and the importance of the post-transcriptional tRNA modifications m^1G and m^1I at tRNA position 37 in general plant growth and development.

accession number IPX0001222000 and is available at https://www.iprox.org//page/project.html?id=IPX0001222000.

Funding: The research was partially supported by ARC grant FT130100525, partially funded an Australia-China Science and Research Fund grant ACSRF48187 awarded to I.S. and an APA awarded to PQ.N and J.L. This research was also partially supported by the National Natural Science Foundation (31570234) awarded to W.Z., W.Z. was supported by the Innovation Program of Chinese Academy of Agricultural Sciences and the Elite Youth Program of the Chinese Academy of Agricultural Science.

Competing interests: The authors have declared that no competing interests exist.

Introduction

RNA has over 100 different post-transcriptional modifications that have been identified in organisms across all three domains of life [1–5]. While several RNA modifications have been recently identified on mRNAs in yeast, plants, and animals, tRNAs are still thought to be the most extensively modified cellular RNAs [6–9]. These tRNA modifications are introduced at the post-transcriptional level by specific enzymes. These enzymes recognize polynucleotide substrates and modify individual nucleotide residues at highly specific sites. Some tRNA modifications have been shown to have a clear biological and molecular function [10, 11]. Several tRNA modifications around the anticodon have been demonstrated to have crucial functions in translation, for example, by enhancing decoding [12], influencing the propensity to ribosomal frameshifting or facilitating wobbling [13–15]. Modifications distal to the tRNA anticodon loop can also directly influence the tRNA recognition and/or translation process [16] or can have roles in tRNA folding and stability [1, 17]. However, the precise functions of many tRNA modifications still remain unknown despite often being conserved across species. Often, loss of a tRNA modification does not negatively impair cell growth or cell viability under standard laboratory growth conditions [18]. However, under environmental stress, such mutants display a discernible phenotype [11].

The tRNA anticodon loop position 37 is important to maintain translational fidelity, prevent frameshift errors and translational efficiency [10, 19–21], and almost all tRNAs are modified at this site. There are two prominent modifications at tRNA position 37: N^1-methylguanosine (m^1G37) and 1-methylinosine (m^1I). Trm5 in humans, yeast, and *Pyrococcus abyssi* has been described as having multifunctionality [22–24]. N^1-methylation of guanosine at position 37, m^1G37, is performed by TrmD-type enzymes in bacteria, functionally and evolutionarily unrelated Trm5-type proteins in Archaea and Eukaryote, Trm5p in yeast *Saccharomyces cerevisiae*, and TRMT5 *in vivo* in humans [21–23, 25–27]. Trm5p complete loss of function mutants in yeast *Saccharomyces cerevisiae* are lethal whereas mutations in TRMT5 lead to multiple respiratory-chain deficiencies and a reduction in mitochondrial tRNA m^1G37 [10, 23, 26]. In humans, TRMT5 (tRNA methyltransferase 5) catalyses the formation of m^1G37 *in vivo* on mitochondrial $tRNA^{Pro}$ and $tRNA^{Leu}$ [22, 28]. N^1-methylguanosine has been described in eukaryotic tRNAs at two positions; at position 37 catalysed by Trm5, and the other at position 9 catalysed by Trm10 [29]. In contrast to bacteria TrmD, which requires a guanosine at position 37, human TRMT5 can also recognise and methylate inosine at position 37 with some limited activity [22]. Similarly,Trm5p has also been shown to catalyse inosine to m^1I modification in yeast in a two-step reaction, where the first adenosine-to-inosine modification was mediated by Tad1p [11, 18, 26, 30]. As m^1G is an intermediate during the modification of guanosine to wybotusine (yW), tRNAs from *trm5* mutants were also devoid of yW [28]. The yeast Trm5p protein has been shown to be localised to the cytoplasm and mitochondria and it is thought that Trm5p protein present in the mitochondria is required to prevent unmodified tRNA affecting translational frameshifting [23, 26]. In the unicellular parasite *Trypanosome brucei*, Trm5 was located in both the nucleus and mitochondria and reducing Trm5 expression led to reduced mitochondria biogenesis and impaired growth [31]. Interestingly, Trm5 and m^1G37 were shown to be essential for mitochondrial protein synthesis but not cytosolic translation [31].

Little is known about tRNA modifying enzymes in plants, especially the plant homolog of this bifunctional methyltransferase. Here, we report the identification and functional analysis of *AtTRM5* (At3g56120) from the model plant *Arabidopsis thaliana*. We demonstrate that *Attrm5* mutant plants are slower growing, have reduced shoot and root biomass and display late flowering. Furthermore, we demonstrate that *in vitro TRM5* is required for m^1G37 and

m^1I37 methylation at the position 3' to the anticodon and *in vivo* tRNAs enriched from *Attrm5* plants have reduced m^1G and m^1I.

Results

Identification of At3g56120 as a TRM5 homolog

In yeast (*Saccharomyces cerevisiae*), m^1G37 nucleoside modification is catalysed by Trm5p/ScTrm5 [26]. We searched for *Arabidopsis thaliana* homologs by using blastp and HMMER and identified a high confidence candidate, At3g56120, with 49% similarity to ScTrm5 (S2 Fig). Alignment of At3g56120 with yeast, human, *Drosophilia*, *Pyrococcus*, and *Methanococcus* Trm5 homologs identified three conserved motifs and catalytically required amino acids (R166, D192, E206) present in At3g56120 (S2 Fig). We subsequently will refer to At3g56120 as AtTRM5. In the *Arabidopsis* genome, AtTrm5 has homology to At4g27340 and At4g04670 and both genes were recently named as TRM5B and TRM5C, respectively (S2 Fig and [32]). We have also identified TRM5 homologs in algae, bryophytes and vascular plants (Fig 1A and S1 Fig). We focussed our experiments on *Arabidopsis* At3g56120/AtTRM5 as the protein had the highest amino acid similarity to yeast ScTrm5.

To functionally characterize AtTRM5 we isolated two T-DNA insertions, SALK_022617 and SALK_032376, and identified homozygous mutant plants for each insertion (Fig 1B). SALK_022617 and SALK_032376 were named *trm5-1* and *trm5-2*, respectively. Next, we measured AtTRM5 mRNA abundance in both mutants and detected almost no transcripts in both mutants (Fig 1C). We generated a genomic construct of AtTRM5 that contained the endogenous promoter, coding region, and UTRs, transformed the construct into *trm5-2* and demonstrated that the AtTRM5 mRNA levels were similar in two complemented lines when compared to wild type plants. Subsequently, the extracted tRNAs from wild type and the *trm5* mutants were purified, digested and modified nucleosides measured by mass spectrometry (Fig 1D). In both *trm5* mutant alleles, nucleoside m^1G levels were reduced to about 30% of the wild type and m^1G levels were restored to wild type levels in both complemented lines (Fig 1D). Nucleoside m^1G is present at tRNA positions 9 and 37 [26], therefore the residual m^1G levels in *trm5* mutants may be the result of tRNA m^1G at position 9. In saying this, we cannot exclude an alternative explanation that the residual m^1G levels in *trm5* plants are the result of activity of either TRM5B or TRM5C.

In yeast, Trm5 has also been reported to also catalyse m^1I on tRNAs [11, 26]. We therefore measured m^1I levels in purified tRNAs from both *Arabidopsis trm5* mutants and wild type control plants. In both *trm5-1* and *trm5-2* mutant alleles, nucleoside m^1I levels were reduced to about 10% of wild type levels and were restored to wild type levels in plants of both complemented lines (Fig 1D). It is possible that the residual m^1I in *trm5* plants may be m^1I at position 57 [4, 33, 34]. In summary, we identified At3g56120 as a TRM5 homolog in *Arabidopsis thaliana*, identified two AtTRM5 mutant alleles, *trm5-1* and *trm5-2*, and both mutants showed a significant reduction in m^1G and m^1I.

AtTRM5 is involved in leaf and root development and flowering time regulation

Before undertaking growth measurements, we grew wild-type Columbia, *trm5-1*, two complemented lines, and two overexpression lines together under long-day conditions, harvested and dried the seeds to minimise any maternal or environmental effects. To observe the early growth stages of seedlings, we grew the six lines (wild type, *trm5-1*, two complemented lines and two overexpression lines) on plates for 10 days (Fig 2A). The *trm5-1* seedlings were

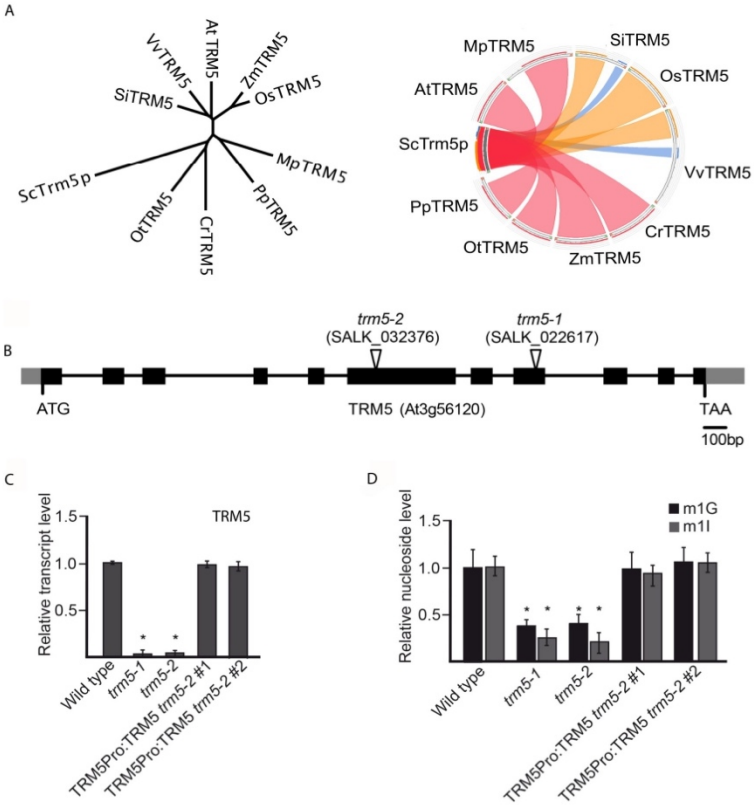

Fig 1. TRM5 is conserved in plants and has dual-functionality in modifying RNA bases. (**A**) Unrooted phylogenetic tree and sequence conservation Circos plot of putative TRM5 proteins from yeast (Sc), tomato (Sl), grape (Vv), *Arabidopsis* (At), maize (Zm), rice (Os), *Marchantia* (Mp), *Physcomitrella* (Pp), *Chlamydomonas* (Cr), and *Ostreococcus* (Ot). The ribbons were coloured based on sequence identity, with blue < = 25%, green 25–50%, orange 51–75% and red for 76–99%. (**B**) Exon-intron structure of the putative TRM5 locus (At3g56120) showing the T-DNA insertion sites of the *trm5-1* and *trm5-2* alleles (as indicated by the open triangles). Black boxes and grey boxes represent coding regions and untranslated regions, respectively. (**C**) Relative transcript level detected by qPCR in wild type, *trm5-1* or *trm5-2* seedlings. (**D**) Relative nucleoside level of modification m^1G and m^1I detected by HPLC/MS in wild type, *trm5-1* or *trm5-2* seedlings.

https://doi.org/10.1371/journal.pone.0225064.g001

noticeably smaller than the wild type. In contrast, no clear differences were evident between wild type, the complemented and overexpression lines. To rule out the possibility that the reduced growth in *trm5-1* seedlings was due to slower germination, we measured the germination of *trm5-1* and wild type and no difference was observed (S3 Fig). Reduced growth of *trm5-1* roots was also evident on plate-grown plants (Fig 2B). Interestingly, *trm5-1* primary, lateral and total (primary + lateral) root lengths were reduced in *trm5-1* when compared to

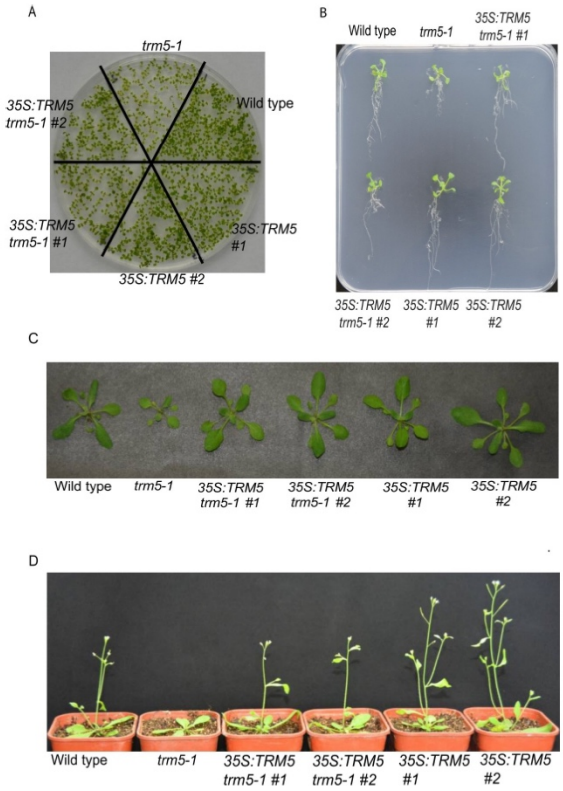

Fig 2. Phenotype analysis of *trm5*, complemented lines (35S:TRM5 *trm5-1*) and TRM5 overexpression lines (35S:TRM5). (**A**) Seedlings were sown on ½ MS media plates and grown for 7 days and photographed. (**B**) Seedlings of wild type, *trm5*, complemented lines (35S:TRM5 *trm5-1*), TRM5 overexpression lines (35S:TRM5) were vertically grown on ½ MS medium for 10 days and then photographed. (**C**) Plants were grown on soil under long day photoperiods and photographed 15 days after germination. (**D**) Wild type, *trm5-1*, two complementing (35S:TRM5 *trm5-1*) and two overexpressing lines (35S:TRM5) were grown under long days and representative plants photographed at flowering.

https://doi.org/10.1371/journal.pone.0225064.g002

wild-type plants (S4 Fig). We also measured the lateral root number and found that *trm5-1* plants had reduced numbers when compared to the wild type (S4 Fig). In contrast, no differences in the root growth were evident upon comparison of the wild type and the complemented lines. In *TRM5* overexpression lines, primary and lateral root lengths were slightly longer than in the wild type (Fig 2B and S4 Fig).

At inflorescence emergence in wild-type plants grown under long days, we observed reduced rosette leaf numbers, smaller leaves and reduced fresh weight in *trm5-1* plants (Fig 2C and 2D; S3 Fig). Sectioning of the shoot apical meristems of wild type and *trm5-1* plants at wild-type floral transition, confirmed that *trm5* plants were later flowering (S3 Fig). We

measured the flowering time of wild type, *trm5-1*, complemented, and overexpression lines under both short and long days and observed that mutants produced more rosette leaves and flowered later than the wild type (Fig 3A; S3 Fig). Plants overexpressing TRM5 flowered slightly earlier than wild type under both long and short-day conditions (Fig 2D; S3 Fig).

AtTRM5 is involved in circadian clock and flowering time gene expression

To explore the molecular basis of delayed flowering in *trm5-1*, we measured the mRNA abundance of circadian clock and flowering time related genes by quantitative RT-PCR over a

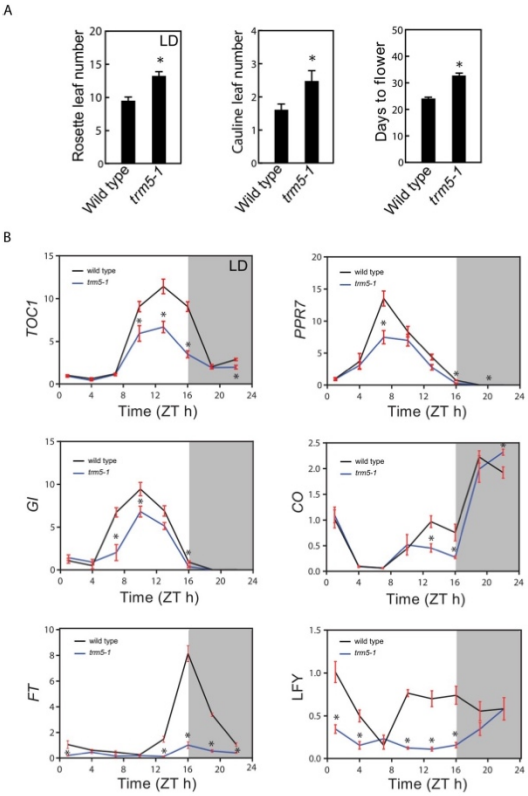

Fig 3. More leaves, slower flowering and impacted photosynthetic genes in trm5 mutant of *Arabidopsis thaliana*. (**A**) Rosette leaf number (long-day conditions), cauline leaf number and days to flower (short day conditions) of wild type and *trm5* mutant. (**B**) The mRNA abundance of circadian clock-related genes over a 24-hour period. 17-day-old seedlings of wild type, *trm5-1*, complemented lines (35S:TRM5 *trm5-1*), TRM5 overexpression lines (35S:TRM5) were grown on ½ MS medium for 10 days and then harvested every 3 hours. The expression levels of *TOC1*, *PRR7*, GI, CO, *FT*, and LFY were measured and normalized relative to *EF-1-α*. Data presented are means. Error bars are ± SE, n = 3 biological replicates. An asterisk indicates a statistical difference ($P<0.05$) as determined by Student's t-test. 0 hours is lights on and 16 hours is light off. Shaded area indicates night, whereas Zeitgeber time is abbreviated as ZT.

https://doi.org/10.1371/journal.pone.0225064.g003

24-hour period (Fig 3). In *trm5-1* plants, lower abundance of the clock genes *TIMING OF CAB EXPRESSION 1* (*TOC1*), and *PSEUDO RESPONSE REGULATOR 7* (*PPR7*), and the flowering time regulator genes *GIGANTEA (GI)*, *CONSTANS (CO)* and *FLOWERING LOCUS T (FT)* were observed at ZT10 to ZT22. The reduced abundance of the flowering time regulators *GI*, *CO*, and *FT* in *trm5-1* mutants correlates with delayed flowering. As expected, the downstream floral meristem identity gene *LEAFY (LFY)* had lower abundance at almost all tested time points in the *trm5* mutant when compared to wild type (Fig 3B). The downregulation of circadian-clock related genes were also detected in the RNA-seq data (S2 Table). Together these results support a role for AtTRM5 in plant growth, development, and flowering time regulation.

AtTRM5 m^1G methyltransferase activity

To test AtTRM5 m^1G methyltransferase activity *in vivo*, a *Δtrm5* mutant strain in yeast *(Saccharomyces cerevisiae*, Sc) that is defective for the tRNA m^1G37 modification was used for genetic complementation. The mutant not only has defective tRNA m^1G37 but also a slow growth phenotype when compared to wild type or a congenic strain (Fig 4A). Full-length *ScTrm5* and *AtTRM5* were cloned into yeast expression vectors. From the *AtTRM5* expression vector, a catalytically inactive mutant *Attrm5* R166D was generated by site-directed mutagenesis. After the three vectors had been transformed into the yeast *Δtrm5* mutant, cell growth and m^1G nucleoside levels were observed (Fig 4). Not only were the slow growth and nucleoside levels rescued when expressing *ScTrm5* but they were also rescued when expressing *AtTRM5* (Fig 4A and 4B). However, the catalytically inactive Attrm5 R166D did not rescue either the slow growth or m^1G nucleoside levels (Fig 4A and 4B).

To test the m^1G methyltransferase activity of AtTRM5 *in vitro*, we incubated purified recombinant proteins with tRNA substrates and measured the m^1G levels. We expressed *AtTRM5* as a GST fusion protein and purified the recombinant GST-AtTRM5 protein. We also generated a catalytically inactive GST-AtTRM5 recombinant protein by using site directed mutagenesis, expressed and purified the GST-AtTRM5 recombinant fusion protein. In yeast, ScTrm5 methylates tRNA-His-GUG, tRNA-Leu-UAA, tRNA-Asp-GUC and other tRNA isoacceptors [11, 26, 32]. Yeast tRNA-Asp-GUC RNA transcripts were generated *in vitro* by using T7 RNA polymerase, the tRNA transcripts incubated with the recombinant fusion proteins in the presence of AdoMet and m^1G nucleoside levels were measured (Fig 4D). m^1G was detected only when AtTRM5 was provided (Fig 4D) and in a dosage dependent manner. No m^1G was detected when the catalytically inactive mutant AtTRM5 was provided (Fig 4D). To test the specificity of the methyltransferase activity on tRNA-Asp guanine at position 37, the guanine nucleotide was mutated to an adenine nucleotide (tRNA-Asp-A37) and the m^1G methyltransferase activity was measured. No m^1G was detected after incubation with the fusion proteins (Fig 4D). The overall results of the yeast complementation experiments suggest that guanosine methylation occurred at position 37 of tRNA.

AtTRM5 tRNA m^1I methyltransferase activity

Previously in plants, TAD1 was demonstrated to oxidatively deaminate adenosine at position 37 of tRNA-Ala-(UGC) to inosine, and subsequently methylated by an unknown enzyme to N1-methylinosine (m^1I; Fig 5A). Human TRM5 has been reported to methylate tRNA I37 but with limited activity [22]. Given our observation that *Attrm5* mutant plants had reduced m^1I (Fig 1D), we asked the question whether AtTRM5 has methyltransferase activity on tRNA I37. We developed a two-step approach, whereby purified AtTAD1 was first incubated with the substrate tRNA-Ala-A37 to produce tRNA-Ala-I37 and then the inosine methyltransferase

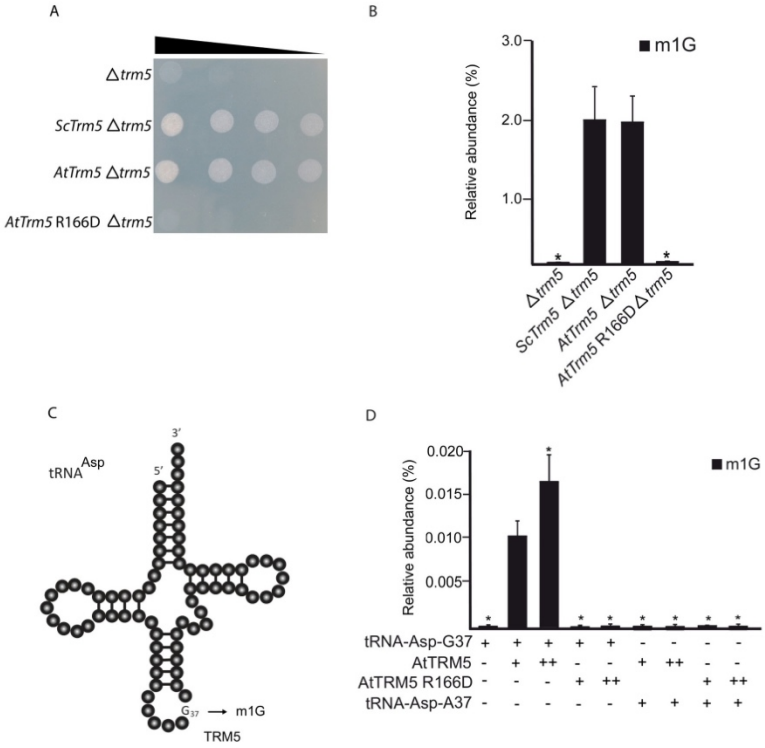

Fig 4. TRM5 modifies $tRNA_{37}$ guanosine (G) to m^1G in yeast. (**A**) Serial-dilution growth assay. Complementation experiment of TRM5 from yeast (Sc), *Arabidopsis thaliana* (At) or a catalytically inactive mutant AtTrm5 R166D in the yeast *trm5* mutant. (**B**) Relative nucleoside level of modification m^1G quantified by HPLC/MS of each complemented yeast strains with either ScTRM5 or AtTRM5. (**C**) Proposed model of TRM5-mediated m^1G modification of yeast tRNA-Asp. (**D**) Relative nucleoside level of modification m^1G with varying conditions of tRNA-Asp-G37, AtTRM5, AtTRM5 catalytic mutant, and tRNA-Asp-A37. + indicates presence, ++ indicates two-fold increase,—indicates absence.

https://doi.org/10.1371/journal.pone.0225064.g004

activity of AtTRM5 was measured by incubating AtTRM5 with the tRNA-Ala-I37 substrate. Previously, in yeast ScTAD1 was demonstrated to deaminate tRNA-Ala-A37 to tRNA-Ala-I37 *in vitro* [26] and *Arabidopsis thaliana tad1* mutants were reported to have reduced tRNA-Ala-I37 [11]. We expressed *AtTAD1* as a GST fusion protein and purified the recombinant GST-AtTAD1 protein. We also generated a catalytically inactive GST-AtTAD1 mutant recombinant protein by using site-directed mutagenesis and expressed and purified the GST-AtTAD1 mutant fusion protein. In a two-step assay, yeast tRNA-Ala-UGC RNA transcripts were generated by *in vitro* transcription using T7 RNA polymerase, the tRNA transcripts were then incubated with the recombinant fusion proteins in the presence of Mg^{2+} and methyl donor S-adenosyl-methionine (AdoMet), and the m^1I nucleoside levels measured (Fig 5B). m^1I was

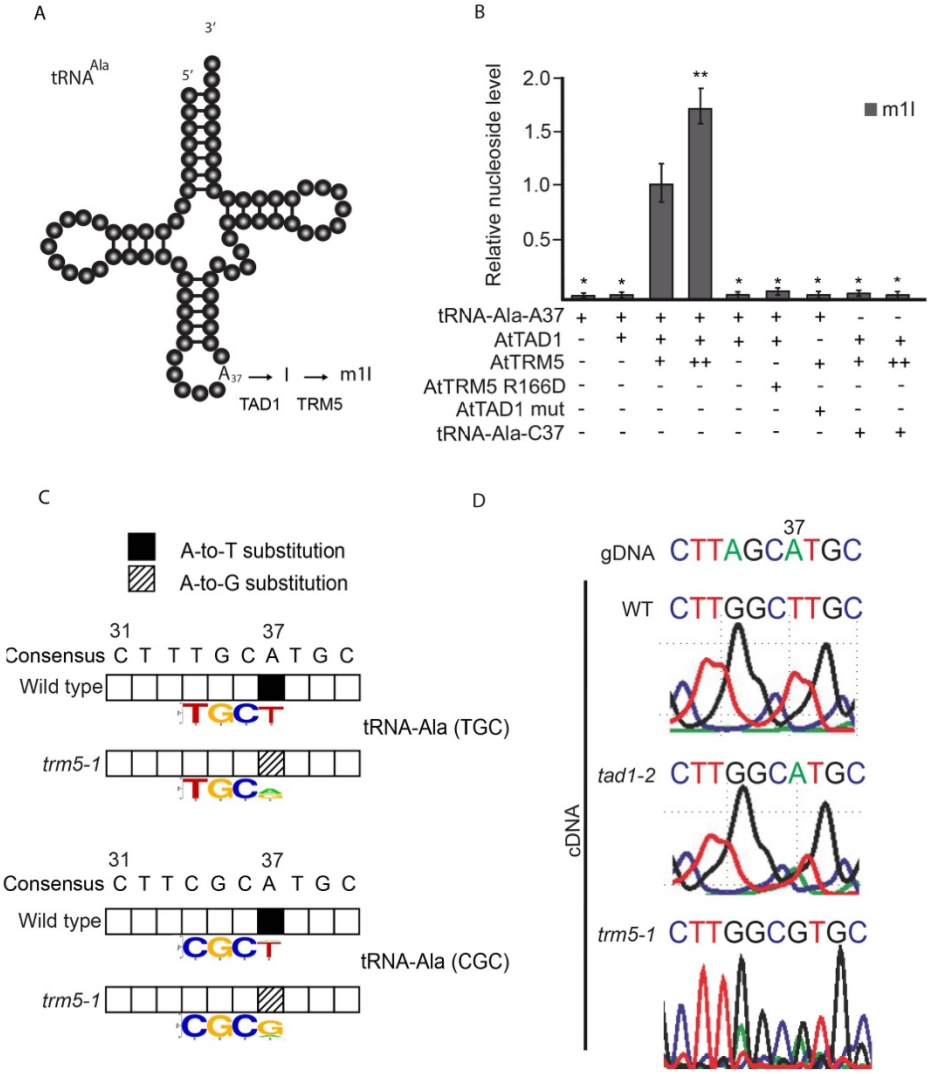

Fig 5. TRM5-mediated m^{1}I modifications in two-step reaction. (**A**) Proposed two-step modification model of TRM5-mediated m^{1}G modification of tRNA-Ala. (**B**) Relative nucleoside level of modification m^{1}I with varying conditions of tRNA-Asp-A37, AtTAD1, AtTRM5 mutant, AtTAD1 mutant, and tRNA-Ala-C37. + indicates presence, ++ indicates two-fold increase,—indicates absence. (**C**) Qualitative analysis of tRNA-Ala$^{(TGC)}$ and tRNA-Ala$^{(CGC)}$ modifications. tRNAs were enriched, deep sequenced, aligned using segemehl to tRNA references and the modifications present were inferred from observed

base substitutions between wild type and *trm5-1*. Position 37 in the gDNA, labelled as consensus, is an adenine. Sequence logo shows the proportion of nucleotides and hence inferred modifications at positon 37. Anticodons TGC and CGC are shown in the sequence logos for $Ala^{(TGC)}$ and tRNA-$Ala^{(CGC)}$, respectively. Base substitutions observed from 3 biological replicates are shown. (**D**) Qualitative analysis of tRNA-$Ala^{(AGC)}$ modifications by Sanger sequencing. tRNA-$Ala^{(AGC)}$ was PCR amplified from wild type, *tad1-2* and *trm5-1* and Sanger sequenced. Position 37 in the gDNA is an adenine. In wild-type cDNA, a thymine was detected, in *tad1-2* cDNA an adenine was observed and in *trm5-1* a guanine was detected.

https://doi.org/10.1371/journal.pone.0225064.g005

detected only when GST-AtTAD1 and GST-AtTRM5 were provided, and its production occurred in a dosage-dependent manner (Fig 5B). No m^1I was detected when the catalytically inactive mutants AtTAD1 E76S or AtTRM5 R166D were provided (Fig 5B). To test the specificity of the methyltransferase activity on tRNA-Ala alanine at position 37, the alanine nucleotide was mutated to a cytosine nucleotide (tRNA-Ala-C37) and the m^1I methyltransferase activity was measured. No m^1I was detected after incubation with the fusion proteins (Fig 5B). Collectively, these findings interestingly suggest that inosine methylation also occurs at position 37, in addition to guanosine methylation.

To test the AtTRM5 inosine methyltransferase activity *in vivo*, we measured tRNA position modifications by cDNA sequencing from either mutant or wild type plants (Fig 5C and 5D). In the sequencing assay, modification events at position 37 of tRNAs can be directly detected by sequencing of amplified cDNA obtained by reverse transcription and comparison to the DNA reference sequence as inosine is read as guanine (G) and m^1I is read as thymine (T) by the reverse transcriptase [10, 35]. As expected, we detected substitutions of A in the reference to T at position 37 for tRNA-Ala-(TGC) and tRNA-Ala-(CGC) by using Illumina sequencing in wild-type plants which is consistent with the presence of m^1I (Fig 5C). m^1I modifications have previously been described in tRNA-Ala at position 37 in eukaryotes [11, 30, 33]. In the *trm5-1* mutant, no T's were detected at position 37 (Fig 5C) which is consistent with AtTRM5 acting as a tRNA m^1I methyltransferase at position 37. Based on our *in vitro* assay results, AtTAD1 first deaminates tRNA-Ala-A37 to tRNA-Ala-I37, and then AtTRM5 methylates tRNA-Ala-I37 to tRNA-Ala-m^1I37. We confirmed this pathway in *tad1* and *trm5* mutant plants by Sanger sequencing of tRNA-Ala-(AGC) (Fig 5D). As expected, at position 37, A was substituted to T in the wild type, whereas in *trm5* mutants a G and in *tad1* mutants an A were observed (Fig 5D). These sequencing results are consistent with AtTAD1 first deaminating A37 to I37 as previously reported by Zhou, Karcher (11), and AtTRM5 then methylating I37 to m^1I. We also attempted to detect the putative loss of m^1G in the tRNA-sequencing data, as it has been reported that m^1G is prone to be called as a T in sequencing [35]. However, this was not observed in our datasets. Together, our *in vitro* and *in vivo* data provide support for AtTRM5 possessing tRNA m^1I methyltransferase activity.

AtTRM5 is localized to the nucleus

In yeast, ScTRM5 is localized to both the nucleus and mitochondria [23, 36]. Localisation to mitochondria is thought to be important as yeast strains with only nuclear-localized ScTRM5 exhibited a significantly lower rate of oxygen consumption [23]. In order to determine to which subcellular compartment(s) AtTRM5 is localized in *Nicotiana benthamiana*, we fused TRM5 to the Green Fluorescent Protein (GFP) reporter, transiently infiltrated the construct into leaves and performed laser-scanning confocal microscopy to detect GFP fluorescence. To unambiguously identify the nucleus, we stained the cells with DAPI. When we imaged the cells (n = 100), we observed distinct DAPI fluorescence in a single large circular structure per cell, as expected for the nucleus (Fig 6). Next, we imaged the same cells for GFP fluorescence (Fig 6C) and overlayed the DAPI and GFP fluorescence. The two fluorescence signals showed perfect overlap (Fig 6D). We then searched for nuclear localisation signals (NLS) using the

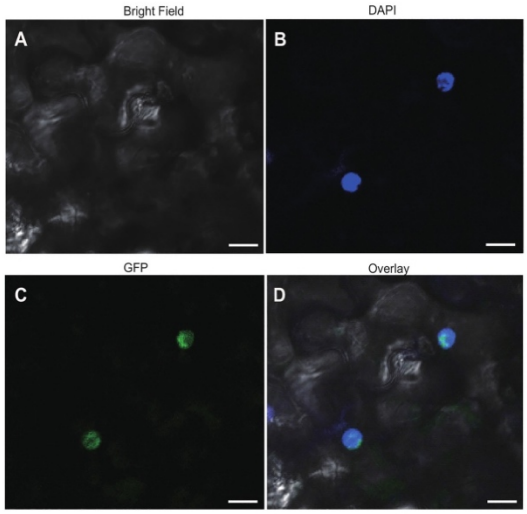

Fig 6. Subcellular localisation of TRM5 translational reporter protein in *Nicotiana benthamiana* leaves. TRM5 was fused to Green Fluorescent Protein (GFP) to yield a TRM5-GFP translational fusion recombinant protein. The construct was transiently expressed in *N. benthamiana* leaves and subcellular localisation was determined by confocal laser-scanning microscopy. (**A**) Bright field, (**B**) DAPI stained, (**C**) GFP fluorescence, (**D**) overlay of DAPI and GFP imagines. Scale bars = 20 μm.

https://doi.org/10.1371/journal.pone.0225064.g006

LOCALIZER (http://localizer.csiro.au/), LocSigDB (http://genome.unmc.edu/LocSigDB/), and cNLS mapper (http://nls-mapper.iab.keio.ac.jp/cgi-bin/NLS_Mapper_form.cgi) programs [37–39]. While LOCALIZER and LocSigDB did not predict any canonical or bipartite NLS, cNLS mapper predicted with high confidence a 29 amino acid importin α-dependent NLS, QKGCFVYANDLNPDSVRYLKINAKFNKVD, that starts at amino acid 236. Previous finding in yeast suggested that no common canonical or bipartite NLS was detected in ScTrm5 [26], which explains the outcome from LOCALIZER and LocSigDB. Multiple sequence alignment of ScTrm5 and AtTRM5 showed that only a few amino acids were conserved at the region which the importin α-dependent NLS is detected for AtTRM5 (S2 Fig). In summary, we conclude that, unlike in yeast, AtTRM5 in *Arabidopsis* is only localized to the nucleus and may be imported from the cytoplasm into the nucleus by the importin α-dependent pathway.

Proteins involved in photosynthesis are affected in *trm5* mutant plants

Next, we performed a proteomic analysis to identify proteins that differentially accumulate in *trm5-1* plants when compared to the wild type by using the Tandem Mass Tag (TMT) method (Fig 7). A total of 61571 peptide-spectrum match (PSM) were recorded, corresponding to 29011 peptides and 23055 unique peptides, respectively. 5242 protein groups were identified by blastp searches against the TAIR_pep database. Proteins with fold changes $\geq$1.20 or $\leq$0.83 and a significance level of $P \leq 0.05$ were considered to be differentially expressed. In this way, a total of 263 proteins were identified (S3 Table). 102 proteins were upregulated, and 151

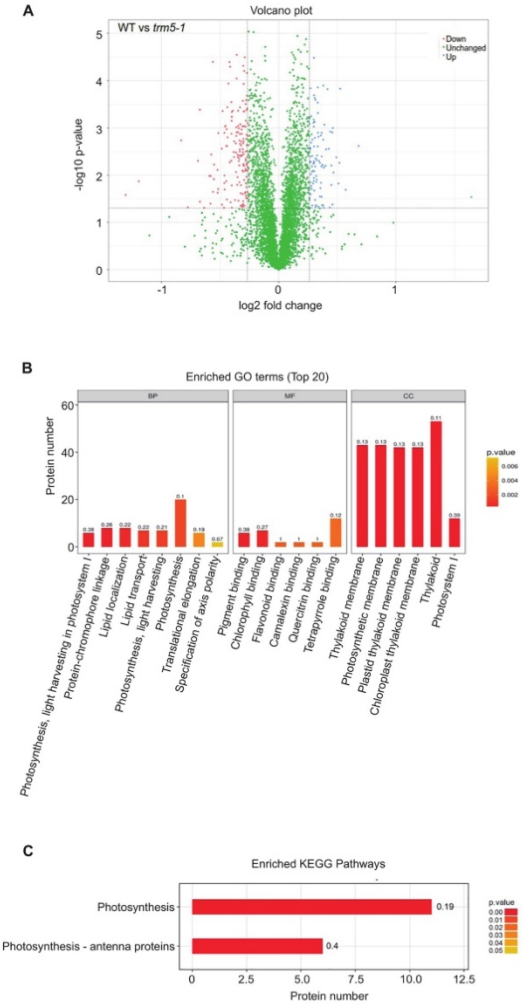

Fig 7. Proteomic analysis of wild type and *trm5-1*. (**A**) Volcano plot of differentially abundant proteins between wild type and *trm5-1*. In *trm5-1*, proteins that were increased in abundance are represented as blue dots, proteins decreased in abundance as red dots, with threshold fold change > 1.2 or < 0.83 (increased or decreased) and *P*-value < 0.05. There were 102 proteins increased and 161 proteins decreased in *trm5-1*. (**B**) GO and (**C**) KEGG terms enrichment analysis. Each differentially abundant protein was first annotated in the GO or KEGG databases, enrichment analysis was performed based on annotated differentially expressed proteins in wild type and *trm5-1*. The top 20 enriched GO terms from Biological Processes (BP), Molecular function (MF), and Cellular Component (CC) are reported.

https://doi.org/10.1371/journal.pone.0225064.g007

Table 1. Comparison between RNA-seq data and proteomics data of selected protein candidates.

Gene ID	Protein	log2FC		Status	
		RNA-seq	Proteomics	RNA-seq	Proteomics
AT1G03540.1	Pentatricopeptide repeat (PPR-like) superfamily protein	N/A	3.12815	non-differentially expressed	upregulated
AT2G45180.1	Bifunctional inhibitor/lipid-transfer protein/seed storage 2S albumin superfamily protein	2.012	0.56136	downregulated	downregulated
AT2G39480.1	P-glycoprotein 6	N/A	0.43734	non-differentially expressed	downregulated
AT5G50160.1	ferric reduction oxidase 8	N/A	0.40435	non-differentially expressed	downregulated

Four protein candidates with the highest fold change (p-$value < 0.05$) reported in the proteomics data were selected for further comparison.

https://doi.org/10.1371/journal.pone.0225064.t001

proteins were downregulated in *trm5* (Fig 7A). GO annotation of these differentially accumulating proteins revealed enrichment of the GO terms thylakoid, chloroplast, and photosystem I (Fig 7B). KEGG annotation revealed enrichment of proteins involved in photosynthesis, and photosynthetic proteins, with most of these proteins encoded by genes found in the nuclear and chloroplast genome. (Fig 7C). A further inspection on these GO terms with our proteomics data showed that the photosynthesis-related proteins were downregulated in *trm5* mutant. In the future, the abundance of these photosynthesis-related proteins could be validation by quantitative western blotting analysis. It is worthwhile to state that the abundance of these photosynthesis-related proteins may be directly or indirectly affected by the loss of TRM5 in our experiment. Taken together, the GO and KEGG analysis demonstrated that most differentially accumulating proteins are involved in processes related to photosynthesis.

Defects in tRNA m^1G methylation can be expected to affect mRNA translation, particularly of proteins that have high numbers of affected codons. Therefore, we were interested in identifying genes that showed reduced expression at the protein level in our proteomics analysis of *trm5* plants, but no detectable reduction in mRNA abundance. To identify such mRNAs, we performed RNA-seq on wild type and *trm5* plants. We identified 1186 transcripts that were reduced in abundance in *trm5* and 580 transcripts that were increased in abundance by at least 2-fold and hierarchically clustered these transcripts (S2 Table and S5 Fig). Comparison of the RNA-seq and proteomics datasets identified 133 proteins with reduced abundance, but with no detectable reduction in mRNA abundance (S5 Fig). We further inspected the data by selecting four candidate proteins with the highest fold change reported in the proteomics data (Table 1). From the selected candidate proteins, we discovered that three of the differentially expressed proteins reported in the proteomics data were not differentially expressed in the RNA-seq data, indicating that there is no change in transcripts levels leading to the fluctuation of their corresponding proteins. Only one protein candidate (AT2G45180.1) showed decreased fold change of mRNA, which correlates with the decrease of its corresponding protein reported in the proteomics data.

Finally, we performed a codon usage frequency analysis for this class of genes and detected no codon bias towards triplets read by both m^1I and m^1G modified tRNAs (S5 Fig).

Modifications at position 37 affects tRNA-halve abundance

Since our previous results showed no bias towards codon usage in *Attrm5* mutants when compared to wild type, we then asked if depleting m^1G37 and m^1I37 affects tRNA abundance. To test this, we performed a northern blot analysis on the AtTRM5 substrates tRNA-Ala-(AGC) and tRNA-Asp-(GTC), respectively (Fig 8A). We did not observe any substantial change in the

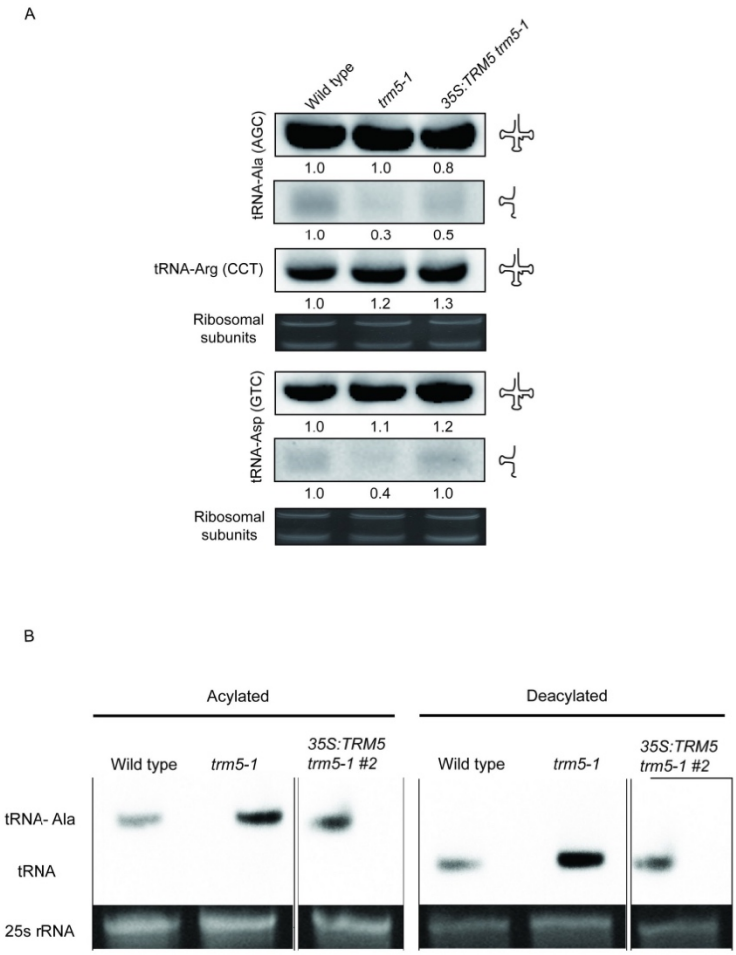

Fig 8. Loss of function of AtTRM5 affects tRNA halve abundance. (**A**) Northern blot analysis of RNA from wild type, *trm5-1* and *35S:TRM5 trm5-1*. tRNA-Ala (AGC) was inspected for changes in m^1G37 and tRNA-Asp (GTC) and m^1I37. tRNA-Arg (CCT) and rRNA were used as loading controls. The blots were probed with either tRNA-Arg (CCT), tRNA-Asp (GTC), or tRNA-Ala (AGC). (**B**) Accumulation and aminoacylation of tRNA-Ala (AGC) in wild-type plants, *trm5-1* mutant plants and *35S:TRM5 trm5-1*. The aminoacylated tRNA migrates slower than its corresponding deacylated species. To visualize the difference in electrophoretic mobility, aliquots of the same samples were deacylated *in vitro*. 10 μg of RNA was separated by electrophoresis, blotted and hybridized to a tRNA-Ala (AGC)-specific probe. The 25S rRNA band of the ethidium bromide-stained gel prior to blotting is shown as a loading control.

https://doi.org/10.1371/journal.pone.0225064.g008

full-length tRNA abundances for both tRNA-Ala-(AGC) and tRNA-Asp-(GTC). However, we unexpectedly observed significant decreases in the 5' half abundance of both tRNA-Ala-(AGC) and tRNA-Asp-(GTC) (Fig 8A), suggesting that the loss of m^1G37 and m^1I37 affects tRNA halve steady state abundance.

The anticodon region of tRNAs are known to impact tRNA aminoacylation as it interacts with tRNA aminoacyl synthetase [40] and that tRNA position 37 at the 3' anticodon region has a significant role in facilitating tRNA structure fidelity and anticodon interactions [20]. Therefore, we investigated if the tRNA position 37 which is proximal to the 3' anticodon could affect tRNA aminoacylation for tRNA-Ala-(AGC). We performed a tRNA aminoacylation experiment to determine if the loss of m^1G37 modification at the anticodon region of tRNA-Ala-(AGC) affects tRNA charging (Fig 8B) and our results show that the loss of function of *AtTRM5* does not affect acylation of tRNA-Ala (Fig 8B). One explanation for this observation can be attributed to the nature of alanyl-tRNA synthetases that recognizes G3:U70 of tRNA acceptor stem for tRNA charging instead of the anticodon region [41]. This showed that the loss of m^1G37 modification does not inhibit aminoacylation.

Discussion

The discovery of m^1G and m^1I at position 37 in tRNAs of a wide range of eukaryotic and prokaryotic organisms underscores its importance as a key regulator of tRNA function and, presumably, translation [10, 21, 23]. Previous studies in bacteria have shown that m^1G37 is required for translational fidelity [21, 42, 43] and that mutations in the enzymes catalysing m^1G37 severely impact growth or cause lethal phenotypes [10, 23, 31]. The presence of m^1G37 modification on tRNA-Asp prevents erroneous amino-acylation by arginyl-tRNA synthetase as both tRNA-Asp and tRNA-Arg have highly similar structures [44].

In eukaryotes, m^1G37 modification requires the methyltransferase TRM5. Here we report that in plants, *trm5* mutants have a 60% reduction in m^1G and m^1I levels, display severely reduced growth and delayed transition to flowering. This is somewhat similar to human patients that are heterozygous for one mutant and one functional allele of *Trm5*. They show childhood failure to thrive and exercise intolerance symptoms [10].

With the 60% reduction of m^1G and 75% reduction of m^1I in *trm5* plants, it is reasonable to anticipate a significant impact on protein translation due to the reduced stacking effect of m^1G37 on base-pairing between position 36 and the first nucleoside in translated mRNA codons. We observed a reduction in abundance of proteins involved in ribosome biogenesis and photosynthesis, and this is likely to account for the observed reduced growth of the mutant plants. A similar study by Jin *et al.* (2019) showed higher levels of polysomes in *attrm5a* mutants compared to wild type and decreased levels of ribosomal subunit, which is anticipated to reduce translation rate [45]. In the future, it would be interesting to test if translational errors, such as ribosome stalling or frame shifting, occur in *trm5* plants which would be similar to what has been previously reported in bacteria with reduced tRNA m^1G [26].

We localized *Arabidopsis* TRM5 to the nucleus which is in contrast to the cytoplasmic and mitochondrial localisation in other eukaryotes: *Trypanosoma brucei*, *Homo sapiens* (HeLa cells) and *Saccharomyces cerevisiae* [10, 23, 31], although in one study *S. cerevisiae* Trm5 has also been localized exclusively to the nucleus [36]. Interestingly, in yeast, Trm5 acts in the nucleus to form m^1G on retrograde imported $tRNA^{Phe}$ after initial export from the nucleus and subsequent splicing at the mitochondrial outer membrane. As retrograde tRNA import is conserved from yeast to vertebrates [46, 47], it is tempting to speculate that TRM5-mediated m^1G formation occurs in retrograde imported tRNAs in *Arabidopsis*.

Direct comparison of RNA-seq and proteomics data has been challenging as variation in protein abundance in proteomics datasets can be confounded by multiple factors. Several factors can cause fluctuation in protein levels with no change of mRNA abundance: mRNA transcript abundance, translation rate, and translation resources availability (as reviewed in Liu, Beyer (48)). This may explain the results of the initial comparison between our RNA-seq and proteomics data, and the seeming discrepancies in the derived sets of differentially expressed genes (S2 and S3 Tables). In our RNA-seq data, microtubule-related genes appeared to be significantly downregulated (AT1G21810, AT1G52 410, AT2G28620, AT2G44190, AT3G23670, AT3G60840, AT3G63670, AT5G67270, AT4G14150, AT5G27000). However, we could not detect any differential expression of these proteins in our proteomics dataset. This is not unexpected, as it has been reported that protein and transcript abundances only rarely correlate in data analysis [48]. However, it has been shown that transcript abundance can still be used to infer protein abundance [49]. Among the selected four candidate proteins (Table 1), we could observe only one event of protein downregulation due to decreased transcript level: the lipid transfer protein (AT2G45180) which is involved in lipid transport in chloroplasts. Lipid transport is crucial in the formation of photosynthetic membranes in plants [50]. As several lipids are important functional components of thylakoidal protein complexes involved in photosynthesis, the impacted lipid transport and lipid synthesis revealed by the GO term analysis may contribute to the observed dysregulation of photosynthesis-related genes. This finding is consistent with Jin *et al.* (2019) [45]. The remaining three candidate genes displayed no changes in transcript levels, but one candidate gene showed upregulation and the other two downregulation at the protein level. The exact function of pentatricopeptide repeat (PPR-like) superfamily protein (AT1G03540.1) is unknown, but the protein was suggested to play a significant role in post-transcriptional modification of tRNAs [51]. The P-glycoprotein 6 (AT2G39480) belongs to the large P-glycoprotein family and is known to play a role in mediating auxin transport, and disturbed auxin transport is known to affect plant growth [52]. Our proteomics data suggested that the auxin transport is affected (AT5G35735, AT3G07390, AT4G12980, AT5G35735) in the *trm5* mutant. This can be inferred to the reduced auxin levels in *attrm5a* as reported by Jin *et al.* (2019) [45]. Ferric reduction oxidase 8 (AT5G50160/AtFRO8) has been shown to participate in iron reduction and was implicated in leaf vein transport [53]. We proposed that disturbed photosynthesis in *trm5* mutant plants is a secondary effect of dysregulated transport processes.

Our findings also show that modified bases at tRNA-Ala at position 37 does not affect tRNA aminoacylation but does affect tRNA-Ala-derived 5' half steady state abundance. Both tRNA aminoacylation and tRNA-derived halves were shown to effect translational fidelity [40, 54]. In yeast, the introduction of tRNA-derived halves, both 5' and 3' fragments, affects tRNA aminoacylation, suggesting that tRNA-derived fragments (tRFs) has a regulatory role in translation [54]. It was also demonstrated that these tRFs regulate tRNA-aminoacylation via interacting with ribosome. The decreased amount of tRNA-Ala 5' halves may explain the polysome profile changes reported by Jin *et al.* (2019) [45].

The role of post-transcriptional RNA modifications in tRNA and mRNA metabolism and their impact on plant growth and development in plants are only beginning to be elucidated. Here, we have described the AtTRM5-mediated m^1G and m^1I methylation in tRNAs and identified crucial links between this modification, photosynthesis, plant growth, and protein translation. It appears likely that the many other tRNA modifications in plant tRNAs also play important roles in translation and/or translational regulation which remain to be discovered.

Materials and methods

Plant material and root growth experiments

Arabidopsis thaliana (Columbia accession) wild type and mutant plants were grown in Phoenix Biosystems growth under metal halide lights as previously described [55]. For plate experiments, seeds were first surface sterilized, plated on ½ MS medium supplemented with 1% sucrose and sealed as previously described [1, 56]. All plants were grown under either long-day photoperiod conditions of 16 h light and 8 h darkness or short-day photoperiods of 10 h light and 14 h darkness.

Characterization of the mutant alleles, *trm5-1* (SALK_022617) and *trm5-2* (SALK_032376) are as described previously [57]. The *tad1-2* mutant was used as described previously [11]. Nucleotide sequence data for the following genes are available from The *Arabidopsis* Information Resource (TAIR) database under the following accession numbers: TRM5 (At3g56120), At4g27340, At4g04670, and TAD1 (At1g01760).

Analysis of root phenotypes was carried out on 11-day-old seedlings grown on ½ MS agar plates. A flatbed scanner (Epson) was used to non-destructively acquire images of seedling roots grown on the agar surface. Once captured, the images were analysed by software package RootNav [58, 59].

Plasmid construction and generation of transgenic plants

For the 35SCaMV:TRM5 construct, the full-length genomic region of At3g56120 including the 5'UTR and 3'UTR was amplified from Col-0 genomic DNA template with primers provided in (S1 Table) and cloned into Gateway entry vector pENTRTM/SD/D-TOPO (Invitrogen). The insert was sequenced and then cloned into the binary destination vector pGWB5 by an LR recombination reaction, using the Gateway cloning system following the manufacturers protocol (Invitrogen), resulting in the 35S:TRM5 construct. For the $TRM5_{Pro}$::TRM5 construct, the full-length genomic region of At3g56120 that included the promoter, 5'UTR and 3'UTR was amplified from Col-0 genomic DNA template with primers provided in (S1 Table) and cloned into Gateway entry vector PCR8 TOPO-TA (Invitrogen). The insert was sequenced and then cloned into the a modified (35S promoter removed) destination pMDC32 vector, using the Gateway cloning system [60] following the manufacturers protocol (Invitrogen), resulting in $TRM5_{Pro}$::TRM5. The 35S:TRM5 construct was transformed into *A. thaliana* wild type Col-0 plants or *trm5-1* mutant plants by *Agrobacterium*-mediated floral dip method respectively [61]. The $TRM5_{Pro}$::TRM5 construct was transformed into *trm5-2* mutant plants by *Agrobacterium*-mediated floral dip method. Transgenic plants were selected on ½ MS media supplemented with 50 μg ml^{-1} kanamycin. TRM5 transcript abundance was assessed in at least five independent T_1 plants using qRT-PCR and two lines showing the highest TRM5 transcript levels were carried through to homozygous T_3 generation for phenotypic analysis.

Sub-cellular localization of TRM5

For analysis of subcellular localization of TRM5, a 35S:TRM5:GFP construct was produced by PCR amplification of the TRM5 coding sequence from *Arabidopsis* seedling cDNA by using the primers described in the supplementary data (S1 Table). The TRM5 cDNA was recombined cloned into pCR8, sequenced and then recombined in frame into pMDC83 to produce 35S:TRM5:GFP. The 35S:TRM5:GFP construct was introduced into *A. tumefaciens* strain GV3101 and transiently expressed in 5-week-old *Nicotiana benthamiana* leaves. Fluorescence was analysed using a confocal laser-scanning microscope (Zeiss microscope, LSM700) and excited with 488-nm line of an argon ion laser. GFP fluorescence was detected via a 505- to

530-nm band-pass filter. The cut leaves were immersed in 10 μM 4´, 6-diamidino-2-phenylindole (DAPI) at room temperature for 45 min, and then washed with PBS for 3 times (5 min each). The blue fluorescence of DAPI was imaged using 404-nm line for excitation and a 435- to 485-nm band pass filter for emission.

Shoot apical meristem sections

14, 18, or 22-day-old seedlings were fixed for 1 day in FAA containing 50% ethanol, 5% acetic acid and 3.7% formaldehyde. The samples were then dehydrated through an ethanol series of five one-hour steps (50, 60, 70, 85, 95% ethanol) ending in absolute ethanol (100%). The ethanol was gradually replaced with Histoclear containing safranine to stain the tissue, as following: incubated in a Histoclear series (75:25, 50:50, 25:75 Ethanol: Histoclear) for 30 min and followed by twice one-hour incubation in 100% Histoclear. The paraffin was polymerised by baking overnight at 60˚C, and the samples were embedded in paraffin. Sections were cut, attached to slides and dried on a slide warmer overnight at 42˚C to allow complete fixation. The shoot apical meristem was observed using light microscopy.

Quantitative real-time PCR (qPCR)

For the transcription profiling of flowering-related genes and circadian clock-related genes, 17-day-old seedlings were sampled from Zeitgeber time (ZT) 1 and collected every 3h during the day and night cycles, respectively. Total RNA was extracted the leaf samples using Trizol reagent (Invitrogen). The relative expression levels of *AtTRM5* were determined using quantitative real-time PCR (qPCR) with gene-specific primers (S1 Table). The qPCR was performed using the StepOnePlus real-time PCR system (Applied Biosystems) using Absolute SYBR Green ROX mix (Applied Biosystems) for quantification. Three biological replicates were carried out for each sample set. The relative expression was corrected using a reference gene *EF1alpha* (At5g60390) and calculated using the $2^{-\Delta\Delta Cq}$ method as described previously [11].

mRNA-sequencing

Total RNA, 1 ug, was extracted from 20-day-old *Arabidopsis* leaf samples using Trizol reagent (Invitrogen) and purified using the RNAeasy Mini RNA kit (Qiagen). One hundred nanograms of RNA were used for RNA-seq library construction according the manufacturer's recommendations (Illumina). First-strand cDNA was synthesized using SuperScript II Reverse Transcriptase (Invitrogen). After second strand cDNA synthesis and adaptor ligation, cDNA fragments were enriched, purified and then sequenced on the Illumina Hiseq X Ten. Three biological replicates were used for RNA-seq experiments.

tRNA purification and tRNA-sequencing

Total RNA was isolated from wild type and *trm5* 10-day-old *Arabidopsis* seedlings using the Spectrum Plant total RNA kit (SIGMA-ALDRICH) and contaminating DNA removed using DNase I (SIGMA-ALDRICH). To enrich for tRNAs, 10μg of total RNA was separated on a 10% polyacrylamide gel, the region containing 65–85 nts was removed and RNA was purified as previously described [56]. Purified tRNAs were used for library construction using NEB Ultradirectional RNA library kit. Given the short sequences of tRNAs, the fragmentation step of the library preparation was omitted, and samples were quickly processed for first-strand cDNA synthesis after the addition of the fragmentation buffer. The remaining steps of library construction were performed as per the manufacturer's instructions. Illumina sequencing was

performed on a MiSeq platform at The Australian Cancer Research Foundation (ACRF) Cancer Genomics Facility, Adelaide.

Yeast complementation

AtTrm5 (At3g56120) and ScTrm5 (YHR070W) was PCR amplified from cDNA and cloned into pYE19 using a Gibson assembly reaction (NEB). Mutant AtTrm5 (R166D) was generated by synthesising gene blocks (IDT) with nucleotides that mutated the translated proteins at R166 and the gene block was cloned into pYE19 using a Gibson assembly reaction (NEB). Yeast △trm5 (*Mat a*, *hisD1*, *leu2D1*, *met15D0*, *trm5*:*KanMX)* was previously described [62]. Recombinant plasmids were transformed into △*trm5* mutant strain and the resulting strain was analysed for growth phenotypes and m^1G nucleoside levels.

AtTrm5, AtTAD1, ScTrm5 protein expression and purification and tRNA methylation

Full length AtTrm5, mutant AtTrm5 (R166D) and AtTAD1 (At1g01760) cDNAs were cloned into pGEX resulting in GST-AtTrm5, GST-AtTRM5-mutant, GST-TAD1, respectively. Mutant AtTAD1 (E76S) was generated by synthesising a gene block (IDT) with mutated nucleotides and the gene block was cloned into pGEX using a Gibson assembly reaction (NEB) resulting in GST-TAD1 mutant. IPTG (0.5 μM) was used to induce expression of the proteins and the recombinant proteins were purified on a GST resin column (ThermoFisher Scientific). tRNA-Asp-GUC or tRNA-Ala-AGC were transcribed in vitro with T7 RNA polymerase (Promega). Methylation reactions were performed in 100 mM Tris-HCl, 5 mM $MgCl_2$, 100 mM KCl, 2 mM DTT, 50 mM EDTA, 0.03 mg/mL BSA and 25 μM AdoMet. Substrate tRNA was provided in a final concentration of 1–5 μM, AtTrm5 or AtTrm5 mutant proteins from 6.0 to 12 μM and AtTAD1 or AtTAD1 mutant proteins at 5.0 μM.

mRNA-seq and tRNA-seq bioinformatics analysis

Global Mapping: Reads were first adapter trimmed using Trim galore v0.4.2 (http://www.bioinformatics.babraham.ac.uk/projects/trim_galore/) with default parameter. The quality of the trimmed reads was checked using Fastqc (https://www.bioinformatics.babraham.ac.uk/projects/fastqc/) and ngsReports (https://github.com/UofABioinformaticsHub/ngsReports). Reads were then globally mapped to *Arabidopsis* reference genomes (TAIR10) [63] using STAR v2.5.3 [64]. Mapped reads were counted using featureCounts [65]. The raw read counts were normalized using sample size factor for sequence depth and differential expression analysis between wild type and *trm5-1* mutant samples was performed using DESeq2 v1.18.1 [66]. The tRNA-enriched reads were mapped to tDNA reference acquired from GtRNAdb (generated from tRNA-Scan SE v2.0) of *Arabidopsis thaliana* derived from TAIR10 reference genome [63, 67–69] using segemehl v0.2.0 [68]. The mapped reads were then processed for variant calling using GATK v3.7 [70]. Haplotype Caller in GATK v3.7 was implied to call for variants, with the variant filtered using hard filtering as recommended.

Proportion estimation: SNPs were identified in the wild type and *trm5-1* samples were then compared. SNPs at position 37 were extracted and analysed using vcftools [71]. Changes in base pair modifications were indicated by base substitution due to the property of next generation sequencing as mentioned in [10, 35]. The ratio of the expected A-to-T conversion in wild type samples and both the ratio of A-to-T (indicating no change in comparison to wild type) and A-to-G in *trm5-1* were analyzed as an indication of m^1I depletion.

Sanger sequence analysis of tRNA editing

tRNA purification and tRNA editing analysis were performed as described previously [11]. Cytosolic tRNA-Ala (AGC) were amplified by reverse transcriptase (RT)-PCR with specific primers (tRNA-Ala-f and tRNA-Ala-r, S1 Table), and purified PCR products were directly Sanger sequenced.

TMT-based proteome determination and data analysis

Total protein was extracted from 20-day-old *Arabidopsis* leaf samples and purified according to a method described by [72]. Protein digestion was performed according to FASP procedure described previously [73], and 100 μg peptide mixture of each sample was labelled using TMT reagent according to the manufacturer's instructions (Thermo Fisher Scientific). LC-MS/MS analysis was performed on a Q Exactive mass spectrometer (Thermo Fisher Scientific) that was coupled to Easy nLC (Thermo Fisher Scientific). MS data was acquired using a data-dependent top20 method dynamically choosing the most abundant precursor ions from the survey scan (200–1800 m/z) for HCD fragmentation (Shanghai Applied Protein Technology Co., Ltd). Determination of the target value is based on predictive Automatic Gain Control (pAGC). SEQUEST HT search engine configured with Proteome Discoverer 1.4 workflow (Thermo Fisher Scientific) was used for mass spectrometer data analyses. The latest *Arabidopsis* protein databases (2018) was downloaded from http://www.arabidopsis.org/download/index-auto.jsp?dir=/download_files/Proteins and configured with SEQUEST HT for searching the datasets. The following screening criteria was deemed as differentially expression: fold-changes >1.2 or <0.83 (up- or down-regulation) and the Benjamini-Hochberg corrected *p*-value, $P < 0.05$ were considered significant.

tRNA nucleoside analysis

tRNAs were purified as previously described [56]. Twenty-five μg of tRNAs were digested with P1 nuclease (Sigma- Aldrich) and 1.75 units of calf intestine alkaline phosphatase in 20 mM Hepes–KOH (pH 7.0) at 37˚C for 3 h. The mixture was diluted to a concentration of 15 ng/uL and samples were injected into an API 4000 Q-Trap (ThermoFisher Scientific) mass spectrometer coupled with LC-20A HPLC system (Shimadzu). All RNA samples analyzed were from three biological replicates. A diode array UV detector monitored the LC signals from the nucleosides, whereas in counts were recorded in positive mode (190–400 nm). The abundance of each modified nucleoside was represented by its unique ion peak area and normalized to the sum of the four canonical nucleosides (A, C, G and U nucleosides). Since m^1G, m^2G and m^7G have the same Q1 and Q3 mass, they were discriminated by retention time, in the order of m^7G, m^1G and m^2G, respectively. The identity of m^7G peak was confirmed with external standard (TriLink Biotechnologies) and the identity of m^1G versus m^2G was indirectly confirmed by results from yeast *trm5* mutant

Northern blot for tRNA detection

Total RNA was isolated from the wild type, *trm5-1* and *35S:TRM5 trm5-1 Arabidopsis* seedlings by using the TRIZOL Reagent (ThermoFisher Scientific). 20μg of total RNA was on 15% urea-polyacrylamide gel and RNA was transferred to Amersham Hybond-N^+membrane. After cross-linking, prehybridization was performed for 3 hours at 68˚C in 20μl of DIG easy Hyb Granules (Roche). 60 pmol of 3-end Digoxin labelled oligonucleotides was added to hybridization buffer (S1 Table) and hybridize for overnight at 40˚C with gentle agitation. The membrane was washed at low-stringency (2X SSC, 0.1% SDS) twice and high-stringency (0.1X SSC,

0.1% SDS) twice. The probe-target hybrid was localised with the anti-DIG-alkaline phosphatase antibody (Roche), and the membrane was put into washing and blocking and detection buffer to visualize using the CDP-Star, ready to use (Roche).

tRNA aminoacylation assay

Total RNA of wild type, *trm5-1* and *35S:TRM5 trm5-1 Arabidopsis* seedlings were isolated and analysed using the tRNA aminoacylation protocol as described in Zhou, Karcher (11), using a specific probe for tRNA-Ala (AGC) (S1 Table).

Supporting information

S1 Fig. Extended phylogenetic analysis of TRM5 orthologues. (**A**) Circos plot of sequence conservation of TRM5 orthologues in yeast (Sc), tomato (Sl), grape (Vv), *Arabidopsis* (At), maize (Zm), rice (Os), *Marchantia* (Mp), *Physcomitrella* (Pp), *Chlamydomonas* (Cr),*Ostreococcus* (Ot), humans (HsTrm5), *Drosophila melanogaster* (DmTrm5), *Pyrococcus horikoshii* (PhTYW2), and *Methanococcus jannaschii* (MjTYW2). The ribbons were coloured based on sequence identity, with blue < = 25%, green 25–50%, orange 51–75% and red for 76–99%. (**B**) Unrooted phylogenetic tree of the same TRM5 orthologues used to for sequence conservation analysis.
(TIF)

S2 Fig. Bioinformatics characterization of TRM5 and related proteins. (**A**) Multiple sequence alignment of TRM5 proteins from *Arabidopsis thaliana* (At), yeast (ScTrm5), humans (HsTrm5), *Drosophila melanogaster* (DmTrm5), *Pyrococcus horikoshii* (PhTYW2), and *Methanococcus jannaschii* (MjTYW2). Black shaded boxes are identical across all species. Light shaded boxes are similar and nearly conserved residues. Asterisk indicates catalytic important amino acids. The predicted 29 aa importin α-dependent NLS is boxed in red. (**B**) Multiple sequence alignment of yeast Trm5p, *Arabidopsis* TRM5 (At3g56120) and the two closest related proteins from *Arabidopsis*. Black shaded boxes are conserved in at least 2 sequences. Met 10+ like domain and S-adenosyl Methyltransferase Motif (SAM) are detected in *Arabidopsis* TRM5 using NCBI Conserved Domains Search (https://www.ncbi.nlm.nih.gov/Structure/cdd/wrpsb.cgi). The position of importin α-dependent NLS is also indicated.
(TIF)

S3 Fig. Characterisation of growth and development in wild type, trm5 mutant, complemented and overexpression lines. (**A**) Seeds (n = 100) of wild type and *trm5-1* were sown on ½ MS plates, stratified at 4 °C and then grown at 21 °C under long day conditions for 32 hours. Germination was measured at 8, 16, 24 and 32 hours after shifting to 21 °C. (**B**) Sections of the shoot apical meristems of wild type and *trm5-1* plants grown under long days for 14, 18 and 22 days. (**C**) The average fresh plant weight of long day grown plants. (**D**) The average rosette leaf number at flowering; (**E**) The average days to flowering under long days. (**F**) The rosette leaf number under short days. Data presented are means. Error bars are ± SE (n = 16). NF = did not flower. An asterisk indicates a statistical difference ($P<0.05$) as determined by Student's t-test.
(TIF)

S4 Fig. Root phenotypic analysis of seedlings. Seedlings of wild type, *trm5*, complemented lines (35S:TRM5 *trm5-1*), TRM5 overexpression lines (35S:TRM5) were vertically grown on ½ MS medium for 10 days and then measured. (**A**) Total root length, (**B**) Primary root, (PR) length, (**C**) average lateral root (LR) length and (**D**) LR number were measured 10 days after

germination. Data presented are means. Error bars are ± SE (n = 10 plants).
(TIF)

S5 Fig. RNA-seq and proteomic analysis of wild type and trm5-1. (**A**) RNA was purified from 10-day-old seedlings of wild type (wt) and *trm5-1* (n = 3). RNA-seq analysis was performed and differentially abundant transcripts were hierarchically clustered. (**B**) An upset plot showing positive overlapping mRNAs and proteins identified by RNA-seq and proteomics analysis. (**C**) Codon bias analysis of codons in the up and down regulated proteins identified by proteomics analysis.
(TIF)

S1 Table. Oligonucleotide primers used in this study.
(DOCX)

S2 Table. Differentially expressed genes identified by RNA-seq analysis of wild type and *trm5-1*.
(XLSX)

S3 Table. Differentially abundant proteins identified by LC-MS/MS analysis of wild type and *trm5-1*.
(XLSX)

Acknowledgments

We thank the staff at The Australian Cancer Research Foundation (ACRF) Cancer Genomics Facility, Adelaide for their technical expertise in sequencing. We would also like to thank the staff members of the University of Adelaide Bioinformatics Hub for bioinformatics consultation.

Author Contributions

Conceptualization: Wenbin Zhou, Iain Searle.

Formal analysis: Qianqian Guo, Pei Qin Ng, Shanshan Shi, Diwen Fan, Jun Li, Jing Zhao, Hua Wang, Rakesh David, Parul Mittal, Trung Do, Ralph Bock, Wenbin Zhou, Iain Searle.

Funding acquisition: Ming Zhao, Iain Searle.

Investigation: Qianqian Guo, Iain Searle.

Methodology: Wenbin Zhou, Iain Searle.

Project administration: Iain Searle.

Supervision: Iain Searle.

Writing – original draft: Pei Qin Ng, Iain Searle.

Writing – review & editing: Qianqian Guo, Pei Qin Ng, Jing Zhao, Hua Wang, Rakesh David, Trung Do, Ralph Bock, Ming Zhao, Wenbin Zhou, Iain Searle.

References

1. Burgess A, David R, Searle IR. Deciphering the epitranscriptome: A green perspective. Journal of integrative plant biology. 2016; 58(10):822–35. https://doi.org/10.1111/jipb.12483 PMID: 27172004
2. Edelheit S, Schwartz S, Mumbach MR, Wurtzel O, Sorek R. Transcriptome-wide mapping of 5-methylcytidine RNA modifications in bacteria, archaea, and yeast reveals m5C within archaeal mRNAs. PLoS Genetics. 2013; 9(6):e1003602. https://doi.org/10.1371/journal.pgen.1003602 PMID: 23825970

3. Jackman JE, Alfonzo JD. Transfer RNA modifications: nature's combinatorial chemistry playground. Wiley interdisciplinary reviews RNA. 2013; 4(1):35–48. https://doi.org/10.1002/wrna.1144 PMID: 23139145
4. Machnicka MA, Milanowska K, Osman Oglou O, Purta E, Kurkowska M, Olchowik A, et al. MODOMICS: a database of RNA modification pathways—2013 update. Nucleic Acids Research. 2013; 41 (Database issue):D262–7. https://doi.org/10.1093/nar/gks1007 PMID: 23118484
5. Motorin Y, Lyko F, Helm M. 5-methylcytosine in RNA: detection, enzymatic formation and biological functions. Nucleic Acids Research. 2010; 38(5):1415–30. https://doi.org/10.1093/nar/gkp1117 PMID: 20007150
6. Dominissini D, Moshitch-Moshkovitz S, Schwartz S, Salmon-Divon M, Ungar L, Osenberg S, et al. Topology of the human and mouse m6A RNA methylomes revealed by m6A-seq. Nature. 2012; 485 (7397):201–6. https://doi.org/10.1038/nature11112 PMID: 22575960
7. Dominissini D, Nachtergaele S, Moshitch-Moshkovitz S, Peer E, Kol N, Ben-Haim MS, et al. The dynamic N(1)-methyladenosine methylome in eukaryotic messenger RNA. Nature. 2016; 530 (7591):441–6. https://doi.org/10.1038/nature16998 PMID: 26863196
8. Meyer KD, Saletore Y, Zumbo P, Elemento O, Mason CE, Jaffrey SR. Comprehensive analysis of mRNA methylation reveals enrichment in 3' UTRs and near stop codons. Cell. 2012; 149(7):1635–46. https://doi.org/10.1016/j.cell.2012.05.003 PMID: 22608085
9. Schwartz S, Agarwala SD, Mumbach MR, Jovanovic M, Mertins P, Shishkin A, et al. High-resolution mapping reveals a conserved, widespread, dynamic mRNA methylation program in yeast meiosis. Cell. 2013; 155(6):1409–21. https://doi.org/10.1016/j.cell.2013.10.047 PMID: 24269006
10. Powell CA, Kopajtich R, D'Souza AR, Rorbach J, Kremer LS, Husain RA, et al. TRMT5 Mutations Cause a Defect in Post-transcriptional Modification of Mitochondrial tRNA Associated with Multiple Respiratory-Chain Deficiencies. American Journal of Human Genetics. 2015; 97(2):319–28. https://doi.org/10.1016/j.ajhg.2015.06.011 PMID: 26189817
11. Zhou W, Karcher D, Bock R. Importance of adenosine-to-inosine editing adjacent to the anticodon in an Arabidopsis alanine tRNA under environmental stress. Nucleic Acids Research. 2013; 41(5):3362–72. https://doi.org/10.1093/nar/gkt013 PMID: 23355609
12. Alfonzo JD, Blanc V, Estévez AM, Rubio MA, Simpson L. C to U editing of the anticodon of imported mitochondrial tRNA(Trp) allows decoding of the UGA stop codon in Leishmania tarentolae. The EMBO Journal. 1999; 18(24):7056–62. https://doi.org/10.1093/emboj/18.24.7056 PMID: 10601027
13. Agris PF, Vendeix FAP, Graham WD. tRNA's wobble decoding of the genome: 40 years of modification. Journal of Molecular Biology. 2007; 366(1):1–13. https://doi.org/10.1016/j.jmb.2006.11.046 PMID: 17187822
14. Allnér O, Nilsson L. Nucleotide modifications and tRNA anticodon-mRNA codon interactions on the ribosome. RNA (New York). 2011; 17(12):2177–88. https://doi.org/10.1261/rna.029231.111 PMID: 22028366
15. Nasvall SJ, Chen P, Bjork GR. The modified wobble nucleoside uridine-5-oxyacetic acid in tRNAPro (cmo5UGG) promotes reading of all four proline codons in vivo. RNA (New York). 2004; 10(10):1662–73. https://doi.org/10.1261/rna.7106404 PMID: 15383682
16. Aström SU, Byström AS. Rit1, a tRNA backbone-modifying enzyme that mediates initiator and elongator tRNA discrimination. Cell. 1994; 79(3):535–46. https://doi.org/10.1016/0092-8674(94)90262-3 PMID: 7954819
17. Phizicky EM, Alfonzo JD. Do all modifications benefit all tRNAs? FEBS Letters. 2010; 584(2):265–71. https://doi.org/10.1016/j.febslet.2009.11.049 PMID: 19931536
18. Gerber A, Grosjean H, Melcher T, Keller W. Tad1p, a yeast tRNA-specific adenosine deaminase, is related to the mammalian pre-mRNA editing enzymes ADAR1 and ADAR2. The EMBO Journal. 1998; 17(16):4780–9. https://doi.org/10.1093/emboj/17.16.4780 PMID: 9707437
19. Gamper HB, Masuda I, Frenkel-Morgenstern M, Hou Y-M. Maintenance of protein synthesis reading frame by EF-P and m(1)G37-tRNA. Nature Communications. 2015; 6:7226. https://doi.org/10.1038/ncomms8226 PMID: 26009254
20. Helm M, Alfonzo JD. Posttranscriptional RNA Modifications: playing metabolic games in a cell's chemical Legoland. Chemistry & Biology. 2014; 21(2):174–85. https://doi.org/10.1016/j.chembiol.2013.10.015 PMID: 24315934
21. Björk GR, Wikström PM, Byström AS. Prevention of translational frameshifting by the modified nucleoside 1-methylguanosine. Science. 1989; 244(4907):986–9. https://doi.org/10.1126/science.2471265 PMID: 2471265

22. Brulé H, Elliott M, Redlak M, Zehner ZE, Holmes WM. Isolation and characterization of the human tRNA-(N1G37) methyltransferase (TRM5) and comparison to the Escherichia coli TrmD protein. Biochemistry. 2004; 43(28):9243–55. https://doi.org/10.1021/bi049671q PMID: 15248782

23. Lee C, Kramer G, Graham DE, Appling DR. Yeast mitochondrial initiator tRNA is methylated at guanosine 37 by the Trm5-encoded tRNA (guanine-N1-)-methyltransferase. The Journal of Biological Chemistry. 2007; 282(38):27744–53. https://doi.org/10.1074/jbc.M704572200 PMID: 17652090

24. Wang C, Jia Q, Zeng J, Chen R, Xie W. Structural insight into the methyltransfer mechanism of the bifunctional Trm5. Science advances. 2017; 3(12):e1700195. https://doi.org/10.1126/sciadv.1700195 PMID: 29214216

25. Christian T, Hou Y-M. Distinct determinants of tRNA recognition by the TrmD and Trm5 methyl transferases. Journal of Molecular Biology. 2007; 373(3):623–32. https://doi.org/10.1016/j.jmb.2007.08.010 PMID: 17868690

26. Björk GR, Jacobsson K, Nilsson K, Johansson MJ, Byström AS, Persson OP. A primordial tRNA modification required for the evolution of life? The EMBO Journal. 2001; 20(1–2):231–9. https://doi.org/10.1093/emboj/20.1.231 PMID: 11226173

27. Hori H. Transfer RNA methyltransferases with a SpoU-TrmD (SPOUT) fold and their modified nucleosides in tRNA. Biomolecules. 2017; 7(1). Epub 2017/03/08. https://doi.org/10.3390/biom7010023 PMID: 28264529; PubMed Central PMCID: PMC5372735.

28. Noma A, Kirino Y, Ikeuchi Y, Suzuki T. Biosynthesis of wybutosine, a hyper-modified nucleoside in eukaryotic phenylalanine tRNA. The EMBO Journal. 2006; 25(10):2142–54. https://doi.org/10.1038/sj.emboj.7601105 PMID: 16642040

29. Jackman JE, Montange RK, Malik HS, Phizicky EM. Identification of the yeast gene encoding the tRNA m1G methyltransferase responsible for modification at position 9. RNA (New York). 2003; 9(5):574–85. https://doi.org/10.1261/rna.5070303 PMID: 12702816

30. Grosjean H, Auxilien S, Constantinesco F, Simon C, Corda Y, Becker HF, et al. Enzymatic conversion of adenosine to inosine and to N1-methylinosine in transfer RNAs: a review. Biochimie. 1996; 78(6):488–501. https://doi.org/10.1016/0300-9084(96)84755-9 PMID: 8915538

31. Paris Z, Horáková E, Rubio MAT, Sample P, Fleming IMC, Armocida S, et al. The T. brucei TRM5 methyltransferase plays an essential role in mitochondrial protein synthesis and function. RNA (New York). 2013; 19(5):649–58. https://doi.org/10.1261/rna.036665.112 PMID: 23520175

32. Wang Y, Pang C, Li X, Hu Z, Lv Z, Zheng B, et al. Identification of tRNA nucleoside modification genes critical for stress response and development in rice and Arabidopsis. BMC Plant Biology. 2017; 17(1):261. https://doi.org/10.1186/s12870-017-1206-0 PMID: 29268705

33. Torres AG, Piñeyro D, Filonava L, Stracker TH, Batlle E, Ribas de Pouplana L. A-to-I editing on tRNAs: biochemical, biological and evolutionary implications. FEBS Letters. 2014; 588(23):4279–86. https://doi.org/10.1016/j.febslet.2014.09.025 PMID: 25263703

34. Juhling F, Morl M, Hartmann RK, Sprinzl M, Stadler PF, Putz J. tRNAdb 2009: compilation of tRNA sequences and tRNA genes. Nucleic Acids Res. 2009; 37(Database issue):D159–62. Epub 2008/10/30. https://doi.org/10.1093/nar/gkn772 PMID: 18957446; PubMed Central PMCID: PMC2686557.

35. Ryvkin P, Leung YY, Silverman IM, Childress M, Valladares O, Dragomir I, et al. HAMR: high-throughput annotation of modified ribonucleotides. Rna. 2013; 19(12):1684–92. https://doi.org/10.1261/rna.036806.112 PMID: 24149843

36. Ohira T, Suzuki T. Retrograde nuclear import of tRNA precursors is required for modified base biogenesis in yeast. Proceedings of the National Academy of Sciences of the United States of America. 2011; 108(26):10502–7. https://doi.org/10.1073/pnas.1105645108 PMID: 21670254

37. Kosugi S, Hasebe M, Tomita M, Yanagawa H. Systematic identification of cell cycle-dependent yeast nucleocytoplasmic shuttling proteins by prediction of composite motifs. Proceedings of the National Academy of Sciences of the United States of America. 2009; 106(25):10171–6. https://doi.org/10.1073/pnas.0900604106 PMID: 19520826

38. Negi S, Pandey S, Srinivasan SM, Mohammed A, Guda C. LocSigDB: a database of protein localization signals. Database: the Journal of Biological Databases and Curation. 2015; 2015(0). https://doi.org/10.1093/database/bav003 PMID: 25725059

39. Sperschneider J, Catanzariti A-M, DeBoer K, Petre B, Gardiner DM, Singh KB, et al. LOCALIZER: subcellular localization prediction of both plant and effector proteins in the plant cell. Scientific reports. 2017; 7:44598. https://doi.org/10.1038/srep44598 PMID: 28300209

40. Giegé R, Sissler M, Florentz C. Universal rules and idiosyncratic features in tRNA identity. Nucleic Acids Res. 1998; 26(22):5017–35. https://doi.org/10.1093/nar/26.22.5017 PMID: 9801296.

41. Chong YE, Guo M, Yang XL, Kuhle B, Naganuma M, Sekine SI, et al. Distinct ways of G:U recognition by conserved tRNA binding motifs. Proc Natl Acad Sci U S A. 2018; 115(29):7527–32. Epub 2018/07/

04. https://doi.org/10.1073/pnas.1807109115 PMID: 29967150; PubMed Central PMCID: PMC6055181.

42. Hagervall TG, Tuohy TM, Atkins JF, Björk GR. Deficiency of 1-methylguanosine in tRNA from Salmonella typhimurium induces frameshifting by quadruplet translocation. Journal of Molecular Biology. 1993; 232(3):756–65. https://doi.org/10.1006/jmbi.1993.1429 PMID: 7689113

43. Li JN, Björk GR. 1-Methylguanosine deficiency of tRNA influences cognate codon interaction and metabolism in Salmonella typhimurium. Journal of Bacteriology. 1995; 177(22):6593–600. https://doi.org/10.1128/jb.177.22.6593-6600.1995 PMID: 7592438

44. Veronique Perret AG, Henri Grosjean, Jean.Pierre Ebel, Catherine Florentz & Richard Giege. Relaxation of a transfer RNA specificity by removal of modified nucleotides. Nature. 1990; 344:787–9. https://doi.org/10.1038/344787a0 PMID: 2330033

45. Jin X, Lv Z, Gao J, Zhang R, Zheng T, Yin P, et al. AtTrm5a catalyses 1-methylguanosine and 1-methylinosine formation on tRNAs and is important for vegetative and reproductive growth in Arabidopsis thaliana. Nucleic acids research. 2019; 47(2):883–98. https://doi.org/10.1093/nar/gky1205 PMID: 30508117

46. Shaheen HH, Horetsky RL, Kimball SR, Murthi A, Jefferson LS, Hopper AK. Retrograde nuclear accumulation of cytoplasmic tRNA in rat hepatoma cells in response to amino acid deprivation. Proceedings of the National Academy of Sciences of the United States of America. 2007; 104(21):8845–50. https://doi.org/10.1073/pnas.0700765104 PMID: 17502605

47. Takano A, Endo T, Yoshihisa T. tRNA actively shuttles between the nucleus and cytosol in yeast. Science. 2005; 309(5731):140–2. https://doi.org/10.1126/science.1113346 PMID: 15905365

48. Liu Y, Beyer A, Aebersold R. On the Dependency of Cellular Protein Levels on mRNA Abundance. Cell. 2016; 165(3):535–50. https://doi.org/10.1016/j.cell.2016.03.014 PMID: 27104977

49. Li JJ, Bickel PJ, Biggin MD. System wide analyses have underestimated protein abundances and the importance of transcription in mammals. PeerJ. 2014; 2:e270. https://doi.org/10.7717/peerj.270 PMID: 24688849

50. LaBrant E, Barnes AC, Roston RL. Lipid transport required to make lipids of photosynthetic membranes. Photosynthesis research. 2018:1–16.

51. Manna S. An overview of pentatricopeptide repeat proteins and their applications. Biochimie. 2015; 113:93–9. https://doi.org/10.1016/j.biochi.2015.04.004 PMID: 25882680

52. Geisler M, Murphy AS. The ABC of auxin transport: the role of p-glycoproteins in plant development. FEBS Letters. 2006; 580(4):1094–102. https://doi.org/10.1016/j.febslet.2005.11.054 PMID: 16359667

53. Wu H, Li L, Du J, Yuan Y, Cheng X, Ling H-Q. Molecular and biochemical characterization of the Fe(III) chelate reductase gene family in Arabidopsis thaliana. Plant & Cell Physiology. 2005; 46(9):1505–14. https://doi.org/10.1093/pcp/pci163 PMID: 16006655

54. Mleczko AM, Celichowski P, Bąkowska-Żywicka K. Transfer RNA-derived fragments target and regulate ribosome-associated aminoacyl-transfer RNA synthetases. Biochimica et Biophysica Acta (BBA)—Gene Regulatory Mechanisms. 2018; 1861(7):647–56. doi: https://doi.org/10.1016/j.bbagrm.2018.06.001.

55. David R, Burgess A, Parker B, Li J, Pulsford K, Sibbritt T, et al. Transcriptome-Wide Mapping of RNA 5-Methylcytosine in Arabidopsis mRNAs and Noncoding RNAs. The Plant Cell. 2017; 29(3):445–60. https://doi.org/10.1105/tpc.16.00751 PMID: 28062751

56. Burgess AL, David R, Searle IR. Conservation of tRNA and rRNA 5-methylcytosine in the kingdom Plantae. BMC Plant Biology. 2015; 15:199. https://doi.org/10.1186/s12870-015-0580-8 PMID: 26268215

57. Alonso JM, Stepanova AN, Leisse TJ, Kim CJ, Chen H, Shinn P, et al. Genome-wide insertional mutagenesis of Arabidopsis thaliana. Science. 2003; 301(5633):653–7. https://doi.org/10.1126/science.1086391 PMID: 12893945

58. Guo Q, Love J, Roche J, Song J, Turnbull MH, Jameson PE. A RootNav analysis of morphological changes in Brassica napus L. roots in response to different nitrogen forms. Plant growth regulation. 2017; 83(1):83–92. https://doi.org/10.1007/s10725-017-0285-0

59. Pound MP, French AP, Atkinson JA, Wells DM, Bennett MJ, Pridmore T. RootNav: navigating images of complex root architectures. Plant Physiology. 2013; 162(4):1802–14. https://doi.org/10.1104/pp.113.221531 PMID: 23766367

60. Curtis MD, Grossniklaus U. A gateway cloning vector set for high-throughput functional analysis of genes in planta. Plant Physiology. 2003; 133(2):462–9. https://doi.org/10.1104/pp.103.027979 PMID: 14555774

61. Davis AM, Hall A, Millar AJ, Darrah C, Davis SJ. Protocol: Streamlined sub-protocols for floral-dip transformation and selection of transformants in Arabidopsis thaliana. Plant Methods. 2009; 5:3. https://doi.org/10.1186/1746-4811-5-3 PMID: 19250520

62. Urbonavicius J, Stahl G, Durand JMB, Ben Salem SN, Qian Q, Farabaugh PJ, et al. Transfer RNA modifications that alter +1 frameshifting in general fail to affect -1 frameshifting. RNA (New York). 2003; 9 (6):760–8.

63. Lamesch P, Berardini TZ, Li D, Swarbreck D, Wilks C, Sasidharan R, et al. The Arabidopsis Information Resource (TAIR): improved gene annotation and new tools. Nucleic Acids Research. 2012; 40(Database issue):D1202–10. https://doi.org/10.1093/nar/gkr1090 PMID: 22140109

64. Dobin A, Gingeras TR. Mapping RNA-seq reads with STAR. Current protocols in bioinformatics. 2015; 51(1):11.4. 1–.4.9.

65. Liao Y, Smyth GK, Shi W. featureCounts: an efficient general purpose program for assigning sequence reads to genomic features. Bioinformatics. 2014; 30(7):923–30. https://doi.org/10.1093/bioinformatics/btt656 PMID: 24227677

66. Love MI, Huber W, Anders S. Moderated estimation of fold change and dispersion for RNA-seq data with DESeq2. Genome Biology. 2014; 15(12):550. https://doi.org/10.1186/s13059-014-0550-8 PMID: 25516281

67. Chan PP, Lowe TM. GtRNAdb 2.0: an expanded database of transfer RNA genes identified in complete and draft genomes. Nucleic Acids Research. 2016; 44(D1):D184–9. https://doi.org/10.1093/nar/gkv1309 PMID: 26673694

68. Hoffmann S, Otto C, Kurtz S, Sharma CM, Khaitovich P, Vogel J, et al. Fast mapping of short sequences with mismatches, insertions and deletions using index structures. PLoS Computational Biology. 2009; 5(9):e1000502. https://doi.org/10.1371/journal.pcbi.1000502 PMID: 19750212

69. Lowe TM, Chan PP. tRNAscan-SE On-line: integrating search and context for analysis of transfer RNA genes. Nucleic Acids Research. 2016; 44(W1):W54–7. https://doi.org/10.1093/nar/gkw413 PMID: 27174935

70. DePristo MA, Banks E, Poplin R, Garimella KV, Maguire JR, Hartl C, et al. A framework for variation discovery and genotyping using next-generation DNA sequencing data. Nature Genetics. 2011; 43 (5):491–8. https://doi.org/10.1038/ng.806 PMID: 21478889

71. Danecek P, Auton A, Abecasis G, Albers CA, Banks E, DePristo MA, et al. The variant call format and VCFtools. Bioinformatics. 2011; 27(15):2156–8. https://doi.org/10.1093/bioinformatics/btr330 PMID: 21653522

72. Lan P, Li W, Wen T-N, Shiau J-Y, Wu Y-C, Lin W, et al. iTRAQ protein profile analysis of Arabidopsis roots reveals new aspects critical for iron homeostasis. Plant Physiology. 2011; 155(2):821–34. https://doi.org/10.1104/pp.110.169508 PMID: 21173025

73. Wiśniewski JR, Zougman A, Nagaraj N, Mann M. Universal sample preparation method for proteome analysis. Nature Methods. 2009; 6(5):359–62. https://doi.org/10.1038/nmeth.1322 PMID: 19377485

Chapter 9

Quantitative and Single-Nucleotide Resolution Profiling of RNA 5-Methylcytosine

Jun Li, Xingyu Wu, Trung Do, Vy Nguyen, Jing Zhao, Pei Qin Ng, Alice Burgess, Rakesh David, and Iain Searle

Abstract

RNA has coevolved with numerous posttranscriptional modifications to sculpt interactions with proteins and other molecules. One of these modifications is 5-methylcytosine (m^5C) and mapping the position and quantifying the level in different types of cellular RNAs and tissues is an important objective in the field of epitranscriptomics. Both in plants and animals bisulfite conversion has long been the gold standard for detection of m^5C in DNA but it can also be applied to RNA. Here, we detail methods for highly reproducible bisulfite treatment of RNA, efficient locus-specific PCR amplification, detection of candidate sites by sequencing on the Illumina MiSeq platform, and bioinformatic calling of non-converted sites.

Key words Bisulfite conversion, Epitranscriptome, Fluidigm Access Array, Illumina, Next-generation sequencing, 5-Methylcytosine

1 Introduction

Cellular RNAs can be modified, or decorated, with more than 120 chemically and structurally distinct nucleoside modifications [1]. The emerging field of epitranscriptomics [2] has been enabled by the development of high-throughput mapping methods for RNA modifications, typically based on second-generation sequencing. Transcriptome-wide positions of N1-methyladenosine (m^1A, [3–5]), N6-methyladenosine (m^6A, [6, 7]), 5-methylcytosine (m^5C, [8]), and pseudouridine [9] have each been reported in this way. To detect m^5C in RNA, a range of methods have been developed, including the indirect (aza-IP [10], miCLIP [11]) immunoprecipitation of methylated RNA or direct methods (meRIP, [7]). Of particular interest here, the bisulfite conversion approach previously used for DNA has been adapted to RNA [12, 13]. Bisulfite conversion of nucleic acids takes advantage of the differential chemical reactivity of m^5C compared to

Mary McMahon (ed.), *RNA Modifications: Methods and Protocols* , Methods in Molecular Biology, vol. 2298, https://doi.org/10.1007/978-1-0716-1374-0_9,

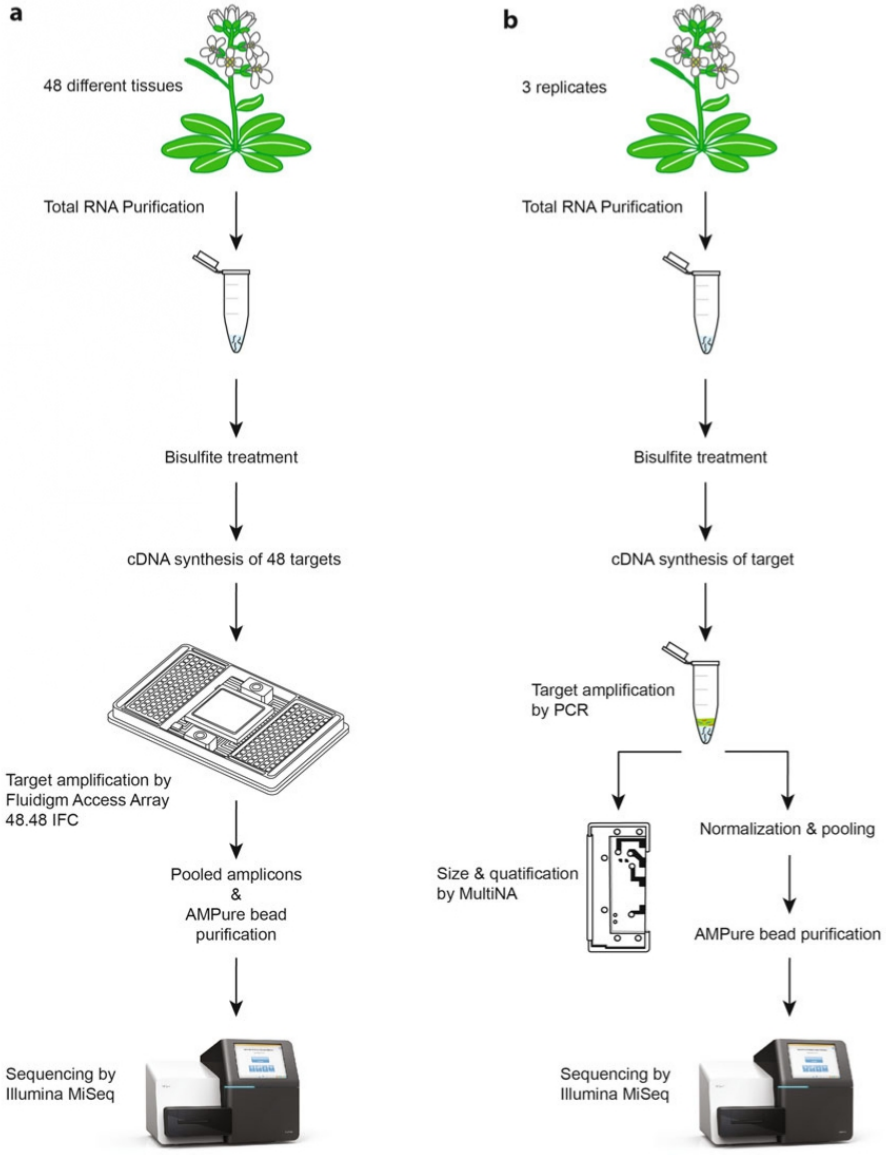

Fig. 1 Protocol overview showing the workflow for either parallel or single amplicon amplification for effective detection of m^5C. (**a**) Parallel amplification and sequencing of up to 2304 amplicons across 48 tissues and 48 primer pairs. Forty-eight different tissues can be selected, total RNA isolated and purified, spiked with MGFP in vitro-transcribed control RNA and bisulfite converted. Bisulfite-converted RNA is reverse transcribed

unmethylated cytosines; unmethylated cytosines are deaminated to uracil while m^5C remains as a cytosine.

The RNA bisulfite conversion method has been applied to animals and plants [8, 14] using second-generation sequencing, for example Illumina, based transcriptome-wide readout and has mapped thousands of novel candidate m^5C sites in a diverse array of RNAs, including mRNAs and long noncoding RNAs (lncRNAs). Here, we detail protocols for RNA bisulfite conversion, locus-specific PCR amplification of up to 2304 amplicons, and bioinformatics calling of converted or non-converted sites. Sequencing of PCR amplicons is conveniently done on the Illumina MiSeq, as this affords multiplexing of multiple distinct amplicons while still achieving ample read depth for estimating the proportion of m^5C at targeted positions. For instance, each of the 96 Fluidigm indexed adapters could be assigned to a separate RNA derived from different tissues, and 96 multiple PCR amplicons per sample could be included in the sequencing pool, potentially generating thousands of independent quantitative measurements of the m^5C levels in a single MiSeq run (Fig. 1).

2 Materials

Prepare all solutions using RNase-free and DNase-free H_2O and analytical grade reagents. Store and prepare all reagents at room temperature unless indicated otherwise. Prepare and perform bisulfite conversion, cDNA synthesis, and PCR amplification experiments in an RNase-free area. Follow all state or national safety and waste disposal regulations when performing experiments.

2.1 Total RNA Extraction and In Vitro Transcription

1. TRIzol™ reagent.
2. Chloroform.
3. Isopropanol.
4. 75% Ethanol.
5. Ultrapure™ H_2O.
6. Monster Green® Fluorescent protein phMGFP vector.

Fig. 1 (continued) (RT) to cDNA using gene-specific RT primers that include the positive control *MAG5* (AT5G47480) and negative control MGFP. Target regions are PCR amplified using a Fluidigm Access Array Integrated Fluidic Circuit (IFC); up to 2304 amplicons are harvested and eluted pools are quantified. Equal concentrations of the pools are combined into a final pool, purified using AMPure beads, accurately quantified, PhiX control library spiked-in, and subjected to sequencing on the Illumina MiSeq platform. (**b**) Single amplicon amplification and sequencing. A single tissue is selected, RNA isolated and purified in triplicate, spiked with MGFP in vitro-transcribed control RNA and bisulfite converted. Bisulfite conversion and cDNA synthesis are the same as outlined above except a specific target RT primer is used. The target amplicon is PCR amplified, triplicate amplicons are pooled, size and concentration are assessed on a Shimadzu MultiNA, and amplicons are pooled at equal concentration. Pooled amplicons are purified, PhiX control library spiked-in, and subjected to sequencing on the Illumina MiSeq platform

7. XbaI restriction enzyme.
8. HiScribe™ T7 In Vitro Transcription Kit.
9. TURBO™ DNase.
10. Phase Lock Gel ™ QuantBio (2.0 mL).
11. UltraPure ™ Phenol:Water (3.75:1 v/v).
12. 100% Ethanol.
13. 3 M sodium acetate, pH 5.2.
14. 5 mg/mL Glycogen.
15. Agilent RNA 6000 Nano Kit.
16. Biological tissue samples (animal or plant).

2.2 Sodium Bisulfite Conversion

1. Sodium bisulfite solution: 40% (w/v) Sodium metabisulfite, 0.6 mM hydroquinone, final pH 5.1.

   To prepare the sodium bisulfite solution, prepare the following:

   0.6 M Hydroquinone: Weigh 66 mg hydroquinone and place into a 1.5 mL tube. Add H_2O to 1 mL and cover in foil to protect from light. Place in an orbital shaker to dissolve.

   40% (w/v) Sodium bisulfite: Dissolve 4 g sodium metabisulfite in 10 mL H_2O in a 50 mL falcon tube and vortex until it completely dissolves.

   Add 10μL 0.6 M hydroquinone to the 40% sodium bisulfite solution, vortex, and adjust pH to 5.1 with 10 M NaOH. Filter the solution through a 0.2μm filter. Cover in foil to protect from light (*see* **Note 1**).
2. 1 M Tris–HCl, pH 9.0.
3. Micro Bio-Spin ™ P-6 Gel Columns.
4. Mineral oil.
5. 75% Ethanol.
6. 100% Ethanol.
7. 3 M sodium acetate, pH 5.2.
8. 5 mg/mL Glycogen.

2.3 cDNA Synthesis

1. SuperScript ™ III Reverse Transcriptase.
2. 10 mM Mixed dNTPs.
3. Single-target priming: 20μM Gene-specific oligo for each amplicon. Here is an example of a positive control (MAG5) and a negative control (mGFP) (all C should be converted to U) primer sequence:

   MAG5: CACACACACCCATACATCCAC.
   mGFP: AACAAAAAAATTAACCCCATC
4. Pool target priming: Up to 48 primers at 20μM each. Design for target genes of interest.

2.4 PCR Amplicon Amplification

1. KAPA HiFi DNA polymerase.
2. First PCR primers: Examples of positive control (MAG5) and negative control (mGFP) first round primer primers are shown (underlined sequence = tag, BC = 8 nt barcode):
   MAG5 F: ACACTGACGACATGGTTCTACAGGTAAAGGTAAAATTGGGTAATGAG.
   MAG5 R: TACGGTAGCAGAGACTTGGTCT-[BC]-AGACCAAGTCTCTGCTACCGTA.
   mGFP F: ACACTGACGACATGGTTCTACAGAGGGTGATGGGAAAGGTAAG.
   mGFP R: TACGGTAGCAGAGACTTGGTCTCAATCATCCACACCCTTCATC
3. Second PCR primers (underlined sequence = tag, BC = 8 nt barcode):
   P5_CS1_F: AATGATACGGCGACCACCGAGATCTACACTGACGACATGGTTCTACA P7_BC_CS2_R: CAAGCAGAAGACGGCATACGAGAT -[BC]-TACGGTAGCAGAGACTTGGTCT
4. 10 mM Mixed dNTPs.
5. Fluidigm Access Array Integrated Fluidic Circuit (IFC) 48.48.
6. FastStart ™ High Fidelity PCR System, dNTPack.
7. 20× Access Array Loading Reagent.
8. 1× Access Array Harvest Solution.
9. 1× Access Array Hydration Reagent v2.
10. Access Array Barcode primers for Illumina Sequencers-384: Single Direction.

2.5 MultiNA Microelectrophoresis System

1. DNA-500 Kit (Shimadzu Corporation).

2.6 PCR Amplicon Purification and Quantification

1. Agencourt AMPure XP beads.
2. Qubit ™ dsDNA Broad Range Assay Kit.
3. KAPA Library Quantification Kit (Universal).

2.7 Library Sequencing Components

1. 0.2 M NaOH.
2. Illumina MiSeq Reagent Kit v3 (150 or 600 cycles) (*see* **Note 2**).

3 Methods

Carry out all procedures described below at room temperature unless otherwise stated.

3.1 RNA Extraction, Purification, and DNase Treatment

Total RNA is extracted and purified directly from tissue with 1 mL of TRIzol™ as per the manufacturer's protocol. RNA is then treated with TURBO™ DNase as per the manufacturer's protocol. Assess the integrity of the RNA by using a RNA 6000 Nano Chip on the Agilent 2100 Bioanalyzer according to the manufacturer's protocol.

3.2 Generation of the MGFP In Vitro Transcript Spike-in Control

1. Linearize the phMGFP vector by using the restriction enzyme *XbaI* and purify the linearized DNA vector according to the HiScribe T7 In Vitro Transcription Kit protocol.
2. Perform in vitro transcription according to the HiScribe T7 In Vitro Transcription Kit protocol by using 1μg of linearized DNA. An incubation period of 4 h at 37 °C with the kit components is sufficient.
3. Add 2 U TURBO™ DNase and incubate at 37 °C for 30 min.
4. Transfer the reaction to a Phase Lock Gel™ tube and make the volume of the reaction up to 100μL with ultrapure H_2O.
5. Add an equal volume of phenol:water and chloroform, shake vigorously for 15 s, and centrifuge at 15,000 × *g* for 5 min.
6. Add the same volume of chloroform as in **step 5** to the tube, shake vigorously for 15 s, and centrifuge at 15,000 × *g* for 5 min again.
7. Transfer the aqueous phase to a clean 1.5 mL tube. Add 1/10 volume 3 M sodium acetate, 3 volumes of 100% ethanol, and 1μL glycogen; vortex; and precipitate the RNA overnight at −80 °C.
8. Centrifuge RNA at 17,000 × *g* at 4 °C for 60 min and carefully remove the supernatant.
9. Add 1 mL 75% ethanol to the RNA, invert five times, and centrifuge at 7500 × *g* at 4 °C for 10 min (*see* **Note 3**).
10. Carefully remove the supernatant and let the pellet air-dry for approximately 15 min (*see* **Note 4**).
11. Resuspend the RNA in 25μL of ultrapure H_2O.
12. Optional step: Treat 5μg of in vitro-transcribed MGFP transcript with 2 U TURBO™ DNase according to the manufacturer's protocol at 37 °C for 30 min.
13. Assess the integrity and size of the MGFP in vitro transcripts by using an RNA 6000 Nano Chip on the Agilent 2100 Bioanalyzer according to the manufacturer's protocol (*see* **Note 5**).

3.3 Bisulfite Conversion of RNA

1. Add 1/2000 of the MGFP RNA transcript to 2μg DNase-treated purified total RNA. Increase the volume of the RNA sample to 20μL with ultrapure H_2O.
2. Denature RNA by heating to 75 °C for 5 min in a heat block.

3. Preheat the sodium bisulfite solution to 75 °C, add 100μL to the RNA, vortex thoroughly, and briefly spin in a microcentrifuge (13,000 × *g* for 1 min).
4. Overlay the reaction mixture with 100μL of mineral oil. Cover the tube in aluminum foil to protect the reaction mixture from light (*see* **Note 6**).
5. Incubate at 75 °C for 4 h in a heat block.
6. About 15 min before the bisulfite conversion reaction is complete, prepare two Micro Bio-Spin Columns for each conversion reaction by allowing the Tris solution in the column to drain into a collection tube. Discard the Tris flow-through, place the column back into the collection tube, and centrifuge at 1000 × *g* for 2 min. Transfer each column to a clean 1.5 mL tube (*see* **Note 7**).
7. Remove the bisulfite reaction mixture from the heat block and gently transfer the aqueous layer (that is under the mineral oil) containing the sodium bisulfite/RNA mixture to the Micro Bio-Spin column (*see* **Note 8**).
8. Centrifuge at 1000 × *g* for 4 min.
9. Carefully transfer the eluate into the second Micro Bio-Spin column placed in a 1.5 mL tube and repeat **step 8**.
10. Preheat the temperature of the heat block to 75 °C in preparation for **step 12**.
11. Add an equal volume of 1 M Tris–HCl pH 9.0 to the second eluate, vortex, spin briefly, and then overlay with 175μL of mineral oil. Cover the tube in aluminum foil to protect the reaction mixture from light.
12. Incubate at 75 °C for 1 h in the heat block.
13. Transfer the bottom aqueous layer containing the RNA to a clean 1.5 mL tube.
14. Precipitate the bisulfite-treated RNA by following **steps 7–11** in Subheading 3.2 and resuspend the bisulfite-converted RNA in H_2O (*see* **Note 9**).

3.4 Bisulfite Oligonucleotide Primer Design for cDNA Synthesis and PCR

1. For efficient parallel amplification of 48 target amplicons on the Fluidigm Access Array, use targeted cDNA synthesis to reduce the amplification of spurious amplicons. Targeted cDNA synthesis is achieved by designing reverse transcriptase (RT) primers 30–40 nt 3′ of the cytosine(s) to be assayed. N. B.: Design the RT primers such that they avoid areas of bisulfite-converted cytosines as inefficient BS conversion may result in unconverted cytosines and biasing of later amplification. See Fig. 2.

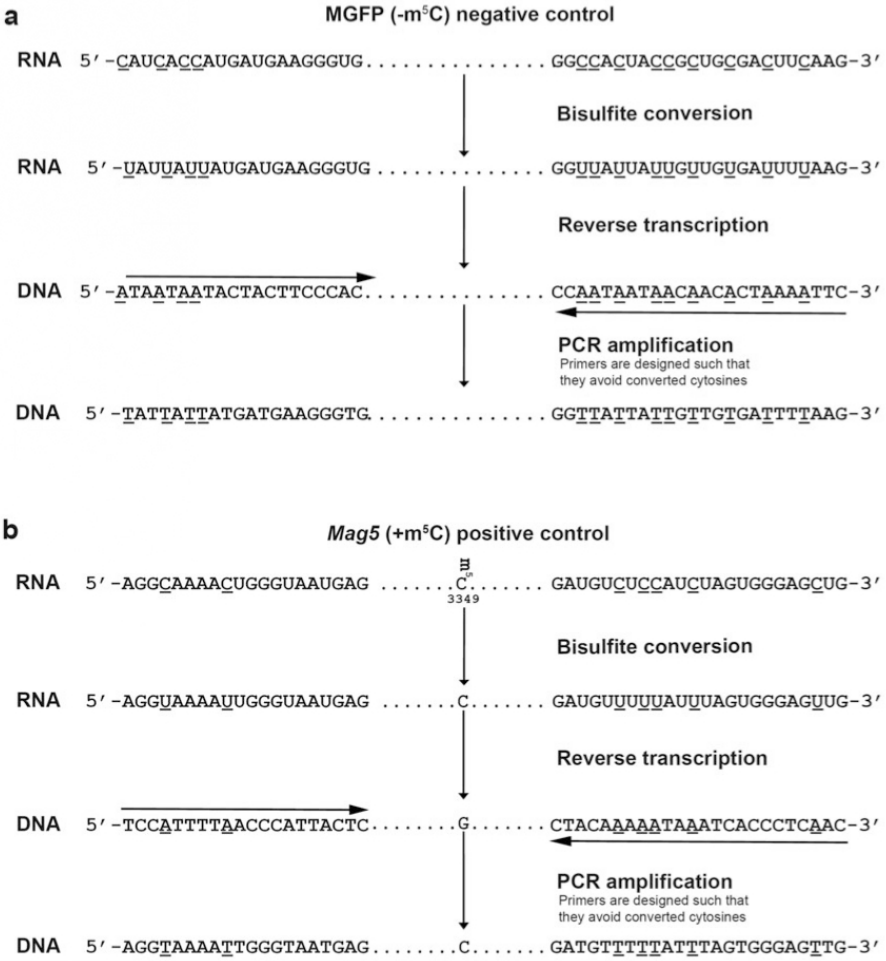

Fig. 2 Overview of bisulfite conversion of RNA, reverse transcription to cDNA, and PCR amplification. (**a**) In the in vitro-transcribed MGFP sequence, unmodified cytosines (underlined) are converted to uracil, reverse transcribed (RT) by reverse transcriptase to cDNA, and then PCR amplified. RT and PCR primers are designed to avoid stretches of converted cytosines to prevent preferential amplification of converted sequences which may incorrectly indicate efficient bisulfite conversion. (**b**) In *MAG5* control and other candidate sequences, primers are designed to span areas containing converted cytosines to preferentially amplify converted sequences. C3349 is methylated in *Arabidopsis thaliana* and serves as an over-conversion control. Flanking cytosines are not methylated and should be completely converted. Primers are designed with a T_m of 59–61 °C, preferably with a 3′ G nucleotide and to amplify PCR products of 170–200 bp

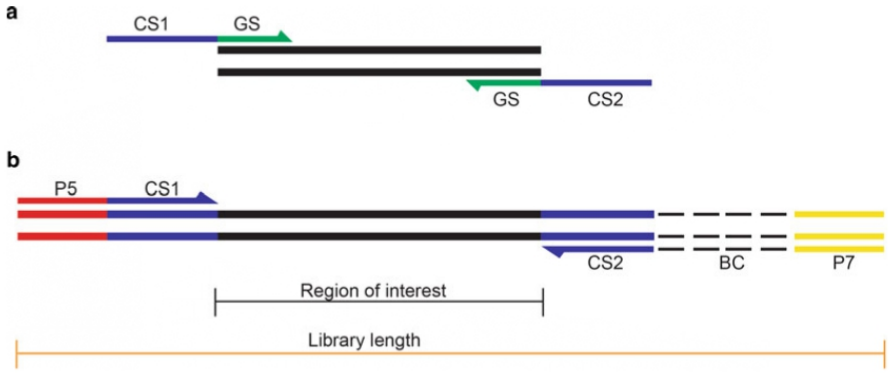

Fig. 3 Overview of first and second PCR amplification of target regions. (**a**) For the first PCR, the forward PCR primer is designed with the gene-specific sequence (GS) and universal forward tag called Common Sequence, CS1 (5′- TACGGTAGCAGAGACTTGGTCT -3′), and reverse PCR primer is designed with the gene-specific sequence (GSS) and universal reverse tag called Common Sequence CS2 (5'-ACACTGACGACATGGTTCTACA -3′). (**b**) For the second PCR, the forward primer is designed with the CS1 and Illumina P5 sequences and the reverse primer contains the CS2, barcoding, and Illumina P7 sequences. The Fluidigm barcodes or indexes are 10 nt in length

2. Design primers for the first round of PCR amplification so that small amplicons are 170–200 bp, to allow efficient amplification (*see* **Notes 10** and **11**). As the G/C content in the template is low, design long primers to ensure that a T_m is in the rage of 59–61 °C. Add the CS1 sequence (5′-TACGGTAGCA GAGACTTGGTCT -3′) to the forward primer gene-specific sequence (GSS) and CS2 (5′- ACACTGACGACATGGTTC TACA -3′) to the reverse primer GSS. For the second PCR amplification, use the forward primer containing the complementary sequences to the P5 Illumina flow cell combined with CS1 (P5_CS1) and the reverse primer containing the barcode, and complementary sequences to the P7 Illumina flow cell combined with CS2 (P7_BC_CS2) primer (*see* **Note 12**). See Fig. 3.

3.5 cDNA Synthesis

1. Mix 500 ng of bisulfite-converted RNA, 1μL of 1 mM dNTP mix, and 2μL of 10× pooled primer mix and add ultrapure H_2O to a final volume of 13μL. Incubate the mix at 65 °C for 5 min to denature the RNA.
2. Reverse transcribe the bisulfite-converted RNA using SuperScript™ III Reverse Transcriptase according to the manufacturer's protocol. Add either pooled 48 RT primers for parallel Access Array amplification or random hexamers for single-PCR amplicons.

Suggested controls: Include RT minus controls for each sample as the PCR primers are not necessarily designed to span exon-exon junctions. In the controls, use 1μL of H_2O instead of reverse transcriptase.

3. After the reaction is complete, dilute the cDNAs 1:10 in ultrapure H_2O for PCR amplification.

3.6 Individual PCR Amplification, Quantification, and Pooling

1. For a 10μL PCR, add 0.2μL of KAPA HiFi DNA Polymerase, 2μL of 5× HiFi Fidelity buffer (with $MgCl_2$), 0.3μL of 10 mM dNTP, 0.4μL of 10μM forward primer (CS1_GSS), 0.4μL of 10μM reverse primer (CS2_GSS), 1μL of diluted cDNA, and H_2O to a final volume of 10μL. Perform PCR for each amplicon in triplicate.
2. Gently finger vortex, briefly centrifuge, and place into a preheated thermal cycler.
3. Perform a two-step thermal cycling PCR program. See Table 1 for more details.
4. Pool the triplicates and perform an AMPure bead cleanup at a ratio of 1.8:1 to remove unincorporated primers and primer dimers. Repeat this step (*see* **Notes 13** and **14**).
5. Assess PCR amplicon size and concentration after separation on a Shimadzu Microchip Electrophoresis System MCE®-202 MultiNA.
6. Normalize the concentration of each amplicon in the experiment by dilution with H_2O to a concentration in the range of 0.5–5 ng/μL.
7. Perform the barcoding and Illumina adapter addition PCR. In a 10μL PCR, add 0.2μL of KAPA HiFi DNA Polymerase, 2μL of 5× HiFi Fidelity buffer (with $MgCl_2$), 0.3μL of 10 mM dNTP, 1μL of 10μM forward primer (P5_CS1), 1μL of 10μM reverse primer (P7_CS2), 2μL of diluted PCR amplicon, and H_2O to a final volume of 10μL.
8. Gently finger vortex, briefly centrifuge, and place into a preheated thermal cycler.
9. Perform a two-step thermal cycling PCR program. See Table 2 for more details.
10. Assess PCR amplicon size and concentration after separation on a Shimadzu Microchip Electrophoresis System MCE®-202 MultiNA.
11. Pool the amplicons in equimolar concentration and purify them using AMPure beads according to the manufacturer's protocol. Use a ratio of beads to pooled amplicons of 0.9:1 to ensure binding of amplicons and not primer dimers or unincorporated primers.

Table 1
Two-step thermal cycling conditions for the amplification of individual amplicons

Stage	Temperature (°C)	Time (s)
Initial denaturation	98	15
Step I (×10 cycles)		
Denaturation	94	10
Annealing	60	30
Extension	72	15
Step II (×20 cycles)		
Denaturation	94	10
Annealing	55	30
Extension	72	15
Final extension	72	60
Hold	4	Forever

Table 2
One-step thermal cycling conditions for the addition of barcodes and Illumina adapters

Stage	Temperature (°C)	Time (s)
Initial denaturation	98	15
One step (×12 cycles)		
Denaturation	94	10
Annealing	63	30
Extension	72	30
Final extension	72	120
Hold	4	Forever

12. First estimate the DNA concentration using a Qubit dsDNA Broad Range Assay Kit according to the manufacturer's protocol. Then accurately assess the DNA concentration by using KAPA Library Quantification Kit for Illumina® Platforms. Perform serial dilution of the pooled amplicons such that they fall into the dynamic range of the assay of 5.5–0.000055 pg/μL.

3.7 Parallel PCR Amplification Using a Fluidigm Access Array Integrated Fluidic Circuit (IFC)

1. Prime the Access Array according to the manufacturer's protocol.
2. Pre-warm the 20× Access Array loading reagent to room temperature before use. Prepare the pooled 48-oligonucleotide

primer mix by mixing 2.0μL of 50μM CS1-GS forward, 2.0μL of 50μM CS1-GS reverse, 5.0μL of 20× Access Array loading reagent, and 91μL of H_2O to a final volume of 100μL.

3. Finger vortex the mix and centrifuge to spin the contents to the bottom of the tube.
4. Prepare the sample premix solution by mixing 30μL 10× FastStart High Fidelity Reaction Buffer (without $MgCl_2$), 54μL 25 mM $MgCl_2$, 15μL DMSO, 6.0μL 10 mM dNTP mix, 3.0μL FastStart High Fidelity Enzyme Blend, 15.0μL 20× Access Array Loading Reagent, and 57μL H_2O.
5. Finger vortex the mix and centrifuge to spin the contents to the bottom of the tube.
6. Prepare the sample mix solutions, 48 in total, in a 96-well plate. Mix 3.0μL sample premix, 1.0μL cDNA, and 1.0μL Access Array Barcode library primers.
7. Thoroughly vortex the solutions for at least 30 s and then centrifuge to spin down the contents to the bottom of the plate. N.B.: Each well should receive a uniquely barcoded primer pair.
8. Load 4.0μL of the primer solution and 4.0μL of the sample mix solution into the primer and sample inlets of the Access Array by using an 8-channel pipette.
9. Load the Access Array into the Pre-PCR IFC Controller AX according to the manufacturer's protocol.
10. Place the Access Array onto the FC1 Cycler and start thermal cycling by selecting the protocol AA 48 × 48 Standard v1. The thermal cycling conditions are presented in Table 3.
11. To harvest the PCR products from the Access Array follow the manufacturer's protocol. Once the final step is completed, eject the Access Array.
12. Collect the harvested PCR products into a labeled PCR 96-well plate. Carefully transfer 10μL of harvested PCR products from each of the sample inlets into columns 1–6 of the labeled 96-well plate by using an 8-channel pipette.
13. Assess PCR amplicon size and concentration after separation on a Shimadzu Microchip Electrophoresis System MCE®-202 MultiNA.
14. Pool the amplicons in equimolar concentration and purify them using AMPure beads according to the manufacturer's protocol. Use a ratio of beads to pooled amplicons of 0.9:1 to ensure binding of amplicons and not primer dimers or unincorporated primers (see **Note 14**).
15. First estimate the DNA concentration using a Qubit dsDNA Broad Range Assay Kit according to the manufacturer's

Table 3
Multistep thermal cycling conditions for the Access Array

Temperature (°C)	Time (s)	Number of cycles
50	120	1
70	1200	1
95	600	1
95 60 72	15 30 60	10
95 80 60 72	15 30 30 60	2
95 60 72	15 30 60	8
95 80 60 72	15 30 30 60	2
95 60 72	15 30 60	8
95 80 60 72	15 30 30 60	5

protocol. Then accurately assess the DNA concentration by using KAPA Library Quantification Kit for Illumina® Platforms. Perform serial dilution of the pooled amplicons such that they fall into the dynamic range of the assay of 5.5–0.000055 pg/μL.

3.8 MiSeq Sequencing

1. Prepare the sample sheet using the Illumina Experiment Manager by following the manufacturer's protocol (*see* **Note 15**).
2. Dilute the library to 10 nM in EBT buffer based on the concentrations determined by the qPCR. From this point, keep the libraries on ice.
3. Dilute the PhiX control library to 2 nM by adding 8μL EBT buffer to 2μL of the 10 nM PhiX control library (*see* **Note 16**).
4. Denature the pooled libraries and PhiX control library separately by adding 10μL of 0.2 M NaOH to 10μL of the 2 nM libraries (*see* **Note 17**).

5. Vortex thoroughly to mix and centrifuge at 1000 × *g* for 30 s. Incubate at room temperature for 5 min.
6. Dilute the denatured pooled libraries and PhiX control library separately to 20 pM by adding 980μL pre-chilled HT1 to 20μL denatured libraries.
7. Dilute the 20 pM pooled libraries and PhiX control library separately to 10 pM by adding 500μL pre-chilled HT1 to 500μL 20 pM libraries.
8. Combine 100μL of the 10 pM PhiX control library with 900μL of the 10 pM pooled libraries and vortex to mix (*see* **Note 18**).
9. Load 600μL of the final sample into the cartridge. Ensure that air bubbles are removed by gently tapping the cartridge.
10. Perform the sequencing run according to the manufacturer's protocol.

3.9 Bioinformatics Analysis of Data

1. To trim the Illumina adaptor sequences that were incorporated into the amplicons to permit sequencing of the 150 bp paired-end reads, use Trimmomatic in palindromic mode [15].
2. Sequencing reads can be aligned with meRanTK by using Bowtie2 internally [16]. Assemble reference sequences for the alignment by using the segments of RNA interrogated by sequencing prior to bisulfite conversion.
3. Extract the methylation state of individual cytosines from bisulfite-read alignments by using meRanCall. The number of reads can be extracted from the aligned sequencing reads in order to determine read coverage at a given cytosine.
4. To call differentially methylated cytosines use meRanCompare. The number of reads can be extracted from the aligned sequencing reads in order to determine read coverage at a given cytosine (Fig. 4).

4 Notes

1. Slowly add 10 M NaOH dropwise to the sodium bisulfite solution while mixing. Slightly less than 1 mL is required to adjust the pH to 5.1.
2. The MiSeq Reagent Kit v3 (150- or 600-cycle) provides 1 × 150 bp or the 600-cycle kit allows combinations of cycles that add to 600, for example 200 and 400 cycles.
3. Do not machine or finger vortex the RNA as this will increase the risk of RNA loss.
4. Air-drying the samples in a sterile laminar flow hood is recommended. Do not allow the RNA to completely dry as this will cause difficulties in resuspending the RNA.

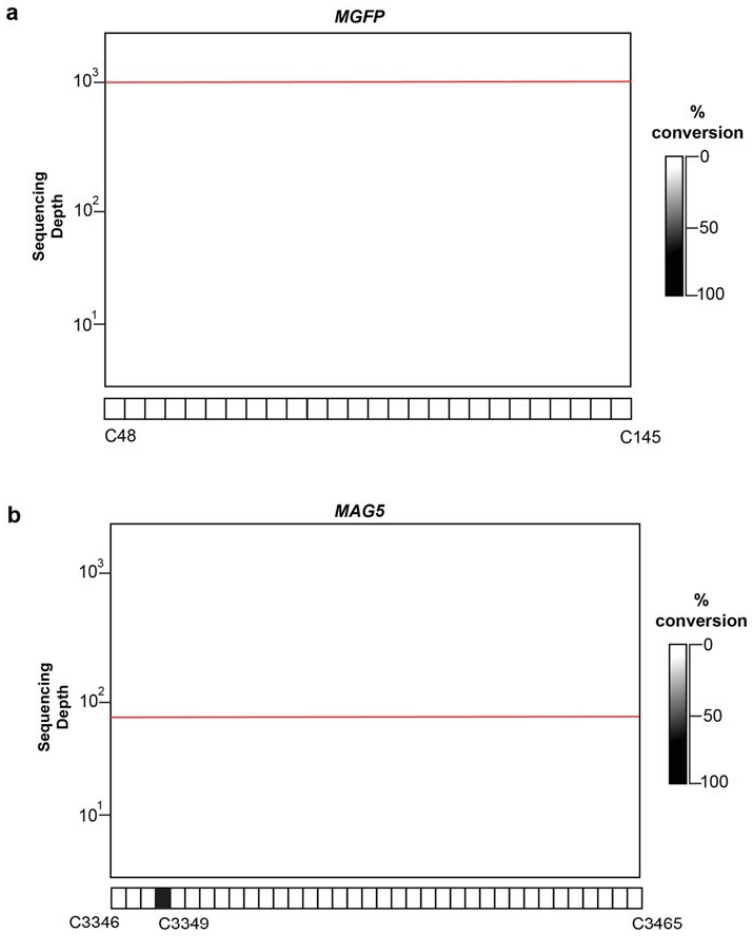

Fig. 4 Representative analysis of an Illumina MiSeq amplicon sequencing of negative and positive controls. (**a**) A region of the MGFP spiked-in in vitro control transcript showing even coverage and all cytosines are converted (no methylation). The *y*-axis shows the read depth and the *x*-axis shows the cytosines (numbers) in the sequenced region. (**b**) A region of the *Mag5* gene that shows converted and non-converted cytosine, C3349. Cytosines flanking C339 are completely converted, demonstrating that bisulfite conversion was very efficient. The heatmaps display the cytosine non-conversion percentage

5. As the in vitro MGFP transcript will most likely be at a high concentration, it is good practice to perform a serial dilution in H_2O such that the estimated concentrations are in the range of 5–50 ng/μL. Prepare and run three dilutions on the RNA Nano chip.

6. Tilt the 1.5 mL tube at a 45° angle and then slowly pipette the mineral oil directly on top of the RNA-bisulfite reaction mixture.
7. Emptying of the Micro Bio-Spin gel column takes about 2 min. If the gel column does not empty by gravity, place the lid back onto the column and remove again.
8. Gently pipette the reaction mixture onto the gel bed and avoid disturbing the gel bed. Minimize the transfer of mineral oil to the column although there will be traces which is unavoidable.
9. About 25% of the RNA is lost during the procedure, and we find that 10μL of H_2O/2μg RNA used in the bisulfite conversion reaction results in concentrations of ~150 ng/μL.
10. Bisulfite treatment of the RNA causes significant shearing and we have observed that shorter amplicons are preferentially amplified over longer amplicons.

    Longer PCR amplicons increase the tendency of detecting non-converted cytosines in RNA exhibiting strong secondary structure.
11. Inefficient bisulfite conversion may result in unconverted cytosines, so it is important to ensure that the PCR primers are not biasing the amplification toward converted cytosines.
12. Occasionally, not all triplicates successfully amplify and it may be necessary to optimize the PCR.
13. We elute the purified PCR products in 10–30μL depending on the amount of amplified PCR products.
14. After purification of the amplicons, residual ethanol may remain in the purified amplicons. We find that concentrating down the pooled amplicons even if there is <55μL and adding H_2O to 55μL are best to remove as much ethanol as possible.
15. The sample sheet is required to insert the sample names and adapter indices used for each sample. We have selected the "Other" as the category followed by "Fastq only." This option generates FASTQ files only and also enables the deselection of downstream processing steps like adapter trimming, allowing trimming and mapping to be performed separately.
16. The prepared PhiX library is added to the pooled amplicon libraries as an internal control for the MiSeq sequencing run.
17. It is best to prepare fresh 0.2 M NaOH for the denaturation of libraries.
18. Loading 10% PhiX control library is sufficient for low-diversity libraries. We have previously loaded between 7 and 10 pM. Underloading of the libraries can give cluster densities below the optimal range and overloading of the libraries can give cluster densities above the optimal range, reducing the quality of the data. The optimal cluster density is 700–1000 K/mm^2.

Acknowledgments

This work was supported by an Australian Research Council Future Fellowship (FT130100525) awarded to IS, a Grains Research and Development Corporation scholarship awarded to AB, a Chinese Scholarship Council scholarship awarded to JZ, and a MOET-VIED PhD scholarship awarded to TD.

References

1. Burgess A, David R, Searle IR (2016) Deciphering the epitranscriptome: a green perspective. J Integr Plant Biol 58(10):822–835
2. Saletore Y, Meyer K, Korlach J, Vilfan ID, Jaffrey S, Mason CE (2012) The birth of the Epitranscriptome: deciphering the function of RNA modifications. Genome Biol 13(10):175
3. Bujnicki JM (2001) In silico analysis of the tRNA: m1A58 methyltransferase family: homology-based fold prediction and identification of new members from Eubacteria and Archaea. FEBS Lett 507(2):123–127
4. Droogmans L, Roovers M, Bujnicki JM, Tricot C, Hartsch T, Stalon V, Grosjean H (2003) Cloning and characterization of tRNA (m1A58) methyltransferase (TrmI) from Thermus thermophilus HB27, a protein required for cell growth at extreme temperatures. Nucleic Acids Res 31(8):2148–2156
5. Oerum S, Dégut C, Barraud P, Tisné C (2017) m1A post-transcriptional modification in tRNAs. Biomol Ther 7(1):20
6. Dominissini D, Moshitch-Moshkovitz S, Schwartz S, Salmon-Divon M, Ungar L, Osenberg S, Cesarkas K, Jacob-Hirsch J, Amariglio N, Kupiec M (2012) Topology of the human and mouse m6A RNA methylomes revealed by m6A-seq. Nature 485 (7397):201–206
7. Meyer KD, Saletore Y, Zumbo P, Elemento O, Mason CE, Jaffrey SR (2012) Comprehensive analysis of mRNA methylation reveals enrichment in 3′ UTRs and near stop codons. Cell 149(7):1635–1646
8. Squires JE, Patel HR, Nousch M, Sibbritt T, Humphreys DT, Parker BJ, Suter CM, Preiss T (2012) Widespread occurrence of 5-methylcytosine in human coding and non-coding RNA. Nucleic Acids Res:gks144
9. Lovejoy AF, Riordan DP, Brown PO (2014) Transcriptome-wide mapping of pseudouridines: pseudouridine synthases modify specific mRNAs in S. cerevisiae. PLoS One 9(10): e110799
10. Khoddami V, Cairns BR (2013) Identification of direct targets and modified bases of RNA cytosine methyltransferases. Nat Biotechnol 31(5):458–464
11. Hussain S, Sajini AA, Blanco S, Dietmann S, Lombard P, Sugimoto Y, Paramor M, Gleeson JG, Odom DT, Ule J (2013) NSun2-mediated cytosine-5 methylation of vault noncoding RNA determines its processing into regulatory small RNAs. Cell Rep 4(2):255–261
12. Cokus SJ, Feng S, Zhang X, Chen Z, Merriman B, Haudenschild CD, Pradhan S, Nelson SF, Pellegrini M, Jacobsen SE (2008) Shotgun bisulphite sequencing of the Arabidopsis genome reveals DNA methylation patterning. Nature 452(7184):215–219
13. Schaefer M, Pollex T, Hanna K, Lyko F (2008) RNA cytosine methylation analysis by bisulfite sequencing. Nucleic Acids Res 37(2):e12–e12
14. David R, Burgess A, Parker B, Li J, Pulsford K, Sibbritt T, Preiss T, Searle IR (2017) Transcriptome-wide mapping of RNA 5-methylcytosine in Arabidopsis mRNAs and noncoding RNAs. Plant Cell 29(3):445–460
15. Bolger AM, Lohse M, Usadel B (2014) Trimmomatic: a flexible trimmer for Illumina sequence data. Bioinformatics 30 (15):2114–2120
16. Rieder D, Amort T, Kugler E, Lusser A, Trajanoski Z (2015) meRanTK: methylated RNA analysis ToolKit. Bioinformatics 32 (5):782–785